The Faint End of the Luminosity Function in Clusters of Galaxies

by

Roberto De Propris
B. Sc., King's College, University of London, 1990
M. Sc., University of Victoria, 1992

A Dissertation Submitted in Partial Fulfillment of the
Requirements for the Degree of

DOCTOR OF PHILOSOPHY

in the Department of Physics and Astronomy

Abstract

Supervisor: Dr. Christopher J. Pritchet

We have determined luminosity functions, surface density distributions and color distributions for galaxies in eight clusters of galaxies at moderate redshift ($z \sim 0.02$) observed at the CFHT.

- In the inner $2'$ of four cD clusters (Abell 2052, 2107, 2199 and 2666) we find very steep LFs, with $\alpha \sim -2.2 \pm 0.2$, where $N_{gal}(L) \propto L^{\alpha}$, where L is luminosity
- For Abell 262, we find no significant contribution from cluster dwarfs in the field around NGC708 (the central cluster elliptical), although there is a small excess over background counts in the inner $3'$ of this field. For galaxies near UGC1308, we derive a LF with $\alpha \sim -1.4 \pm 0.1$. Galaxies in this field are concentrated towards UGC1308, so that the LF may be due to a population of satellites.
- For the field centred on NGC1275 in Abell 426 we find a very steep LF, with $\alpha \sim -1.9 \pm 0.1$. We find that galaxies are not centrally concentrated towards NGC1275, except for a central 'spike' in their surface density distribution. We see a weak sequence of galaxies in the V vs $V - I$ plot. There is a small color gradient in the sense of bluer galaxies near NGC1275.

- For the field centred on NGC1265, we find again a very steep LF. Galaxies in this field tend to avoid the neighbourhood of NGC1265 and there is a mild red color gradient towards NGC1265. The LF within 100 kpc of NGC1265 is somewhat flatter than outside of this region, although the significance of this result is marginal.

- For the field centred on UGC3274 in A539 we find a LF with $\alpha \sim -1.4 \pm 0.1$. We see that the galaxy distribution as a function of distance from UGC3274 is flat, except for a central spike. The LF appears to steepen towards UGC3274. There is a tight sequence of cluster galaxies in the V vs. $V - I$ plot. There also appears to be a blueing trend towards UGC3274.

- For Hercules (A2151) we derive a LF with $\alpha \sim -1.5$ and $M^* = 12.2$, where M^* is a characteristic luminosity here converted to magnitudes.

We interpret these results as supporting the conclusions by Biviano et al. (1995b) in Coma, namely that a population of dwarf galaxies with a steep LF constitutes the main body of the cluster, into which brighter giants fall later, thereby flattening the LF. We also find evidence that steep LFs are correlated with high gas densities. The blueing trend towards NGC1275 and UGC3274 is also consistent with recent star formation in dwarfs due to accretion of intracluster gas.

Contents

List of Figures

List of Tables

Acknowledgements

I would like to acknowledge the many people who helped me in this endeavour. In the first place, my supervisor, Dr. Christopher J. Pritchet, for his constant encouragement and support. I would also like to thank Drs. F. David A. Hartwick and Don A. VandenBerg for their help and friendship. Many thanks also go to Dr. James E. Hesser and family.

My fellow graduate students deserve some mention (praise, blame...): among them Luc 'The friendly IRAF guru' Simard (aka Money Mart), John 'Boy' Ouellette, Ana 'Can We Fake It ?' Larson, Dave 'Peter' Patton and Robert 'Sturm Graz' Greimel.

I would also like to thank very much Ms. Claudia Fabbri for her friendship and her company.

"Unfit to mend the azure sky,
I passed some years to no avail.
My life in both worlds written here,
whom can I ask to pass it on ?"

Inscription on the jade stone rejected by the goddess Nu Wa when she repaired the sky. From *A Dream of Red Mansions* by Tsao Hsueh-Chin.

Chapter 1

Introduction

1.1 Introduction

The galaxy Luminosity Function (LF) is a representation of the space density of galaxies as a function of luminosity L, or absolute magnitude M, within an arbitrarily large region of space, normalised to one cubic megaparsec (Mpc – a non SI unit corresponding to a million parsecs, where a parsec is the distance at which the radius of the Earth's orbit subtends an angle of 1″). In simplistic terms, the LF estimates the number of galaxies having luminosities between $L - dL/2$ and $L + dL/2$, where dL is an interval of luminosity, within a given (large) volume.

The LF holds great importance for a number of topics in modern astronomy. For example, the LF may be integrated over the cosmological volume element, assuming an appropriate redshift distribution (i.e., evolutionary history) for galaxies, to yield a geometrical estimate of the deceleration parame-

ter q_0, by matching the observed number counts of faint galaxies as a function of apparent magnitude to theoretical predictions (e.g., Narlikar 1992; Peebles 1993).

It is well known that observed faint galaxy counts exceed predictions of the simplest 'no evolution' models (in which galaxies are assumed to have the same luminosity in the past as at the present epoch) at $B > 20$, the excess reaching factors of 5-15 at $B \sim 24$ (e.g., Tyson 1988; Maddox et al. 1990; Lilly et al. 1991; Metcalfe et al. 1991; Pritchet & Infante 1992a and references therein). Yet, observed redshift distributions are consistent with little or no evolution of galaxy populations for $z < 0.6$, with most objects lying at $z \sim 0.3$ (Broadhurst et al. 1988; Colless et al. 1990; Cowie et al. 1991; Colless et al. 1993; Lilly 1993; Tresse et al. 1993; Songaila et al. 1994; but see Lilly et al. 1995 for evidence of evolution in I selected samples and Steidel et al. 1995 for absorption-line selected samples). One possibility is that the LF is 'steep' at low luminosities (i.e., the number of intrinsically faint galaxies increases rapidly with decreasing luminosity); Koo et al. (1993) show that this might account for the excess population in number counts, while salvaging 'no evolution' models and without resorting to exotic cosmologies. This requires a population of nearby blue low surface brightness dwarfs, which are missed in redshift surveys because of selection effects. It would therefore be very interesting to determine LFs to low luminosities, in order to test these hypotheses.

The LF is also a cornerstone observation for theories of galaxy formation, which must eventually succeed in reproducing its observed shape. In the popular Cold Dark Matter (CDM) model (see Ostriker 1993 for a review), dwarf galaxies contributing to the faint regime are believed to form from 1σ fluctuations in density, whereas spirals and ellipticals originate from 2σ and 3σ perturbations respectively. Thus, the LF of dwarf galaxies is expected to be steep, because of the relative abundance of small perturbations with respect to large ones. Furthermore, dwarf galaxies are expected to trace the underlying matter distribution better, as they form from plentiful 1σ perturbations, whereas spirals and ellipticals may only form where a large scale perturbation (on protocluster scales, for example) 'boosts' the peaks in density fluctuations above the required threshold to initiate collapse and galaxy formation (i.e., galaxy formation is 'biased' to occur in high density regions). Thus, we expect, as a consequence of CDM, steep dwarf galaxy LFs (e.g., White & Frenk 1991) and a larger number of dwarf galaxies, with respect to giants, in low density regions such as the field (e.g., Dekel & Silk 1986). The observed LF is, on the other hand, not very steep, with faint end slopes of $\alpha = -1$ to -1.3 (e.g., § 1.2.3 and 1.2.4) and the dwarf to giant ratio *increases* in high density environments (e.g., § 1.2.4), which both are in strong disagreement with CDM predictions.

Dwarf galaxies are, on the other hand, expected to be strongly affected by their surroundings, and differential evolution in different environments may be invoked to explain these discrepancies. An interesting scenario for dwarf

galaxy evolution has been presented by Babul & Rees (1992), and we will briefly discuss it in § 1.3. Clearly, determining LFs in different environments would help in resolving these issues.

Finally, the LF provides information on the nature of faint galaxies, for which little information may be gathered by methods other than broadband photometry. In particular, it would be interesting to obtain information on the colors of dwarf galaxies and on their clustering properties.

In this thesis we discuss determinations of the LF to low luminosities in four clusters of galaxies, selected according to their X-ray properties. We derive LFs to faint absolute magnitudes in V and I in two different fields in each cluster, in order to gain an understanding of how LFs vary with environmental density from cluster to cluster and within each cluster. We also determine colors for dwarf galaxies in these clusters and we produce surface density distributions for galaxies in V, I and $V - I$, in order to determine the nature of the dwarf galaxy population and their clustering properties with respect to bright galaxies in each cluster.

The outline of this thesis is as follows. In the remainder of this Introduction we review LF determinations in the Local Group (§ 1.2.2), the general field (§ 1.2.3) and clusters (§ 1.2.4). Environmental effects are discussed in § 1.3. We outline our project, explain our rationale for observing in clusters and our cluster selection procedures in § 1.4.

Observations for this project were taken at the Canada-France-Hawaii

3.6m Telescope (CFHT), using the High Resolution Camera (Chapter 3) and the new Mosaic CCD Camera (Chapters 5-8). We discuss the procedures used in preprocessing and initial data reduction in § 2.2. Data for Abell 2151 were taken at the Kitt Peak 4.2m Mayall Telescope, and reduction procedures are discussed in Chapter 7. Finding and photometry algorithms are presented in § 2.3. Our earlier study in four cD clusters is presented in Chapter 3.

One crucial step in obtaining cluster LFs is discrimination against contamination by stars and foreground or background galaxies. In most cases it is impossible to safely separate cluster members from galaxies in the background or foreground field. Discrimination of cluster members is therefore carried out statistically, using background galaxy counts from the literature and from observed fields. We discuss our background correction and star-galaxy separation in Chapter 4.

Chapters 5, 6, 7 give the main results of this work for Abell 262, Abell 426 and Abell 539; LFs in V for each field observed, radial distributions in V, I and $V-I$ for galaxies in these fields and fits to these distributions. Chapter 8 presents R observations of Abell 2151.

We summarise and discuss our findings in Chapter 9.

For the remainder of this work we assume a $H_0 = 75$ km/s/Mpc and $\Omega_0 = 1$ unless quoting the results of others.

1.2 The Luminosity Function in Different Environments

In order to place our findings in the proper frame of reference we will need to consider the LF in different environments, such as the Local Group, the general field and clusters of galaxies (that are the main focus of this work). In the following we present a brief historical introduction and discuss LFs in these environments.

1.2.1 Historical Note

The first attempts to determine the galaxy LF were carried out by Hubble (1936) who derived a Gaussian luminosity distribution with small (0.84 magnitudes) dispersion from the small scatter of galaxies in the Hubble m-z (apparent magnitude - redshift) diagram, compiled from the redshift survey by Humason (1936).

This approach was soon criticized by Zwicky (1942, 1957, 1964) who drew attention to magnitude and surface brightness selection effects, and favoured an exponentially rising LF, apparently on purely theoretical grounds, drawn from thermodynamics.

Inclusion of the (then) newly discovered dwarf spheroidal galaxies in the Local Group (e.g., Fornax - Shapley 1938) was soon shown to skew Hubble's Gaussian distribution to one side (Holmberg 1950). Further work in clusters of galaxies by Abell (1958, 1962, 1964, 1972) established the existence of

power-law LFs, with two different regimes for 'bright' and 'faint' galaxies.

The currently accepted form of the LF was derived by Schechter (1976) from Press & Schechter (1974) formalism:

$$\Phi(L)dL = \Phi^* \exp(-L/L^*)(L/L^*)^\alpha dL/L^*$$

$$\Phi(M)dM = \Phi \exp[-10^{0.4(M^*-M)}]10^{0.4(M^*-M)(\alpha+1)}dM$$

where Φ^* is a normalisation parameter, L^* is a characteristic luminosity approximately equivalent to an absolute B magnitude of -20.3, which is, coincidentally, close to the luminosity of M31, and α is a power-law slope. This function drops rapidly for $L > L^*$ and rises steeply, with asymptotic power-law slope α, for $L < L^*$. An example is shown in Figure 1.1, which is a plot of $\log N$ as a function of absolute magnitude from Felten (1985). Note the large error bars at the bright and faint end. These are due to the fact that intrinsically bright galaxies are rare and are surveyed over very large volumes, whereas low luminosity galaxies are only observed nearby. It is worth noting that for a magnitude-limited sample most galaxies will fall close to L^*, which may explain Hubble's early result.

Ultimately, both Hubble and Zwicky were correct for the galaxies they were considering. Hubble's sample consisted mostly of high surface brightness giant ellipticals and spiral galaxies, whose LF is approximately Gaussian (see Figures 1.2, 1.3 and 1.4). Dwarf galaxies, on the other hand, have exponential LFs (again, see Figures 1.2, 1.3 and 1.4) as required by Zwicky (1942).

This form of the LF was shown to be a very good approximation to the observed luminosity distribution of galaxies (Schechter 1976; Felten 1977, 1985) both in the field and in clusters. Its shape parameters (L^* and α) appear to be approximately universal, although there is considerable variation from one cluster to the other (e.g., Dressler 1978; Lugger 1986). This feature is actually due to the fact that the observed LF represents the average of contributions of LFs for each galaxy morphological type. These contributions are known to vary with environmental density (cf. the well-known morphology density relation — Dressler 1980 – see §§ 1.2.3 and 1.2.4). Possibly the best example of this effect, as far as we are concerned, is the steepening of the dwarf galaxy LF in dense environments, from the field (e.g., Binggeli et al. 1990; – see § 1.2.3) to clusters (e.g., Sandage et al. 1985; – see § 1.2.4).

Currently, there is considerable interest in determining the LF of field galaxies and of galaxies in clusters. The latter is an easier proposition, as we shall see below, but less general than the field LF. The LF for nearby dwarfs in the Local Group is also very instructive, as we can obtain information on their stellar populations. Accordingly, we will review the Local and nearby groups in the first place, before dealing with current knowledge on the LF of field galaxies and cluster galaxies.

Figure 1.1: The Schechter LF - from Felten (1985)

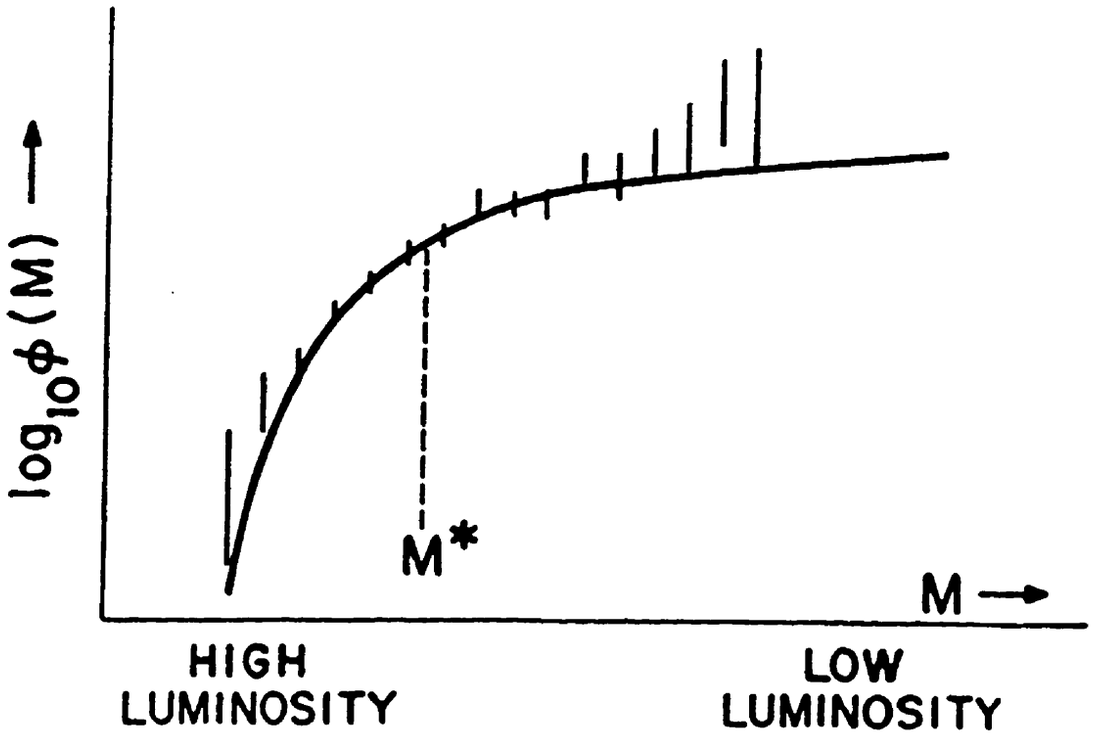

Figure 1.2: The LF for field galaxies by Marzke et al. (1994a)

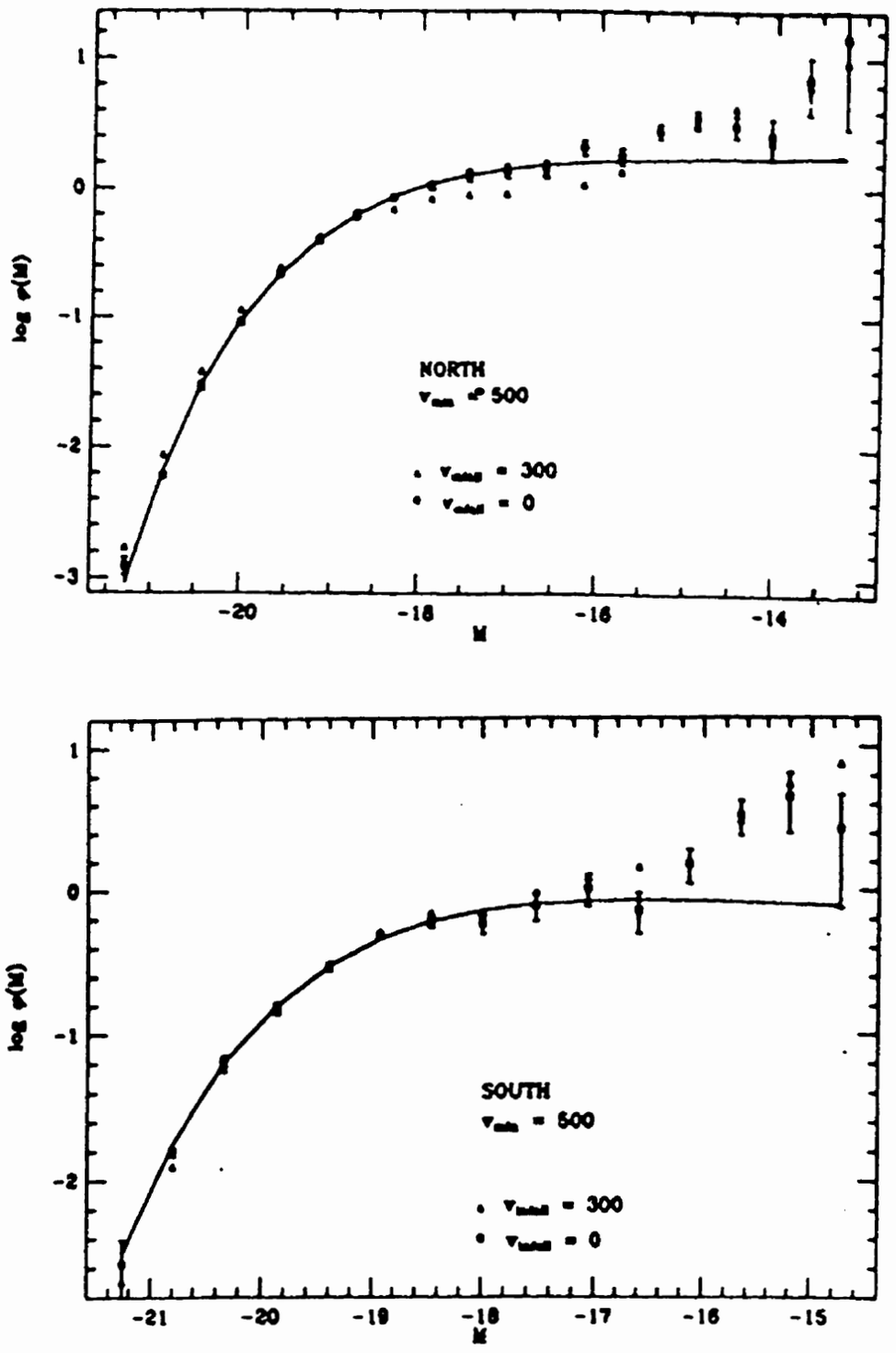

Figure 1.3: The type-resolved LF for field galaxies by Marzke et al. (1994b)

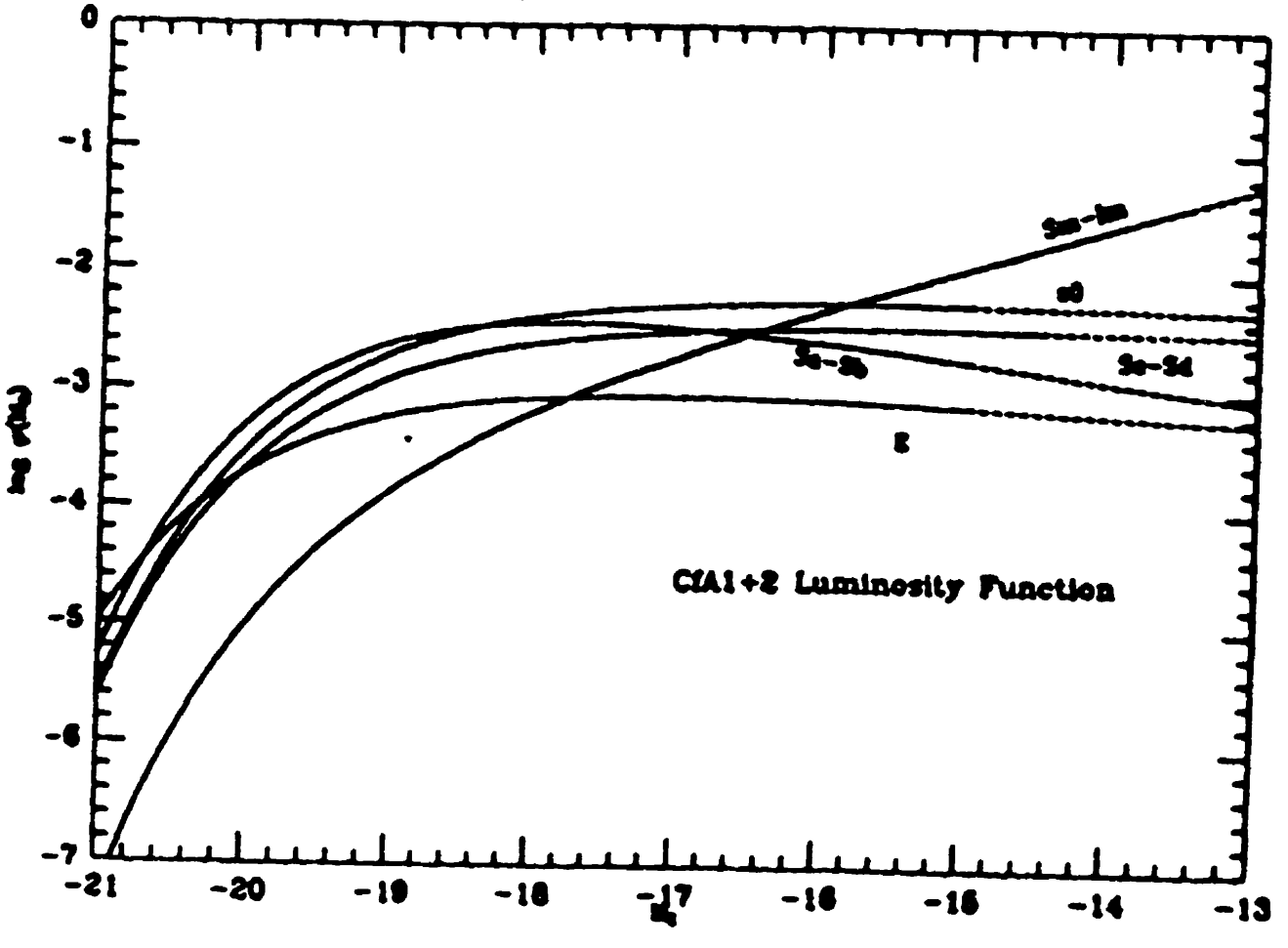

Figure 1.4: The LF for Virgo by Binggeli et al. (1988)

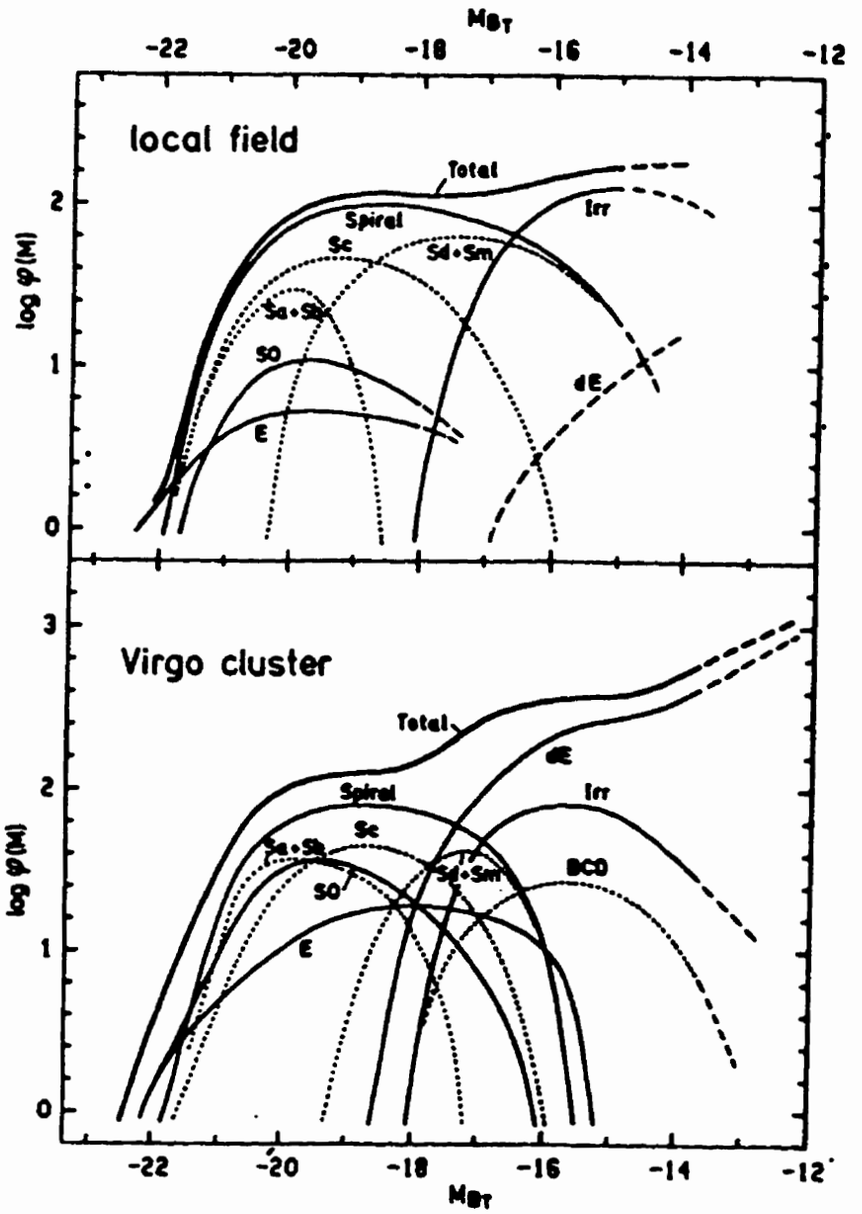

Table 1.1: MEMBERS OF THE LOCAL GROUP

ID	Type	M_V
M31	Sb I-II	–21.1
Galaxy	SABb/c	–20.6
M33	Sc II-III	–18.9
LMC	Im III-IV	–18.1
NGC6822	Im IV-V	–16.4
SMC	Im IV-V	–16.2
IC1613	Im V	–14.9
WLM	Im IV-V	–14.1
DDO 210	Im V	–11.5
LGS 3	dIm/dSph	–10.2
Phoenix	dIm/dSph	– 9.5
M32	E2	–16.4
NGC 205	dE	–16.3
NGC 185	dE	–15.3
NGC 147	dE	–15.1
Fornax	dSph	–13.7
Sagittarius	dSph	–13:
And I	dSph	–11.8
And II	dSph	–11.8
Leo I	dSph	–11.7
Sculptor	dSph	–10.7
And III	dSph	–10.3
Leo II	dSph	–10.2
Sextans	dSph	–10.0
Tucana	dSph	–9.5
Carina	dSph	–9.2
Ursa Minor	dSph	–8.9
Draco	dSph	–8.5

1.2.2 The Local Group

The Local Group is the natural environment to identify dwarf galaxies and to obtain detailed information concerning their structure, dynamics, and stellar populations. Dwarf galaxies are now known in the Local Group to absolute magnitudes approaching those of globular clusters. Thus LFs in the Local Group may be obtained to depths which are unachievable in other systems.

The Local Group consists of two giant spirals (M31 and the Milky Way), one dwarf elliptical (M32), a low luminosity spiral (M33) and a number of dwarf irregular (e.g., the Large and Small Magellanic Clouds, IC 1613) and dwarf spheroidal (e.g., Fornax, Draco) galaxies. A list of Local Group members is given in Table 1.1.

A short digression is now needed to detail a peculiar nomenclature problem; when dwarf spheroidals are encountered outside of the Local Group they are called 'dwarf ellipticals'. Unfortunately, this is confusing. Elliptical galaxies have de Vaucouleurs surface brightness profiles, i.e., when their surface brightness in magnitudes is plotted as a function of radius, it is found to decline as $r^{1/4}$. Spiral galaxies and irregulars have exponential profiles, in which their surface brightness declines exponentially. Dwarf spheroidal galaxies also have exponential surface brightness profiles, rather than the de Vaucouleurs profiles of true ellipticals. Thus the term 'dwarf elliptical' is a misnomer for dwarf spheroidals and may lead to considerable confusion.
The LF for the Local Group has been recently reviewed by van den Bergh

(1992), who finds it to be well fit by a Schechter function with $M_B^* \approx -20.3$ and $\alpha \approx -1$. This result appears to be robust, when analysed with maximum likelihood methods (Pritchet, private communication), despite the small number of objects.

It should be mentioned that the list of Local Group members may not be complete. The recent discovery of a bright dwarf spheroidal galaxy (Sagittarius: Ibata et al. 1994; 1995), albeit at low galactic latitudes, hints at the possibility that many more dwarfs lie hidden. One argument in favour of this is that the number of satellites of the Milky Way is larger than that of M31, despite the fact that M31 is more luminous and more bulge-dominated and thus, by analogy with globular cluster systems (e.g., Harris 1991), may be expected to possess a richer cohort of satellites. If the M31 satellite system resembles ours, most companions should lie 100 to 200 kiloparsecs from M31's centre, which is about 7° when projected on the sky. This region has only been surveyed with shallow Schmidt plates, which are ill suited to the discovery of dwarf spheroidal galaxies. An extensive search for new members of the Local Group has so far yielded only negative results (Irwin 1994; but see Ibata et al. 1994; 1995). Searches tailored to the discovery of extremely low surface brightness galaxies have also been unsuccessful (Eder et al. 1989; Phillips et al. 1994), but a number of low surface brightness giants have been detected in HI surveys (e.g., Sprayberry et al. 1995). These objects are discussed in § 1.2.3 below. Therefore, it appears that many new members of the Local Group are not forthcoming, although it has been suggested that they

may lie in the zone of obscuration (Hartwick 1996, private communication) along an axis connecting the centre of our Galaxy with the centre of M31.

The Local Group is the only system for which it is possible to obtain information concerning the stellar populations of its component galaxies. The stellar populations of dwarf spheroidals have been recently reviewed by van den Bergh (1994) and Ferguson & Binggeli (1994). Very detailed analysis has been carried out for Carina by Smecker-Hane et al. (1994), which show that Carina has undergone multiple episodes of star formation, occurring as early as 5 billion years ago. Clearly, Carina was able to retain most of its interstellar medium and undergo further episodes of star formation. This is somewhat unexpected for a galaxy as massive as Carina, in the framework of the Babul & Rees (1992) model (for which see § 1.3). Other nearby dwarfs (Draco, Sextans, Sculptor and Ursa Minor) have mostly old populations, but none has been surveyed to the level of detail of Carina; further investigations are needed before conclusions may be drawn on the influence of the proximity to the Milky Way galaxy on the star formation history of dwarf spheroidals (van den Bergh 1994); in particular, observations of Draco, Ursa Minor, Sextans and Sculptor are needed to the same level of detail as Carina. This project is now being underway, using the new large field capabilities on CFHT. The newly discovered Sagittarius dwarf seems to possess a number of stellar populations with different ages, which is indicative of multiple episodes of star formation (Sarajedini & Layden 1995), and it is thus similar to Fornax (Buonanno et al. 1985), despite its position, only 25

kpc away from the Galaxy. Further studies of stellar populations in these galaxies would help elucidate their star formation history.

Surveys have also been carried out for other groups. Tully (1988) has reviewed the LF for six of the nearest groups, including the Local Group, and finds considerable variation in the slope of the LF at low luminosities. Only the Local group and the CVn I group have LFs as steep as $\alpha \sim -1$. More recent work has confirmed the variation in the slope of the LF, with some groups having very flat LFs and others with extremely steep ones. Ferguson (1992) has claimed a very steep slope for the M81 group ($\alpha = -1.9$), albeit with very large errors. De Oliveira & Hickson (1991) have explored a number of compact groups and find a shallow LF ($\alpha \sim -0.2$). This is very interesting, as these objects are expected to merge on timescales smaller than a Hubble time into giant field ellipticals. The 'turnover' in their LF demonstrates that tidal interactions and mergers may destroy dwarf galaxies and therefore decrease the slope of the galaxy LF, since fainter and less massive objects will be preferentially destroyed. Finally, Ribeiro et al. (1994) claim $\alpha = -0.9$ from a study of numerous groups. Thus, the LF of groups seems consistent with moderately flat LFs.

1.2.3 The Field

A much more general approach involves determining LFs for galaxies in the general field, which constitute most of the galaxy population in the Universe.

Of course, this is a much more complex problem than obtaining cluster LFs.

In order to derive accurate LFs for field galaxies we need large bodies of photometry (from plate material or, nowadays, CCD drift scans) and redshift information, to determine distances and absolute luminosities. A serious problem in these studies concerns the possibility of biases in galaxy selection. Disney (1976), Davies & Phillips (1983) and Davies et al. (1988) have pointed out that galaxies are selected, in galaxy catalogs such as the Uppsala General Catalog (UGC; Nilson 1973), as objects that, on shallow survey plates, subtend more than $1'$ at some faint isophotes. This discriminates against low surface brightness objects, whose faintest isophote may well be within $1'$, or unusually compact galaxies. Thus, we may only survey a small section of a much broader distribution of galaxies in the luminosity-surface brightness plane.

In general, low surface brightness galaxies are also intrinsically faint, so that galaxies are indeed selected by surface brightness but, thanks to the fact that faint galaxies have low surface brightnesses, they are also selected by luminosity. All of this has recently been challenged by the discovery of intrinsically luminous low surface brightness spirals, of which the prototypical example is Malin 1 (Impey et al. 1988). More examples of such galaxies, although not as extreme as Malin 1, are now known (e.g., Schombert et al. 1992; Sprayberry et al. 1995), although this type of galaxy does not seem to be common enough to significantly alter the shape of the LF.

Another problem to be considered in this respect is the possibility of incompleteness in the redshift surveys needed to determine distances and absolute magnitudes. These will be most serious for low surface brightness objects. These are generally quite faint, and since field LFs are generally computed for $M_B < -16$, this should not affect the result. More detail on the subject of the field LF at low luminosities is given below.

Galaxy samples are generally magnitude-limited and suffer from incompleteness at faint magnitudes. This can generally be corrected for by using objects from other catalogs (Kiang 1961), or by computing an incompleteness function from deeper observations (Sandage et al. 1979). An ingenious method is to use the V/V_{max} estimator (Huchra & Sargent 1973), in which the volume V between the galaxy and the observer is compared with the maximum volume (V_{max}) the galaxy could occupy without falling out of the sample. A sample is complete if V/V_{max} is 0.5.

A last correction to be applied to the raw data arises from the fact that galaxies of different intrinsic luminosity are sampled over different volumes. In particular, dwarf galaxies are only observed close to the Milky Way, and are thus affected by local inhomogeneities in galaxy distribution (i.e., superclustering). There are a number of elegant ways to correct for this problem (e.g., Sandage et al. 1979; Efstathiou et al. 1988). These methods all assume that the LF is independent of density, an assumption that may not be correct (because of the morphology-density relation), especially for faint dwarfs that

may be the more strongly clustered galaxies (Vader & Sandage 1991).

Loveday et al. (1992) have determined the field LF from analysis of plate material taken at Mount Stromlo and studied with the Automatic Plate Measuring machine. The field LF is found to be well fit by a Schechter function with $M^*_{b_J} \sim -19.5$ and $\alpha \sim -0.97$. Early type galaxies are found to have a much flatter ($\alpha \sim +0.2$) LF than late type objects, for which $\alpha \sim -0.8$. Thus, late type galaxies contribute most to the LF at low luminosities.

Marzke et al. (1994a) have derived the field LFs from the Center for Astrophysics (CfA) redshift survey. They find a good fit to a Schechter function with $M^*_Z = -18.8$ (where M^*_Z is a Zwicky magnitude from the Catalog of Galaxies and Clusters of Galaxies – Zwicky et al. 1961-1968) and $\alpha = -1$. As can be seen from Figure 1.2, there is an excess of faint galaxies with $-16 < M_Z < -13$, above the extrapolated Schechter function. Figure 1.3 shows the type-dependent LF in the CfA study (Marzke et al. 1994b). As we can see, early type galaxies follow Schechter LFs with $\alpha > -1$. Galaxies of type earlier than Sd and Im have a very steep LF, with $\alpha = -1.8$. Such objects are therefore the major contributors to the LF at low luminosities and provide the above mentioned excess over the extrapolated 'flat' Schechter LF at bright luminosities.

Da Costa et al. (1994) determine a LF, from southern hemisphere data, with $M^*_{B(0)} = -19.5$ and $\alpha \sim -1.2$. This is steeper than Marzke et al. (1994a) but no faint galaxy excess is detected. Again, blue galaxies contribute most

to to the LF at low luminosities. It is possible that the difference between Marzke et al. (1994a) and da Costa et al. (1994) comes about because of different statistical treatments. Another possibility is that the local overdensity of dwarf galaxies (due to the neighbouring Virgo cluster concentration) has not been properly subtracted in Marzke et al. (1994).

Lin et al. (1995) have derived a LF from observations of 19,000 galaxies in Gunn r, using CCD drift scans. A good fit is found to a Schechter LF with $M_r = -20.5$ and $\alpha = -0.7$ over $-23.5 < M_r < -17.5$. Early-type galaxies have a declining LFs, with $\alpha = -0.3$, whereas late type objects have flatter LFs with $\alpha = -0.9$. Thus, late type, blue galaxies are the major contributors to the faint end of the LF.

This last point is worthy of further discussion. In all field LFs produced so far, we find that the faint end of the LF is dominated by late-type, blue objects, which have steeper LFs than early-type galaxies. As we shall see, this is still flatter than the LF for the Virgo cluster, as measured by Sandage et al. (1985), but, if the dwarfs in the field follow a similar LF as in Virgo, an upturn of the field LF at faint absolute magnitudes cannot be ruled out; this would account for the result by Marzke et al. (1994).

If the trend for blue galaxies to contribute most of the objects at low luminosities continues even fainter, these galaxies may be excellent candidates for the population of blue, low surface brightness galaxies required by Koo et al. (1993). Recent observations, and morphological typing of faint field

galaxies by Driver et al. (1995a,b) appear to support the hypothesis of an upturn in the LF at low luminosities, which is perhaps as steep as $\alpha \sim -1.8$. This is of course in conflict with the absence of a population of nearby dwarfs in redshift surveys, although these may have been missed because of surface brightness selection effects.

It should be noted that faint field galaxies seem to be mostly HI rich, with LFs similar to that of irregulars in Virgo (Eder et al. 1989). Among galaxies in the Driver et al. sample, most appear to be late type spirals, but fainter galaxies seem to be *bona fide* dwarfs. Thus the 'flat' LF for the field at low luminosities reflects the 'flat' LF of irregulars (but see Marzke et al. 1994b).

The field LF has only been determined for galaxies which are generally brighter than $M_B \sim -16$. Below this luminosity, the smaller and smaller volumes surveyed, strong incompleteness in magnitude and redshift catalogs, and selection effects make it all but impossible to obtain reliable LFs. For very faint galaxies we are therefore forced to turn to clusters.

1.2.4 Clusters of Galaxies

Following the early work by Abell (1958, 1962, 1964, 1972) photographic surveys were carried out in most nearby clusters, although these only reached a few magnitudes below M^*. The main conclusion of these early studies was that the LF shape parameters are approximately universal, with $M_R^* \sim -21.4$ and $\alpha \sim -1.25$ (e.g., Oemler 1974, Dressler 1978; 1980; Lugger 1986).

There are of course variations in the shape of the LF from cluster to cluster, with dips and bumps being quite common. Some clusters are found to have unusually flat LFs (Dressler 1978). Recently, the LF for Coma (see below) has been shown to have a 'dip' at about 10% of L^* (Biviano et al. 1995a).

Another important result of these early surveys was the discovery of a morphology density relation (Oemler 1974; Dressler 1978; 1980; Giovanelli et al. 1986). Ellipticals, lenticulars and early-type galaxies prefer environments in which the galaxy density is high, and their relative frequency increases towards such environments. Spirals and late type objects are found in lower density environments, and their relative frequency decreases in high density environments, reaching zero in cluster cores. Giovanelli et al. (1986) show that galaxies of progressively later type are less and less confined to the main filament in the Perseus-Pisces supercluster. Sandage et al. (1985) show that dwarf ellipticals are strongly clustered toward cluster cores. It has been claimed that nucleated dwarfs are strongly concentrated toward the Virgo cluster core (e.g., discussion in Ferguson & Binggeli 1994). Evidence for a morphology density relation is now present even in the field (Postman & Geller 1984).

The morphology-density relation is evidence for mechanisms altering the morphological type of galaxies within each cluster. These may strip spirals of their gas via collisions (a favourite way of producing ellipticals, e.g., Zepf 1995), tidal interactions or ram stripping. Such objects could easily evolve

into lenticulars or ellipticals.

Whitmore et al. (1993) have instead argued that the observed run of elliptical or lenticular fractions is better fit as a function of clustercentric radius, and suggest that this is due to the formation history of galaxies. In other words, the position of a galaxy within a cluster determines its morphological type *at the epoch of its formation.* Environmental density would still *cause* morphological changes, by 'predetermining' the morphological type of galaxies forming in a specified region of space. It may be argued that the fit to a morphology-radius relation occurs because cluster density profiles follow a r^{-1} law (Hubble law). It is, however, difficult to understand how a morphology radius relation may explain the morphology-density relation around secondary density peaks in clusters or in the field (Postman & Geller 1984).

Recently, deep LFs have been derived in a number of nearby clusters. For very nearby objects, cluster members are 'betrayed' by their morphologies. This approach has been used in the pioneering studies of the LF of the Virgo cluster by Sandage and collaborators. Binggeli et al. (1985) observed the inner 6° of the Virgo cluster using high resolution plates taken at the DuPont 2.5m Telescope on Las Campanas. Cluster membership was established on the basis of morphological arguments, using a sample of dwarf galaxies for which distance information and surface photometry were available (Binggeli et al. 1984).

Sandage et al. (1985) find a good fit to a Schechter function with $M_B^* \sim$

-21.4 and $\alpha \sim -1.30$, which is somewhat steeper than the field LF. Sandage et al. (1985) also derive LFs for individual galaxy types. Their conclusions are shown in Figure 1.4 (from Binggeli et al. 1988). Early type galaxies and spirals follow Schechter or Gaussian luminosity distributions, and their contribution is minimal fainter than $M_B \sim -18$. At low luminosities, dwarf ellipticals dominate the LF. A similar result is found for the Fornax cluster (Ferguson & Sandage 1988).

More recently, studies of distant clusters have been carried out using statistical discrimination of cluster members. In these surveys cluster members are not identified, but an estimate of their number is made by comparing number counts in cluster fields with number counts in blank sky fields.

Coma has been analysed in this way by Bernstein et al. (1995) and Secker & Harris (1995). The R LF for this cluster is found to fit a power-law with $\alpha = -1.40$ at low luminosities. Dwarf galaxies in Coma are found to be confined to a relatively narrow color-magnitude sequence in a R vs. $B-R$ plot (Secker & Harris 1995). Dwarfs in Coma also seem to follow a blueing trend at large clustercentric distances, which is interpreted as evidence for a metal abundance gradient. As we shall see below this is interpreted as evidence for the Babul & Rees (1992) effect.

Kashikawa et al. (1995) have determined LFs for four clusters (Abell 1367, 1631, 1644 and 1656) using CCD mosaics on 1m class telescopes. They find it impossible to fit all faint end LFs with a single α. Dividing their sample

into early type and late type galaxies, Kashikawa et al. (1995) find that the variation is due mostly to blue galaxies. This is in contrast with Sandage et al. (1985) who argue that different dwarf elliptical LFs are responsible for variations in faint cluster LFs. Kashikawa et al. (1995) integrate a 'no evolution' LF to estimate the amount of background contamination, and this may underestimate the number of contaminants, which would be preferentially 'blue'.

Biviano et al. (1995a) have carried out an extensive redshift survey in the Coma cluster, which is now complete to $m_b \sim 17$. They find that the LF in Coma is not well represented by a Schechter function, but rather by a Gaussian plus an exponentially rising contribution at faint luminosities. Substructure in Coma seems to indicate that the main body of the cluster consists of faint galaxies, over which a population of giant ellipticals and S0's has been superposed after infall of groups resembling perhaps our Local Group or Hickson compact groups.

The LF for dwarfs to $R = 21$ in a more recent study of Coma (Lobo et al. 1996), seems to be very steep ($\alpha = -1.8$). Curiously, the LF flattens in the proximity of the two giant D galaxies NGC4874 and NGC4889, with $\alpha = -1.5$, which may imply that some dwarfs are being destroyed by interactions with the giants. A steep LF is also apparent, when a two component LF is fit to the data, in the distant clusters Abell 963 (Driver et al. 1994) and Shapley 8 (Metcalfe et al. 1994).

The above methods have been adopted here and in our previous work (De Propris et al. 1995), where we find an extremely steep LF ($\alpha \sim -2.2$) in the cores of four cD clusters (Abell 2052, 2107, 2199 and 2666). This may be a consequence of the extremely dense environment of these objects or may represent an universal feature of the LF at low luminosities. In this thesis, we survey cluster fields using mosaic CCD cameras, to understand how the LF and surface density of dwarfs varies with clustercentric distance.

The LF of clusters therefore appears to be generally steeper than in the field. In some cases, the LF may be considerably steeper. For these reasons, we started a program to determine the LF in clusters of galaxies and in different cluster environments. Eight clusters are studied in this thesis (more observations are forthcoming – see Discussion). The four clusters dealt with in Chapter 3 were observed using the High Resolution Camera (HRCAM – McClure et al. 1991) and only small fields in the proximity of the central cD galaxy were observed. The three clusters observed at CFHT were images using the new mosaic camera described in Chapter 2. Two fields were taken in each cluster. Finally, three large, lower resolution images of the Hercules cluster were taken at KPNO.

One of the aims of our project is to study environmental influences on dwarf galaxies. Before describing our methods we wish to review the theoretical and observational knowledge on the effects of environment on galaxies.

1.3 Environmental Effects

Dwarf galaxies, because of their low mass, may be expected to be strongly affected by their surroundings. The first indication that this may be so was provided by Einasto et al. (1974), who showed how dwarf irregular and other gas-rich objects generally avoid the immediate proximity of giant galaxies, whereas dwarf ellipticals prefer such environments. Einasto et al. (1974) attributed this behaviour to ram stripping from a gaseous corona surrounding our Galaxy, a conclusion which is still controversial. These observations of course suggest that interactions between giant galaxies and dwarfs may affect their star formation history (van den Bergh 1994).

Lin & Faber (1983) and Faber & Lin (1983) have proposed that dwarf ellipticals may evolve from dwarf irregulars that have lost their gas to interactions with neighbouring galaxies. This approach unfortunately conflicts with the different LFs for dwarf ellipticals and dwarf irregulars (Sandage et al. 1985) and the fact that most dwarf ellipticals have higher surface brightness than irregulars (Hunter & Gallagher 1985) and are generally rounder (Binggeli 1986). The presence of nuclei in many bright dwarf ellipticals is also a contrary argument (Caldwell 1985). It is therefore unlikely that a 'simple' conversion of dwarf irregulars into dwarf ellipticals may explain the observed characteristics of dwarf galaxies.

Silk et al. (1987) have instead proposed that dwarf ellipticals may accrete gas from the intracluster medium and 'convert' into dwarf irregulars. This

approach may conflict with the observed trend for dwarf irregulars to avoid higher density regions.

The evolution of dwarf galaxies may of course depend on their environment. Davies & Phillips (1988) have proposed that star formation may occur in 'knots' and that these may then evolve to resemble nuclei. An appropriate analogy appears to be the class of amorphous dwarf galaxies, of which one well studied example is NGC1705 (Meurer et al. 1992; Marlowe et al. 1995; other nearby specimens include NGC3077 and NGC5253). In these objects star formation occurs in 'knots', and is followed by a rearrangement or expulsion of the interstellar medium, after the gas is heated by supernova explosions or strong stellar winds. This process may well alter the shape of the resulting galaxy, and therefore explain the differences between dwarf ellipticals and dwarf irregulars.

A very detailed scheme for dwarf galaxy evolution has been proposed by Babul & Rees (1992). In this scenario, star formation in dwarf galaxies is delayed in the early universe, because the interstellar medium in these objects is heated by the ultraviolet (UV) background from active galactic nuclei (AGN) and from primeval galaxies. At $z < 1$ this background is diluted because of the expansion of the universe and the LF of AGN's declines very rapidly, plus galaxy formation is ceasing at approximately this epoch. Star formation may then begin in dwarf galaxies. This is likely to occur violently, probably around 'knots' as in amorphous dwarfs. A large input of energy

from supernova explosions and from strong stellar winds from young, hot stars will accelerate the interstellar medium to beyond the escape velocity. This process may stop further star formation in dwarf galaxies, which would then fade as their stellar populations age. Loss of a significant fraction of a dwarf's mass may also disrupt the galaxy, or, if the mass lost was less than 50% of the original total, the galaxy will relax and expand, evolving to low surface brightness. Thus, dwarfs would fade and disappear from the sample.

In clusters of galaxies, it is possible that pressure from the surrounding intracluster medium (ICM) would confine the expanding gas to the dwarfs, which would eventually be able to reaccrete it and therefore to undergo further episodes of star formation. These objects would *not* fade away because of reduced surface brightness and aging of their old stellar populations. Indeed, the presence of central surface brightness excesses (nuclei, see below) may aid in the detection of these dwarfs.

The Babul & Rees (1992) mechanism (hereafter BR) would have the following consequences: the LF may be expected to steepen in higher density regions, as more faint dwarfs survive their epochs of star formation. A metal abundance gradient may result, as dwarfs are better able to retain their enriched gas. Finally, a greater incidence of central nucleation should be present in cluster cores, as star formation is likely to have started first in central 'knots'.

The tendency for the LF to become steeper in clusters, and possibly the

very steep LF claimed by De Propris et al. (1995), may be evidence for the existence of the BR effect. Secker & Harris (1995) claim that a metal abundance gradient is evident in Coma, but more investigations are needed (for reasons explained below). Finally, it has been claimed that nucleated dwarfs (in the Virgo cluster) are more concentrated towards M87. These points are evidence for a BR effect, but may be explained otherwise. It is thus important to obtain more information on the nature of faint galaxies.

1.4 The Project

From the preceding discussion we see that it would be of great interest to (i) determine LFs to low luminosities, in order to better define the LF for intrinsically faint galaxies; (ii) verify how LFs vary with environment from cluster to cluster and within each cluster as well; (iii) obtain color information, to ascertain the nature and stellar populations of these galaxies, and (iv) explore the clustering properties of dwarf galaxies in the neighbourhood of bright giants.

This is only practical in clusters of galaxies, for the following reasons:

1. The galaxy density in clusters of galaxies is high enough that the problem of foreground and background contamination may be dealt with statistically, by using surveys in the literature or observations of blank (i.e., clusterless) sky fields.

2. The fact that the nearest rich clusters are somewhat more distant than Virgo or Fornax (by about a factor of 5) is actually an advantage for dwarf galaxy completeness, as the detectability of a given dwarf increases as its apparent radius decreases (i.e., as its distance increases) because of the scale dependence of flatfield noise.

3. The ratio of the number of cluster members to the number of background contaminants is approximately constant for non-cosmological distances, but, since fainter galaxies contribute to contamination for distant clusters, and since the amplitude of the correlation function is smaller for fainter objects, fluctuations in the background counts are smaller for fields in distant clusters, which allows us to recover the cluster LF with greater confidence.

4. Since all cluster members lie at the same distance from us, all galaxies will be subject to the same selection effects. By using blank sky fields to estimate background contamination, we also subject our background fields to the same selection effects as applied to the cluster fields, so that the problem of differential biases is minimised.

5. Clusters allow us to select environments in a variety of evolutionary stages, with different galaxy and gas densities and practically any other feature which we wish to explore.

Eight clusters are observed for this thesis. For four of them we use deep

images taken with the High Resolution Camera (HRCAM – McClure et al. 1991) to survey the inner 2′. These are described in Chapter 3. Four other clusters were observed at the Canada-France-Hawaii Telescope (CFHT) and at the Kitt Peak National Observatory (KPNO). For these objects we imaged one field centred on the brightest cluster galaxy and another on a bright galaxy outside of the cluster core. At KPNO we imaged three very large fields at various positions within the Hercules cluster, which has, in any case, a very complicated structure (consisting of two major lumps, with a filamentary appearance). This procedure allows us to obtain information on the variation of the LF with environment within each cluster. These observations are discussed in Chapters 5-8.

Clusters are selected from the Abell catalog (Abell et al. 1989) among those with $z < 0.05$. Clusters are then chosen according to their X-ray properties, as classified by Jones & Forman (1984). In this scheme clusters are classified as XD (X-ray dominated) or nXD (non X-ray dominated) according to the presence of an optically first ranked galaxy at the centre of their X-ray emission. This is found to correlate with the size of the X-ray core radius, as computed by fitting an isothermal profile to the X-ray distribution; XD clusters have small (< 300 kpc) core radii whereas nXD objects have large ones. Jones & Forman (1984) also classify clusters as 'early' and 'late' according to their X-ray luminosity. Early objects have low X-ray luminosities ($L_X \approx 10^{43}$ ergs/s), whereas late clusters have high luminosities ($L_X \gtrsim 10^{44}$ ergs/s). This is in turn found to correlate with cluster populations. Early

clusters tend to be dominated by spirals whereas late clusters are rich in ellipticals and lenticulars. A simplified table of the Jones & Forman (1984) classification may be found in Table 1.2.

For example, Abell 1367 and Hercules are examples of early nXD clusters, with 'low' X-ray luminosities, large core radii and spiral-rich populations. Both clusters seem to be in an early stage of their collapse and have numerous interacting galaxies (e.g., Oemler 1974). Abell 262 and Virgo are early XD clusters, in which the presence of an optically bright galaxy at the centre of X-ray emission (i.e., at the bottom of the cluster potential well) is evidence for some dynamical evolution. Coma is an example of a late nXD cluster, whose core is dominated by two giant ellipticals. There is indeed evidence that considerable substructure is present in Coma (Biviano et al. 1995a,b), which is a sign of relative dynamical youth, despite earlier claims that Coma is an example of virialized system (e.g., Dressler 1984). Finally, Abell 426 and Abell 2199 are excellent examples of late XD clusters. In Abell 426 there is evidence for a cooling flow centred on the peculiar elliptical NGC1275.

As we can see, our observational plan spans a large range of cluster environments, from the very dense cores of cD clusters to rarefied environments on the outskirts of clusters. In addition, we observe some background fields to gain a handle on the amount of background contamination. Procedures for photometry and data reduction are described in the next chapter.

Table 1.2: THE JONES & FORMAN (1984) SCHEME

	nXD	XD
Early	Large Core Radius (400-800 kpc)	Small Core Radius
		Central Dominant Galaxy
	Low X-ray Luminosity ($L_X < 10^{44}$ ergs/s)	Low X-Ray Luminosity
	Cool X-ray gas (1–4 KeV)	Cool X-ray gas
	No Central Cooling Flow	Central Cooling Flow
	X-ray emission around galaxies	X-ray emission from central galaxy
	High spiral fraction (40%+)	High spiral fraction
	Low central galaxy density	Low central galaxy density
	Irregular cluster structure	Irregular cluster structure
	Example: A1367	Virgo
Late	Large Core Radius	Small Core Radius
	High X-ray Luminosity ($> 10^{44}$ ergs/s)	High X-ray Luminosity
	Hot X-ray gas (> 6 KeV)	Hot X-ray gas
	No central cooling flow	Central cooling flow
	High velocity dispersion	High velocity dispersion
	Low spiral fraction ($< 20\%$)	Low spiral fraction
	High central galaxy density	High central galaxy density
	Regular cluster structure	
	Example: Coma	Perseus

Chapter 2

Observations and Data Reduction

2.1 Introduction

In this thesis we describe observations of eight clusters of galaxies analysed between 1994 and 1995. The four clusters we treat in Chapter 3 were observed during a program to detect globular clusters in the proximity of giant elliptical galaxies in cluster centres. Of these considered here, Abell 2199 was observed using FOCAM and an RCA 640 $\times$ 1024 CCD chip in the B band by Pritchet & Harris (1990). Preprocessing and initial reductions for these images were carried out by the now standard methods of overscan subtraction, trimming, debiasing and flatfielding, followed by a median operation on all frames. These procedures are better described below and in the original reference by Pritchet & Harris (1990).

Abell 2052, 2107 and 2666 were observed at CFHT using the HRCAM

and a SAIC 1024 × 1024 CCD in the I band by Harris et al. (1995). Again, standard procedures were used to reduce these data, as detailed above.

Hercules (A2151) was observed in the R band at KPNO, using the Mayall 4.2m Telescope and a Tek2 2048 × 2048 chip, during an unrelated program by Ciardullo, Pritchet and Shafter to observe novae in nearby galaxies. Details are given in Chapter 8.

Table 2.1 shows the basic data for the observed clusters and the associated background fields. Column 1 identifies the observed field, column 2 gives the classification by Jones & Forman (1984), column 3 the Bautz-Morgan type, column 4 the redshift and column 5 the distance modulus.

The bulk of this thesis deals with observations in Hercules and in three more clusters (Abell 262, 426, 539) observed at the CFHT by De Propris & Pritchet. The initial reduction and preprocessing of these data is dealt with in detail below.

2.2 1994 CFHT Observations and Data Reduction

Observing time for this project was awarded during the nights of December 03-06, 1994. We observed at the prime focus of the CFHT, using a mosaic CCD camera (MOCAM - Cuillandre et al. 1995), equipped with four thick Loral 2048 × 2048 chips. This configuration yields a field of view of $14' \times 14'$, with a pixel scale of $0''.21$ per pixel. Weather was photometric for two nights,

with the third night being lost to clouds. Seeing was below average (0".8) or mediocre. A drawing of the camera on the sky may be seen in Figure 2.1. Note that this approach is similar to the one adopted by Kashikawa et al. (1995), except that we trade field size for survey depth and resolution by observing at the prime focus of a 4m telescope.

In the version of MOCAM used during our run, engineering grade chips were used. Their cosmetic quality was, overall, very good, but one of the chips was affected by a very large defect, which forced us to discard data imaged with this chip. Other minor defects slightly reduced the total area observed by the camera and this was corrected for as described below.

One problem we encountered was that the threshold for saturation was very low and heavily saturated stars have a tendency to 'streak', i.e., to bleed uncontrollably along the region perpendicular to readout (bleeding is well confined to a few columns in the direction of readout). Some areas of the chips were thus contaminated and we had to eliminate these areas, with an appropriate correction as outlined below.

Another problem consisted in the long readout time. The exposure time of 1200s was essentially the same as readout time and this severely limited our efficiency.

We carried out some tests on the camera to determine its characteristics and as an aid for further engineering on the device. Using bad columns and 'streaking' stars we checked that no crosstalk was present among the chips.

We also obtained exposures of the 'dipper' asterism in M67 for calibration purposes in the northernmost chips and shifted the images into coincidence to verify the horizontal alignment between the chips. We find that the chips in the mosaic are aligned to within $0''.05$.

We imaged two fields in three different clusters and a number of background fields, in two colors (V and I). Two frames were taken for each field, for a total exposure time of 1200s in each color (see Table 4.1 for more information). Reduction of these data was carried out in the following way:

1. We split the CCD mosaic into each of the component 2048^2 chips and transposed all of the overscan strips to a single location (in the frame of reference of each chip) to facilitate automatic preprocessing.

2. We computed an average 'pedestal level' (the level added to all exposures prior to readout) from the overscan strips and subtracted this level from each image.

3. We then trimmed the chips of their overscan strips.

4. We subtracted the median of 32 bias frames from each image. These were kindly provided by Mellier & Cuillandre (1995, private communication), out of their testing data.

5. We produced flatfields from the average of three V and I dome flats. It was impossible to obtain a suitable set of twilight sky flats, because of the very long readout time. Sky flats are not suitable either, since

many bright stars are present in the large field of view of MOCAM. Combining our images is not suitable either, since many bright galaxies are also present.

6. We divided each image by the appropriate flatfield.

7. We averaged all images for each field, to eliminate cosmic ray contamination and to improve our signal to noise ratio.

Note that a very similar procedure was carried out for both the HRCAM and the KPNO data, with the obvious differences that no mosaic splitting was necessary, and flatfielding was carried out by using twilight sky flats or the median of all images in each color (superflat).

These completely reduced images were then analyzed as described below.

2.3 Finding and Photometry

As can be seen in the images of the field presented in the sections dealing with each cluster, many bright galaxies are present in each frame. Our first priority is to delete these objects, to reveal faint galaxies covered by light from the giants and remove light gradients across the frame. In order to do so we computed isophotes for these galaxies using the IRAF STSDAS program ELLIPSE. These isophotes were then used to produce a smoothed model of these galaxies, using the task BMODEL (e.g., Jedrzejewski 1987). These models were then subtracted from each image to eliminate the bright

galaxies. Examples of this procedure (and its results) may be found in the discussion for each cluster.

Our next step was to find all objects in our frame and carry out simulations to correct for inefficiencies in our algorithm. We first convolved the image with a lowered Gaussian, whose Full Width at Half Maximum (FWHM) was approximately equivalent to the image seeing and with a kernel about 4×FWHM. This is found to be the best set of parameters, for our finding program, to find low surface brightness objects, while minimizing computer time requirements.

We then found all objects which, in the convolved images, are above a 1σ threshold from the mean sky level. This is equivalent to a 4σ detection in the original image. The found objects were then examined interactively on an image display and we eliminate detections along the frame edge, on cosmic ray residuals and multiple hits on extended objects or saturation spikes. We also eliminated objects affected by 'streaking' stars.

We compute Kron (1980) image parameters for all remaining objects. In the first place, we eliminated all objects for which r_1 is less or equal than zero as spurious. We then carried out photometry for all remaining objects in $2r_1$ apertures. Here r_1 is defined as:

$$r_1 = \int_1^\infty x g(x) dx / \int_1^\infty g(x) dx$$

where $g(x)$ is the radial light distribution. Thus r_1 may be interpreted as the weighted moment of an image and coincides with its half-light radius (Kron

1980).

We computed completeness corrections for our data by introducing artificial stars and 'galaxies' (stars with 'seeing' of 1.5 FWHM) in our frames and repeating our procedure for finding and photometry. This is also used to identify a stellar sequence for star-galaxy separation.

For very bright objects, we computed isophotes as above and carried out photometry in elliptical apertures to a large enough isophote to enclose all of the galaxy light, using the tasks NOAO POLYPHOT.

Finally, we aligned images in V and I and carried out photometry for all objects (except bright galaxies, for which see above) in $3\times$ FWHM apertures. This procedure is preferable to using $2r_1$ apertures for all objects, since it is possible that the apertures used correspond to different isophotal levels.

The photometry lists produced were then calibrated using images of standard stars and photometry by Christian et al. (1985) and Montgomery et al. (1993). Extinction was corrected for using the reddening maps by Burstein & Heiles (1982) and converting from $E(B-V)$ to $E(V-I)$ and to A_V or A_I using tables by Johnson (1965).

Star-galaxy separation was then carried out, using the r_{-2} parameter, as explained in Chapter 4. Where this method is impossible or impractical, because of bad seeing or at faint magnitudes, we use galaxy star count models by Bahcall & Soneira (1980; 1981) and Pritchet (1983) to statistically distinguish stars and galaxies.

We then binned these data in 0.5 magnitude bins, produced number counts as a function of magnitude and carried out corrections for field size and for completeness. We thus obtain numbers of objects as a function of magnitude in each field.

In order to derive a LF we first used the images of the background fields (or literature surveys) to obtain an estimate of the number of background galaxies present in each field. This is detailed in Chapter 3. We subtract our estimates of contamination from each field and are left with an estimate of the number of cluster members as a function of magnitude. We then fit these data to a power-law to recover α, using a non-linear weighted least squares algorithm and maximum likelihood methods to fit to a power-law. Results of this procedure for each cluster and each field studied are presented in Chapters 5-8.

We also determined colors for all galaxies present in the field and analyze their color distribution. We also analyze the radial distributions of galaxies in each color and the radial distributions of $V-I$ color. Finally, we compare fields taken within the cluster core and outside of it and different regions in each field.

As an example of this procedure reference may be made to De Propris et al. (1995) in which our determination of the LF slope of the inner regions of four cD clusters was reported.

Table 2.1: BASIC CLUSTER DATA

ID	JF Type[1]	BM Type	Redshift[2]	$m - M$
A262	E XD	III	0.0167	34.12
Bkgd A262	—	—	—	—
A426	L XD	II-III	0.0183	34.32
Bkgd A426	—	—	—	—
A539	N/A[1]	II	0.027	35.17
A2052	N/A	I-II	0.035	35.73
Bkgd A2052	—	—	—	—
A2107	E XD	I	0.042	36.13
A2151	E nXD	III	0.036	35.79
A2199	L XD	I	0.031	35.47
A2666	N/A	I	0.026	35.12

[1] N/A: Not classified by Jones & Forman (1984).
[2] Data from Abell et al. (1989)

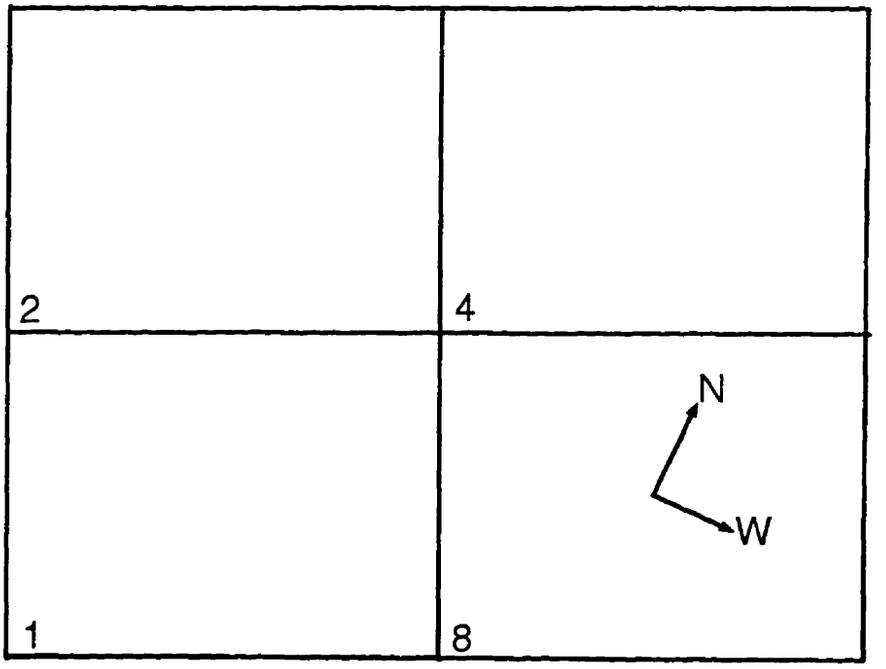

Figure 2.1: Schematic representation of the MOCAM camera

Chapter 3

The LF of Four cD Clusters

We have used data from previous CFHT runs to determine the LF for four cD clusters (Abell 2052, 2107, 2199 and 2666). Abell 2199 was observed in the B band with FOCAM and a RCA 640×1024 CCD. Abell 2052, 2107 and 2666 were observed in the I band using HRCAM. These data were originally used to search for globular clusters in the field of the giant ellipticals lying at the centre of each cluster by Pritchet & Harris (1990) and Harris et al. (1995).

The sample consisted of four cluster fields and one background I band field. Table 3.1 shows the field identification, redshift, exposure time, field size and seeing. The field size variation is due to the fact that we eliminated the region within the original image where the light intensity from the central galaxy was equal or greater than the sky level, and to our correction for vignetting by HRCAM optics.

Data were analyzed in the same way as described above. Number counts

were cut at one magnitude brighther than the brightest globular cluster identified in these objects by Pritchet & Harris (1990) and Harris et al. (1995). Numbers of background stars were computed from galaxy star count models (Bahcall & Soneira 1980; 1981; Pritchet 1983). Numbers of background galaxies were computed from literature surveys, i.e., the B counts by Tyson (1988), Lilly et al. (1991) and Metcalfe et al. (1991) and the I counts by Tyson (1988) and Lilly et al. (1991). Tables 3.2 and 3.3 show the number of objects in each frame, numbers of stars, contaminating galaxies and estimated number of cluster members.

We fit the B band data for Abell 2199 and the sum of all I band data for Abell 2052, 2107, 2666 (the total area surveyed by HRCAM is only 3-4 arcmin^2) with a power-law, to recover the slope α, using a maximum likelihood technique and fitting the data to an equation of the form:

$$N_{obs}(m) = f(m)[s(m) + g(m) + K\,10^{0.4m(\alpha+1)}] \qquad (3.1)$$

where $s(m)$ and $g(m)$ are the assumed contributions of stars and galaxies, $f(m)$ is the known incompleteness fraction and K and α are determined by the program. We plot the data, the best fit and a 'Virgo-like' LF with arbitrary normalization in Figures 3.1 and 3.2. The best fit to the B data is given by a LF with $\alpha = 2.16 \pm 0.18$ and, for the I band data (A2052 + A2107 + A2666), with $\alpha = -2.28 \pm 0.30$. We find nearly identical results with non-linear least squares, but, in this case, maximum likelihood methods are to be preferred, given the small number of objects.

Table 3.1: BASIC DATA FOR cD CLUSTERS

Field	Redshift[a]	Exposure Time	Field Size[b]	FWHM
			[arcmin^2]	
A2052	0.035	12 × 1000s	3.53	0″.8
A2107	0.042	12 × 1000s	3.68	0″.8
A2199	0.031	6 × 1800s	6.54	1″.0
A2666	0.026	6 × 1000s	3.13	0″.8
A2052bkg	—	9 × 1000s	4.42	0″.8

[a] From Abell, Corwin, and Olowin (1989). [b] Solid angle coverage after removing (i) vignetted areas due to HRCam optics, and (ii) areas near the center of the cD galaxy with I(galaxy) > I(sky).

Table 3.2: NUMBER COUNTS FOR A2052, A2107 AND A2666 IN I

A2052

I	M_I	N_{raw}	N_{corr}	N_{bkgd}	$N_{cluster}$
19.98	−15.75	5 ± 2.24	5 ± 2.24	3.15 ± 1.77	1.85 ± 2.85
20.48	−15.25	5 ± 2.24	5 ± 2.24	4.17 ± 2.04	0.83 ± 3.03
20.98	−14.75	10 ± 3.16	10 ± 3.16	5.58±2.36	4.42 ± 3.94
21.48	−14.25	8 ± 2.83	8 ± 2.83	7.61 ± 2.76	0.39 ± 3.95
21.98	−13.75	16 ± 4	16 ± 4	10.57 ± 3.25	5.43 ± 5.15
22.48	−13.25	37 ± 6.08	39.36 ± 6.47	14.89 ± 3.86	24.47 ± 7.5

A2107

I	M_I	N_{raw}	N_{corr}	N_{bkgd}	$N_{cluster}$
20.38	−15.75	6 ± 2.45	6 ± 2.45	3.78 ± 1.94	2.22 ± 3.13
20.88	−15.25	4 ± 2	4 ± 2	5.11 ± 2.26	−1.11 ± 3.02
21.38	−14.75	10 ±3.16	10±3.16	7.05±2.66	2.95 ± 4.13
22.38	−13.75	28 ± 5.29	29.79 ± 5.63	14.02 ± 3.74	15.77 ± 5.76
22.88	−13.25	28 ± 5.29	34.15 ± 6.45	20.10 ± 4.48	14.05 ± 7.05

A2666

I	M_I	N_{raw}	N_{corr}	N_{bkgd}	$N_{cluster}$
19.34	−15.75	0	0	1.68 ± 1.30	−1.68 ± 1.30
19.84	−15.25	4 ± 2	4 ± 2	2.24 ± 1.50	1.76 ± 2.50
20.34	−14.75	6 ± 2.45	6 ± 2.45	3.03 ± 1.74	2.97 ± 3.00
20.84	−14.25	6 ± 2.45	6 ± 2.45	4.16 ± 2.04	1.84 ± 3.19
21.34	−13.75	12 ± 3.46	12 ± 3.46	5.78 ± 2.40	6.22 ± 4.21
21.84	−13.25	9 ± 3	9 ± 3	8.07 ± 2.84	0.93 ± 4.13

Table 3.3: NUMBER COUNTS FOR A2199 IN B

B	M_B	N_{raw}	N_{corr}	N_{bkgd}	$N_{cluster}$
20.21	−15.25	1 ± 1	1 ± 1	1.07 ± 1.03	−0.07 ± 1.44
20.71	−14.75	2 ± 1.41	2 ± 1.41	1.43 ± 1.20	0.57 ± 1.85
21.21	−14.25	3 ± 1.73	3 ± 1.73	1.91 ± 1.38	1.09 ± 2.22
21.71	−13.75	2 ± 1.41	2 ± 1.41	2.63 ± 1.62	−0.63 ± 2.15
22.21	−13.25	6 ± 2.45	6 ± 2.45	3.77 ± 1.94	2.23 ± 3.13
22.71	−12.75	13 ± 3.61	13 ± 3.61	5.57 ± 2.36	7.43 ± 4.31
23.21	−12.25	17 ± 4.12	17.89 ± 4.34	8.56 ± 2.93	9.33 ± 5.24
23.71	−11.75	36 ± 6	39.56 ± 6.59	13.50 ± 3.67	26.06 ± 7.54
24.21	−11.25	30 ± 5.48	34.48 ± 6.30	21.66 ± 4.65	12.82 ± 7.83
24.71	−10.75	58 ± 7.62	82.86 ± 10.88	35.36 ± 5.95	47.50± 12.40

Figure 3.1: Plot of number of objects vs. absolute B magnitude for the A2199 data. Panel (a) shows raw numbers of objects (before subtraction of background and foreground contaminants), whereas panel (b) shows the result after subtraction of contaminants. The *solid squares* with error bars represent the data. The *solid line* represnts our best maximum likelihood fit to the data ($\alpha \simeq -2.2$). The *dotted line* in panel (a) shows the extimated background (see text for details). The *dashed line* shows an $\alpha = -1.3$ ("Virgo-like") LF normalized to pass through the data at the bright end. This illustrates the discrepancy between our data and a "flat" LF.

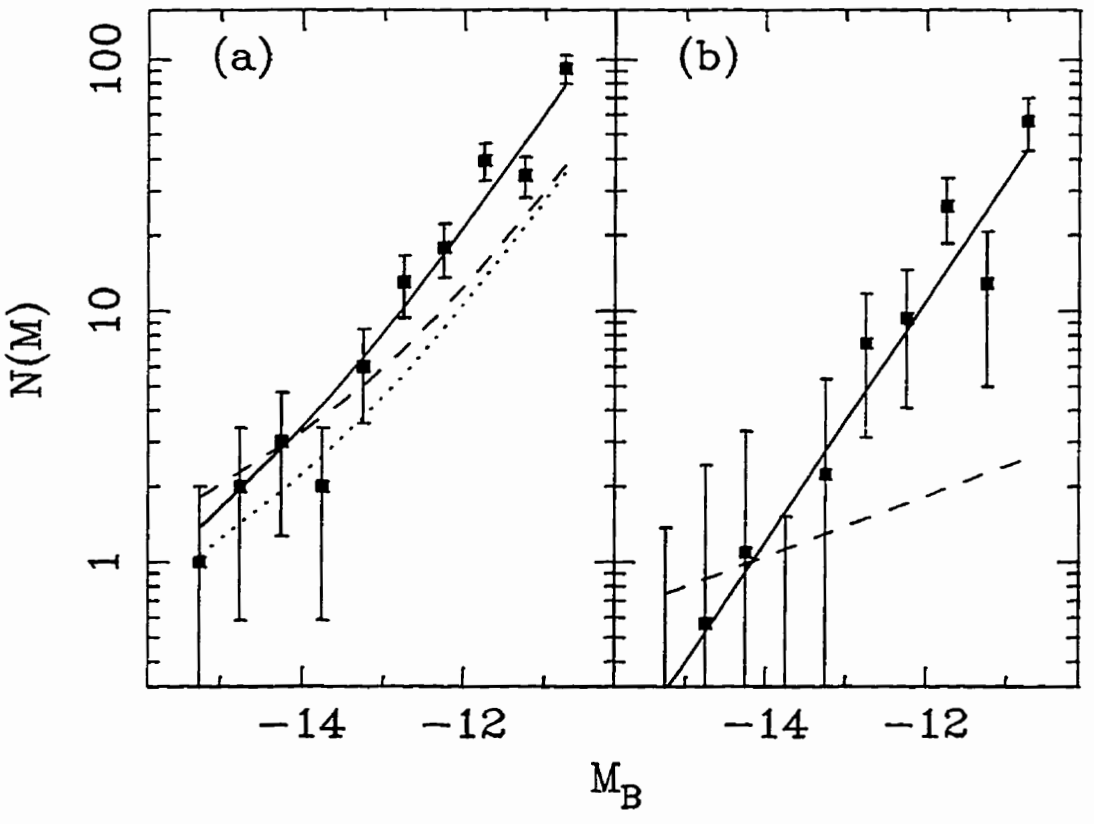

Figure 3.2: As for Figure 3.1, but for the combined I band data

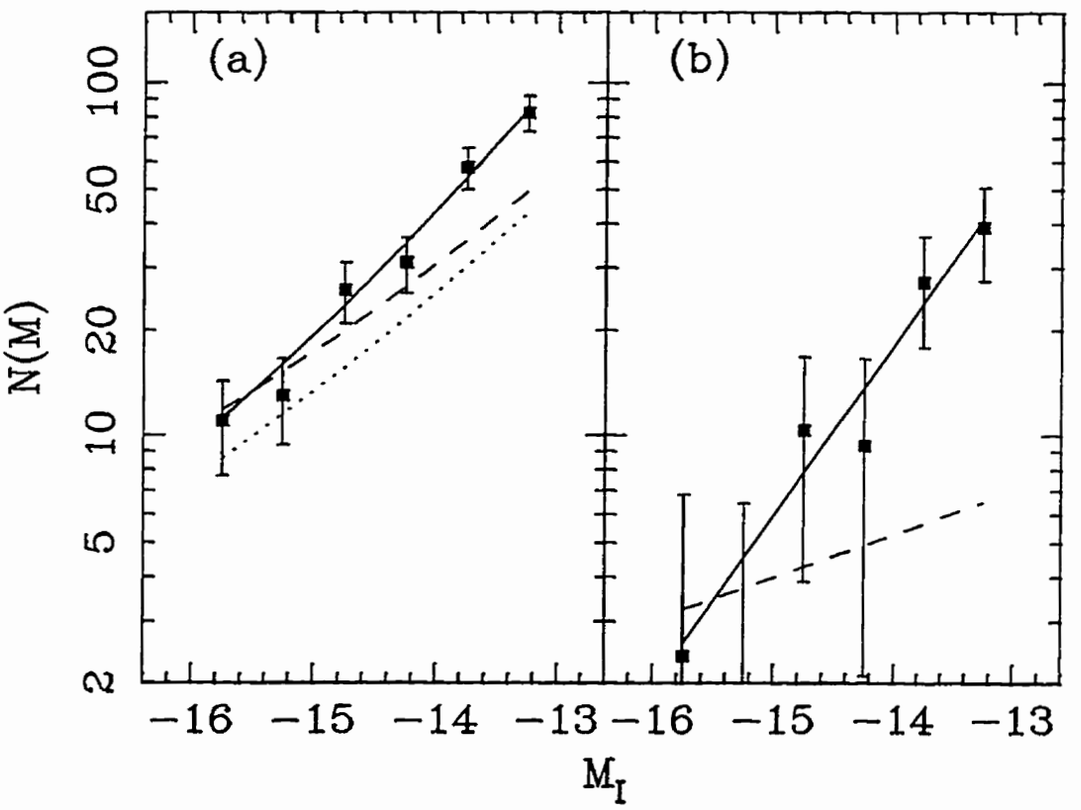

The errors quoted are 1σ errors. Values of α shallower than -1.5 can be ruled out to the 99% level; values shallower than -1.7 can be ruled out at the 99% (97%) level for the B (I) band data. These results are insensitive to the range of data using in the fit or to whether these data are completeness corrected or not.

The slope of the background counts is, within errors, similar to the slope of the LF in our clusters, and this raises the possibility that an incorrect subtraction of background galaxies is responsible for our result. If we lower the number of contaminants, we increase the robustness of our result that $\alpha \sim -2$. The effect of raising the number of contaminants is determined as follows. The field-to-field variance in number counts may be calculated from the angular correlation function of faint galaxies (Peebles 1975; 1980). Taking faint galaxy correlation amplitudes from Pritchet & Infante (1992b) and field sizes from Table 3.1 we find that the probability that the background counts exceed the expected values by more than 1.4 is $< 1\%$. Raising the number of contaminants by 40% still produces $\alpha < -1.5$ at the $> 99.5\%$ level in the B data and $\alpha < -1.3$ at the $> 90\%$ level.

To verify the robustness of this result we have also carried out some Monte Carlo simulations using the maximum likelihood estimator. The procedure for each simulation was as follows:

1. A total of n_c cluster galaxies was chosen from a LF with $\alpha = -2$. Here n_c is drawn from a Gaussian distribution with mean N_c^0 and disper-

sion $(N_c^0)^{1/2}$, where N_c^0 is the number of galaxies after completeness corrections (sum of columns 6 in Tables 3.2 and 3.3).

2. A total of n_g background objects were drawn from a LF as described above. The number of objects is drawn from a Gaussian distribution with mean N_g^0 and dispersion $2(N_g^0)^{1/2}$, where N_g^0 is the completeness-corrected number of contaminants (sum of columns 5 in Tables 3.2, 3.3, 3.4 and 3.5). The extra factor of 2 in the dispersion allows for the effects of clustering (see previous discussion and Table 5 of Metcalfe et al. 1991).

3. Some of the objects in each bin were discarded to allow for the completeness fraction.

4. Maximum likelihood methods were applied to fit the data to equation 3.1.

The mean result of thousands of simulations of this kind is that the input α is recovered to very high accuracy, with errors as quoted earlier. We find $> 99.5\%$ (98%) confidence that the LF for faint galaxies in these rich clusters is steeper than -1.5. This result includes the effect of stochastic variations in the background due to both Poisson fluctuations and galaxy clustering.

We have considered a number of effects that may affect our LF determination. Photometric errors at faint magnitudes may be responsible for an artificial steepening of the LF (Eddington 1940; Scott 1957), but this is un-

likely, as the frame limits are about 3 magnitudes fainter than the faintest galaxy considered here (these data reached to $B > 26$ and $I > 24.5$).

All objects used in the present study have been confirmed optically and we therefore rule out the possibility that spurious detections contribute to our data. We may note that these objects are slightly resolved and somewhat elongated, and their average linear diameter is 1 to 1.2 kpc, which is similar to those of Local Group dwarfs (e.g., Lin & Faber 1983).

We cannot rule out the presence of a population of young globulars or 'double clusters' (van den Bergh 1995, private communication). Young globulars are, on the other hand only encountered in the vicinity of recent merger remnants (e.g., NGC7252 – Holtzman et al. 1992; NGC1275 – Whitmore et al. 1993) and none of our central galaxies shows signs of a recent merger.

Our data therefore suggest that an excess population of faint galaxies above the extrapolated Virgo cluster LF exists in these clusters. This may not be a general characteristics of the LF at low luminosities, but due to the very special environment of cluster cores. On the other hand, there have been indications that the LF inflects upward at low luminosities (e.g., Marzke et al. 1994a) and our result may be explained by an upward inflection of the LF for dwarf spheroidal galaxies. This dichotomy may only be solved by carrying out further observations, as described in § 1.4.

We have therefore carried out observations of four clusters at CFHT and KPNO. These are described in the following chapters.

Chapter 4

Background Counts

4.1 Introduction

One crucial step in studies such as those presented here is removal of contaminating stars and galaxies from the sample. In order to do so we image a number of background fields (see Table 4.1), chosen to lie at major grid intersections of the POSS plates in the neighbourhood of the observed cluster, but farther than 1° from the cluster centre and void of other Abell or Zwicky clusters. Photometry from the literature (mainly Tyson 1988; Lilly et al. 1991; Metcalfe et al. 1991 and Pritchet & Infante 1992a) is used to constrain the number of contaminating objects in each field. Table 4.1 identifies the fields, gives their equatorial and galactic coordinates for epoch 1950.0, and the exposure times in V and I, seeing, extinction and field size correction (see § 2.2) adopted. Extinction in these fields was corrected as in § 2.3. The corrected field size for all images is 147 square arcminutes before correcting for saturated stars

Table 4.1: SUMMARY OF OBSERVATIONS

(1)	(2)	(3)	(4)	(7)	(8)	(9)	(10)
		(5)	(6)				
NGC 708	V	01 49 50.0	35 54 21	1200	0.18	1.6	137.13
		136.57	-25.09				
UGC1308	V	01 47 55.1	36 01 42	1200	0.18	1.2	134.74
	I	136.12	-25.07	1200	0.13	0.8	128.20
A262 Bckgd	V	01 55 00	35 00 00	1200	0.18	1.3	140.94
	I	137.96	-25.68	1200	0.13	1.0	134.86
NGC1275	V	03 16 29.6	41 19 52	1200	0.54	1.0	138.94
	I	150.58	-13.26	1200	0.40	1.1	134.04
NGC 1265	V	03 14 56.9	41 40 32	1200	0.54	0.9	134.49
	I	150.13	-13.13	1200	0.40	0.9	130.86
A426 Bckgd	V	03 20 00	43 00 00	1200	0.90	0.9	139.87
		150.19	-11.51				
UGC3274	V	05 13 55.0	06 22 46	1200	0.36	0.8	142.58
	I	195.72	-17.72	1200	0.20	0.9	123.88
A2151 NE	R	16 03 31	17 59 59	300	0.00	1.5	268.43
		31.80	44.45				
A2151 NW	R	16 02 32	17 59 59	300	0.00	1.5	268.43
		31.68	44.67				
A2151 SE	R	16 03 31	17 45 59	300	0.00	1.5	268.43
		31.50	44.36				

(1) Field ID (2) Filter (3) RA (1950) (4) Dec (1950) (5) l (6) b (7) Exposure time (seconds) (8) Reddening (9) Seeing (arcseconds) and (10) Field size (square arcminutes). The difference in field sizes is due to 'streaks' from bright saturated stars and areas within each field where the residual photon noise from the central galaxy was too high, i.e. where I(galaxy) $\geq$ I(sky).

4.2 V Background Counts

Large numbers of stars are present in these fields, which lie at low galactic latitudes, as shown in Table 4.1 above. This stresses the importance of star removal in this work.

In order to do so we use the r_{-2} parameter (e.g., Kron 1980). This is a measure of central concentration of light from an object:

$$(1/r_{-2}) = \int_1^\infty g(x)/x^2 dx / \int_1^\infty g(x) dx$$

whereas stars are the most centrally concentrated objects of all and have a single value of r_{-2}, as this is set by the seeing. We plot r_{-2} vs. V in Figure 4.1. As we can see, brighter than $V \sim 21$ (dereddened) a clear stellar sequence is identifiable. Fainter, we can use our simulations (§ 2.2) to compute the r_{-2} for stars (and its standard deviation $\sigma_{r_{-2}}$) as a function of magnitude and use these estimates to carry out star-galaxy separation to $V \sim 22.5$, where noise makes it impossible to safely separate stars and galaxies, which are dominated by the seeing profile. For this field we find that for stars with FHWM $\sim 1''.6$ $r_{-2} = 2.20 \pm 0.16$ at $V = 21.15$, $r_{-2} = 2.12 \pm 0.21$ at $V = 22.65$ $r_{-2} = 2.09 \pm 0.26$ at $V = 23.15$. The slight decrease in r_{-2} is due to the smaller number of pixels sampled for fainter stars (since this parameter is basically a size estimator for objects). Based on these simulations we choose $r_{-2} = 2.54$ as our parameter for star-galaxy discrimination down to $V = 22.5$ (i.e., r_{-2} plus 2σ at this magnitude). Assuming Gaussian distributions, there is only a 2% chance that a star will be misidentified as a galaxy. Using an

objects with 1.5 FWHM as a galaxy for our simulations shows there is very little overlap between 'stars' and 'galaxies' in the r_{-2} vs V plot, so that there is only a 2% chance that a galaxy will be misclassified as a star. Note the envelope in r_{-2} vs V sloping downwards and to the right in this and similar plots. This is due to the fact that for fainter galaxies we are surveying more distant objects and their apparent angular sizes decrease.

We show the total number of objects, stars and galaxies in the Abell 262 V background field in Table 4.2. The magnitudes quoted in the table are dereddened by 0.18 magnitudes in V and by 0.13 magnitudes in I. Data are binned in 0.5 magnitudes bins, the central magnitude of each bin being quoted in the table. The errors quoted are $\sqrt{N}$ (Sandage et al. 1985). We plot these data in Figure 4.2. Note how stars outnumber galaxies at nearly all magnitudes. This reiterates the importance of star galaxy separation in these low galactic latitude fields. Because of this, it is not advisable to use galaxy star count models (e.g., Bahcall & Soneira 1980; 1981; Pritchet 1983) as has been done for our previous work (Ch. 3), because of the greater uncertainty in these models at low galactic latitudes. We will comment on this later on as well.

Figure 4.1: The plot of r_{-2} vs V for the Abell 262 Background Field. Open squares are data points. The thick dashed line is the 'cut' made for star-galaxy separation to $V = 22.5$

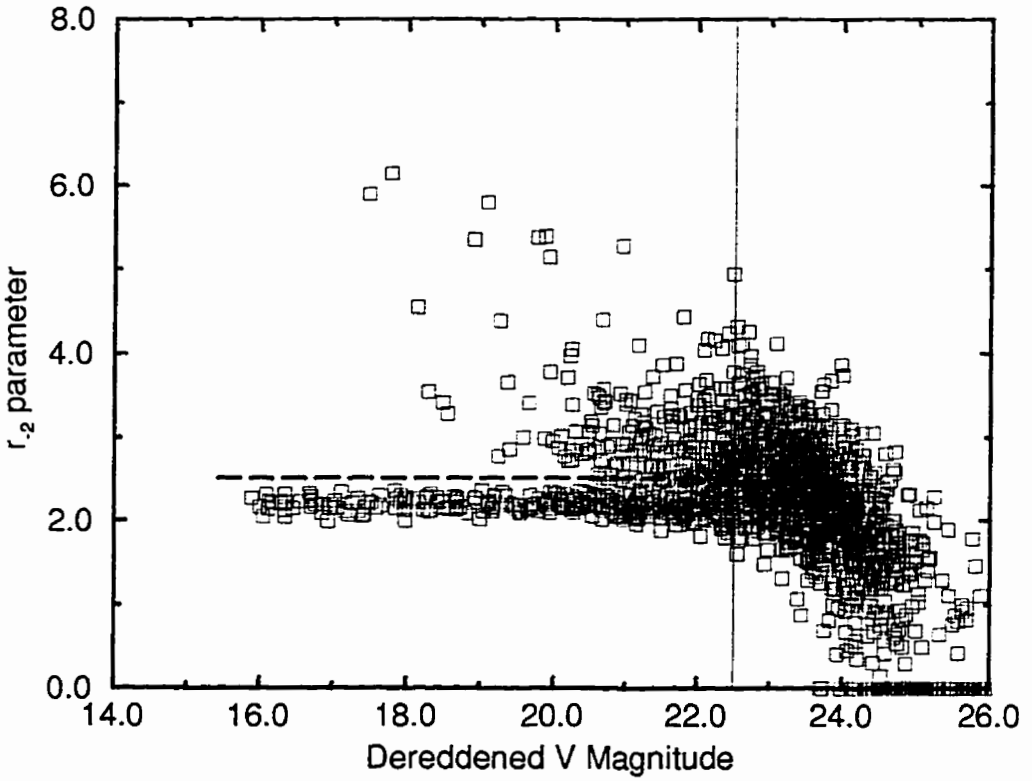

Table 4.2: NUMBER COUNTS IN A262 BACKGROUND FIELD IN V

V	N. of objects	N. of galaxies	N. of stars	Completeness
15.25	0.00 ± 0.00	0.00 ± 0.00	0.00 ± 0.00	1
15.75	1.00 ± 1.00	0.00 ± 0.00	1.00 ± 1.00	1
16.25	12.47 ± 3.53	0.00 ± 0.00	12.47 ± 3.53	1
16.75	13.52 ± 3.68	0.00 ± 0.00	13.52 ± 3.68	1
17.25	13.68 ± 3.70	1.08 ± 1.04	12.60 ± 3.55	1
17.75	16.50 ± 4.06	1.00 ± 1.00	15.50 ± 3.94	1
18.25	16.66 ± 4.08	3.21 ± 1.79	13.45 ± 3.67	1
18.75	19.73 ± 4.44	2.05 ± 1.43	17.67 ± 4.20	1
19.25	24.22 ± 4.92	5.34 ± 2.31	18.88 ± 4.35	1
19.75	29.30 ± 5.41	8.24 ± 2.87	21.06 ± 4.59	1
20.25	51.34 ± 7.17	16.83 ± 4.10	34.51 ± 5.87	1
20.75	73.14 ± 8.55	34.64 ± 5.89	38.50 ± 6.20	1
21.25	91.08 ± 9.54	42.99 ± 6.56	48.09 ± 6.93	1
21.75	109.59 ± 10.47	57.35 ± 7.57	52.24 ± 7.23	1
22.25	186.25 ± 13.65	114.03 ± 10.68	72.22 ± 8.50	0.98

Figure 4.2: Plot of number of objects, stars and galaxies (data in Table 4.2) for the Abell 262 background field

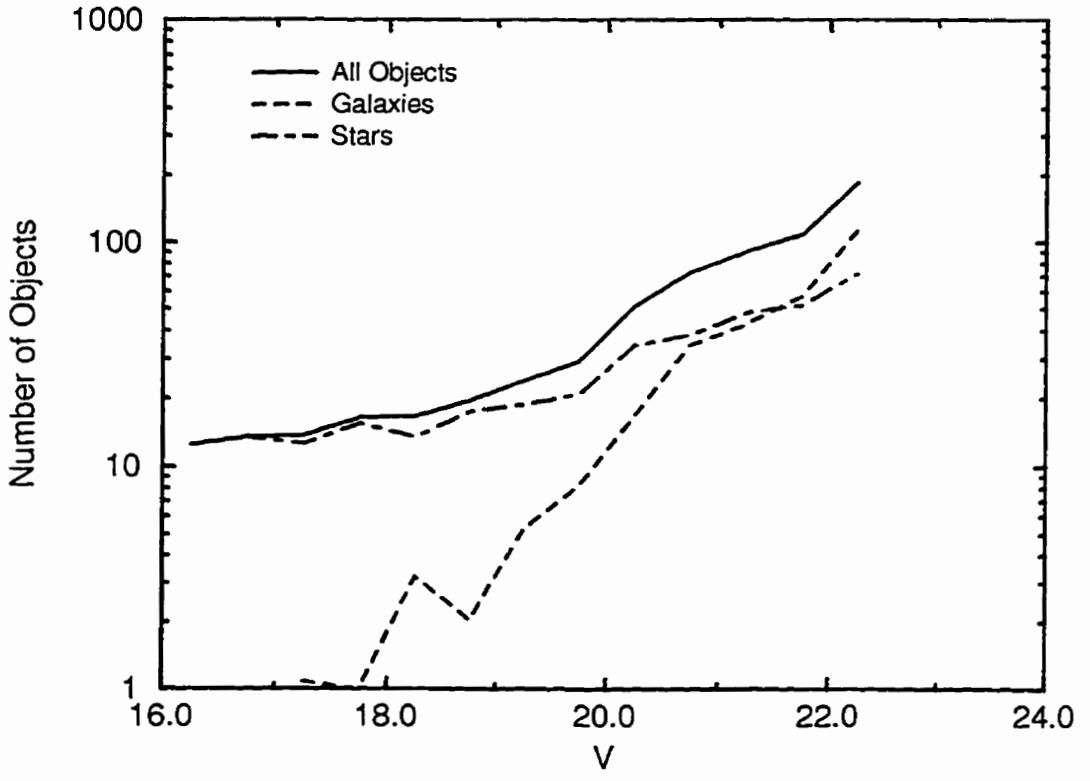

Figure 4.3: The plot of r_{-2} vs V for the Abell 426 Background Field. Open squares are data points. The thick dashed line is the 'cut' made for star-galaxy separation to $V = 21.5$

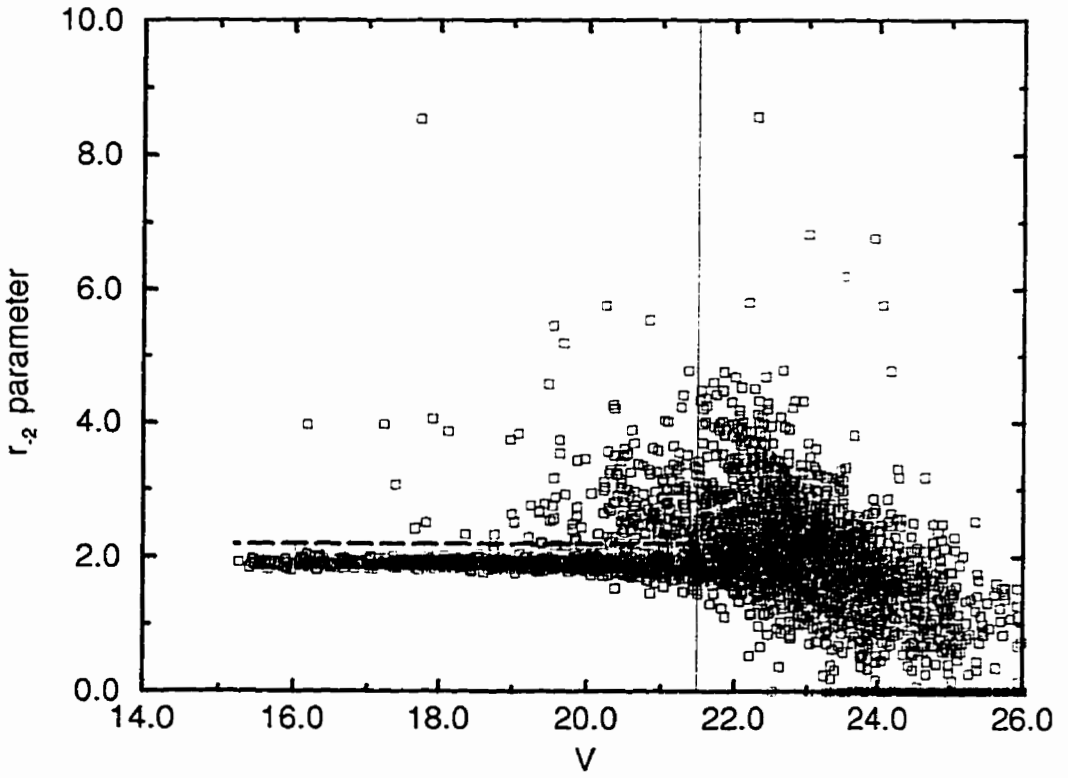

A background field for Abell 426 has been observed in V. We plot the r_{-2} vs V for this field in Figure 4.3. Our simulations show that $r_{-2} = 1.92 \pm 0.13$ at $V = 21.43$, $r_{-2} = 1.91 \pm 0.17$ at $V = 21.93$ and $r_{-2} = 1.94 \pm 0.17$ at $V = 22.43$. We choose $r_{-2} = 2.20$ at $V = 21.5$ for our star-galaxy separation cut, as shown in Figure 4.4. This is brighter than in the previous field and it is due to the high extinction present in this field (about 0.9 magnitudes). Table 4.3 shows the same information as Table 4.2 for the A426 background field. These data are plotted in Figure 4.5, as in Figure 4.2.

Since both background fields cover about 300 arcmin^2 we decided to average counts in both fields and use these averages for background subtraction in all of our cluster fields. This is permissible since the number of background galaxies is the same in all direction, except for variations due to large scale structure. Since the correlation function has no power on large scales, it is not important whether a background field is observed in the immediate neighbourhood of the cluster being considered or not.

The background counts derived from the average of the two fields being considered are shown in Figures 4.6 and 4.7, together with the best fitting line in a $\log N$ vs. V plot. The slope of the line was forced to be 0.4, which is appropriate to J and F counts at bright magnitudes (Pritchet & Infante 1992a). The best fitting line in Figure 4.6 and 4.7 is represented by the equation:

$$\log N = 0.40V - 6.84 \tag{4.1}$$

We compare this to the observed counts in J and F by Pritchet & Infante (1992a) and to the B and R counts by Tyson (1988) in Figure 4.7. Counts in V have never been published in the literature, but $(J+F)/2$ is very close to V. These counts are not published as well. In any case we sample much brighter galaxies than Pritchet & Infante (1992a) or any other author, so that any comparison is not fully justified.

Following Pritchet & Infante (1992a) V counts should lie between J and F counts. As we can see the agreement with previous determinations is quite good.

Table 4.3: NUMBER COUNTS FOR A426 BACKGROUND FIELD IN V

V	N. of objects	N. of galaxies	N. of stars	Completeness
15.25	7.37 ± 2.72	0.00 ± 0.00	6.37 ± 2.52	1
15.75	25.03 ± 5.00	0.00 ± 0.00	25.03 ± 5.00	1
16.25	44.74 ± 6.69	1.07 ± 1.03	43.67 ± 6.61	1
16.75	40.02 ± 6.33	0.00 ± 0.00	40.02 ± 6.33	1
17.25	62.93 ± 7.93	2.07 ± 1.44	60.86 ± 7.80	1
17.75	82.61 ± 9.09	4.13 ± 2.03	77.48 ± 8.80	1
18.25	83.36 ± 9.13	2.15 ± 1.47	81.20 ± 9.01	1
18.75	108.28 ± 10.41	4.33 ± 2.08	103.95 ± 10.20	1
19.25	112.39 ± 10.60	10.66 ± 3.26	100.73 ± 10.04	1
19.75	107.04 ± 10.35	24.39 ± 4.94	82.65 ± 9.09	1
20.25	126.63 ± 11.25	33.43 ± 5.78	93.20 ± 9.65	1
20.75	162.81 ± 12.76	57.71 ± 7.6	104.10 ± 10.20	1
21.25	196.55 ± 14.02	75.81 ± 8.71	117.74 ± 10.85	1

Figure 4.4: Plot of number of objects, stars and galaxies (data in Table 3.3) for the Abell 426 background field

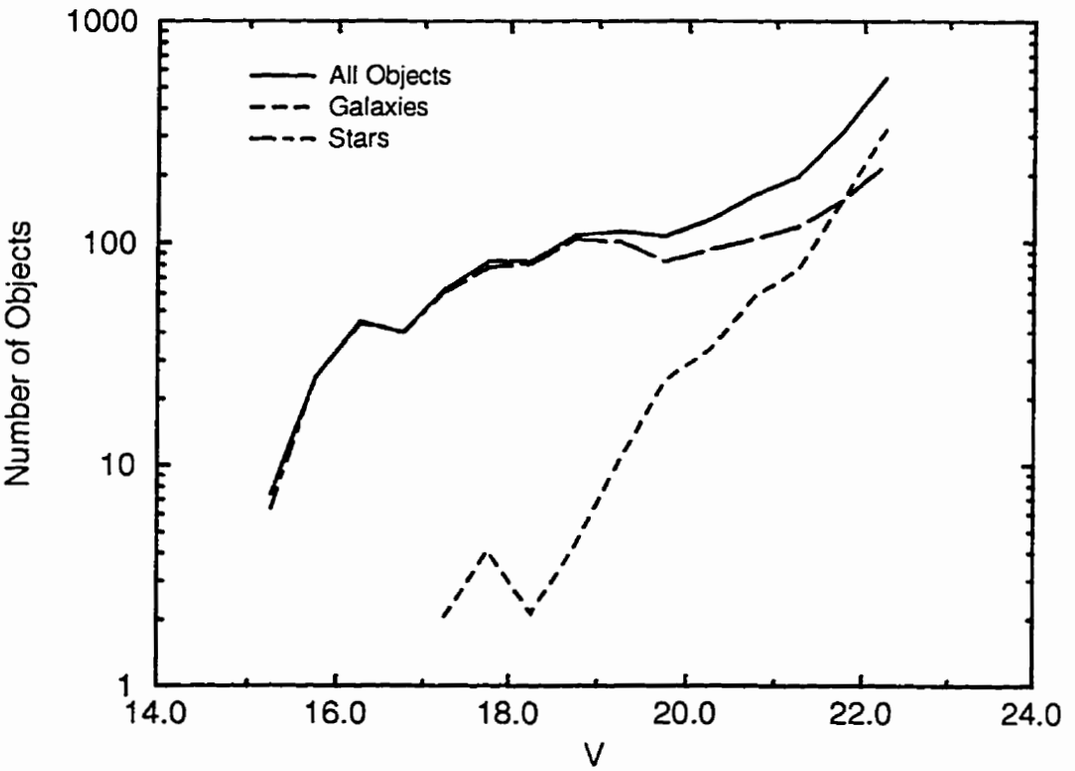

Figure 4.5: Number of background galaxies in V (average of two fields) and best fitting line

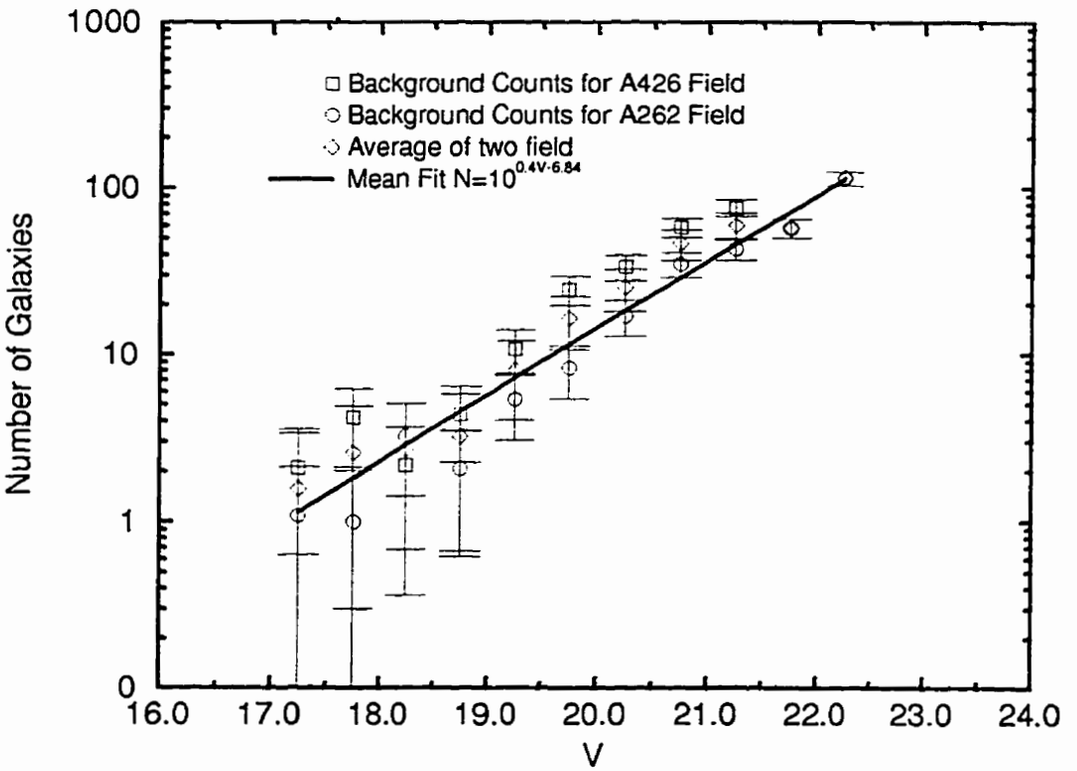

Figure 4.6: Number of background galaxies in V (average of two fields) and best fitting line

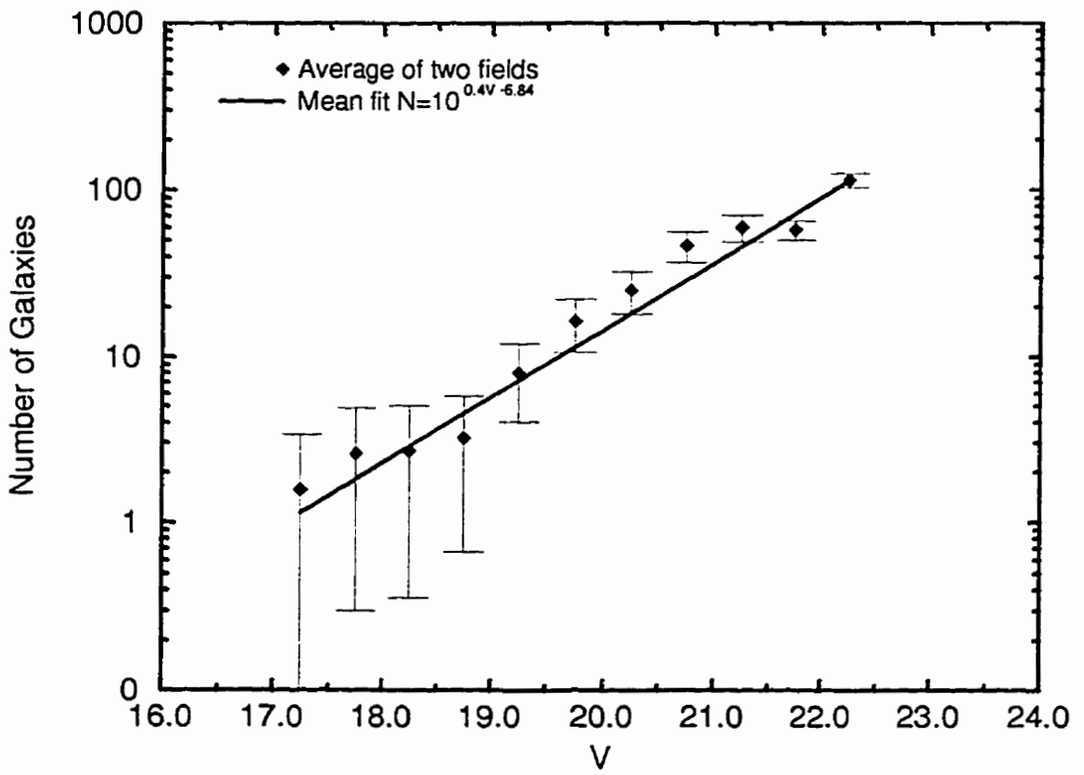

Figure 4.7: Comparison of V counts with surveys in J, F (Pritchet & Infante 1992a) and B and R (Tyson 1988). See figure legend for further information

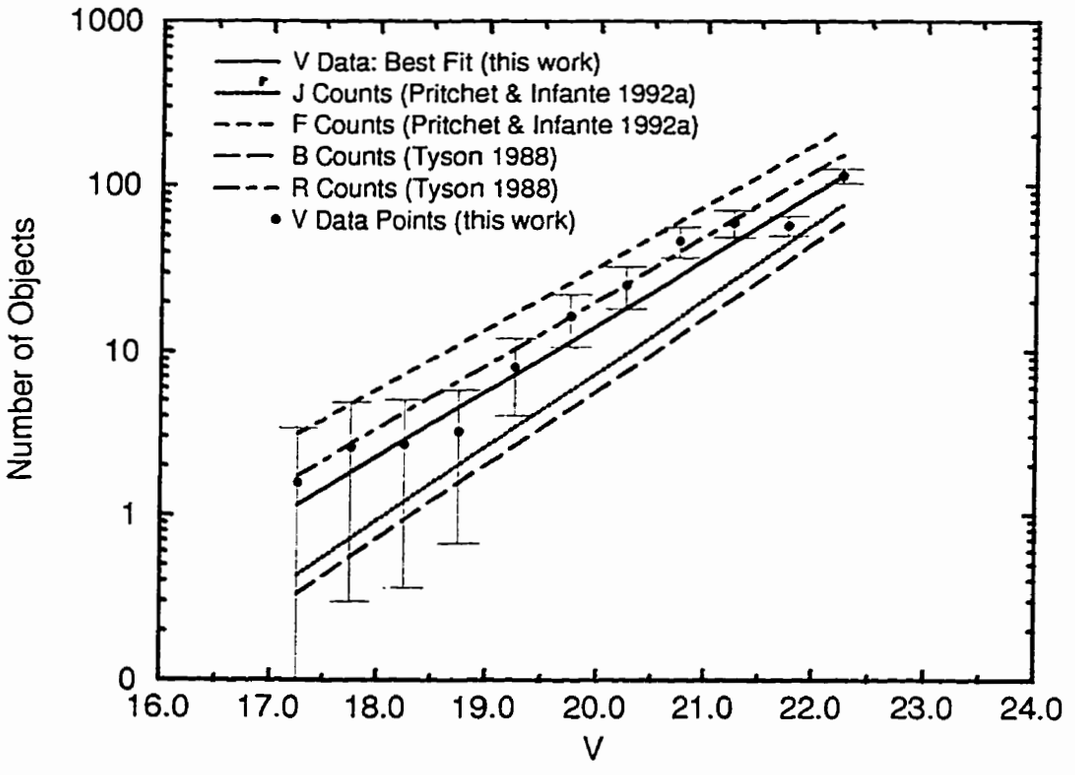

4.3 I Background Counts and Colors

An I band background field was also imaged for Abell 262. A plot of r_{-2} vs I (dereddened) is shown in Figure 4.8 for star-galaxy separation. For this field, we find that $r_{-2} = 1.98 \pm 0.13$ for $I = 21.0$, $r_{-2} = 1.96 \pm 0.14$ for $I = 21.50$ and $r_{-2} = 1.94 \pm 0.20$ for $I = 22$. We therefore choose $r_{-2} = 2.24$ as our 'cut' for star-galaxy separation, to $I = 21.5$. Table 4.4 shows the same information as Tables 4.2 and 4.3 for this field. Figure 4.9 shows the number of objects, stars and galaxies.

These data are again fitted with a straight line in a $\log N$ vs I plot, as shown in Figure 4.10. The best fit is for:

$$\log N = 0.43I - 6.84 \tag{4.2}$$

which is considerably steeper than the counts by Tyson (1988) and Lilly et al. (1991), although the fit is quite good. Imposing a slope of 0.34 (as in Tyson 1988 and Lilly et al. 1991) on the I counts we find:

$$\log N = 0.34I - 5 \tag{4.3}$$

The fit to equation 4.3 is quite poor, and overestimates the number of bright galaxies. On the other hand, as shown in Figure 4.11, it provides an excellent match to Tyson (1988).

Our objects are very much brighter than objects surveyed by Tyson (1988) and Lilly et al. (1991), and it is well known that galaxy counts steepen for

bright objects. The discrepancy between our results and the Tyson fit is likely due to this. We therefore adopt the relation in equation 4.2 as our background counts fit.

For the Abell 262 field we can determine the $V-I$ distribution for galaxies in the field. We plot V vs $V-I$ for this field in Figure 4.12. A histogram of the number of galaxies in 0.25 color bins is shown in Figure 4.13. We see that galaxies are mostly confined to a 'strip' between $V-I$ of 0.75 and 2, with almost equal numbers of galaxies in these bins. The median color for these objects if $V-I \sim 1.24$, which compares well with $J-F \sim 1.2$ for galaxies in Pritchet & Infante (1992a). This is about 1.0 in $B-V$ (for stars). Transforming to $V-I$ using giant colors we get a color of 1.3, which is in reasonable agreement with our result, considering the uncertainties involved in the conversion.

We can compare these star counts to the model by Bahcall & Soneira (1980; 1981). Figure 4.14 plots the number of stars versus V for the Abell 262 background field and the Bahcall & Soneira model. The model appears to fit the obsevations well, but overestimates the number of stars in this field by about 50%. For the I band, we see in Figure 4.15 that the data follow the model quite well, but the normalization is again wrong by about 50%. This is not surprising, considering that the model is not intended to work at low galactic latitudes. We can finally compare the color distributions for stars in this field in Figure 4.16. The color distributions follow the model

qualitatively well, although the normalization is uncertain, because of the areas excluded from analysis and saturated objects. Moreover, the model tends to overestimate the number of stars in these fields, as shown above. A color magnitude diagram is shown in Figure 4.17, where we note some features of interest. Most stars have $0.5 < V - I < 3$. There is a 'color edge' at $V - I \sim 0.5$ and the reddening line can be identified as an envelope in this diagram.

We also plot the number of stars in the A426 background field versus V in Figure 4.18. As we see, the agreement with the model is qualitatively very good, but the model overpredicts the number of stars in these fields. Note that all of these plots are carried out with raw data, without reddening corrections.

Figure 4.8: The plot of r_{-2} vs I for the Abell 262 background field, with the appropriate cut for star-galaxy separation

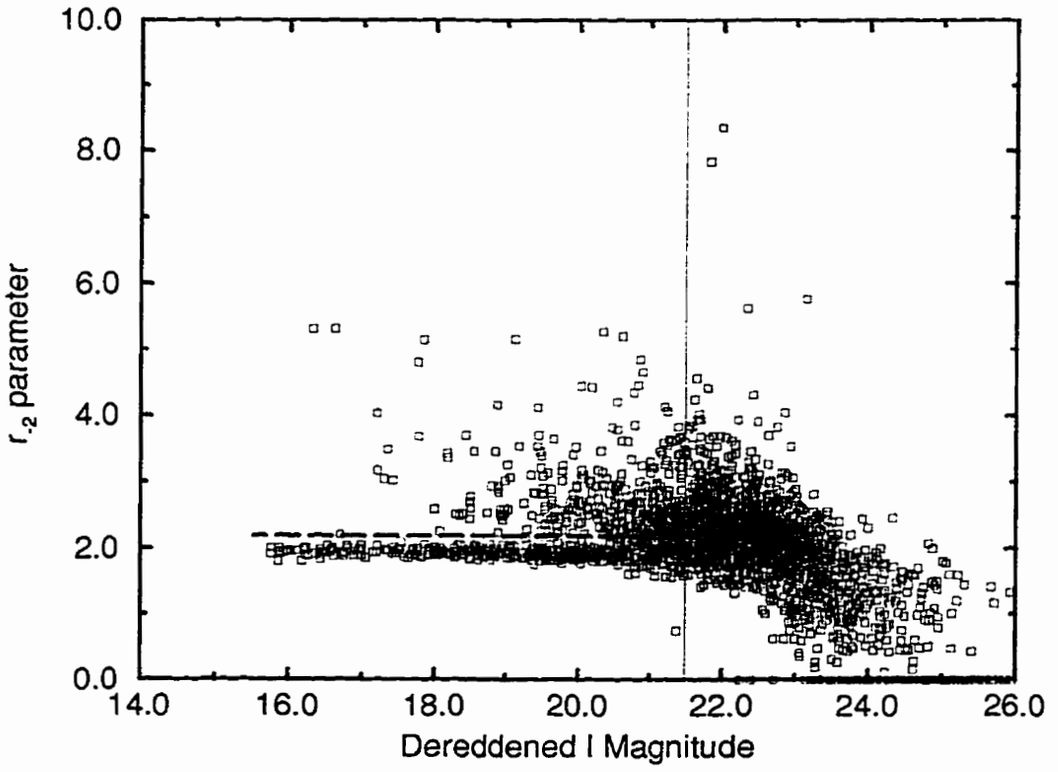

Table 4.4: NUMBER COUNTS FOR A262 BACKGROUND FIELD IN I

I	N. of objects	N. of galaxies	N. of stars	Completeness
15.25	0.00 ± 0.00	0.00 ± 0.00	0.00 ± 0.00	1
15.75	8.45 ± 2.91	0.00 ± 0.00	8.45 ± 2.91	1
16.25	14.72 ± 3.84	1.09 ± 1.04	13.63 ± 3.69	1
16.75	21.17 ± 4.60	2.09 ± 1.45	19.08 ± 4.37	1
17.25	20.08 ± 4.48	5.45 ± 2.33	14.63 ± 3.82	1
17.75	29.71 ± 5.45	4.18 ± 2.04	25.53 ± 5.05	1
18.25	43.97 ± 6.63	10.90 ± 3.30	33.07 ± 5.75	1
18.75	63.69 ± 7.98	19.44 ± 4.41	44.25 ± 6.65	1
19.25	63.69 ± 7.98	23.26 ± 4.82	40.43 ± 6.36	1
19.75	115.84 ± 10.76	49.97 ± 7.07	65.87 ± 8.12	1
20.25	106.49 ± 10.32	51.34 ± 7.17	55.15 ± 7.43	1
20.75	179.71 ± 13.41	114.93 ± 10.72	64.78 ± 8.05	1
21.25	262.06 ± 16.19	177.96 ± 13.34	84.10 ± 9.17	1

Figure 4.9: Number of objects, stars and galaxies for the Abell 262 I background field

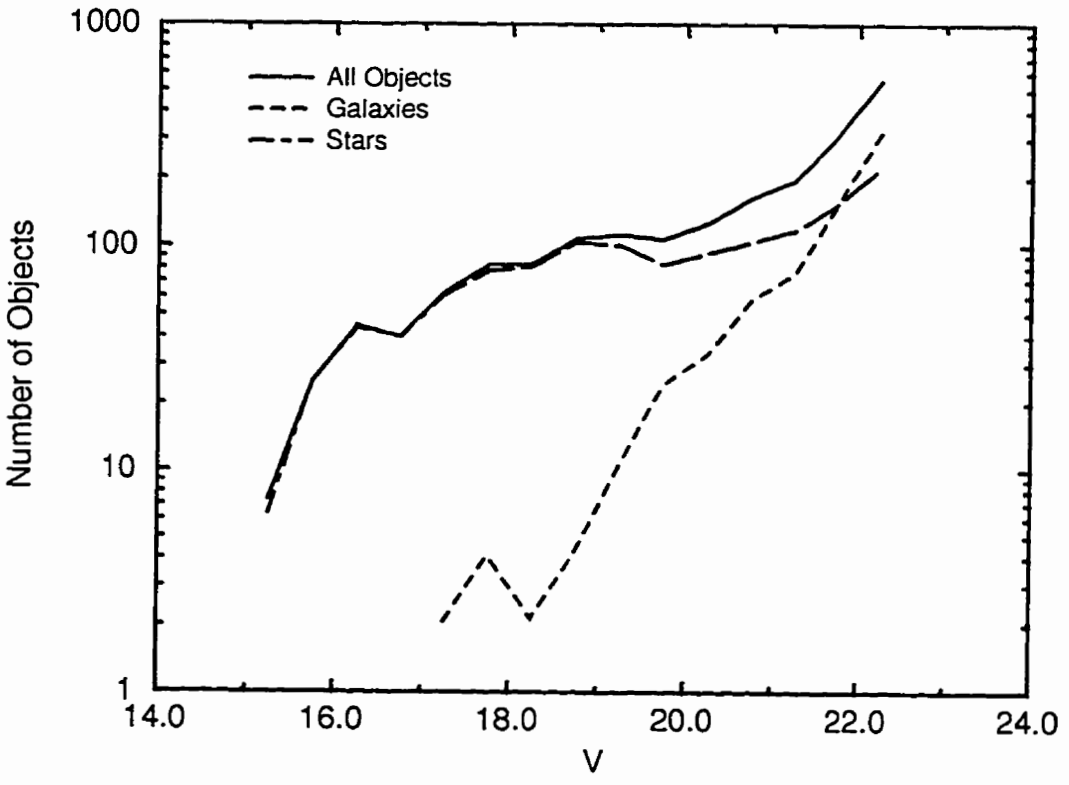

Figure 4.10: Number counts and fits for the I band galaxy counts

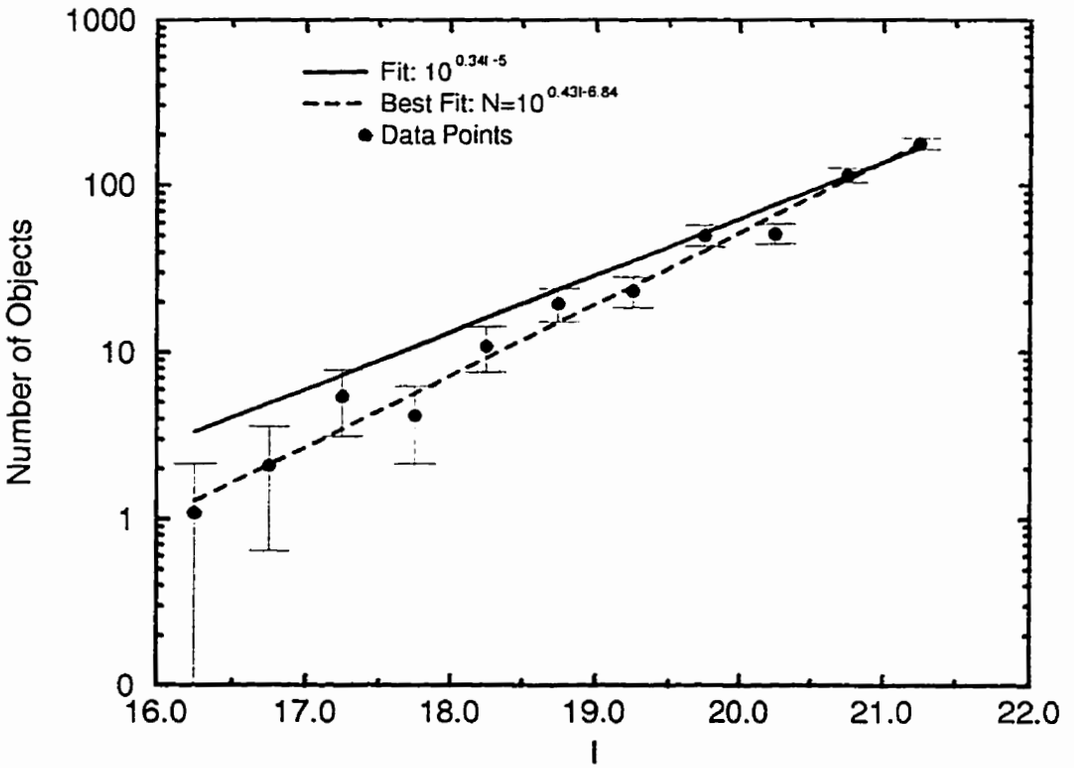

Figure 4.11: Number counts and 'forced' fit to the I counts. Note the excellent agreement with Tyson (1988) counts

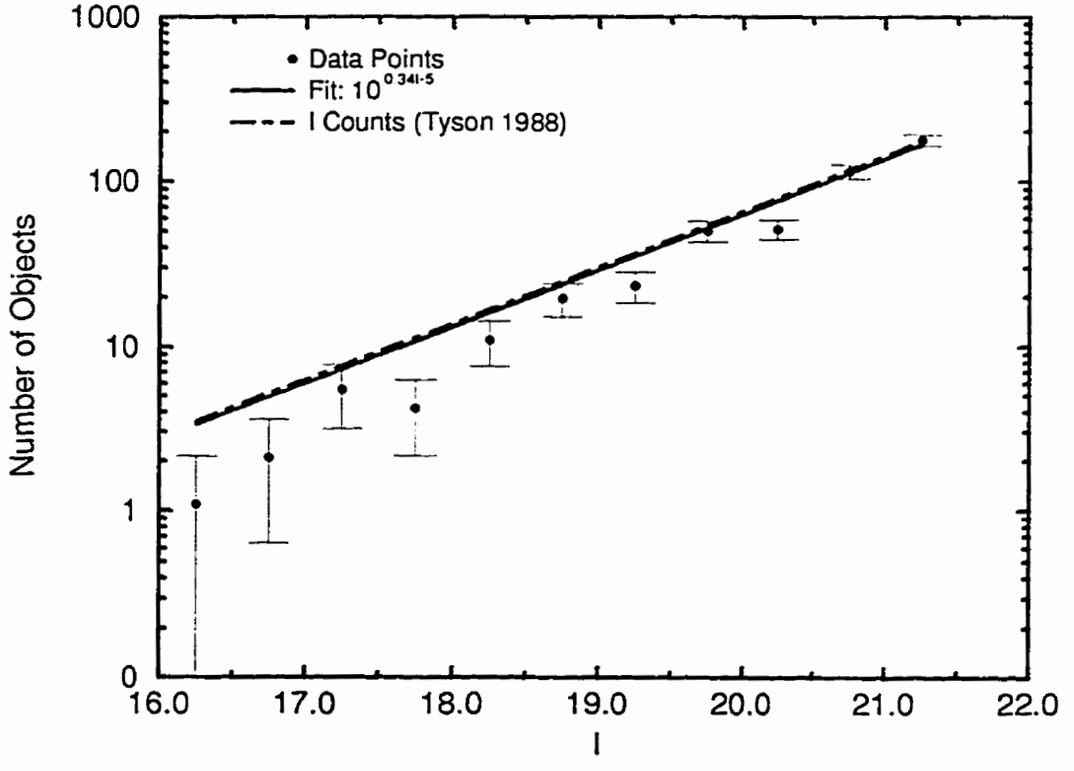

Figure 4.12: Color magnitude diagram for galaxies within the Abell 262 background field

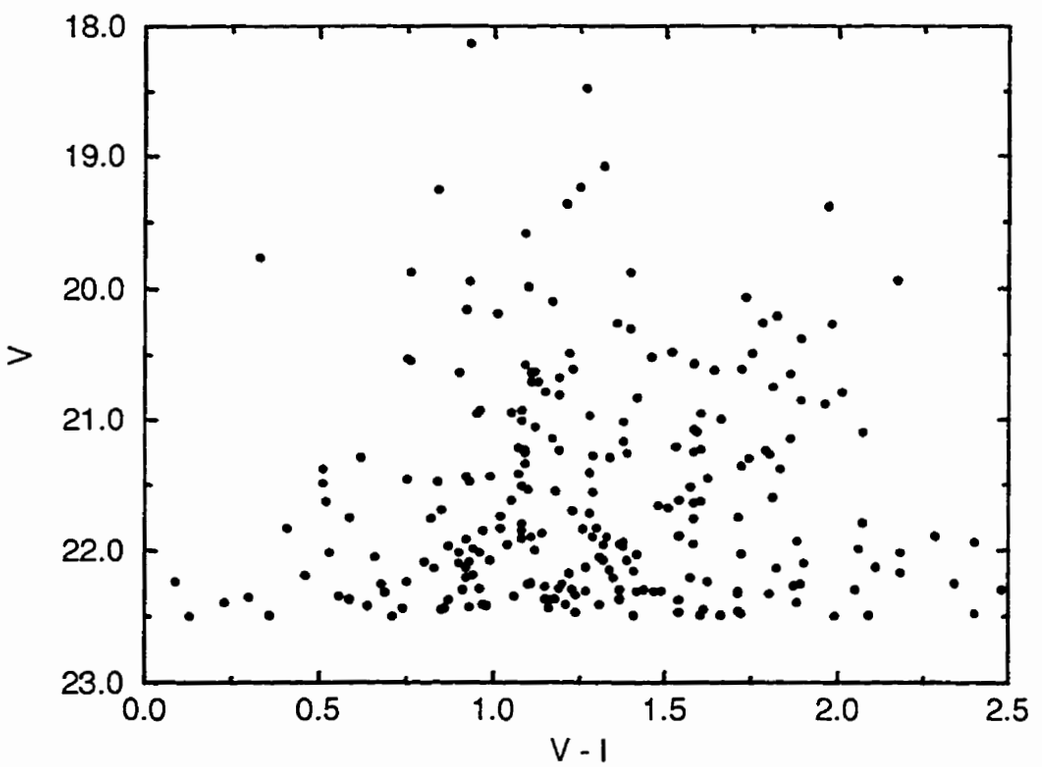

Figure 4.13: Color magnitude histogram for galaxies within the Abell 262 background field: galaxies are binned in 0.25 bins in $V - I$

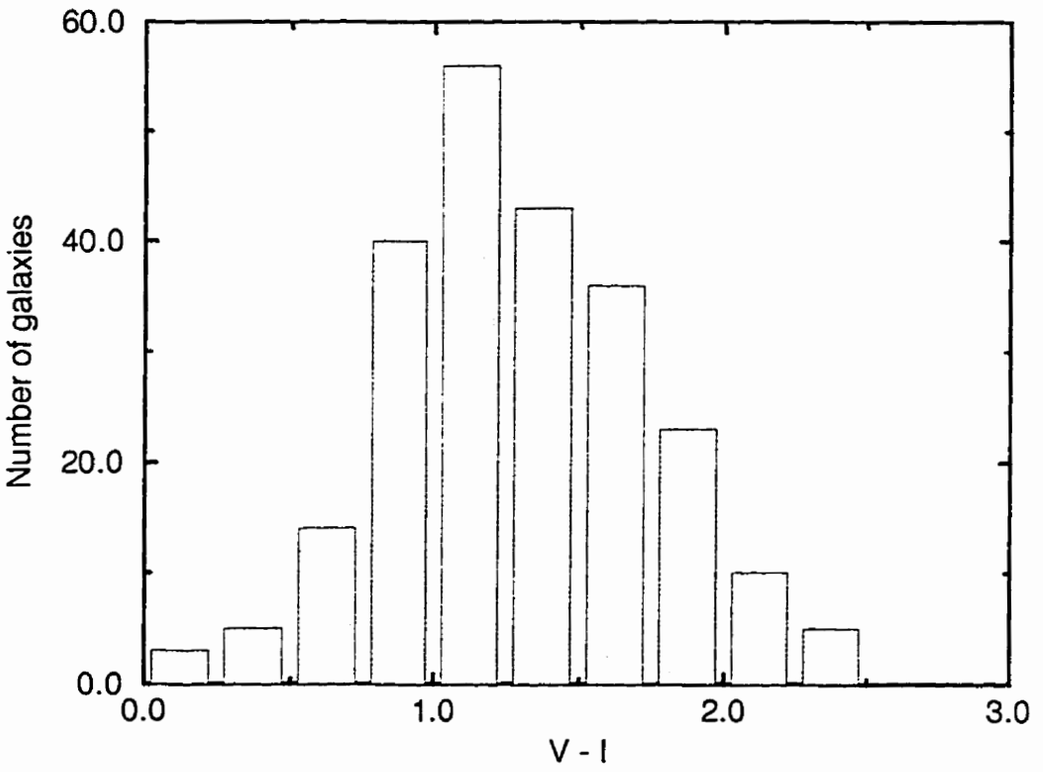

Figure 4.14: Number of stars and starcount model within the Abell 262 background field in V

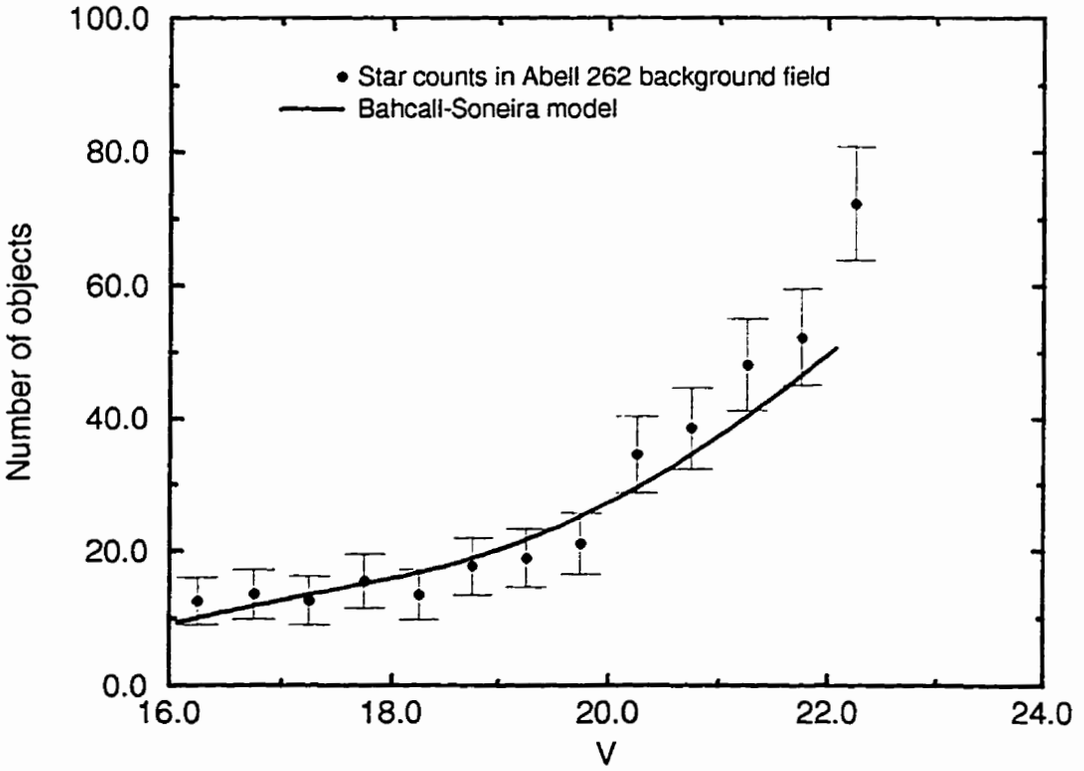

Figure 4.15: Number of stars and starcount model within the Abell 262 background field in I

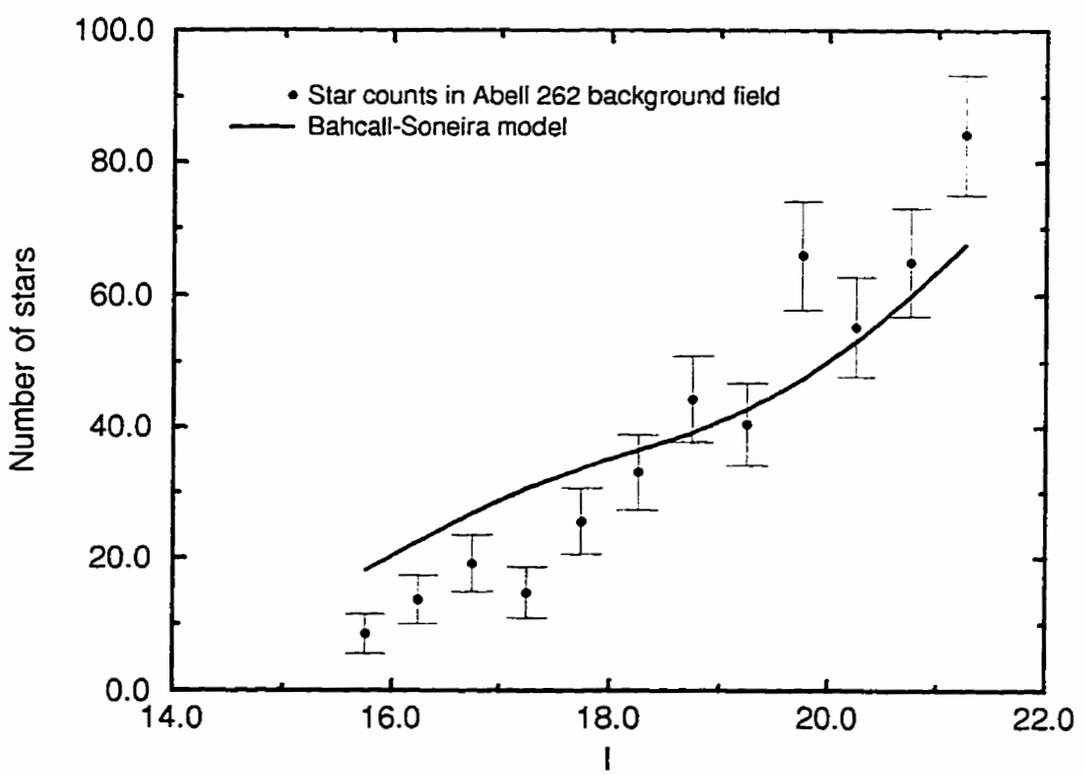

Figure 4.16: Distribution of colors for stars in A262 background field

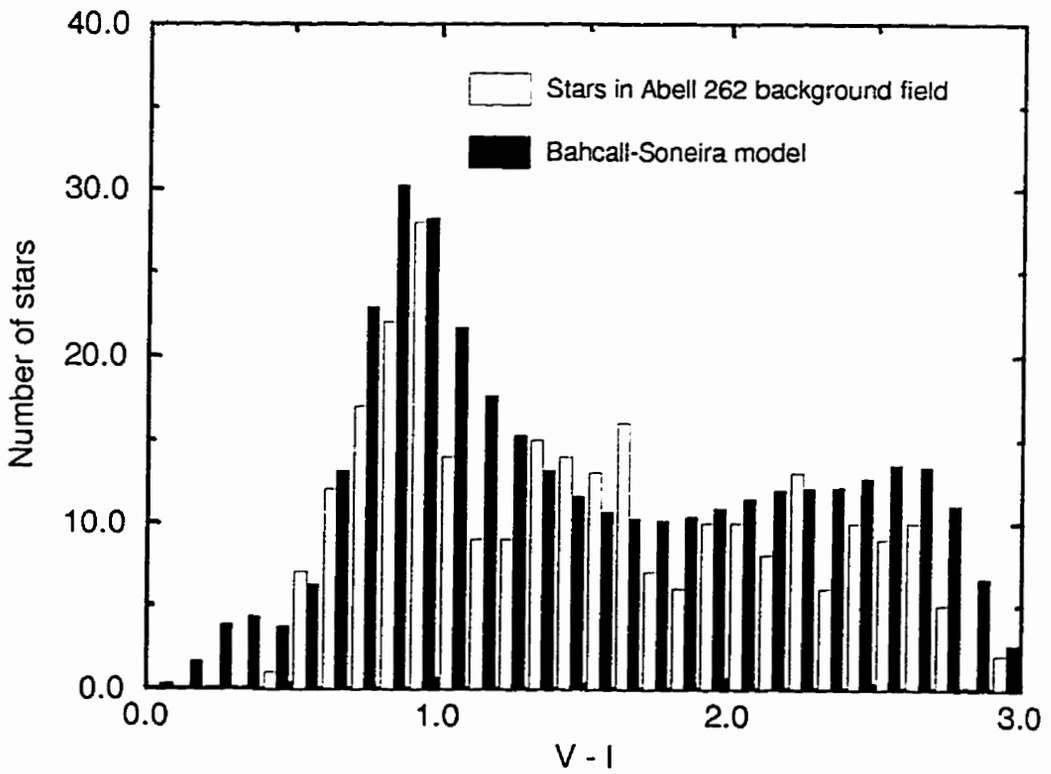

Figure 4.17: Color magnitude diagram for stars within the Abell 262 background field

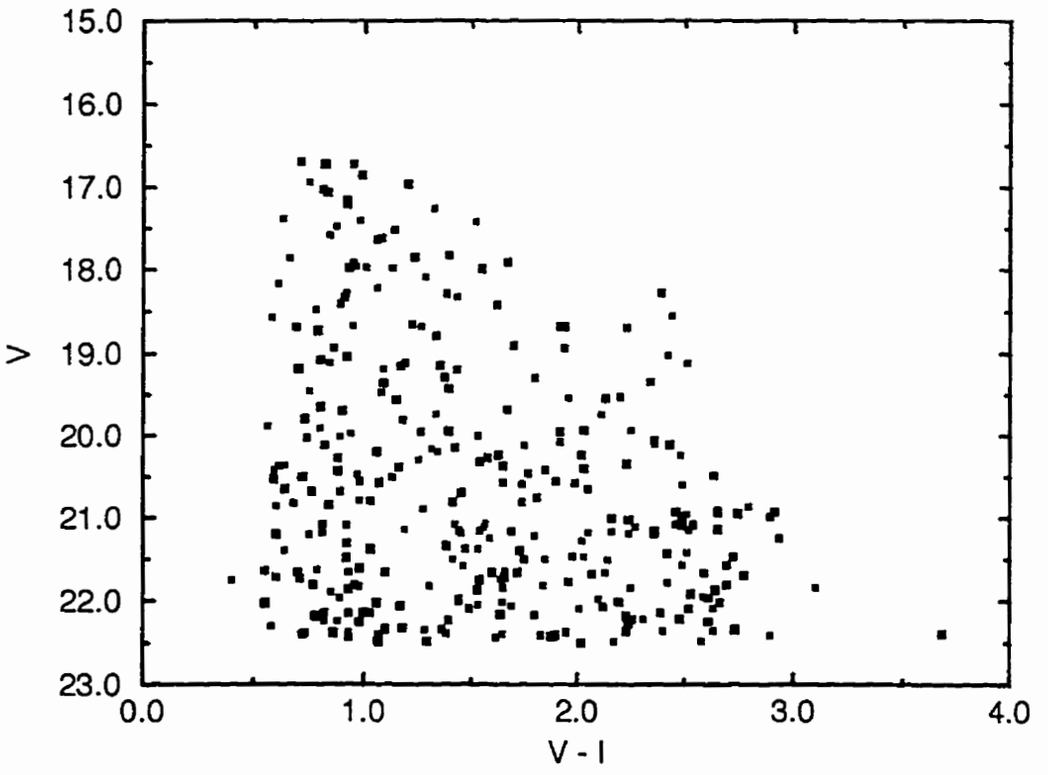

Figure 4.18: Stars and model for A426 background field

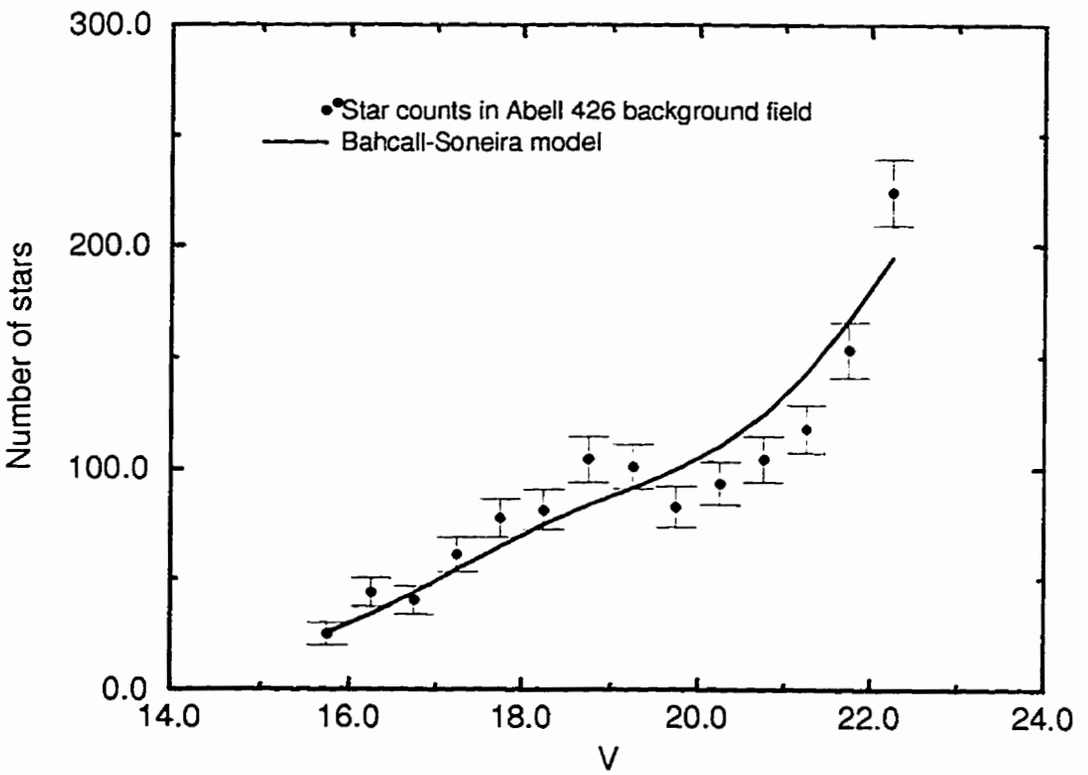

Chapter 5

Abell 262

5.1 Introduction

Abell 262 is one of the major concentrations of the Perseus-Pisces filament. It lies at $l = 136.6$ and $b = -25.1$, with a redshift of 0.016. Abell 262 is classified by Jones & Forman (1984) as an early XD cluster, with $L_X = 3.07 \times 10^{43}$ ergs/s and $r_c = 0.07$ - 0.12 Mpc. The presence of a giant elliptical galaxy at the bottom of the cluster potential well is evidence of some dynamical evolution.

We observed two fields in these clusters, one centred on the dominant elliptical NGC708, and another on a bright cluster member outside of the cluster core (UGC1308). Table 4.1 gives further details on these observations.

We describe observations and results in each field separately below.

5.2 NGC 708

The field around the giant elliptical NGC708 was observed in V and I for a total exposure time of 1200s in each color. The V image for this field before and after removal of bright galaxies is shown in Figures 5.1 and 5.2. Seeing was quite mediocre, as shown in Table 4.1 (about $1''.6$). The I band data were discarded because of focussing problems.

We carry out star-galaxy separation using the r_{-2} parameter, as shown in Figure 5.3. For this field we find that $r_{-2} = 2.80 \pm 0.15$ at $V = 22.15$, $r_{-2} = 2.71 \pm 0.20$ at $V = 22.65$. We choose $r_{-2} = 3.20$ as our 'cut' for star galaxy separation in this plot, to $V = 22.5$.

Table 5.1. shows the number of objects, stars and galaxies in these fields and we plot these data in Figure 5.4. Note that all photometry is dereddened by 0.18 magnitudes in V and 0.13 magnitudes in I, as are the colors. An additional problem in the cluster fields involves contamination by globular clusters, which are abundant in the vicinity of giant ellipticals. These objects are too faint to be safely separated from galaxies, so that our LFs are truncated at a magnitude brighter than the one at which the brightest globular clusters are expected to contribute.

We compare the number of galaxies in the field with the expected number of background contaminants in Figure 5.5.

The number of cluster members in each magnitude bin is estimated by

subtracting the number of contaminating galaxies from the number of objects in each bin. A table showing these data is in Table 5.5. We plot them in Figure 5.6.

As we can see, there does not appear to be a large number of cluster members in this field. As a matter of fact these data are not consistent with a large number of cluster galaxies at low luminosities. This is somewhat surprising, since NGC708 lies at the cluster centre, where the galaxy density should be higher, even if Abell 262 is not a particularly rich object and may have a 'flat' LF (Dressler 1978). Clearly, we are unable to derive a meaningful LF for this cluster.

We compute the surface density of cluster galaxies as a function of radius. This is done by counting the number of objects in 2′ annuli and dividing by the area of each annulus. We then subtracted the average density of background galaxies, as computed by integrating the fit to the V (or I) background counts over the magnitude range of interest and dividing by the total observed area. The error bars are obtained by assuming that the error in galaxy and background counts is $\sqrt{N}$ and adding these errors in quadrature after normalizing for the area covered by each annulus. Figure 5.7 shows the radial surface density distribution for galaxies in the NGC708 field. As we can see, this is not consistent with a large number of cluster members in this field. There is a significant (at the 1σ level) excess of galaxies over background in the inner 5′ of this field, and we plot the number of objects vs

V in Figure 5.8. As above the data are too noisy for any LF to be derived by any method.

We plot the number of stars as a function of magnitude and the Bahcall & Soneira model in Figure 5.9. As before, there is good qualitative agreement with the model, but the model overestimates the number of stars in this region, as for the A262 background field. This is not unexpected since the two fields are not very distant on the sky. Note that no correction for reddening is applied for this field and for the model.

We will comment on these findings after discussing the second field observed in Abell 262.

Figure 5.1: The V image for NGC708 (one of three chips in mosaic)

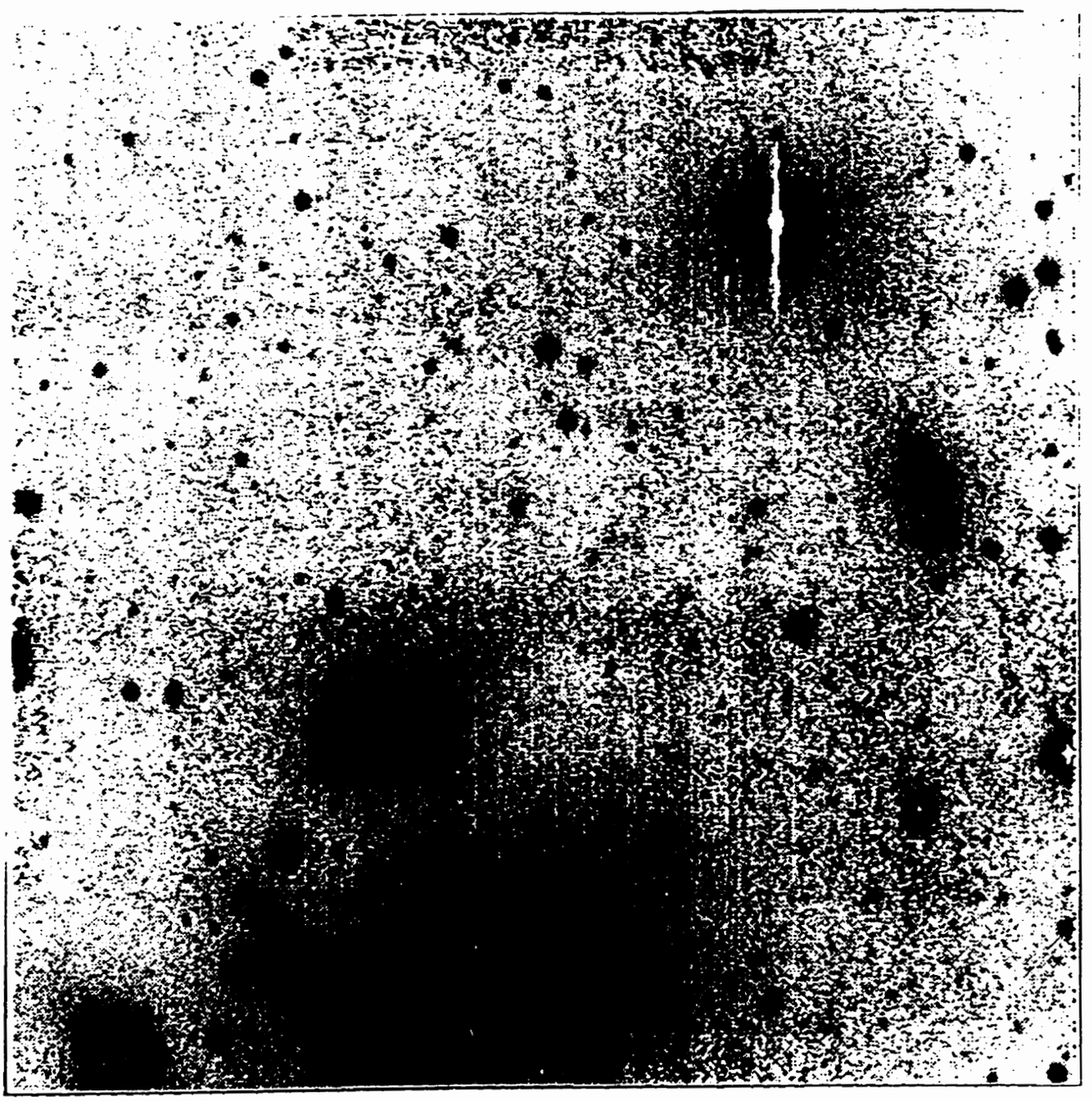

Figure 5.2: The V image for NGC708 after removal of bright galaxies

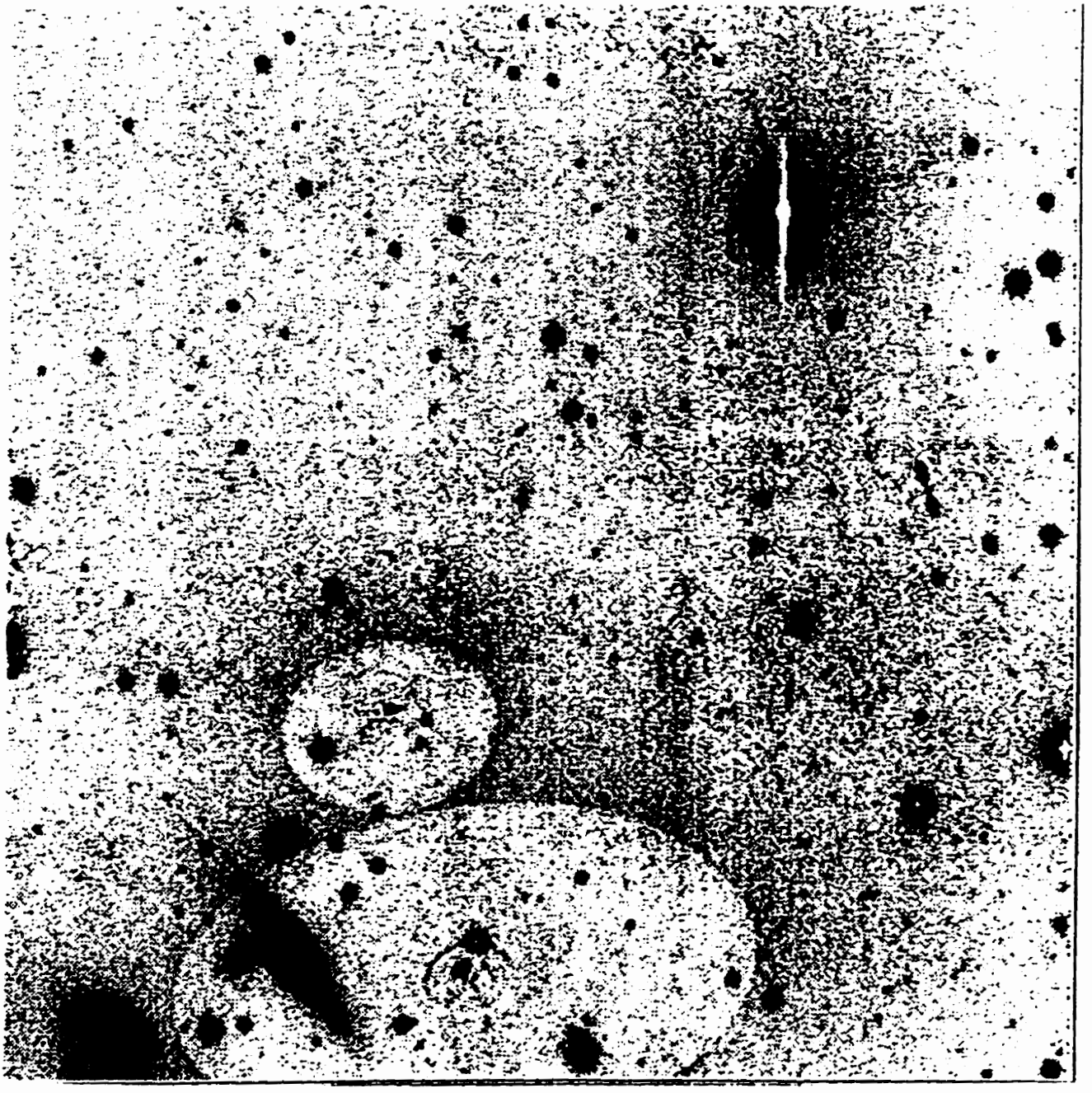

Figure 5.3: Plot of r_{-2} vs V for the NGC708 field in A262 with 'cut' for star-galaxy separation.

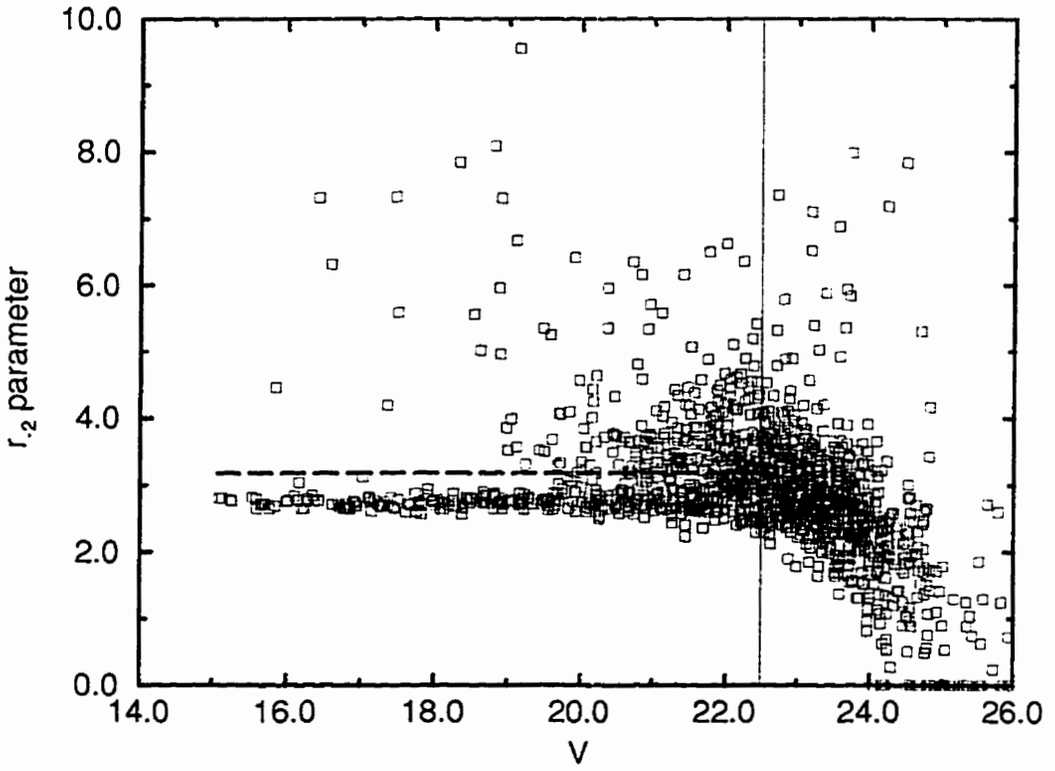

Table 5.1: NUMBER COUNTS IN NGC708 FIELD IN V

V	N. of objects	N. of galaxies	N. of stars	Completeness
16.25	15.66 ± 3.96	2.22 ± 1.49	13.45 ± 3.67	1
16.75	12.61 ± 3.55	1.00 ± 1.00	11.61 ± 3.41	1
17.25	19.95 ± 4.47	4.22 ± 2.05	15.73 ± 3.97	1
17.75	16.08 ± 4.01	0.01 ± 0.00	16.08 ± 4.01	1
18.25	21.14 ± 4.60	1.20 ± 1.09	19.95 ± 4.47	1
18.75	30.31 ± 5.51	7.45 ± 2.73	22.86 ± 4.78	1
19.25	31.94 ± 5.65	8.52 ± 2.92	23.42 ± 4.84	1
19.75	39.44 ± 6.28	16.30 ± 4.04	23.14 ± 4.81	1
20.25	54.93 ± 7.41	20.77 ± 4.56	34.16 ± 5.84	1
20.75	74.05 ± 8.61	36.68 ± 6.06	37.38 ± 6.11	1
21.25	90.83 ± 9.53	48.70 ± 6.98	42.13 ± 6.49	1
21.75	118.26 ± 10.87	63.02 ± 7.94	55.24 ± 7.43	1
22.25	176.60 ± 13.29	117.17 ± 10.82	59.43 ± 7.71	1

Figure 5.4: Number of objects, stars, galaxies for the NGC708 field in A262

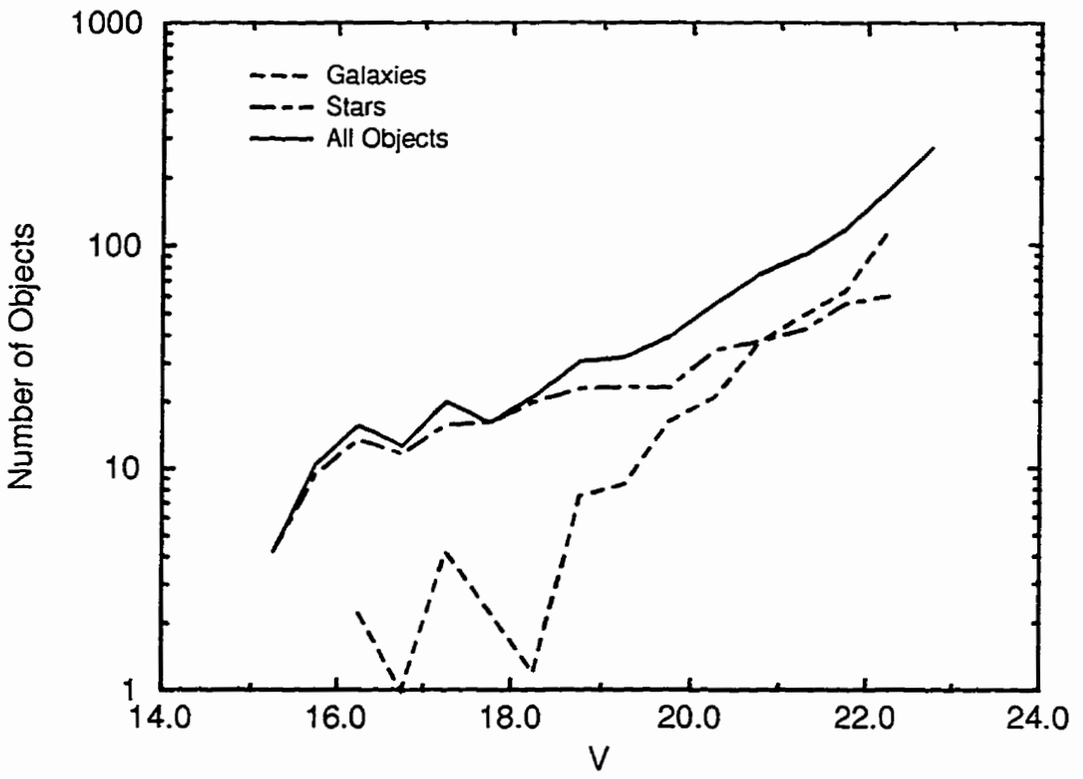

Table 5.2: GALAXY COUNTS FOR NGC708 FIELD IN V

V	N. of galaxies	Background counts	Cluster members
16.25	2.22 ± 1.49	0.46	1.76 ± 1.64
16.75	1.00 ± 1.00	0.72	0.28 ± 1.31
17.25	4.22 ± 2.05	1.15	3.07 ± 2.31
17.75	0.00 ± 0.00	1.82	-1.82 ± 1.35
18.25	1.20 ± 1.09	2.88	-1.68 ± 2.02
18.75	7.45 ± 2.73	4.57	2.88 ± 3.47
19.25	8.52 ± 2.92	7.24	1.28 ± 3.97
19.75	16.30 ± 4.04	11.48	4.82 ± 5.27
20.25	20.77 ± 4.56	18.20	2.57 ± 6.24
20.75	36.68 ± 6.06	28.84	7.84 ± 8.10
21.25	48.70 ± 6.98	45.71	2.99 ± 9.72
21.75	63.02 ± 7.94	72.44	-9.42 ± 11.64
22.25	117.17 ± 10.82	114.82	2.35 ± 15.23

Figure 5.5: Number of objects and V background counts for the NGC708 field in A262

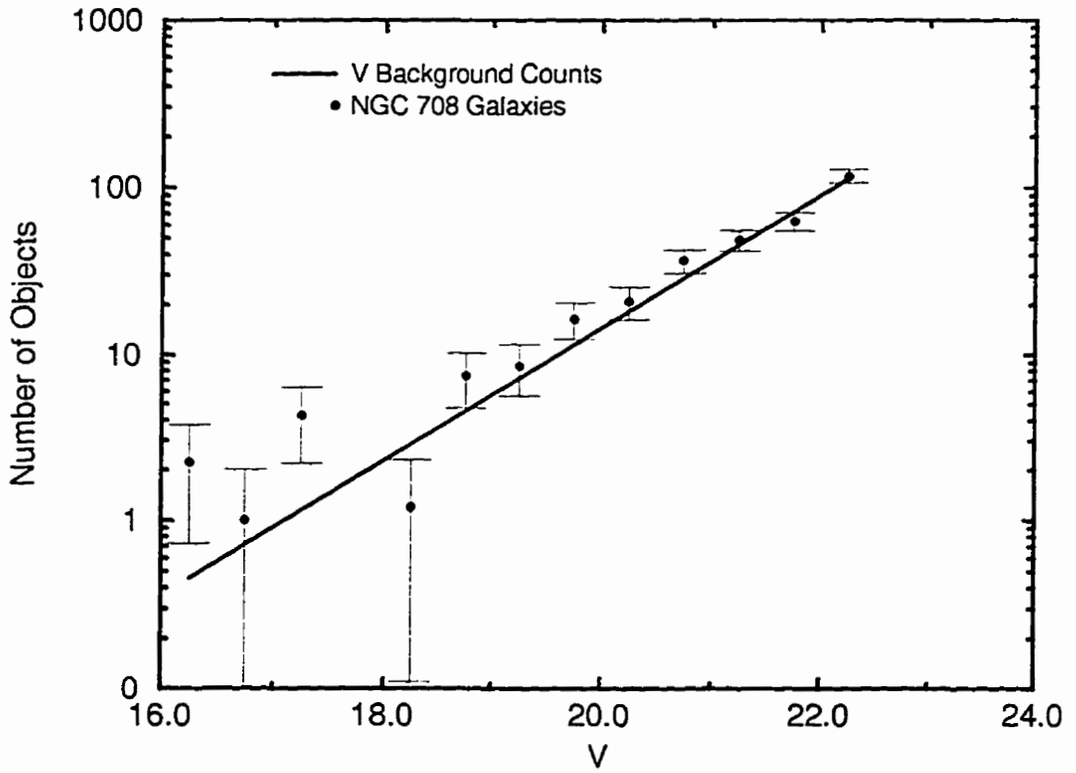

Figure 5.6: Number of objects and V LF NGC708 field in A262

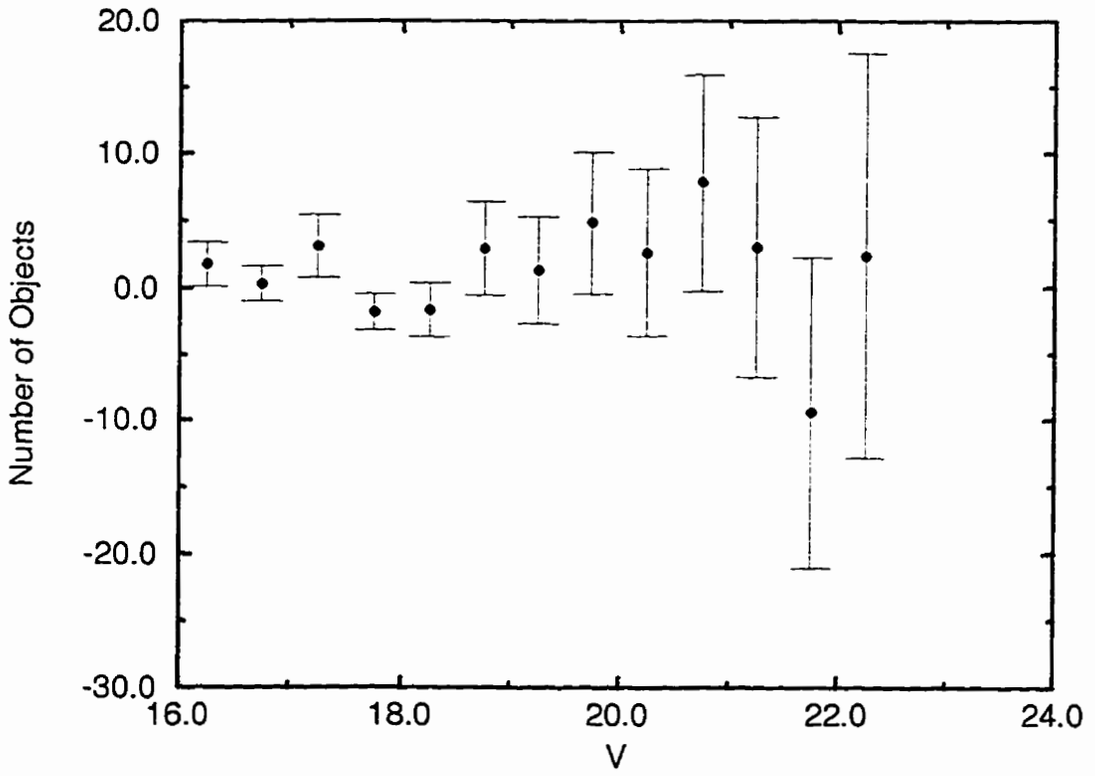

Figure 5.7: Surface density distribution of galaxies in the NGC708 field – see text for further details

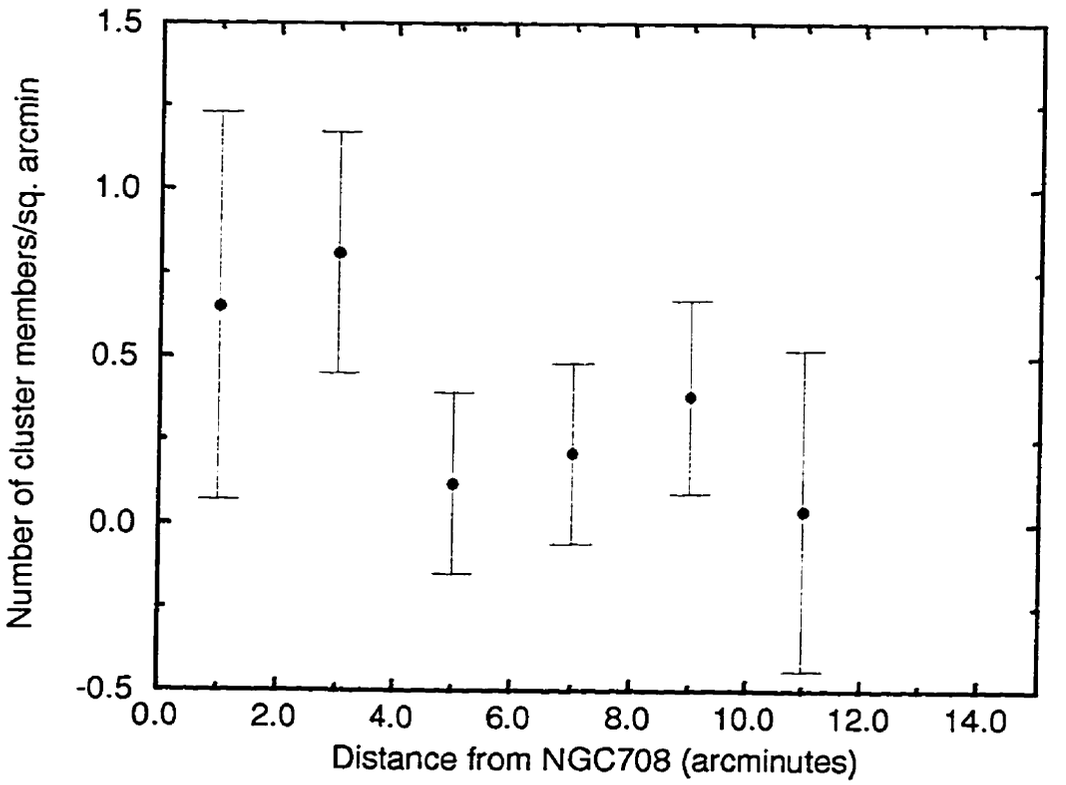

Figure 5.8: Number of objects in the inner 5′ of NGC708 field

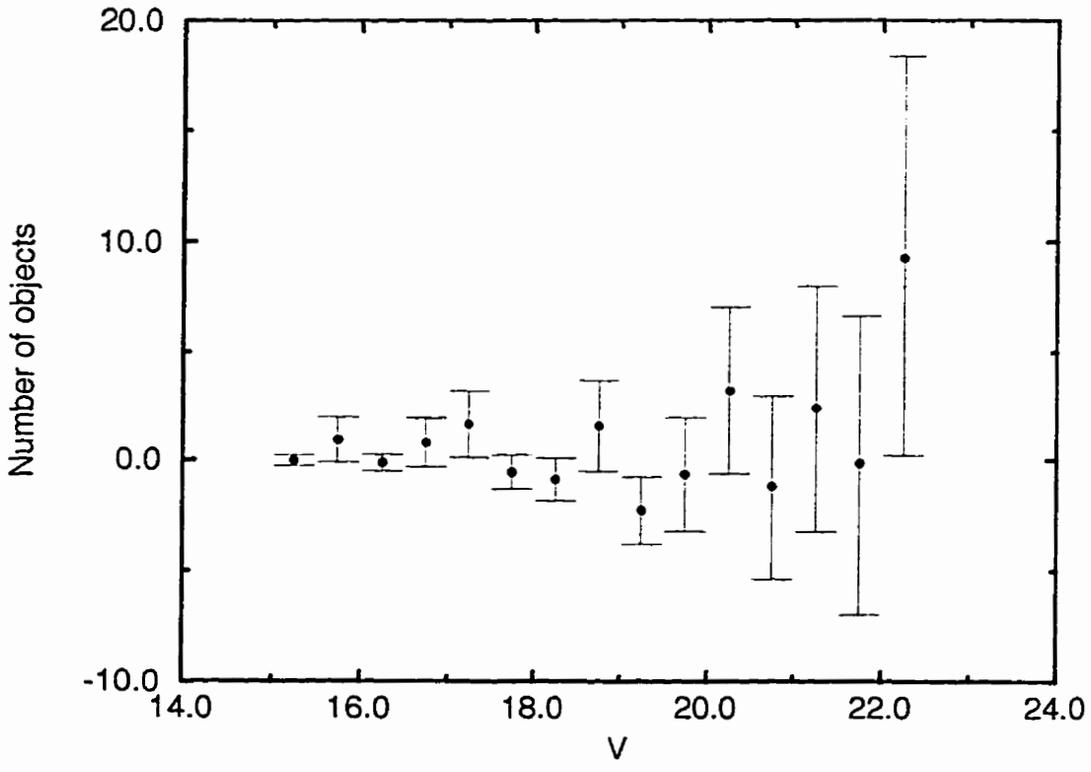

Figure 5.9: Number of stars in NGC708 field and model

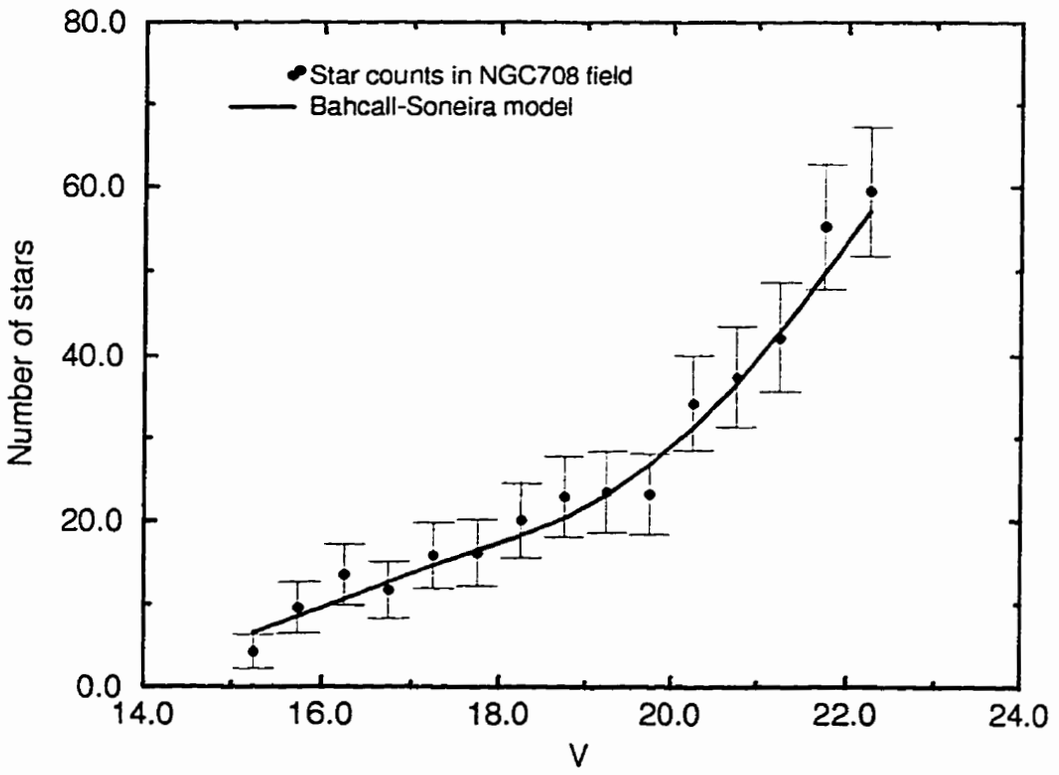

5.3 UGC1308

The field around UGC1308 was observed in V and I for a total of 1200s. The usual procedure of subtraction of bright galaxies was applied.

We plot r_{-2} vs V for this field in Figure 5.10, where we also show the 'cut' made for star-galaxy separation. As above, our simulations show that $r_{-2} = 1.80 \pm 0.08$ at $V = 22.15$, $r_{-2} = 1.75 \pm 0.18$ at $V = 22.65$ and $r_{-2} = 1.75 \pm 0.28$ at $V = 23.15$. We choose $r_{-2} = 2.15$ as our 'cut' for star galaxy separation to $V = 22.5$ A table of objects, galaxies and stars is shown in Table 5.3 and the data are plotted in Figure 5.11. Figure 5.12 shows the number of galaxies in this field and the estimated background count fit. We can notice a clear excess of bright objects above the background counts in this field. We compute the number of background galaxies in Table 5.4 and plot the data in Figure 5.13.

Using maximum likelihood methods, we find that the slope of the counts is best fit by:

$$\alpha = -1.38 \pm 0.09$$

There is only a 5% chance that the slope of the LF is steeper than $\alpha = -1.5$, and a 22% chance that it is flatter than $\alpha = -1.3$. The error quoted above is 1σ; the LF slope may not be flatter than $\alpha = -1.15$ at the 99% percentile level.

It is of course surprising that a LF may be derived for this 'outer' field

and not for the inner field. If we analyze the radial distribution of galaxies as plotted in Figure 5.14 we note that galaxies appear to cluster in the proximity of UGC1308, even if this is not the central cluster elliptical.

Figure 5.10: Plot of r_{-2} vs V for UGC1308 field in A262 and cut for star galaxy separation

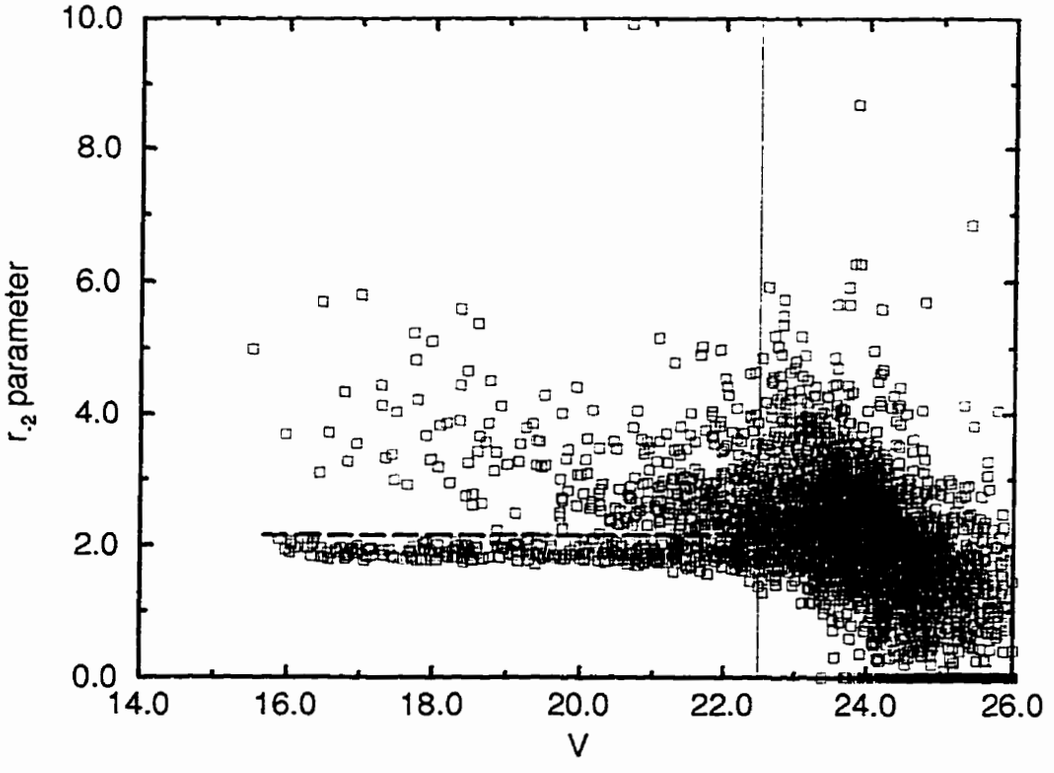

Table 5.3: NUMBER COUNTS FOR UGC1308 FIELD IN V

V	N. of objects	N. of galaxies	N. of stars	Completeness
15.75	4.55 ± 2.13	2.27 ± 1.51	2.27 ± 1.51	1
16.25	14.46 ± 3.80	2.18 ± 1.48	12.27 ± 3.50	1
16.75	23.82 ± 4.88	4.28 ± 2.07	19.55 ± 4.42	1
17.25	18.55 ± 4.31	6.45 ± 2.54	12.09 ± 3.48	1
17.75	29.09 ± 5.39	8.46 ± 2.91	20.64 ± 4.54	1
18.25	36.55 ± 6.05	10.45 ± 3.23	26.09 ± 5.11	1
18.75	31.72 ± 5.63	13.91 ± 3.73	17.81 ± 4.22	1
19.25	41.46 ± 6.44	12.00 ± 3.46	29.45 ± 5.43	1
19.75	33.37 ± 5.78	16.37 ± 4.05	17.00 ± 4.12	1
20.25	54.02 ± 7.35	22.82 ± 4.78	31.19 ± 5.59	1
20.75	69.57 ± 8.34	34.74 ± 5.89	34.83 ± 5.90	1
21.25	114.56 ± 10.70	62.83 ± 7.93	51.74 ± 7.19	1
21.75	133.47 ± 11.55	89.57 ± 9.46	43.91 ± 6.63	1
22.25	227.59 ± 15.09	144.00 ± 12.00	83.59 ± 9.14	1

Figure 5.11: Number counts for objects, stars and galaxies in the UGC1308 field in A262: V band

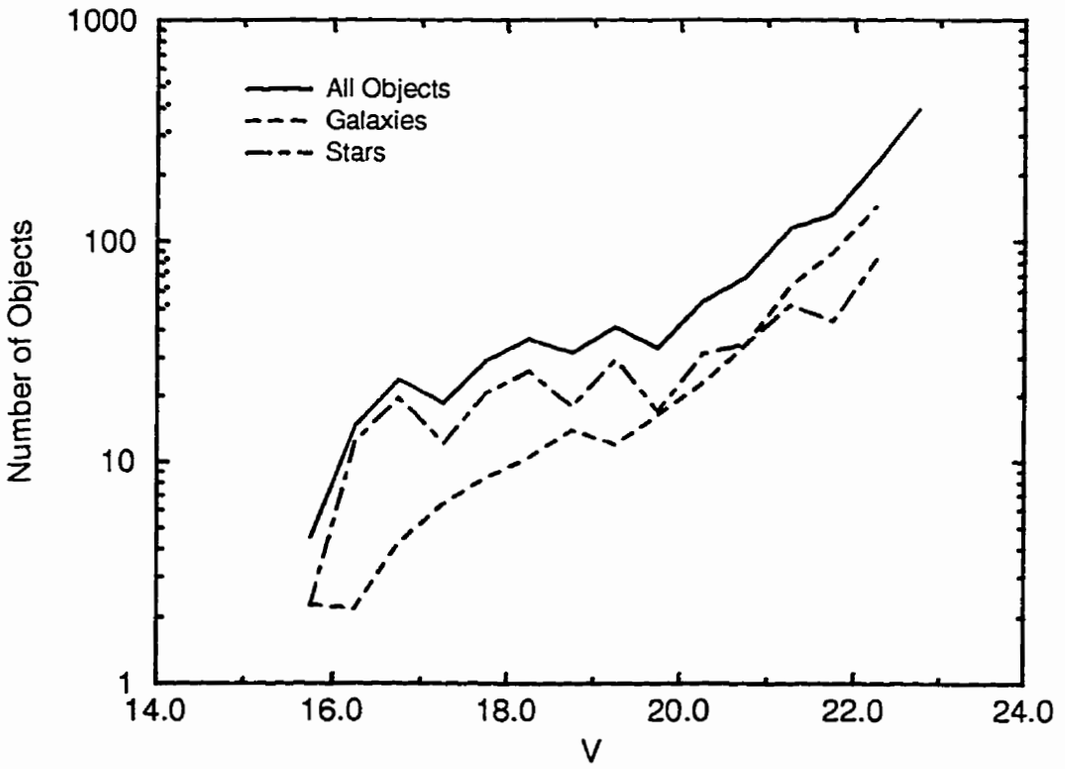

Table 5.4: GALAXY COUNTS IN UGC1308 FIELD IN V

V	N. of galaxies	Background counts	Cluster members
15.75	2.27 ± 1.51	0.29	1.98 ± 1.60
16.25	2.18 ± 1.48	0.46	1.72 ± 1.63
16.75	4.28 ± 2.07	0.72	3.56 ± 2.24
17.25	6.45 ± 2.54	1.15	5.30 ± 2.76
17.75	8.46 ± 2.91	1.82	6.64 ± 3.21
18.25	10.45 ± 3.23	2.88	7.57 ± 3.65
18.75	13.91 ± 3.73	4.57	9.34 ± 4.30
19.25	12.00 ± 3.46	7.24	4.76 ± 4.38
19.75	16.37 ± 4.05	11.48	4.89 ± 5.28
20.25	22.82 ± 4.78	18.20	4.62 ± 6.41
20.75	34.74 ± 5.89	28.84	5.90 ± 7.97
21.25	62.83 ± 7.93	45.71	17.12 ± 10.42
21.75	89.57 ± 9.46	72.44	17.13 ± 12.73
22.25	144.00 ± 12.00	114.82	29.18 ± 16.09

Figure 5.12: Number of galaxies and background counts for UGC1308 field

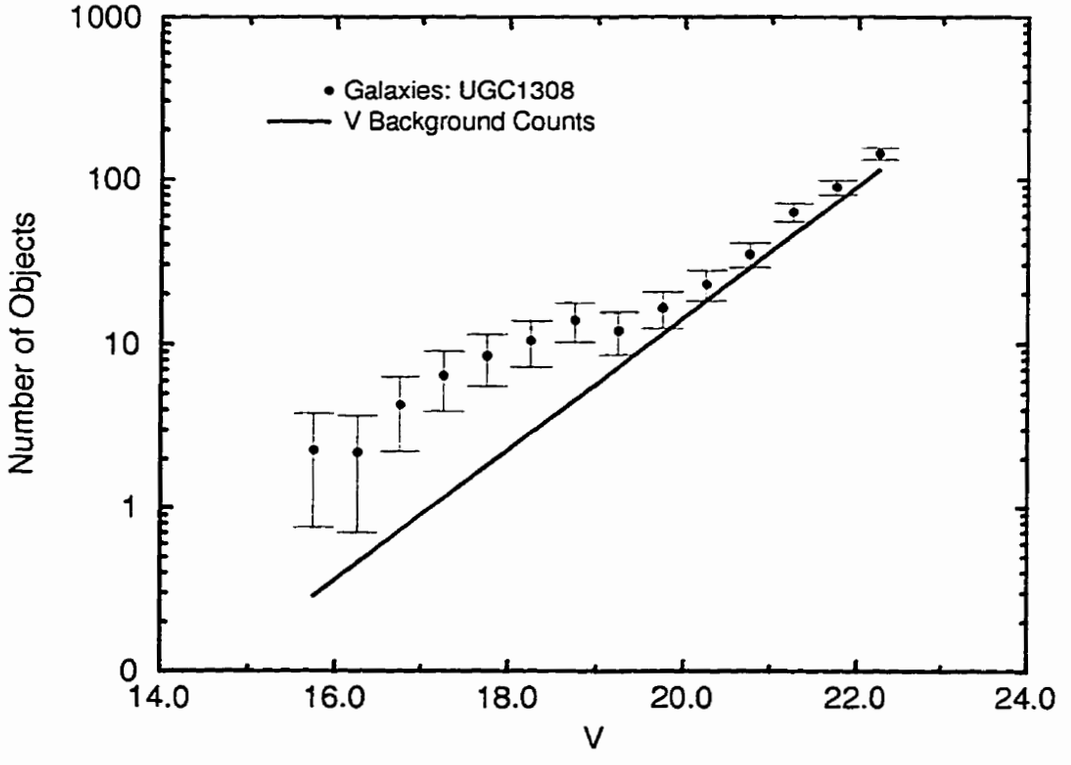

Figure 5.13: Number of galaxies and LF fit for UGC1308 field in V

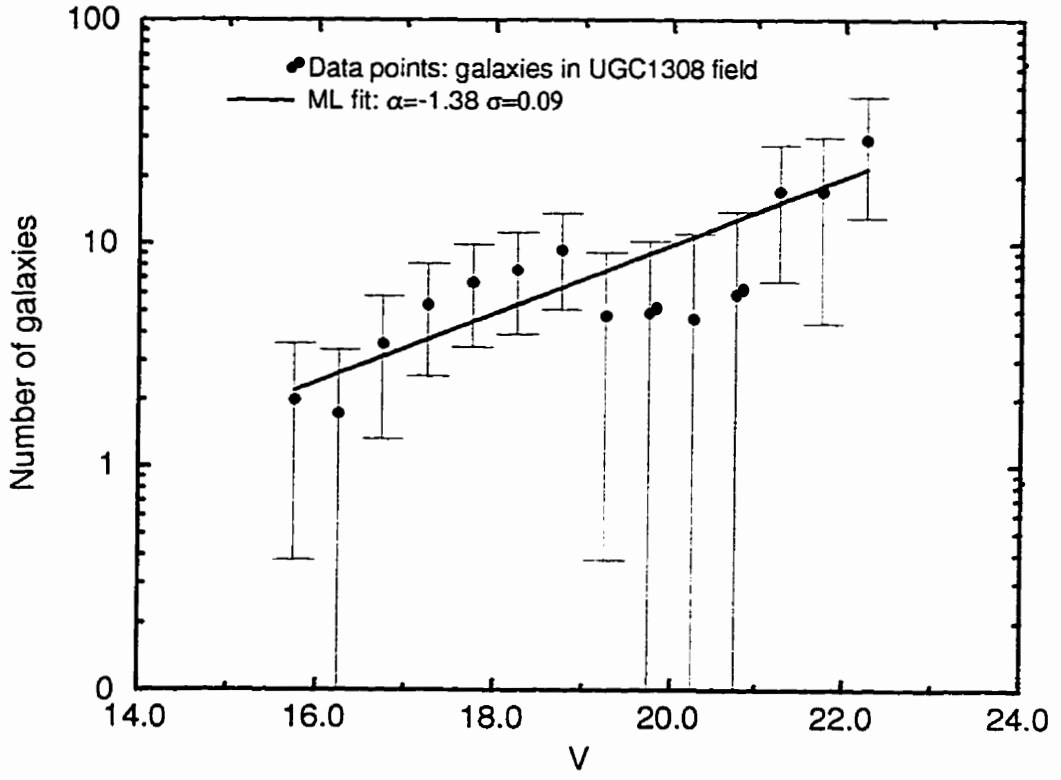

Figure 5.14: Radial distribution of galaxies for UGC1308 field in V

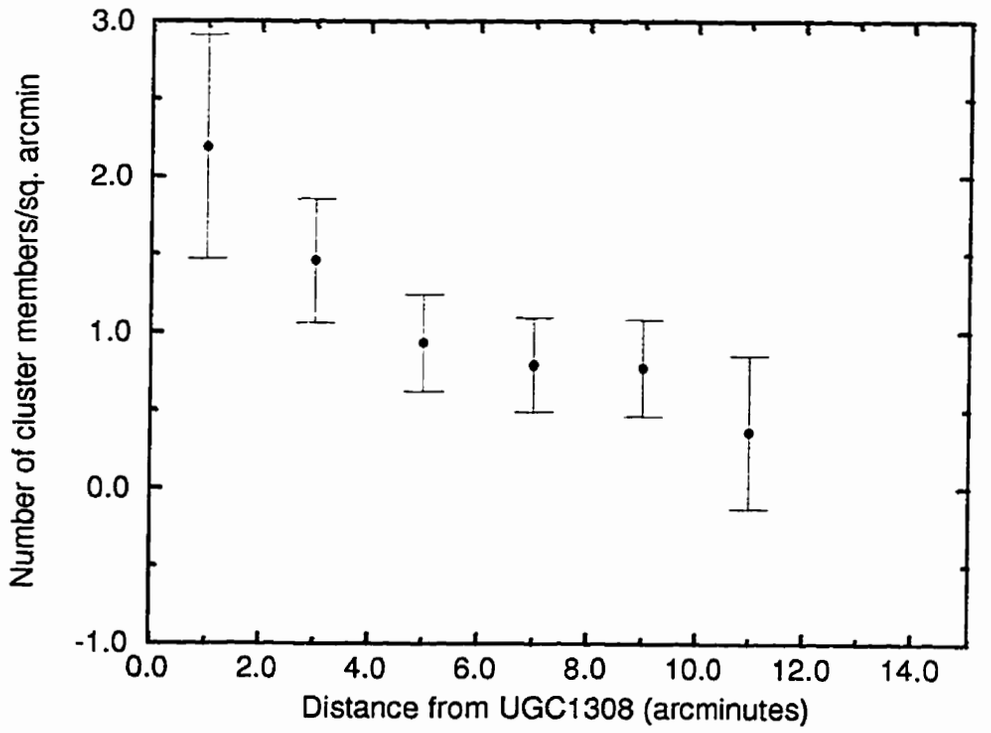

Figure 5.15: Galaxies in the inner 5′ of the UGC1308 field in V

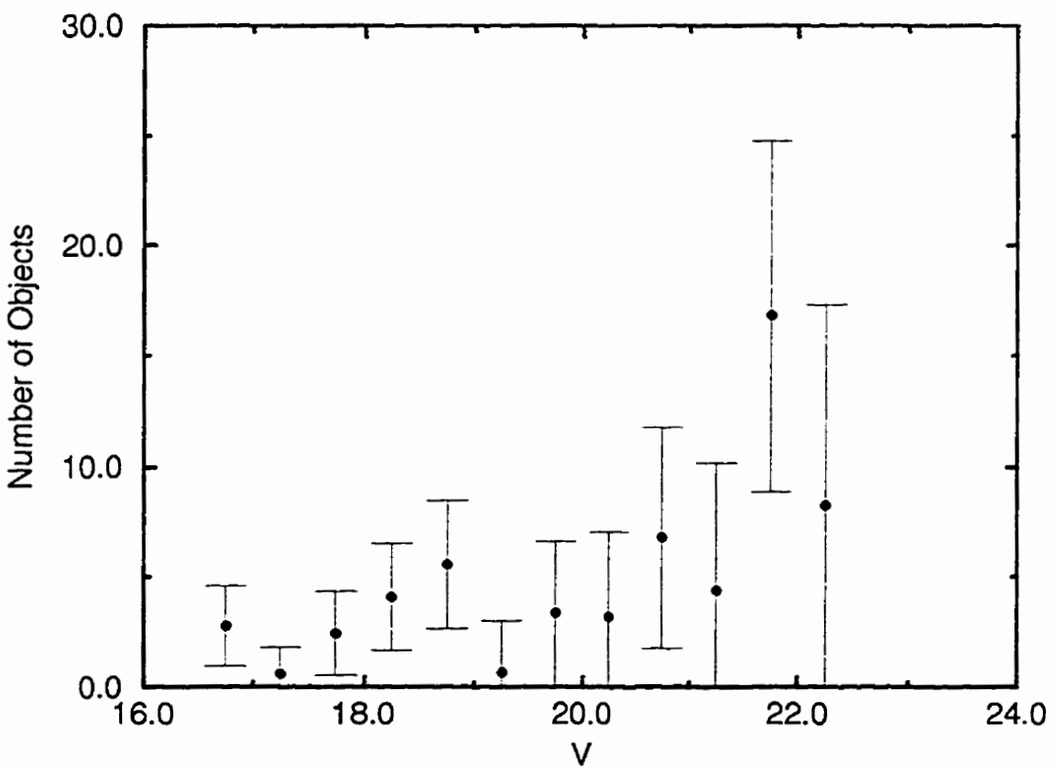

Figure 5.16: Galaxies more distant than 5′ from UGC1308 field in V

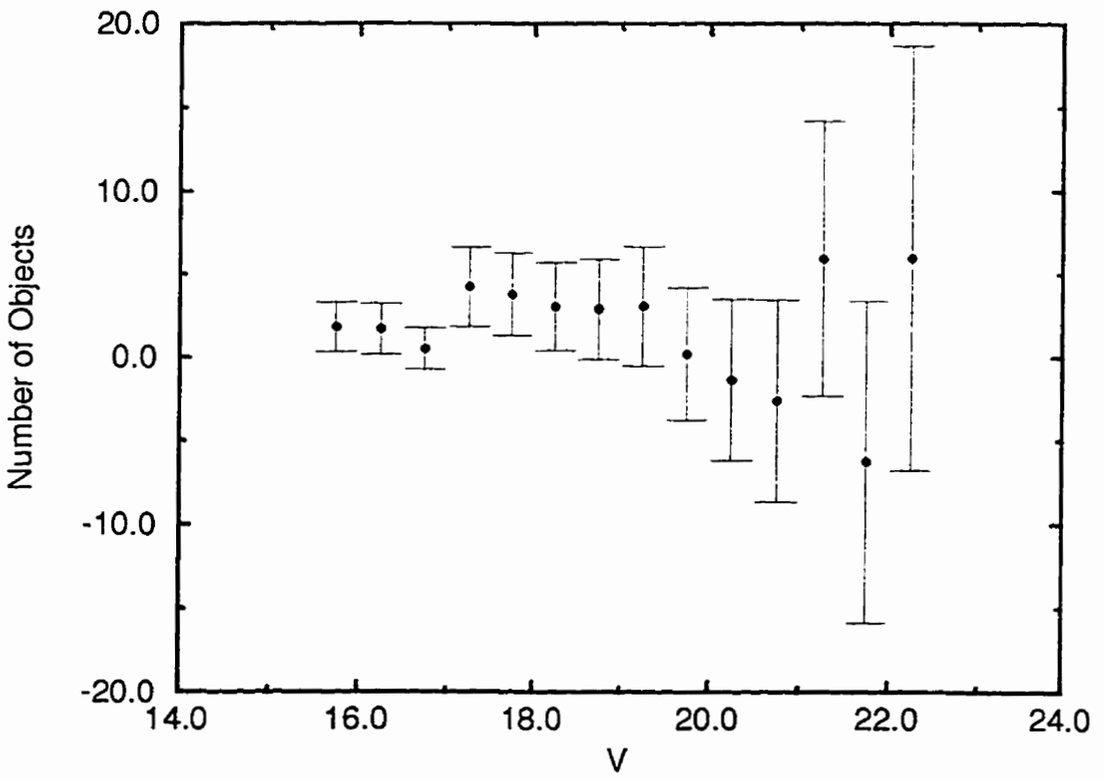

Figure 5.17: Comparison of 'inner' and 'outer' fields for UGC1308 field in V

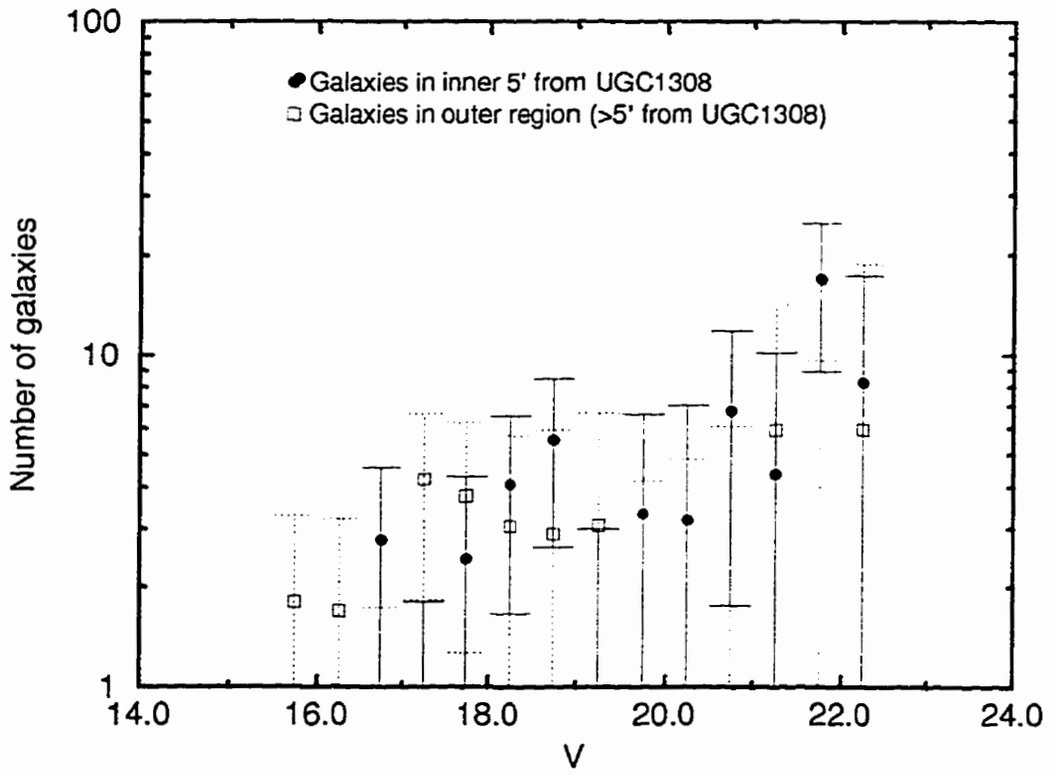

Figure 5.18: LF for galaxies in inner 5′ of UGC1308 field in V

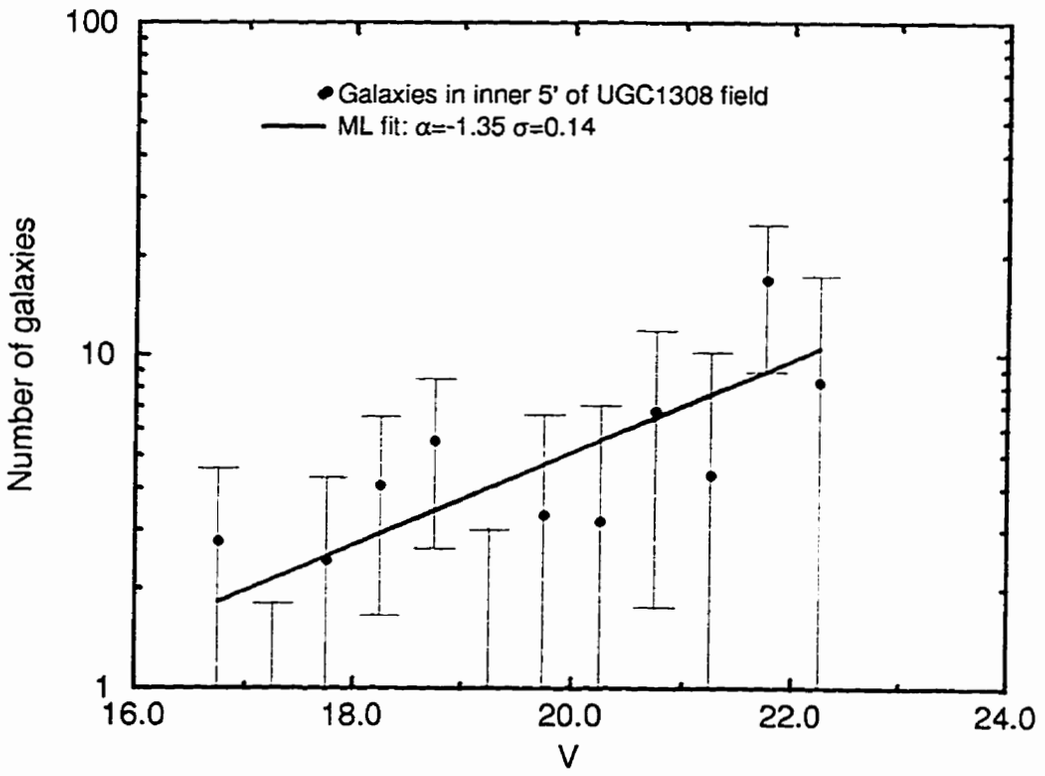

We plot the number of objects vs V in Figure 5.15 for the inner 5′ and in Figure 5.16 for the region outside of 5′ from UGC1308. A comparison of data in these two regions is shown in Figure 5.17. A fit to the LF for galaxies in inner 5' is shown in Figure 5.18. Maximum likelihood methods yield $\alpha = -1.35 \pm 0.14$, which is consistent with the slope derived for the entire field. No LF may be derived for galaxies in the outer regions of this field.

We now analyze findings for our I band data.

We plot r_{-2} vs I in Figure 5.19, with the 'cut' made for star galaxy separation shown. At $I = 21$, we find that $r_{-2} = 1.62 \pm 0.12$ and at $I = 21.5$ $r_{-2} = 1.60 \pm 0.12$. We therefore choose $r_{-2} = 1.85$ as our 'cut' for star-galaxy separation to $I = 21.5$. Table 5.5 shows the number of objects. galaxies and stars present in the field, which are also plotted in Figure 5.20. Figure 5.21 plots the total number of objects in the field and the I band fit by Tyson (1988) after normalization for field size.

The quality of the I data is insufficient to determine an accurate LF, but we see that there is a significant excess of faint galaxies in I. We plot the radial distribution of objects in Figure 5.22, where we again see that there is an excess over the 'smooth' distribution of background galaxies at small distances from UGC1308.

We plot the number of galaxies within 5′ of UGC1308 and galaxies outside of this region in Figures 5.23 and 5.24 and compare these data in Figure 5.25.

The two distributions do not appear to differ significantly. The data are too noisy to obtain a reliable α for galaxies in this field.

Similar results are obtained if we use the steeper fit we obtained for the I band background field. The I data are too poor for any meaningful result to be derived.

Figure 5.19: The plot of r_{-2} vs I for UGC1308 in I

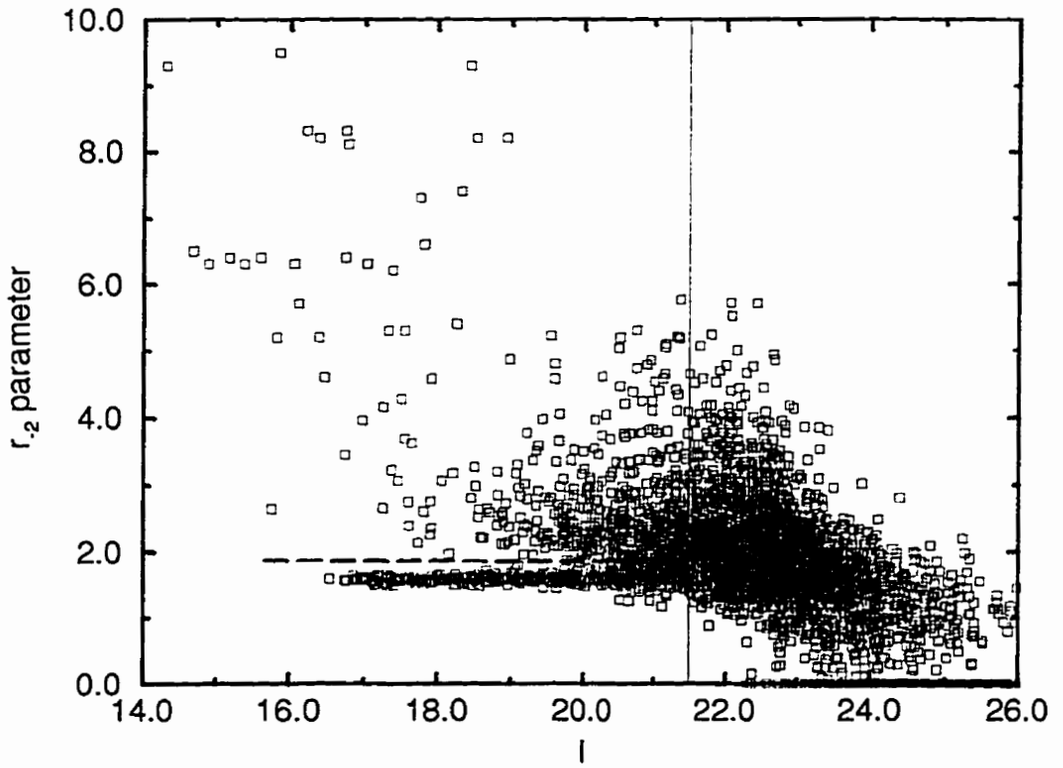

Table 5.5: NUMBER COUNTS IN UGC1308 FIELD IN *I*

V	N. of objects	N. of galaxies	N. of stars	Completeness
15.25	2.00 ± 1.41	2.00 ± 1.41	0.00 ± 0.00	1
15.75	5.00 ± 2.24	5.00 ± 2.24	0.00 ± 0.00	1
16.25	8.88 ± 2.98	8.88 ± 2.98	0.00 ± 0.00	1
16.75	18.76 ± 4.33	6.44 ± 2.54	12.32 ± 3.51	1
17.25	43.96 ± 6.63	11.88 ± 3.45	32.08 ± 5.66	1
17.75	43.96 ± 6.63	16.32 ± 4.04	27.64 ± 5.26	1
18.25	43.52 ± 6.60	9.00 ± 3.00	34.52 ± 5.88	1
18.75	59.28 ± 7.70	25.20 ± 5.02	34.08 ± 5.84	1
19.25	73.72 ± 8.59	32.20 ± 5.67	41.52 ± 6.44	1
19.75	124.68 ± 11.17	66.64 ± 8.16	58.04 ± 7.62	1
20.25	169.20 ± 13.01	119.68 ± 10.94	48.52 ± 6.97	1
20.75	247.80 ± 15.74	162.00 ± 12.73	85.80 ± 9.26	1

Figure 5.20: Number counts for objects, stars and galaxies in UGC1308 *I*

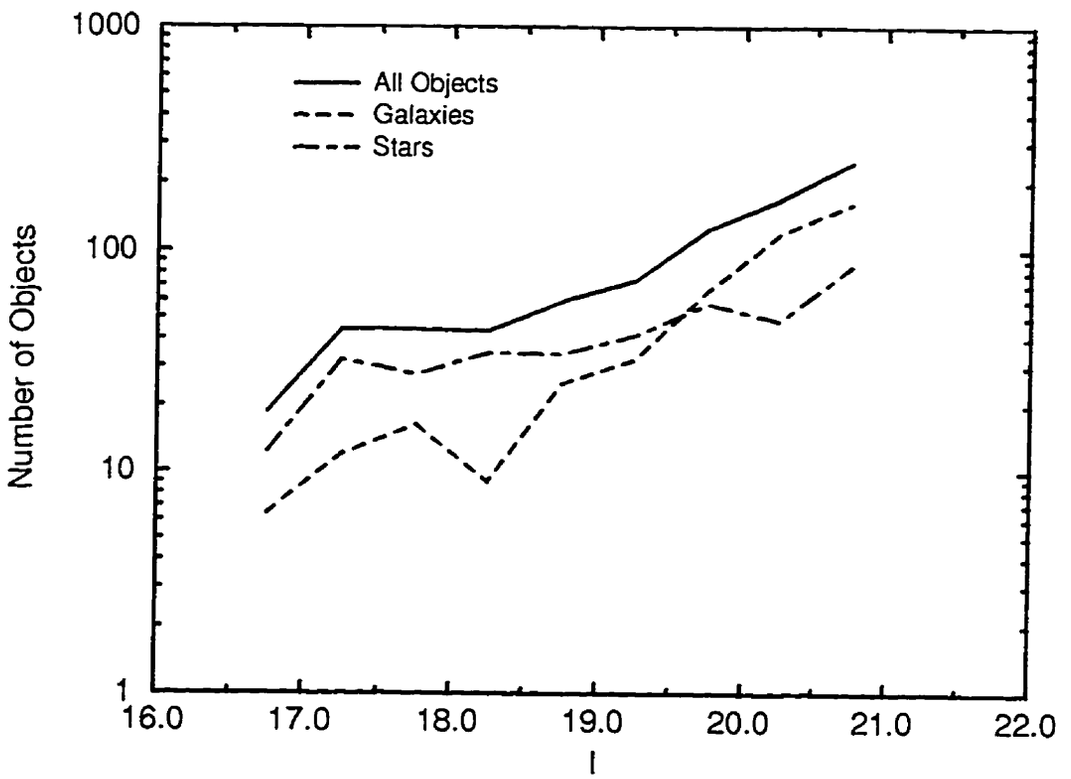

Table 5.6: GALAXY COUNTS IN UGC1308 FIELD IN I

V	N. of galaxies	Background counts	N. of cluster members
15.25	2.00 ± 1.41	1.53	0.47 ± 1.88
15.75	5.00 ± 2.24	2.26	2.74 ± 2.70
16.25	8.88 ± 2.98	3.35	5.53 ± 3.50
16.75	6.44 ± 2.54	4.95	1.49 ± 3.38
17.25	11.88 ± 3.45	7.33	4.55 ± 4.39
17.75	16.32 ± 4.04	10.84	5.48 ± 5.21
18.25	9.00 ± 3.00	16.03	-7.03 ± 5.00
18.75	25.20 ± 5.02	23.71	1.49 ± 6.99
19.25	32.20 ± 5.67	35.08	-2.88 ± 8.20
19.75	66.64 ± 8.16	51.88	14.76 ± 10.88
20.25	119.68 ± 10.94	76.74	42.94 ± 14.01
20.75	162.00 ± 12.73	113.50	48.50 ± 16.60

Figure 5.21: Number counts for cluster members in UGC1308 *I*

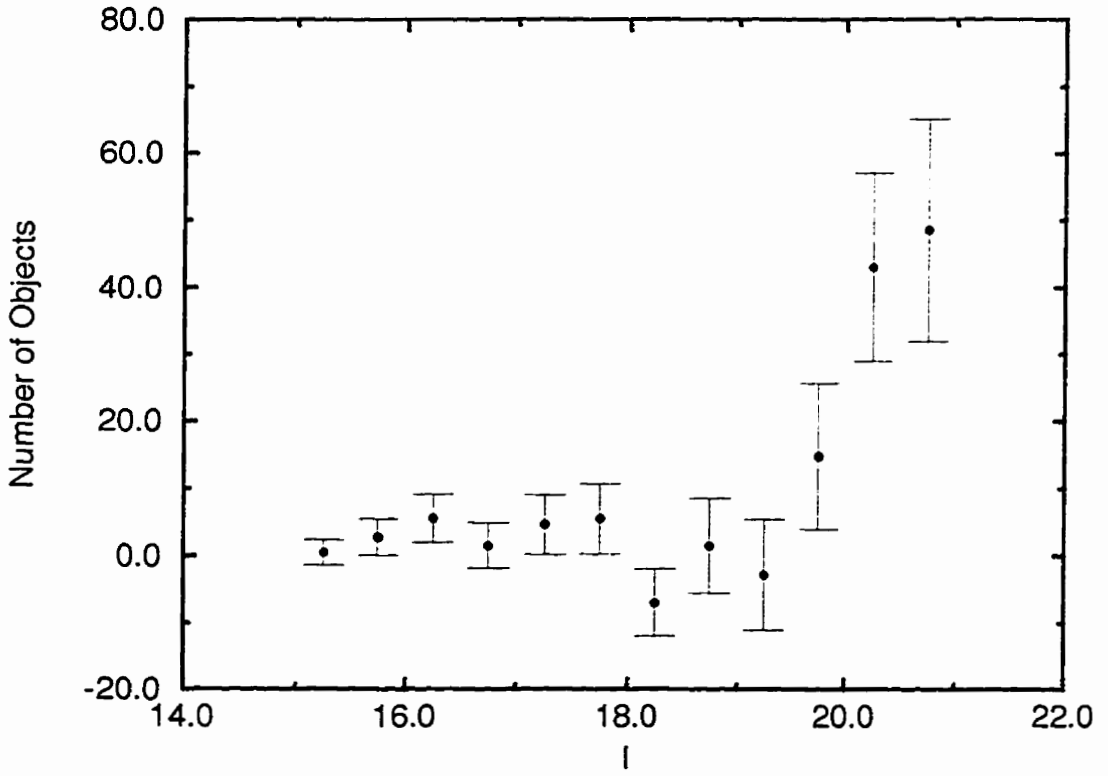

Figure 5.22: Radial distribution for cluster members in UGC1308 *I*

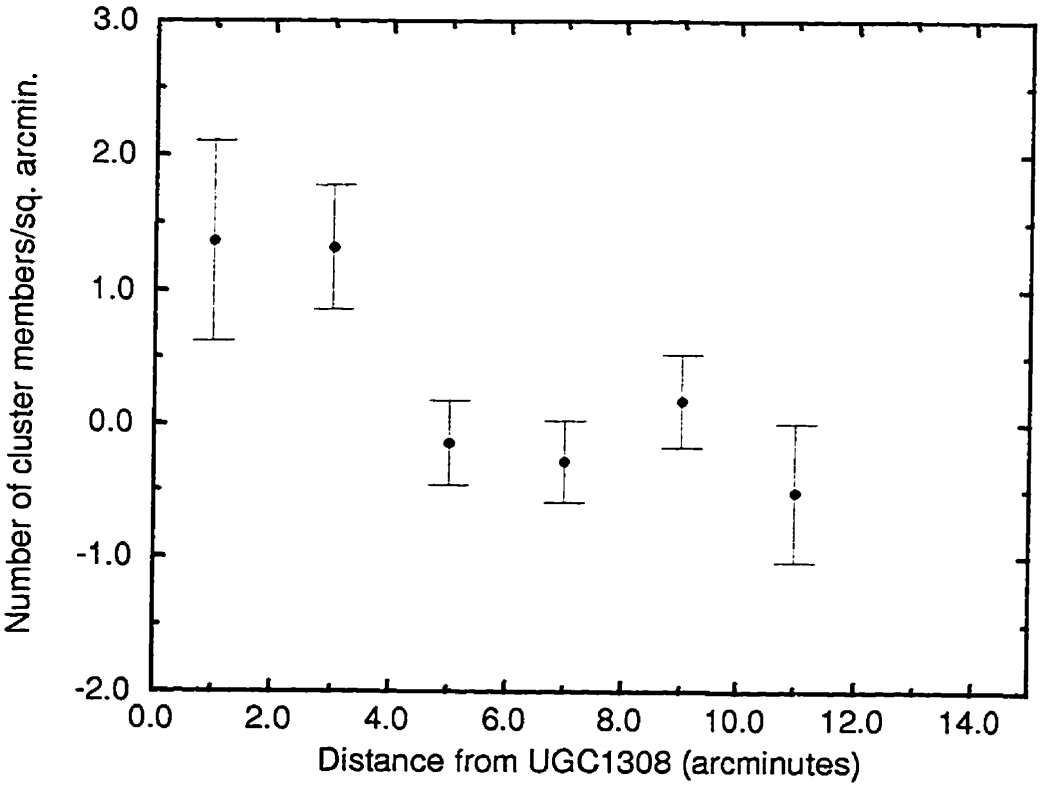

Figure 5.23: Number counts for cluster members in the inner 5′ of UGC1308
I

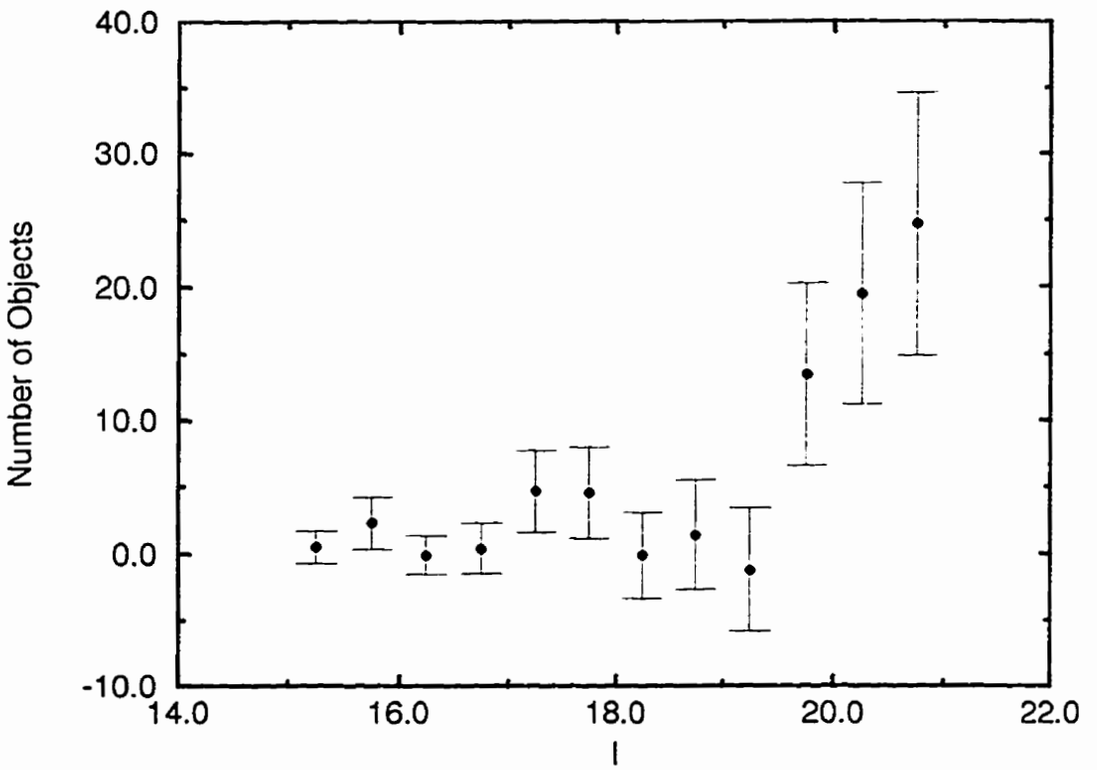

Figure 5.24: Number counts for cluster members more distant than 5′ from UGC1308

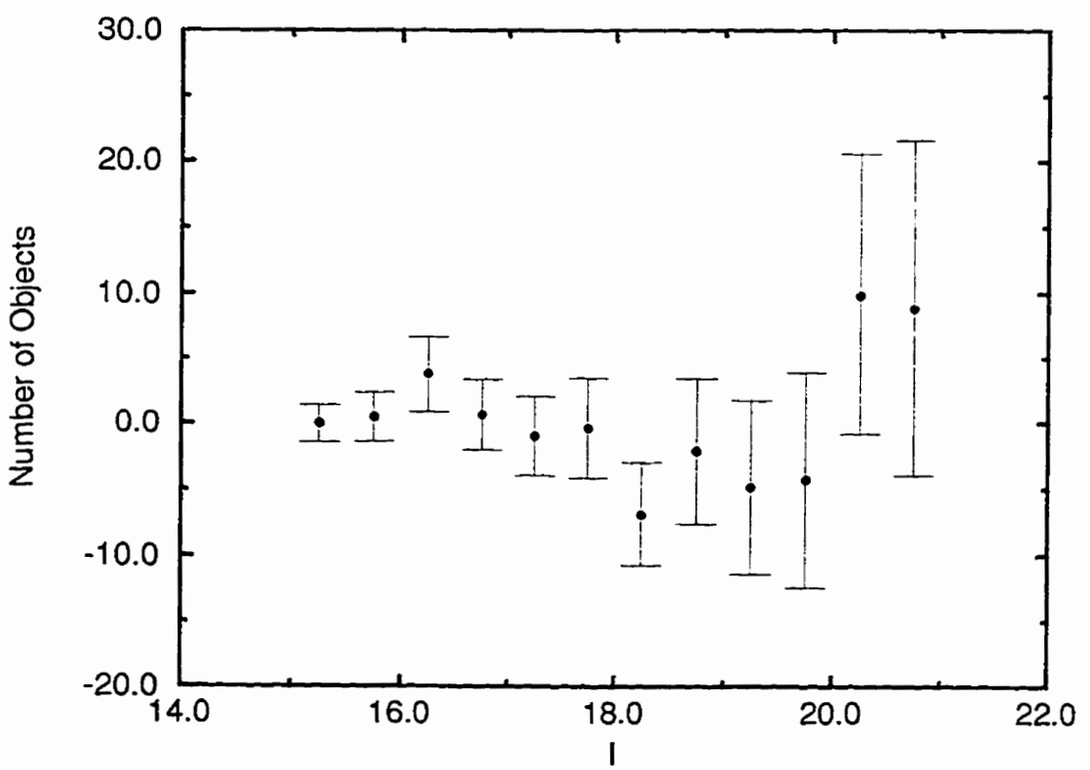

Figure 5.25: Comparison of number counts in inner and outer regions of UGC1308 field

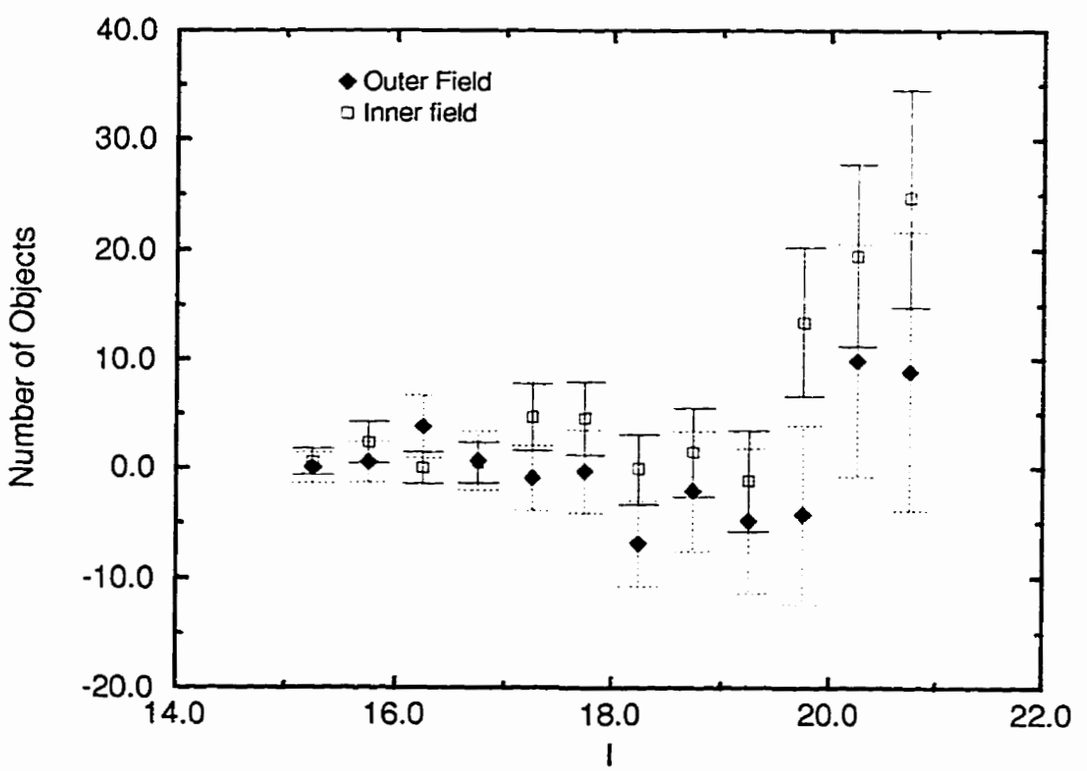

We can now consider the distribution of galaxy colors in the UGC1308 field. We plot V vs $V-I$ for galaxies in this field in Figure 5.26. No strong signal is detectable from cluster members: as a matter of fact the median color of galaxies in this field is about 1.2, which is consistent with the median color of field objects (see above); thus the cluster contribution is probably not strong enough to yield the tight color-magnitude correlation observed by Secker & Harris (1995) in Coma.

A histogram of the color distribution is given in Figure 5.27. As we can see the distribution peaks at $V-I \sim 1.2$ (the median $V-I$ is 1.18) with a decline to redder colors. This should be compared with the distribution for background galaxies above, which appears to be somewhat more symmetrical.

In this particular case, it appears to be impossible to determine a color magnitude diagram for cluster members (only) by statistical subtraction, as described for NGC1275 below, as too few objects are left to obtain any meaningful results.

Is there a color gradient in the proximity of UGC1308 ? We plot average color as a function of radius in Figure 5.28 and see that the average color is approximately constant at all distances from UGC1308.

The color magnitude for stars is shown in Figure 5.29.

A comparison of V and I star counts and their color distribution for the UGC1308 field is shown in Figures 5.30 – 5.32. The shapes of the distributions agree very well, but the model overestimates the number of stars in

this field by about 40%. The normalization shown here is arbitrary and is chosen by taking the mean of the ratio between the number of stars in each magnitude bin in the observations and in the model over a 1 square degree field.

Finally we plot the number of stars in NGC708, UGC1308 and the Abell 262 background field in V in Figure 5.33. The agreement between the three fields is excellent. The same plot is shown for I in Figure 5.34 and the agreement is again very good.

Figure 5.26: Color magnitude diagram for galaxies in UGC1308 field

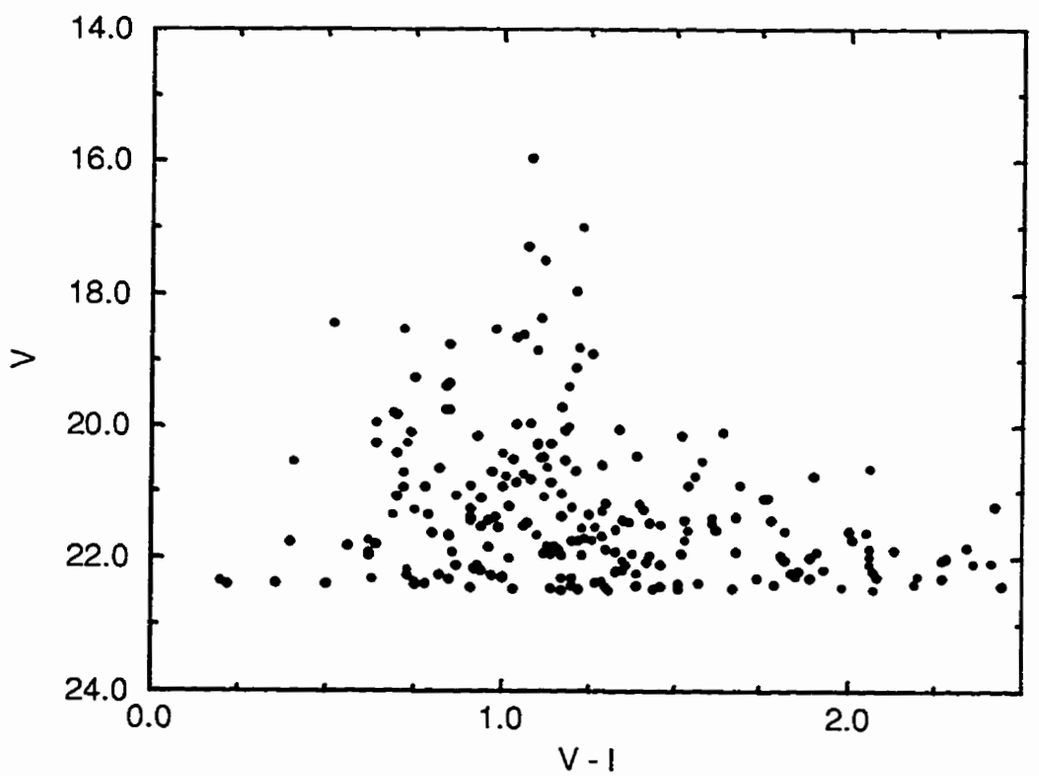

Figure 5.27: Histogram of color distribution for galaxies in UGC1308 field

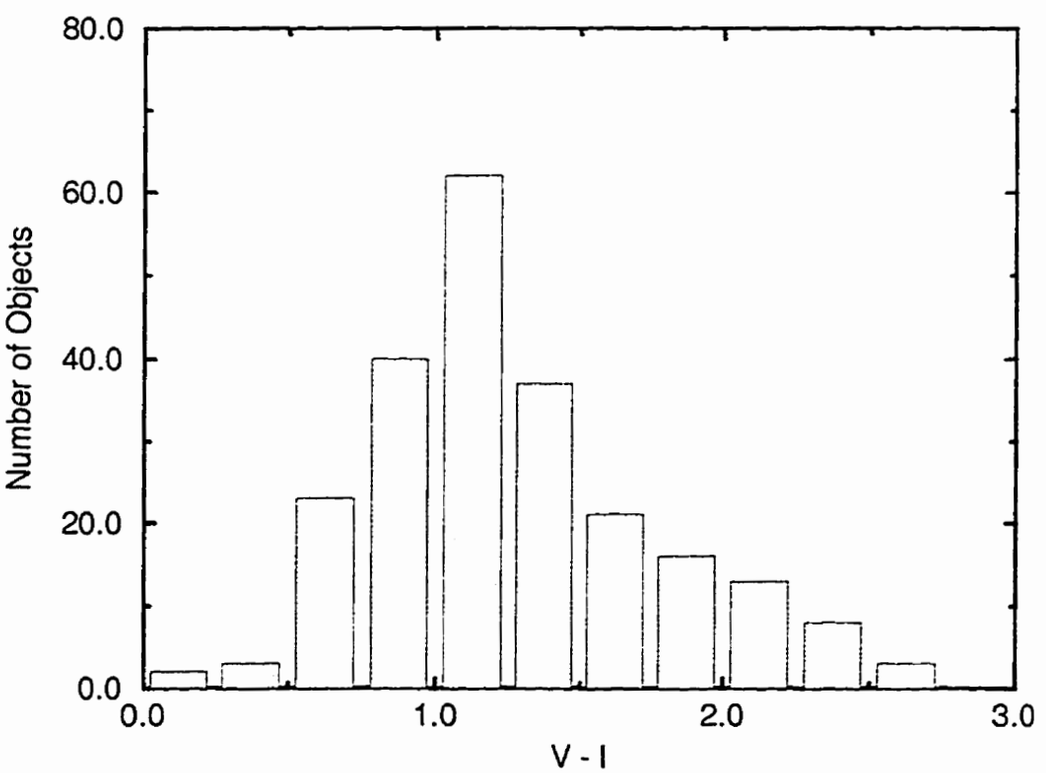

Figure 5.28: Radial distribution of average galaxy color for UGC1308 fields

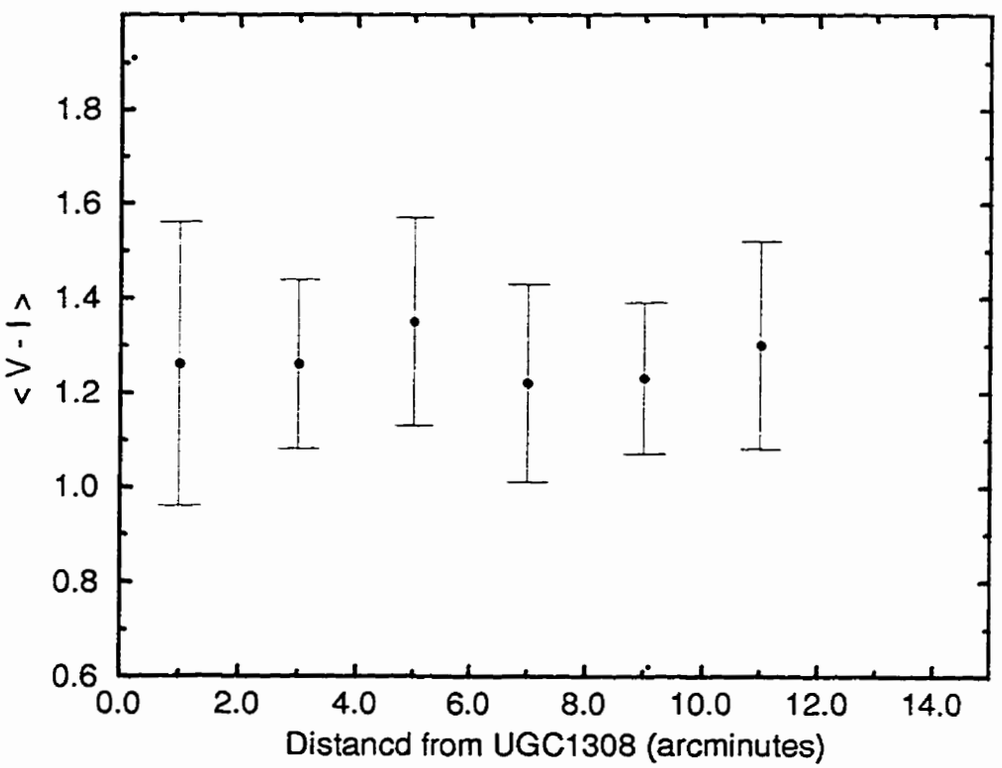

Figure 5.29: Color magnitude diagram for stars in UGC1308 field

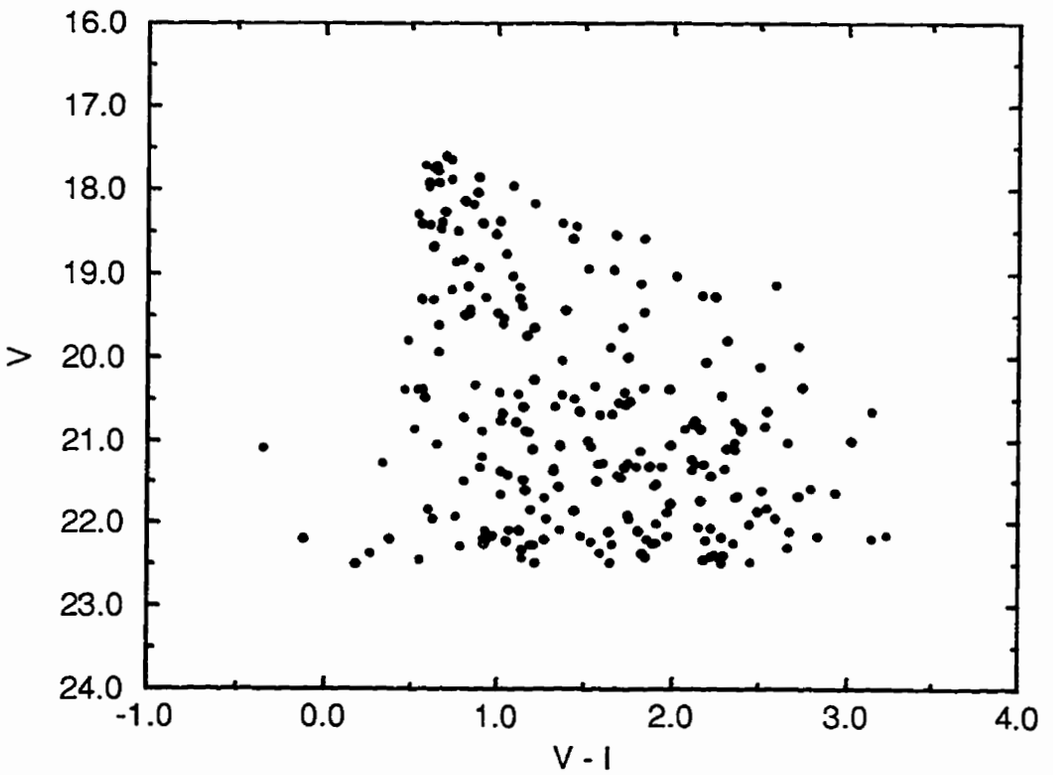

Figure 5.30: Star counts and model for UGC1308 field in V

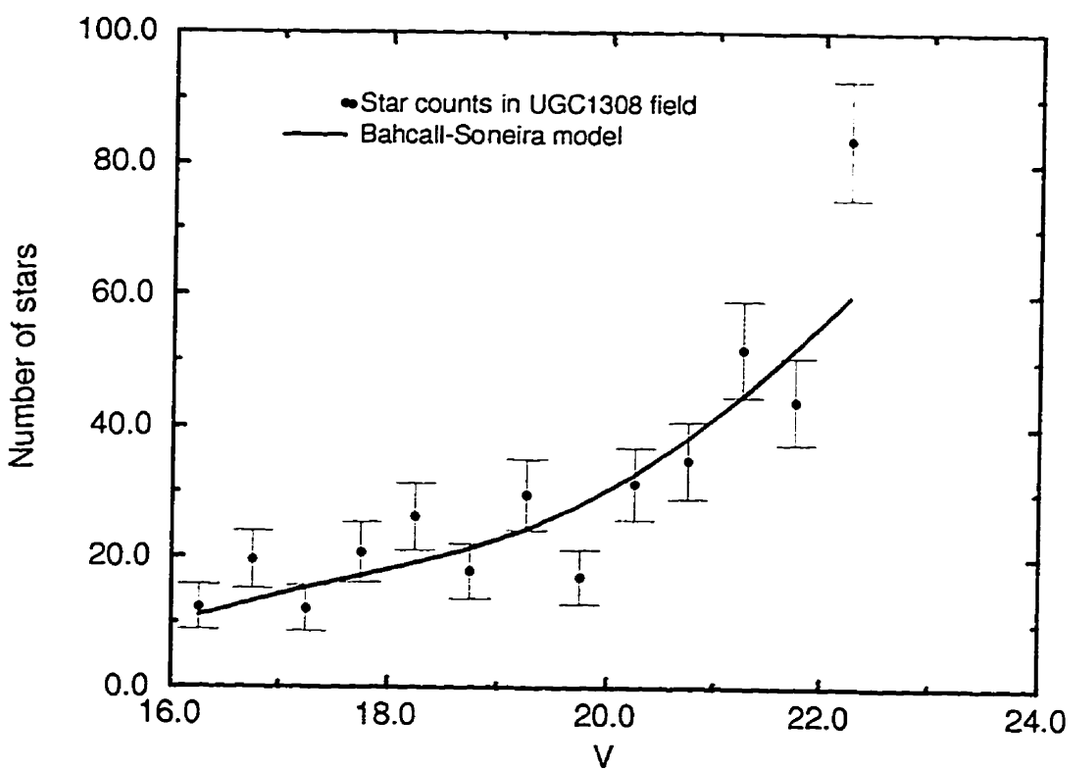

Figure 5.31: Star counts and model for UGC1308 field in I

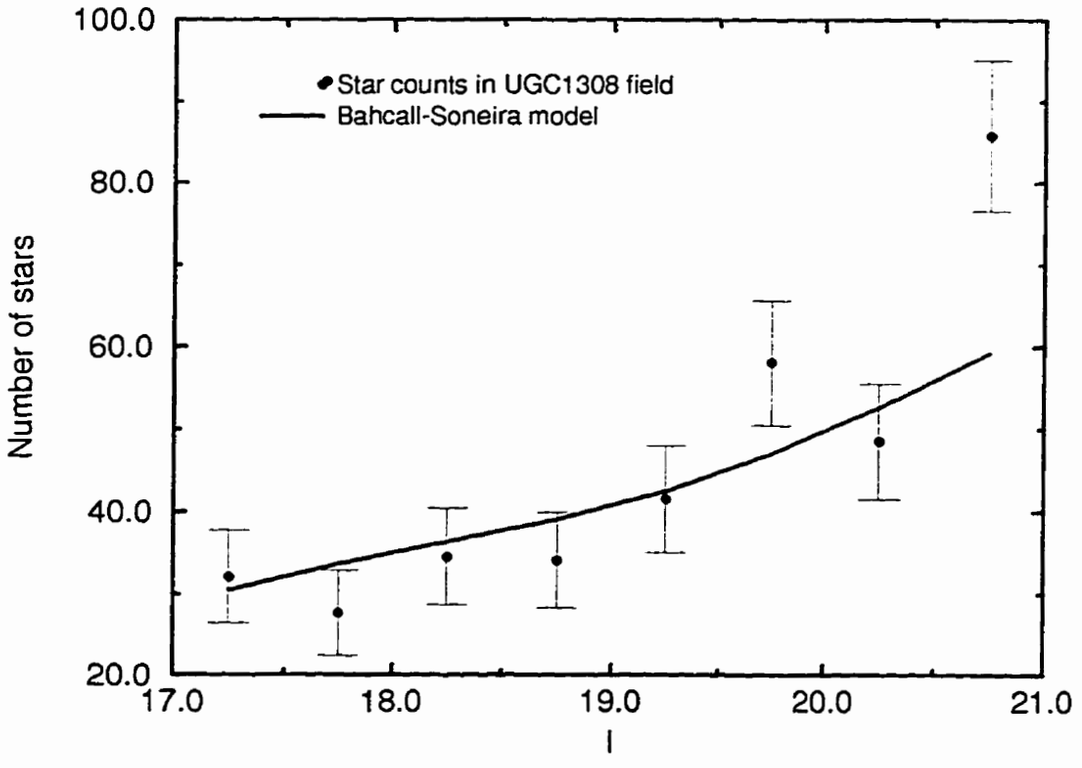

Figure 5.32: Color distribution and model for stars in UGC1308 field

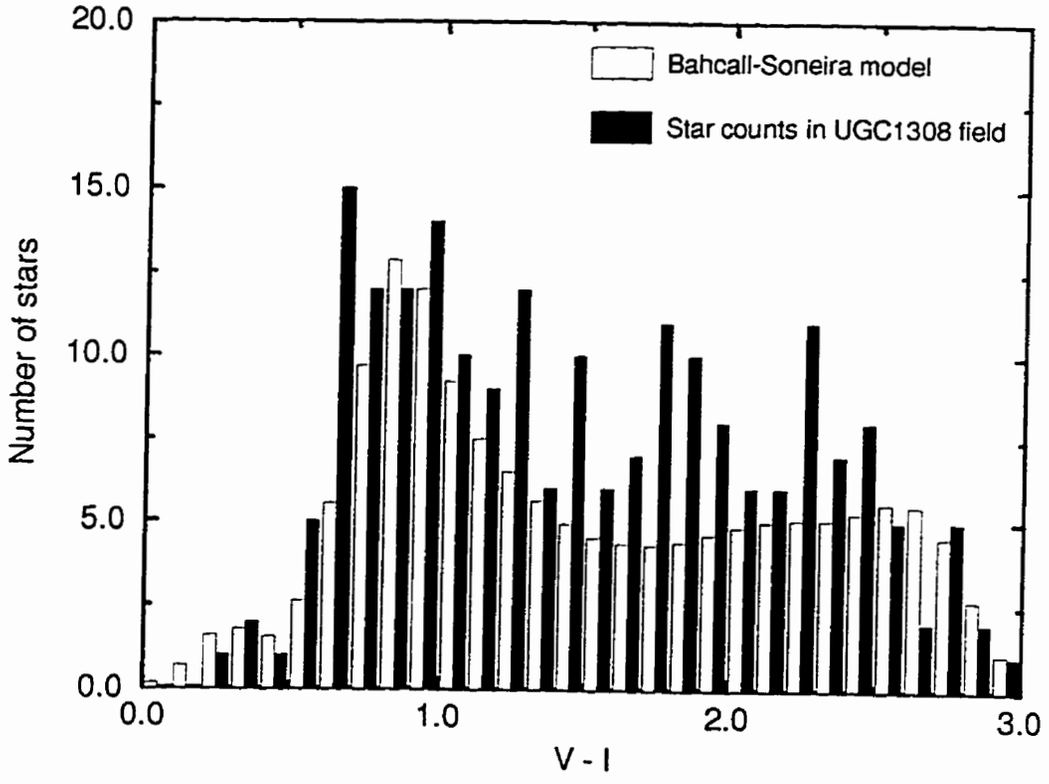

Figure 5.33: Star counts in V for NGC708, UGC1308 and background fields

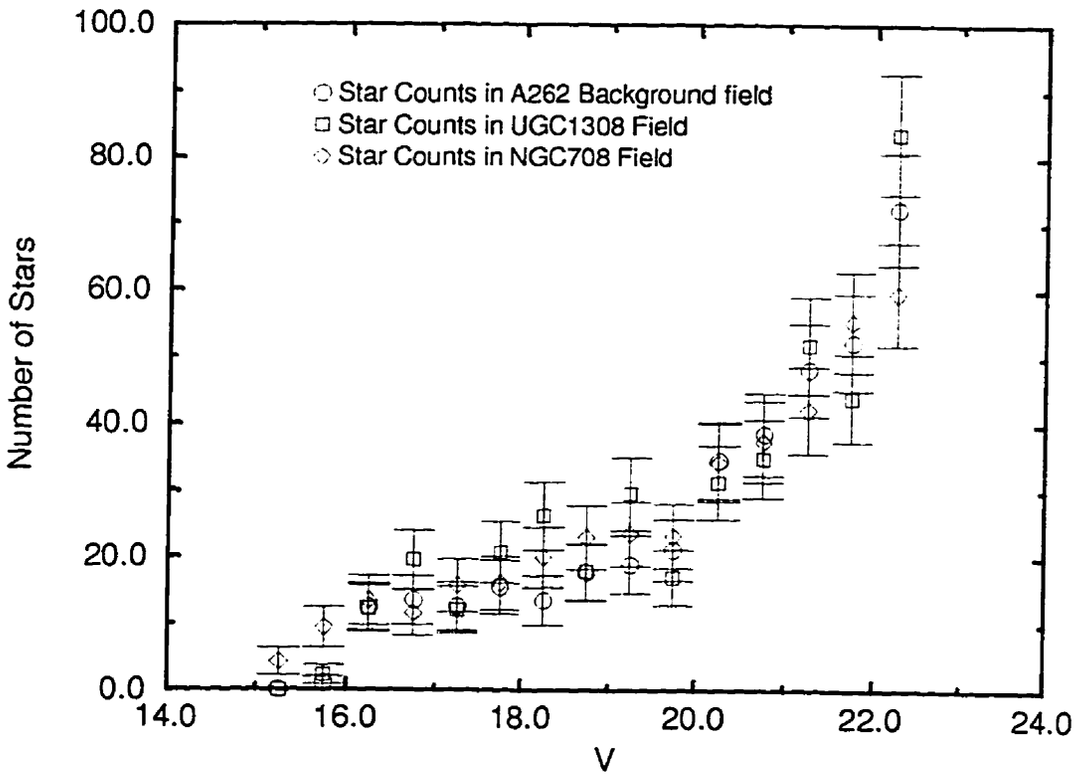

Figure 5.34: Star counts in I for UGC1308 and background fields

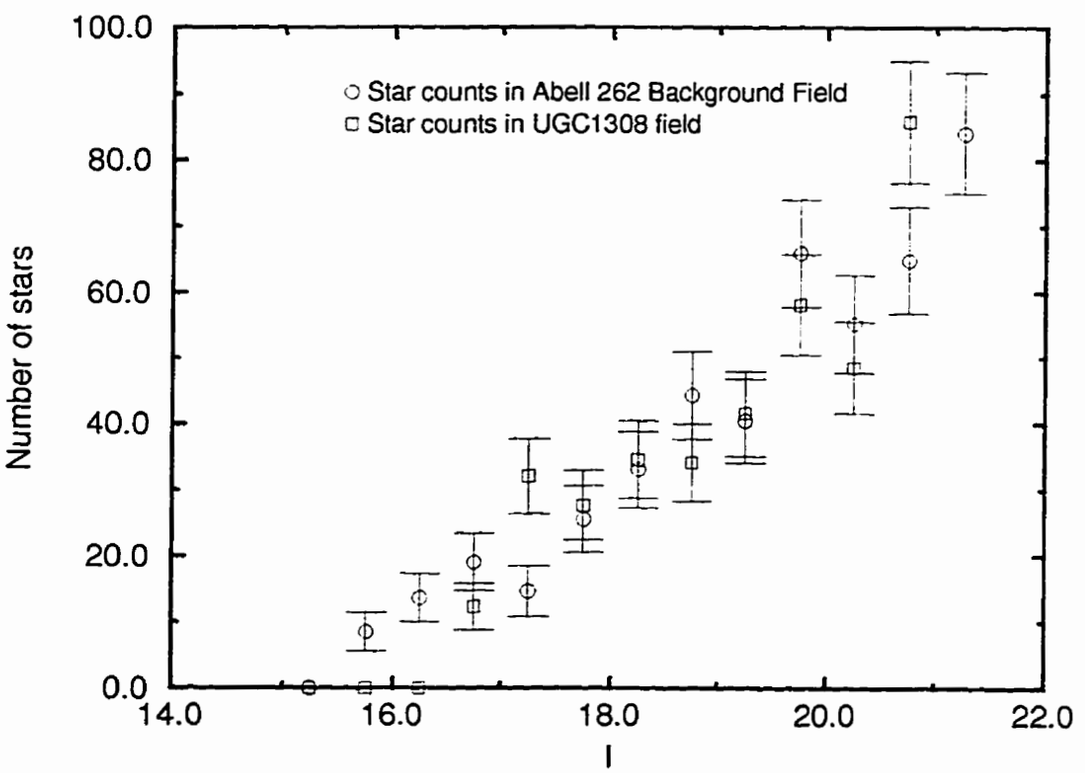

5.4 Interpretation

Our observations of two fields in Abell 262, centred on the bright ellipticals NGC708 and UGC1308 show that: (i) there appears to be little contribution from cluster dwarfs in the central field of the cluster (NGC708); (ii) a LF with a slope of $\alpha \sim -1.35$ can be derived for the field around UGC1308 (V images); (iii) these galaxies appear to be concentrated near UGC1308 and (iv) there is no strong signal from cluster galaxies in the color-magnitude plot.

We may interpret our result in UGC1308 as being due to satellites of this giant elliptical galaxy. This would be consistent with the apparent central concentration of these objects around UGC1308, even if this is not a central galaxy.

It is more complex to explain the null result in the NGC708 field. One possibility is that the cluster contribution is too rarefied to be detected by our relatively crude methods of statistical subtraction. A more intriguing possibility is that dynamical evolution has destroyed dwarf galaxies in this environment. Dwarfs around UGC1308 would survive because this galaxy has not yet fallen in the cluster core.

Chapter 6

Abell 426

6.1 Introduction

Abell 426 is the major cluster concentration in the Perseus-Pisces filament. It lies at $l = 150.6$ and $b = -13.3$ and a redshift of 0.0183. Jones & Forman (1984) classify this cluster as a late XD object, with a high X-ray luminosity ($L_X = 4.61 \times 10^{44}$ ergs/s) and a small core radius ($r_c = 0.23 - 0.34$). It is dominated by elliptical galaxies (see Figure 6.1) and a cooling flow is present, centred on NGC1275 (Jones & Forman 1984).

Two fields have been observed in this object. One centred on the bright peculiar elliptical NGC1275 and another on the giant elliptical NGC1265, which has the peculiarity that it is one of the few second-ranked galaxies to be found outside of the cluster core. Objects were observed in V and I for a total of 1200s each. Further details may be found in Table 4.1.

6.2 NGC1275

Observations of NGC1275 were taken in slightly substandard seeing (1".0). Both V and I information is available for this field. In Figures 6.1 and 6.2 we show the field around NGC1275 (in V) before and after removal of the brightest giants, as described above. Figures 6.3 shows r_{-2} vs V and the 'cut' made to determine star-galaxy separation. At $V = 21.75$ our simulations show that $r_{-2} = 1.90 \pm 0.18$. At $V = 22.25$ we find that $r_{-2} = 1.86 \pm 0.17$, and at $V = 22.75$ we find $r_{-2} = 1.85 \pm 0.23$. We therefore choose $r_{-2} = 2.25$ as an appropriate 'cut' to $V = 22.5$. Table 6.1 shows the number of objects, galaxies and stars present. We plot these data in Figure 6.4. Photometry was dereddened by 0.54 magnitudes in V and by 0.40 magnitudes in I. These values are consistent with previous determinations (such as those from the NED extragalactic database). We then plot the number of galaxies in these fields and the number of background galaxies in this field in Figure 6.5. Clearly, an excess of faint galaxies is present in this field above the level of contamination.

Table 6.2 gives the number of objects, background galaxies and cluster members, estimated as in § 4.2. We plot these in Figure 6.6, together with the best maximum likelihood fit, which yields:

$$\alpha = -1.93 \pm 0.08$$

There is larger than 99% probability that this LF is steeper than $\alpha = -1.7$. The error quoted above is 1σ. At the 99% percentile, $\alpha < -1.75$. This LF is

consistent with the one found for Abell 2199 by De Propris et al. (1995).

We consider the radial distribution of galaxies in the NGC1275 field in Figure 6.7. As we can see there is a concentration of galaxies in the inner 3′ of this field. At large radii the distribution is flat.

We plot the number of galaxies in the inner 5′ in Figure 6.8 and in the outer fields in Figure 6.9. We compare these in Figure 6.10, where we can see that the distributions appear similar.

We compute the LF for galaxies in the inner 5′ of the NGC1275, and we show this fit in Figure 6.11. A ML fit yields $\alpha = -1.89 \pm 0.15$, which is consistent with the result for the whole field. The LF in this region is certainly steeper than $\alpha = -1.3$, and there is 86% confidence that the LF is steeper than $\alpha = -1.7$. At the 99% percentile level, the LF must be steeper than $\alpha = -1.56$.

Figure 6.12 shows the corresponding plot for the outer regions of the NGC 1275 field. We find that $\alpha = -1.88 \pm 0.10$, which is consistent with both the LF for the entire field and the LF for the inner region of the field. There is 94% confidence that the LF is steeper than $\alpha = -1.75$; the error quoted above is again 1σ. At the 99% percentile level, the LF is steeper than $\alpha = -1.62$. We can now consider the I band data. As usual we use the r_{-2} parameter to separate stars from galaxies, which we plot in Figure 6.13 Our simulations show that at $I = 20.5$, $r_{-2} = 1.92 \pm 0.12$, and at $I = 21.0$ $r_{-2} = 1.88 \pm 0.20$. We therefore choose $r_{-2} = 2.30$ to $I = 21$ as our 'cut' for

star-galaxy separation.

Table 6.3 shows the number of objects, stars and galaxies, and these data are plotted in Figure 6.14. We plot the number of galaxies and the estimated I band counts in Figure 6.15. We tabulate the number of objects, background galaxies and cluster members (Table 6.4) and we plot the number of cluster members vs I in Figure 6.16. Using our fit to data in the A262 background field and maximum likelihood methods, we obtain:

$$\alpha = -1.74 \pm 0.13$$

there is only a 25% chance that the true LF is flatter than $\alpha = -1.7$ and at the 99% percentile level, the LF must be steeper than $\alpha = -1.6$. This result is consistent, within errors, with the V band data. It must be remembered that the background counts for I are more uncertain and the LF is not sampled as faint as the V band data, plus background counts are much larger in this band.

The surface density of galaxies as a function of radius in Figure 6.17 shows us that there does not appear to be any strong concentration of galaxies in I in the NGC1275 field. It must of course be noticed that a large portion of the I frame in NGC1275 is excised because of the difficulty in removing NGC1275. Comparing with Figure 6.7 shows that there is a concentration when the field is imaged in V. We plot the number of galaxies in the inner $5'$ and outside of this region in Figure 6.18 and 6.19. These are compared in Figure 6.20.

Figure 6.21 shows the LF and fit for galaxies in the inner 5′ of the NGC1275 field in I. We get $\alpha = -1.73 \pm 0.08$, which is consistent with the result for the entire field. At the 99% percentile the LF is steeper than $\alpha = -1.5$. Again, there is the obvious caveat about the uncertainty of the I background correction.

For the outer region of this field (Figure 6.22) we obtain $\alpha = -1.74 \pm 0.11$, which is in very good agreement with results for the two fields and for the entire observed area in I. These LFs are somewhat shallower but in good agreement with V LFs for these same fields.

Color distributions for these objects are analyzed in Figure 6.23, which shows the V vs $V - I$ plot for the NGC1275 field. The histogram of color distribution is shown in Figure 6.24. This shows that the majority of the objects are found at $V - I > 0.75$. The median color of galaxies in these fields is again 1.20. We can also plot the distribution of average $V - I$ versus distance from NGC1275 and we see that the distribution is 'flat' with a slight blueing trend toward the cluster centre (Figure 6.25).

Figure 6.26 shows the color magnitude diagram for cluster members. This has been computed in the following way. In the V vs $V - I$ plane for objects in the cluster field, we found the nearest 'background' objects, i.e., the nearest object in the V vs. $V - I$ plane for galaxies in the Abell 262 background field. The remaining objects were then considered to be cluster members and a color-magnitude diagram computed. As we can see, there is a broad swath

of galaxies at $V-I \sim 1.2$. This is confirmed by simulating the distribution of colors and magnitudes of background galaxies and reproducing an 'artificial' color-magnitude diagram, as shown in figure 6.27. In this plot we see a broad strip of galaxies at $V-I \sim 1$. There is a modest trend for fainter galaxies to be somewhat bluer. This strip is not as well defined as that claimed for Coma or seen later for galaxies in the UGC3274 field, which may indicate a complex star formation history for dwarfs in this field. Note that other explanations are possible, such as strongly variable extinction in this low galactic latitude field. The above conclusions are also borne out of the histogram shown in Figure 6.28. As we can see from Figure 6.29, the average color is approximately constant at all magnitudes. Thus, the 'cleaned' CMD for this field appears to confirm Secker & Harris (1995)'s claim that dwarfs obey a very tight color-magnitude relation, although we cannot detect any strong radial gradient in colors.

The corresponding color plot for stars is shown in Figure 6.30. Here we clearly note the main sequence for field stars and a scatter of redder objects (field giants and dwarfs) at all magnitudes. There is a tendency for the color distribution of fainter stars to be broader, presumably as stars at different distances are in the line of sight. Note the reddening line in these plots as an envelope in the V vs. $V-I$ diagram.

Star counts in V and I are compared in Figures 6.31 and 6.32 with predictions from the Bahcall-Soneira model. Here, as before, no correction for

reddening was applied. In both cases the agreement is good, but the model overestimates the number of stars by about 50% (again normalization in these plots is arbitrary). The color distribution for stars is again well reproduced (Figure 6.33), although there is an excess of red stars.

Figure 6.1: The V image of the NGC1275 field (one of three chips in mosaic)

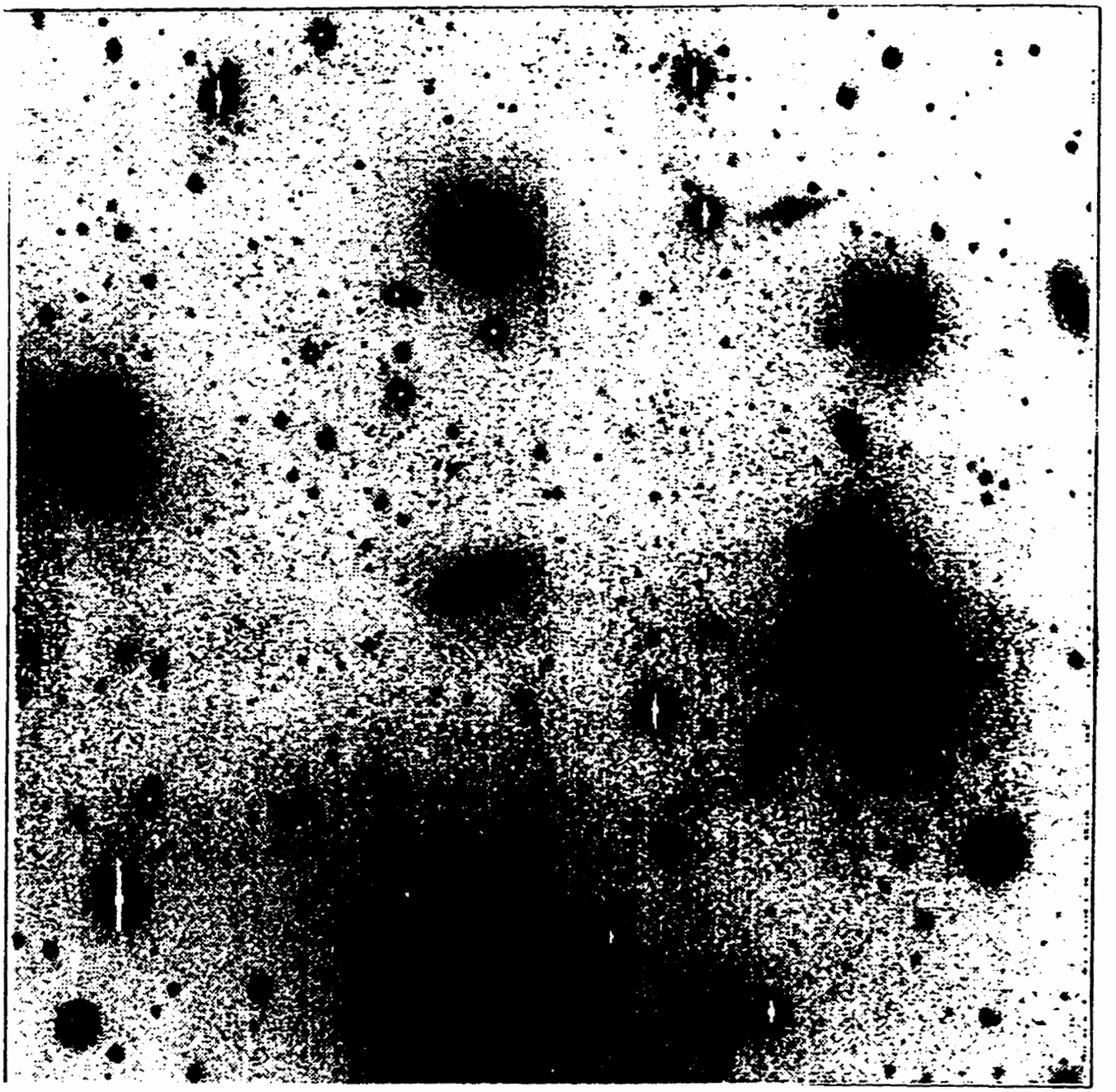

Figure 6.2: The V image of the NGC1275 field after removal of bright galaxies

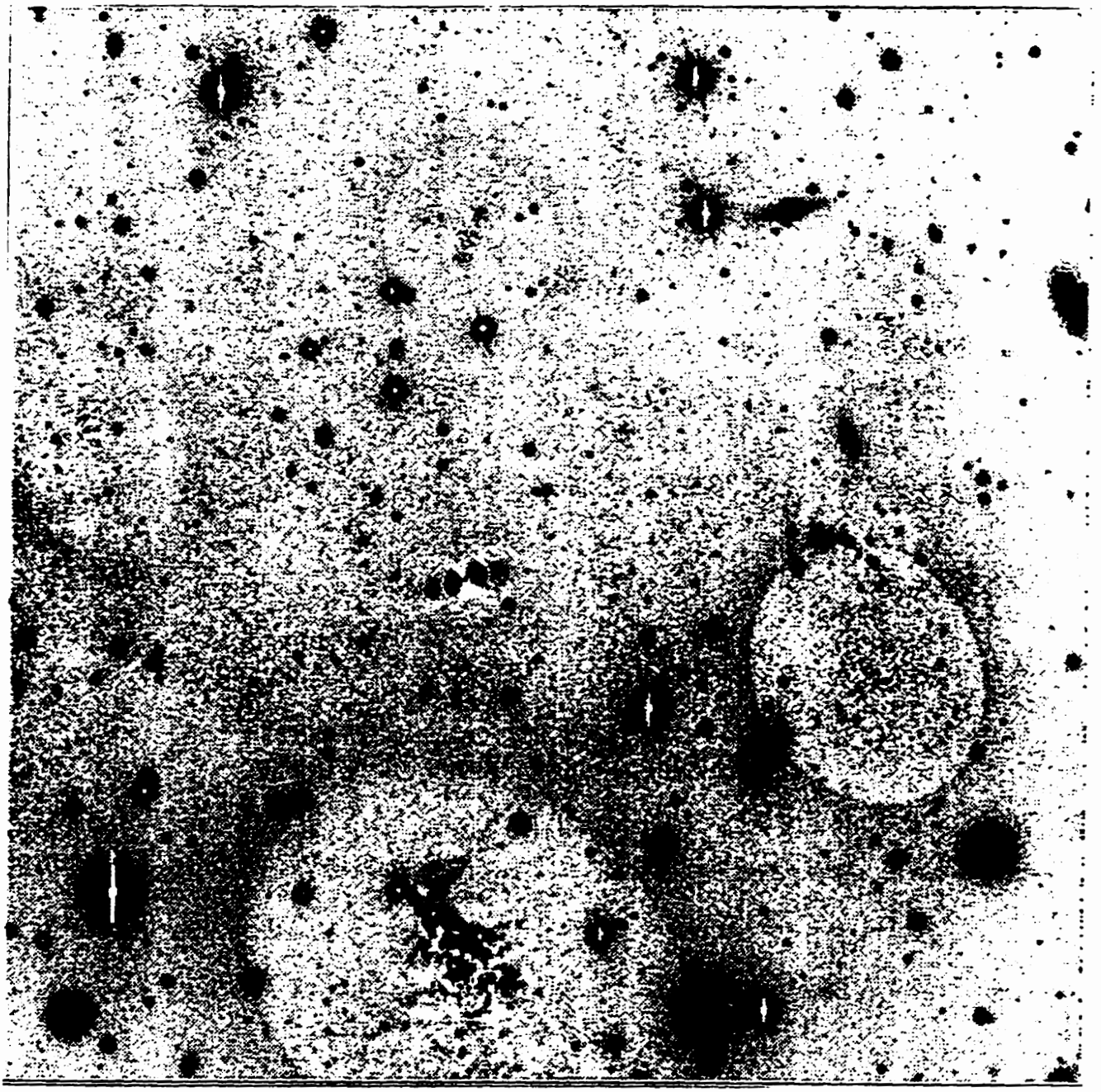

Figure 6.3: Plot of r_{-2} vs. V for NGC1275 field

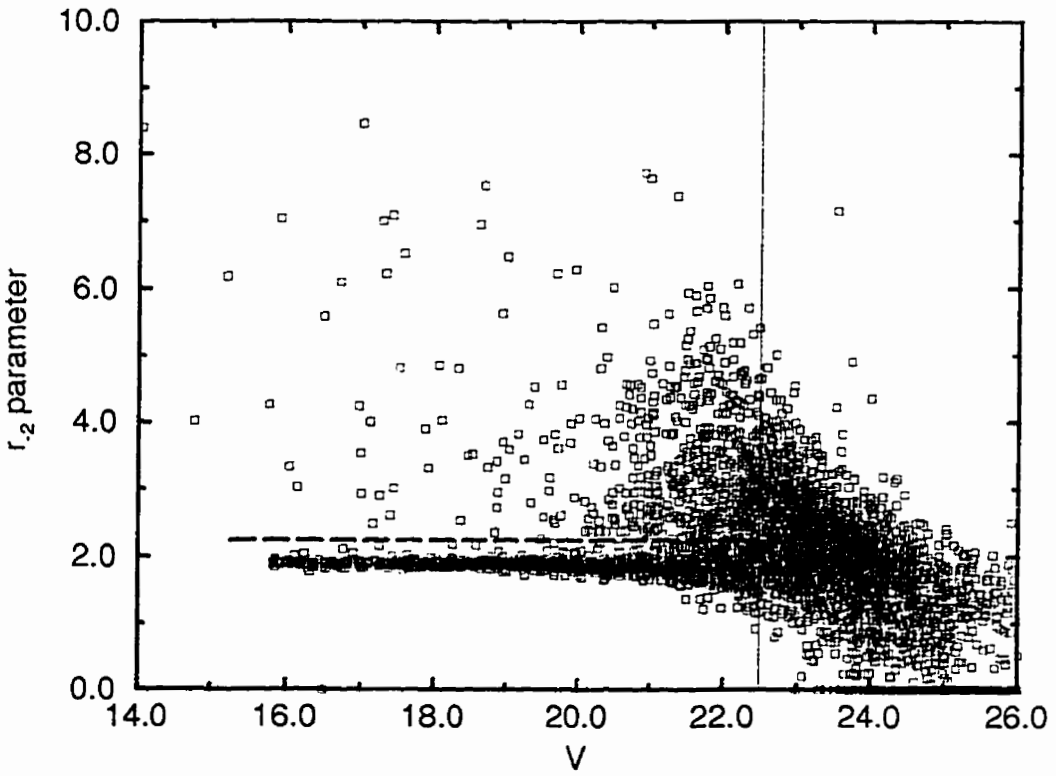

Table 6.1: NUMBER COUNTS FOR NGC1275 FIELD IN V

V	N. of objects	N. of galaxies	N. of stars	Completeness
15.25	1.00 ± 1.00	1.00 ± 1.00	0.00 ± 0.00	1
15.75	11.61 ± 3.41	2.09 ± 1.44	9.53 ± 3.09	1
16.25	37.01 ± 6.08	3.09 ± 1.76	33.93 ± 5.82	1
16.75	34.27 ± 5.85	2.17 ± 1.47	32.10 ± 5.67	1
17.25	48.63 ± 6.97	11.53 ± 3.39	37.10 ± 6.09	1
17.75	54.15 ± 7.36	4.18 ± 2.04	49.97 ± 7.07	1
18.25	69.94 ± 8.36	5.44 ± 2.33	64.50 ± 8.03	1
18.75	89.64 ± 9.47	12.70 ± 3.56	76.94 ± 8.77	1
19.25	78.98 ± 8.89	8.53 ± 2.92	70.46 ± 8.39	1
19.75	118.81 ± 10.90	15.96 ± 3.99	102.85 ± 10.14	1
20.25	112.68 ± 10.62	28.57 ± 5.35	84.11 ± 9.17	1
20.75	168.53 ± 12.98	61.59 ± 7.85	106.94 ± 10.34	1
21.25	201.79 ± 14.21	90.63 ± 9.52	111.16 ± 10.54	1
21.75	291.13 ± 17.06	159.57 ± 12.63	131.56 ± 11.47	1
22.25	435.63 ± 20.87	253.69 ± 15.93	181.93 ± 13.49	0.9

Figure 6.4: Number of objects, galaxies and stars in NGC1275 field

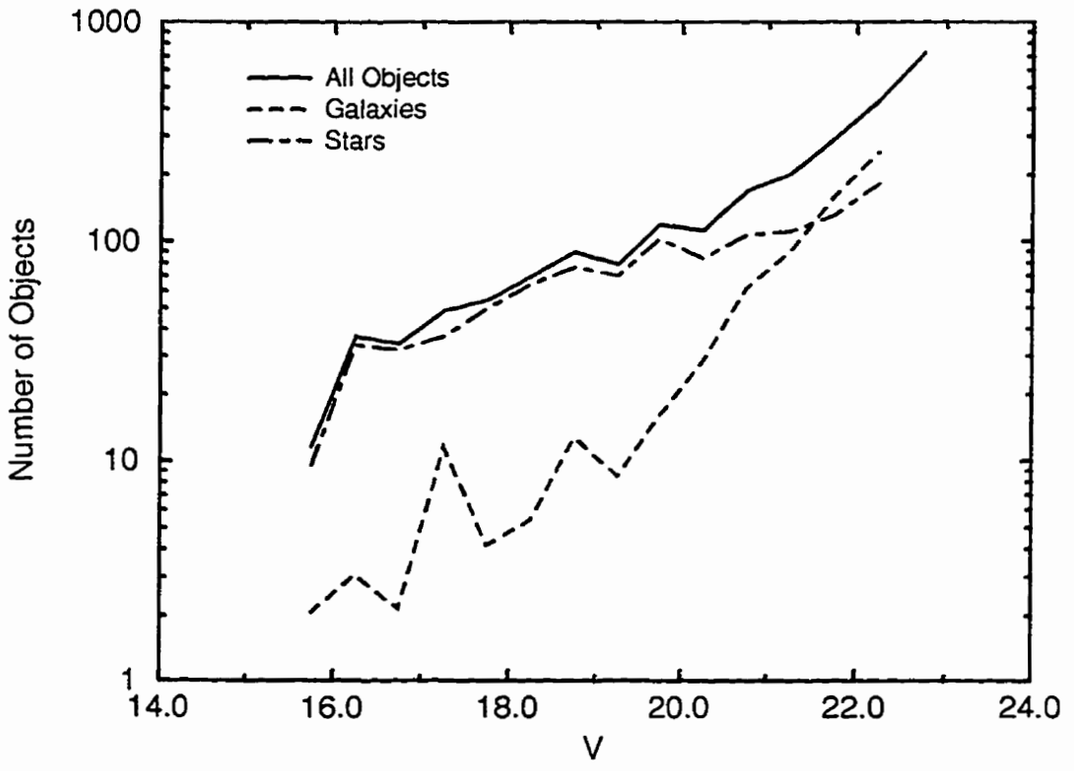

Table 6.2: GALAXY COUNTS IN NGC1275 V FIELD

V	N. of galaxies	Background counts	N. of cluster members
15.25	1.00 ± 1.00	0.18	0.82 ± 1.09
15.75	2.09 ± 1.44	0.29	1.80 ± 1.54
16.25	3.09 ± 1.76	0.46	2.63 ± 1.89
16.75	2.17 ± 1.47	0.72	1.45 ± 1.70
17.25	11.53 ± 3.39	1.15	10.38 ± 3.56
17.75	4.18 ± 2.04	1.82	2.36 ± 2.45
18.25	5.44 ± 2.33	2.88	2.56 ± 2.88
18.75	12.70 ± 3.56	4.57	8.13 ± 4.15
19.25	8.53 ± 2.92	7.24	1.29 ± 3.97
19.75	15.96 ± 3.99	11.48	4.48 ± 5.23
20.25	28.57 ± 5.35	18.20	10.37 ± 6.84
20.75	61.59 ± 7.85	28.84	32.75 ± 9.51
21.25	90.63 ± 9.52	45.71	44.92 ± 11.68
21.75	159.57 ± 12.63	72.44	87.13 ± 15.23
22.25	253.69 ± 15.93	114.82	138.87 ± 19.20

Figure 6.5: Number of galaxies and background objects in NGC1275 field

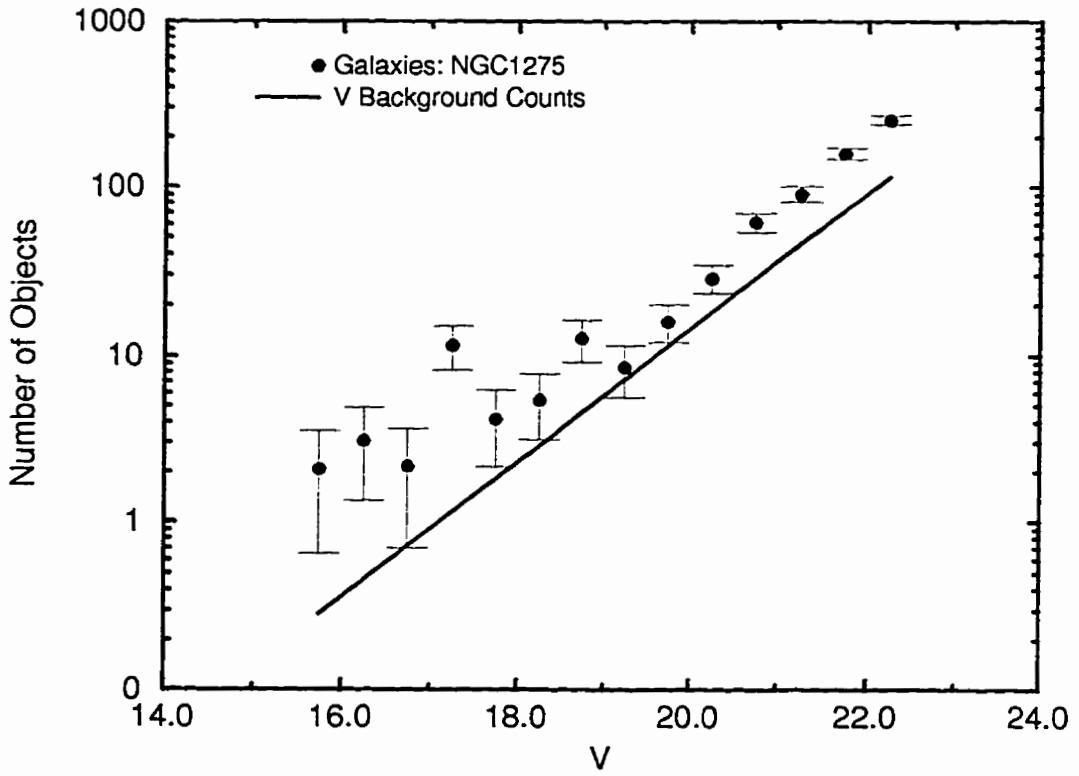

Figure 6.6: Number of cluster members and LF fit in NGC1275 field

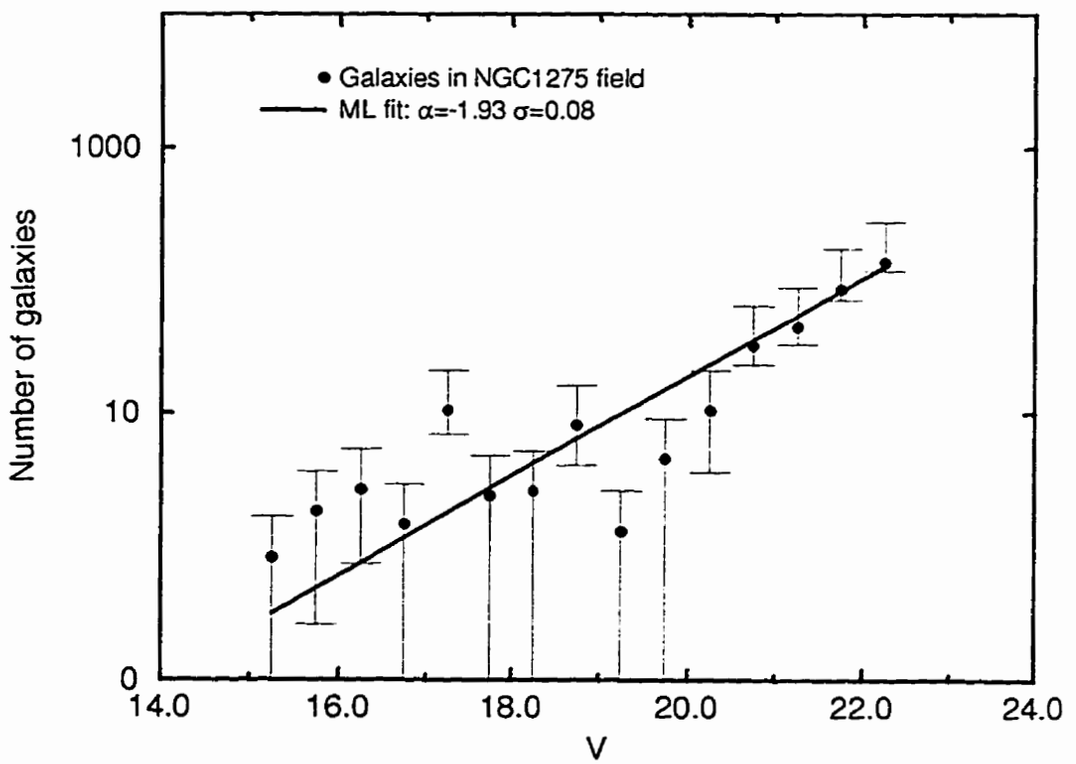

Figure 6.7: Radial distribution of galaxies in NGC1275 V field

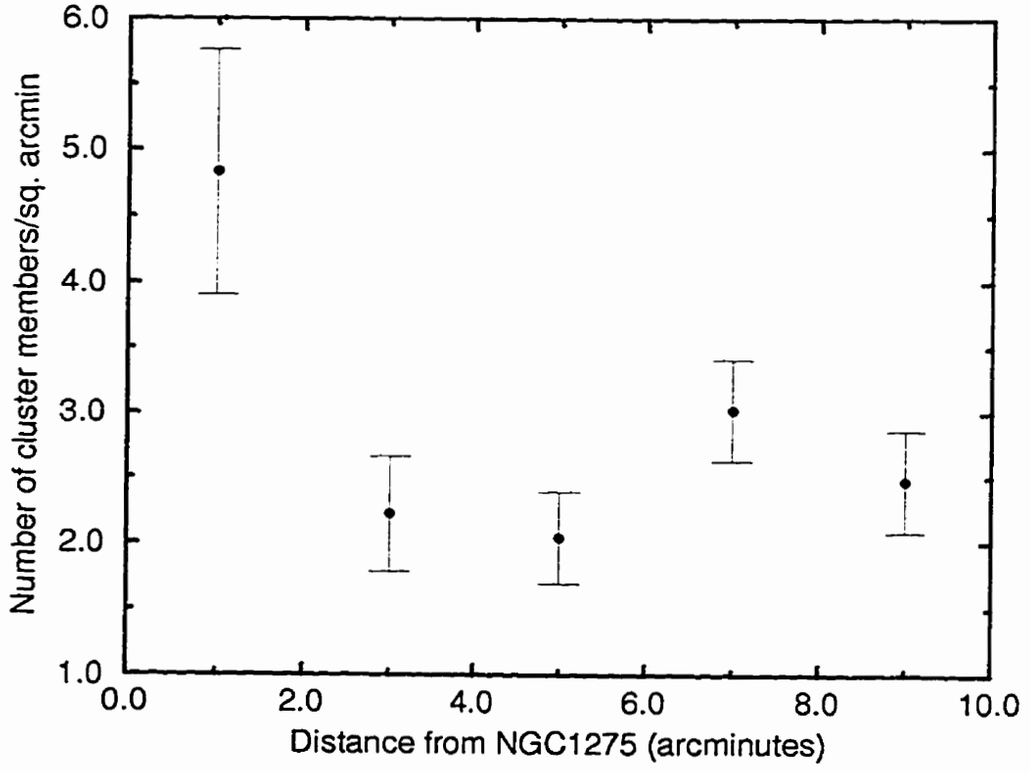

Figure 6.8: Number counts of galaxies in inner 5′ NGC1275 V field

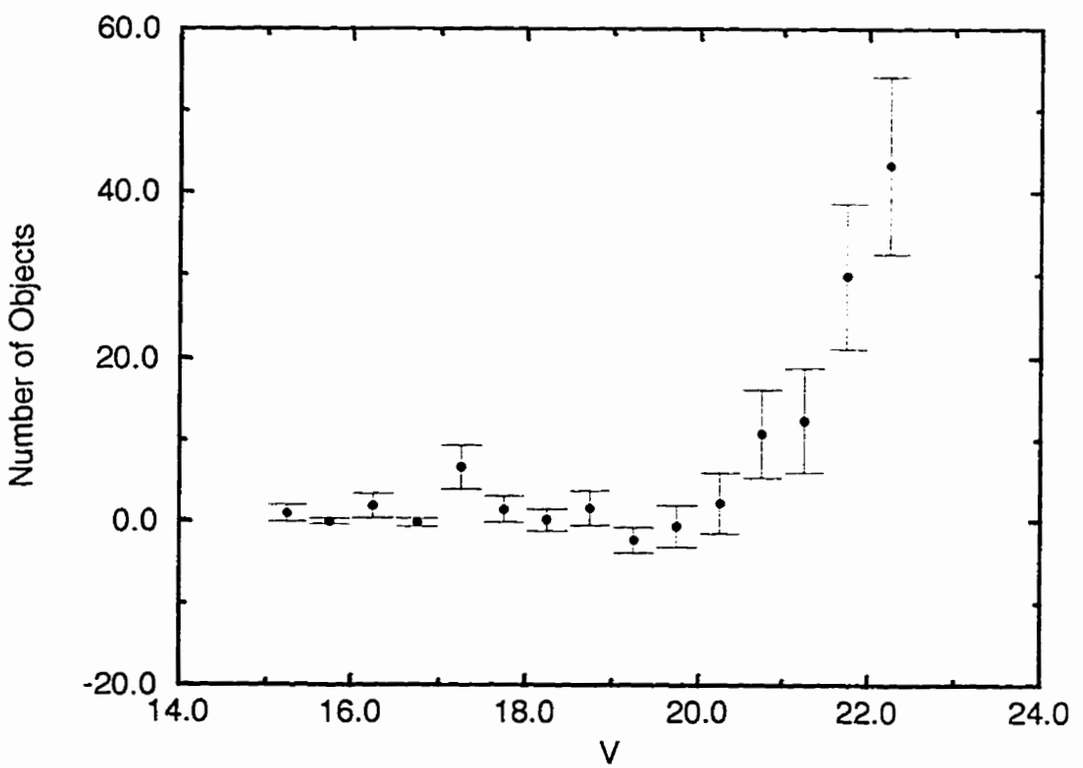

Figure 6.9: Number counts of galaxies more distant than 5′ from NGC1275

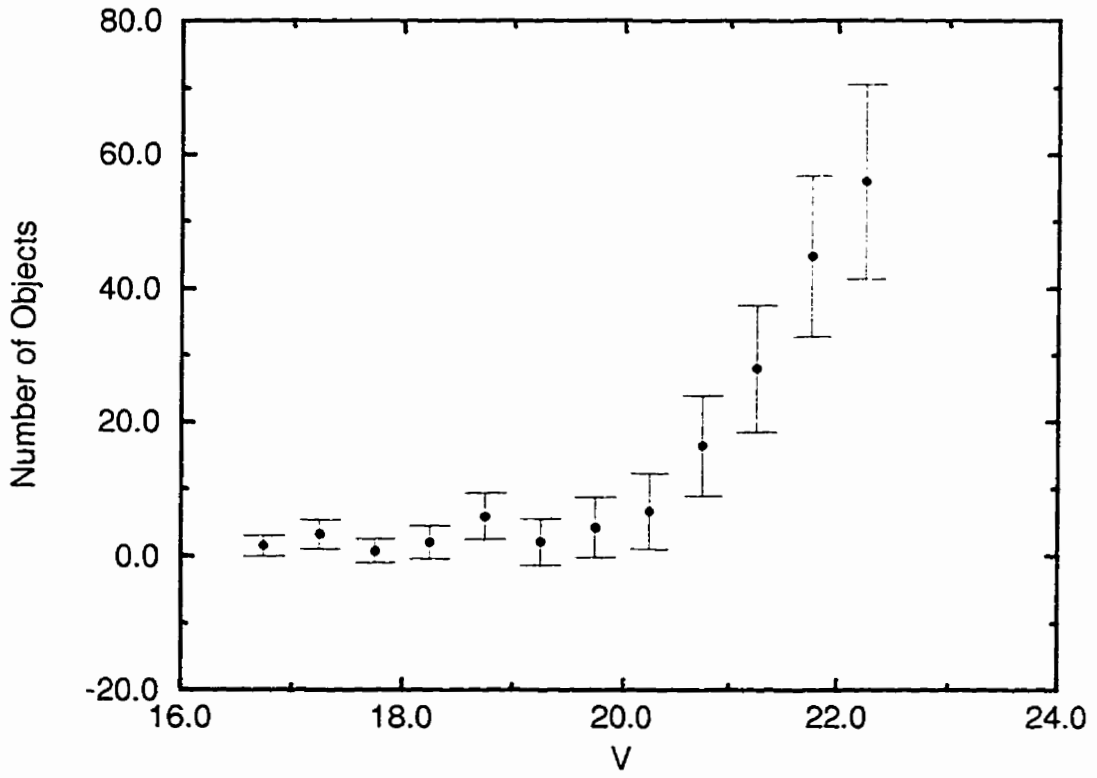

Figure 6.10: Comparison of inner and outer fields

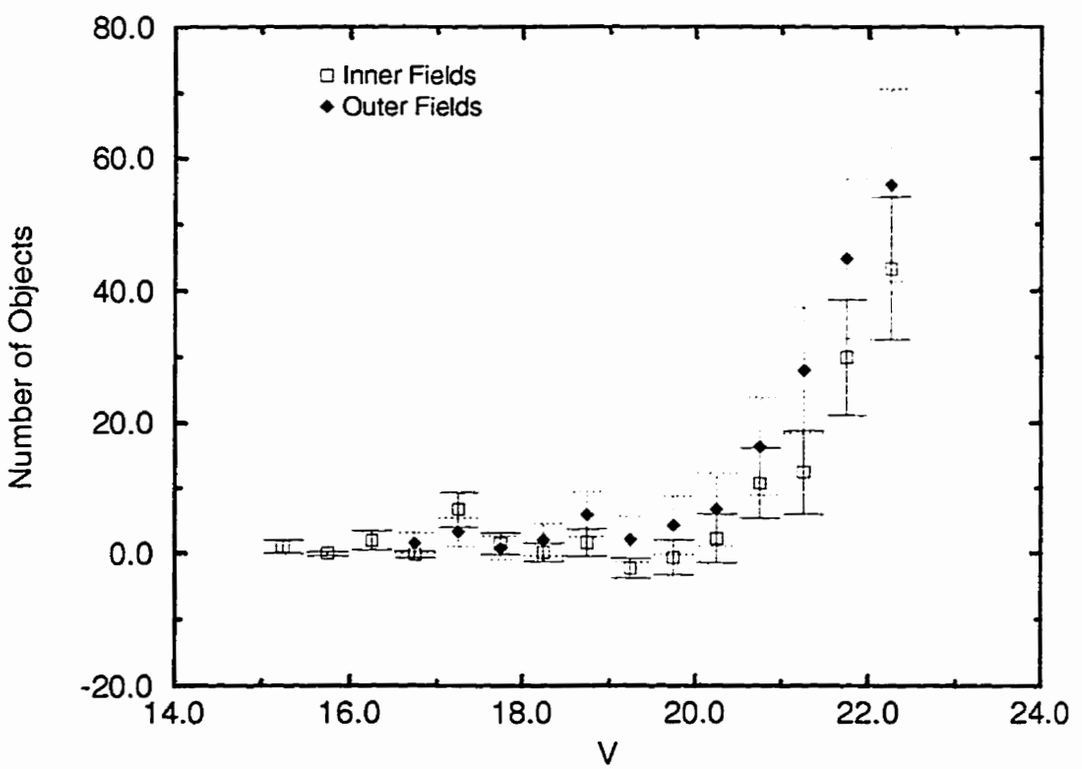

Figure 6.11: Luminosity function for galaxies in inner 5′ of NGC1275 field in *V*

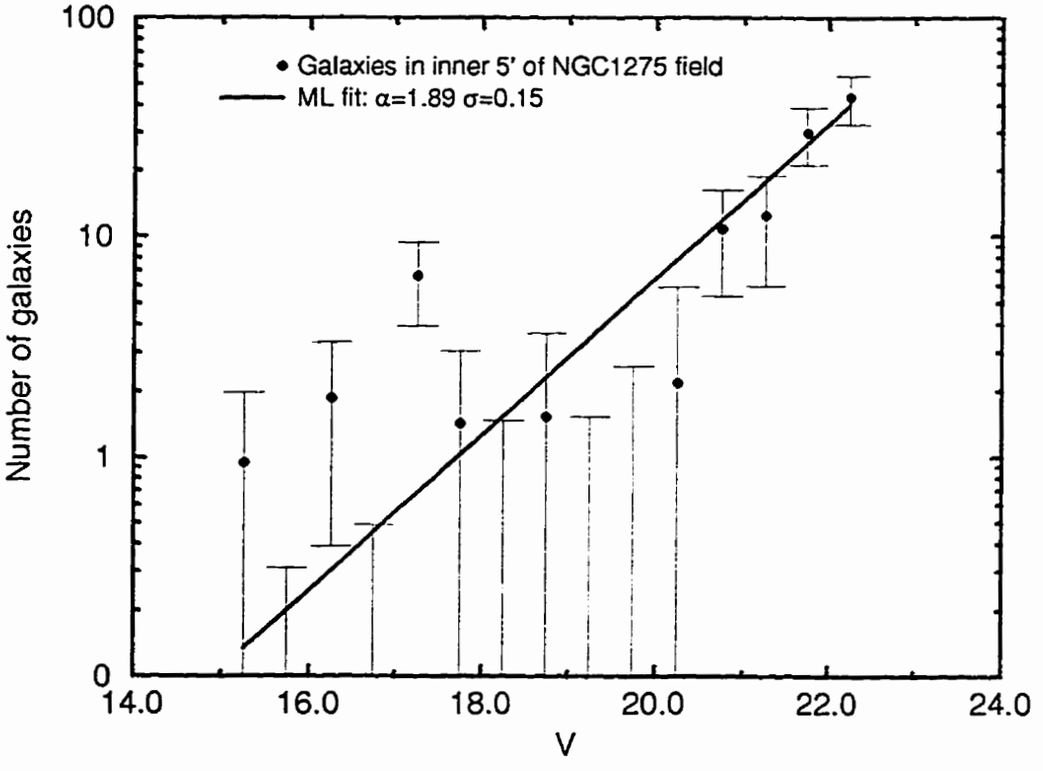

Figure 6.12: Luminosity function for galaxies in outer regions of NGC1275 field in V

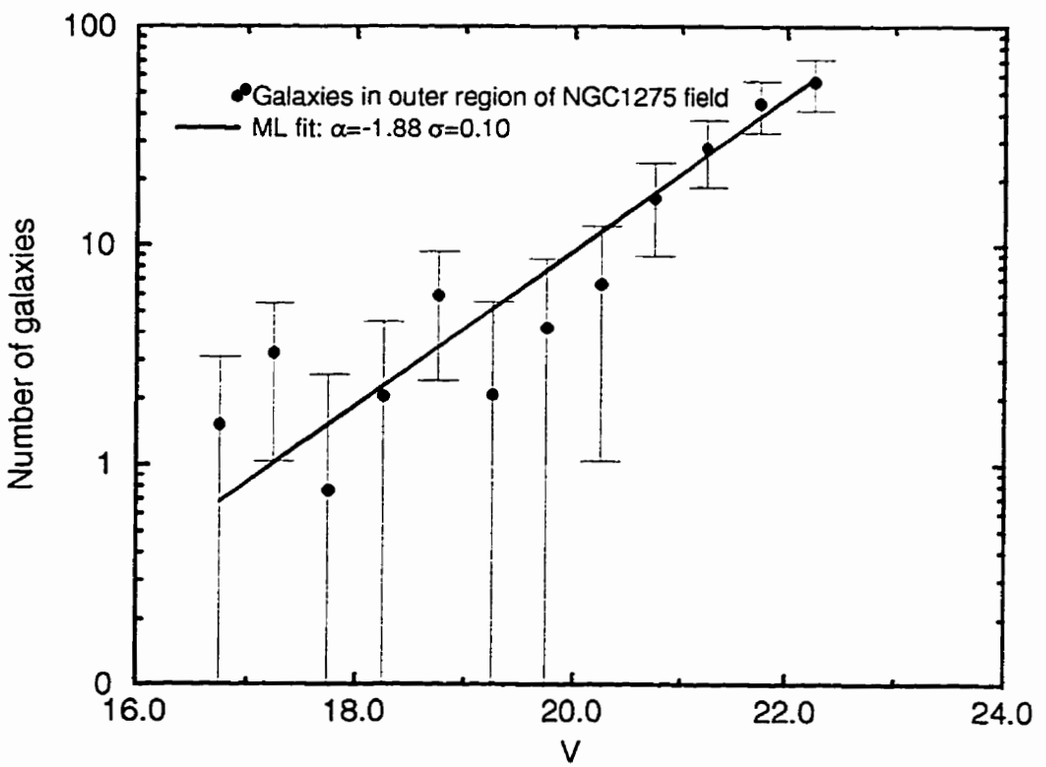

Figure 6.13: Plot of r_{-2} vs I for NGC1275 field

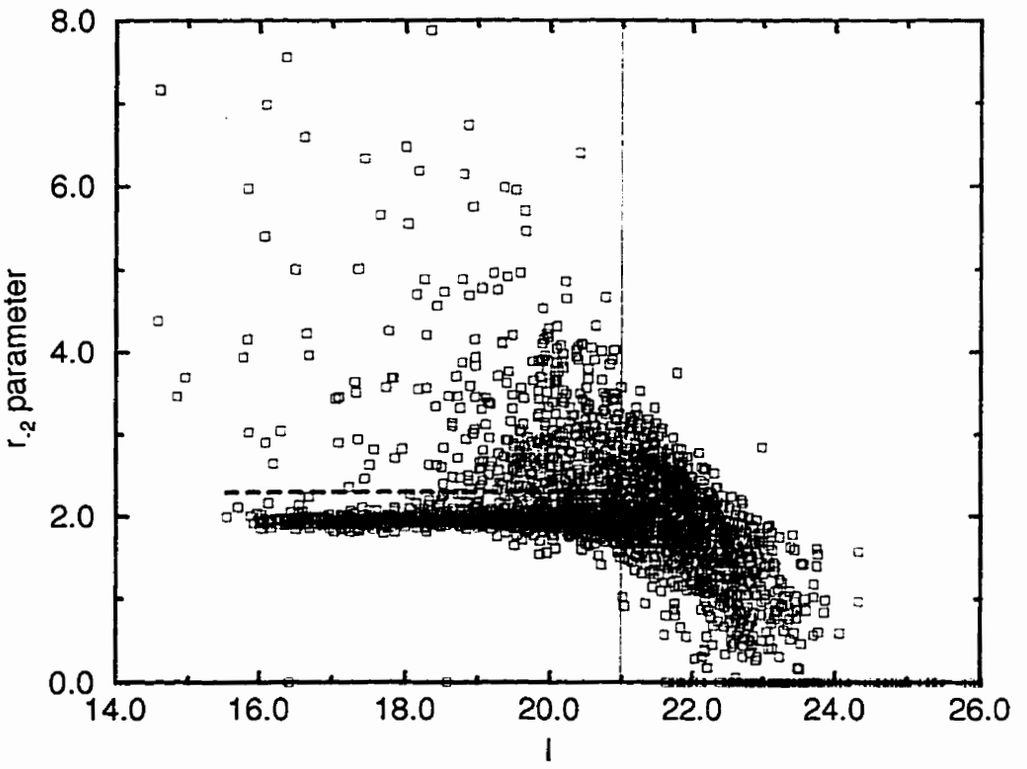

Table 6.3: NUMBER COUNTS FOR NGC1275 *I* FIELD

I	N. of objects	N. of galaxies	N. of stars	Completeness
15.75	11.13 ± 3.34	5.58 ± 2.36	5.55 ± 2.36	1
16.25	51.04 ± 7.14	7.33 ± 2.71	43.71 ± 6.61	1
16.75	65.33 ± 8.08	4.29 ± 2.07	60.04 ± 7.75	1
17.25	85.94 ± 9.27	10.98 ± 3.31	74.96 ± 8.66	1
17.75	85.70 ± 9.26	9.98 ± 3.16	73.72 ± 8.59	1
18.25	127.21 ± 11.28	15.34 ± 3.92	110.87 ± 10.53	1
18.75	146.70 ± 12.11	36.75 ± 6.06	107.95 ± 10.39	1
19.25	184.05 ± 13.57	50.99 ± 7.14	133.06 ± 11.54	1
19.75	242.67 ± 15.58	95.39 ± 9.77	147.28 ± 12.14	1
20.25	287.48 ± 16.96	118.45 ± 10.88	167.03 ± 12.92	1
20.75	330.39 ± 18.18	144.73 ± 12.03	183.12 ± 13.53	1

Figure 6.14: Number of objects, stars and galaxies in NGC1275 *I* field

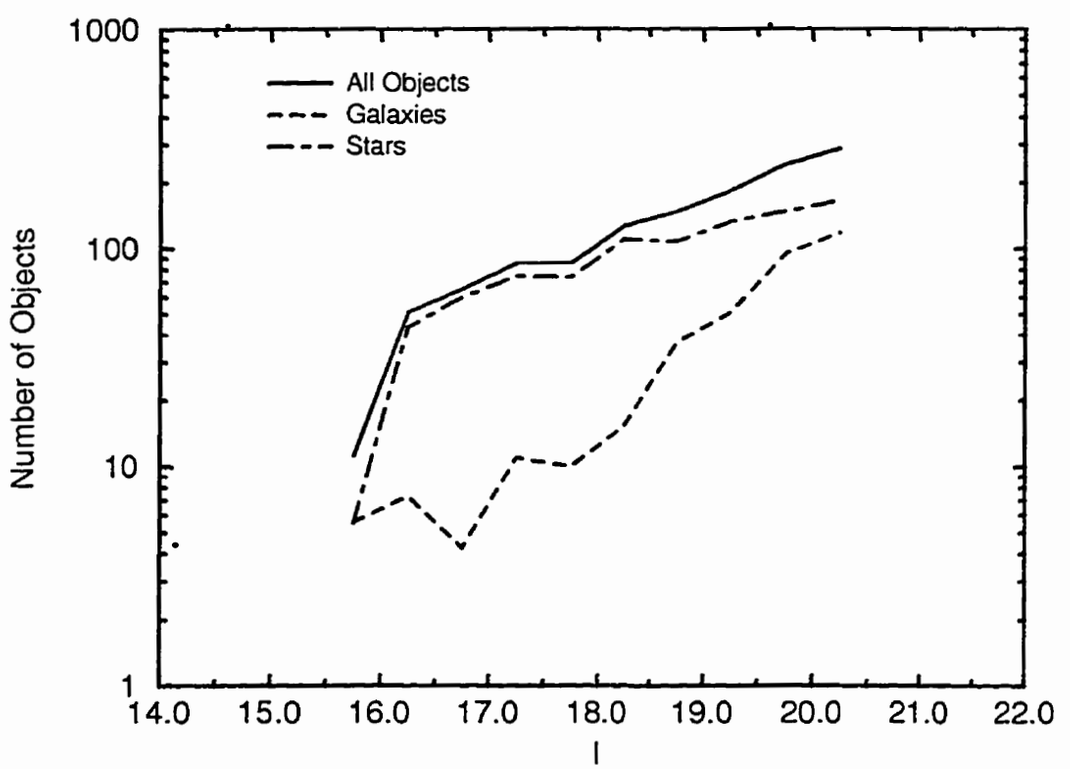

Table 6.4: NUMBER COUNTS OF GALAXIES AND BACKGROUND OBJECTS FOR NGC1275 *I* FIELD

15.75	5.58 ± 2.36	2.26	3.32 ± 2.80
16.25	7.33 ± 2.71	3.35	3.98 ± 3.27
16.75	4.29 ± 2.07	4.95	-0.66 ± 3.04
17.25	10.98 ± 3.31	7.33	3.65 ± 4.28
17.75	9.98 ± 3.16	10.84	-0.86 ± 4.56
18.25	15.34 ± 3.92	16.03	-0.69 ± 5.60
18.75	36.75 ± 6.06	23.71	13.04 ± 7.77
19.25	50.99 ± 7.14	35.08	15.91 ± 9.28
19.75	95.39 ± 9.77	51.88	43.51 ± 12.14
20.25	118.45 ± 10.88	76.74	41.71 ± 13.97
20.75	144.73 ± 12.03	113.50	31.23 ± 16.07

Figure 6.15: Number of galaxies and background objects in NGC1275 *I* field

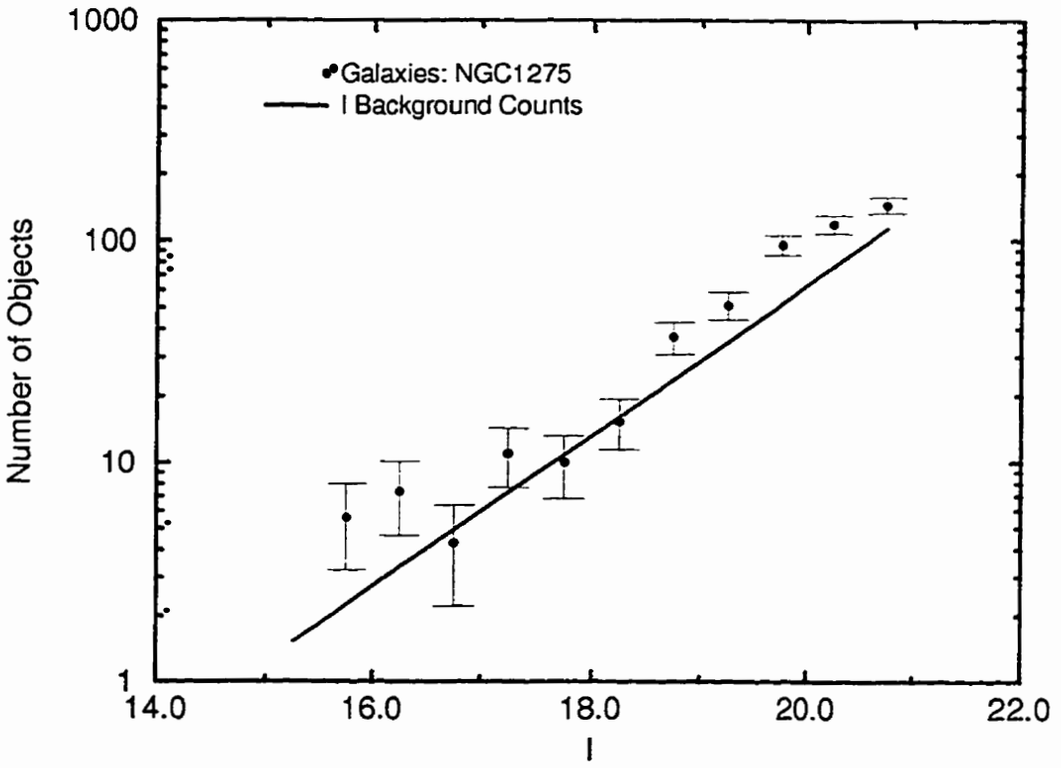

Figure 6.16: Number of cluster members NGC1275 I field

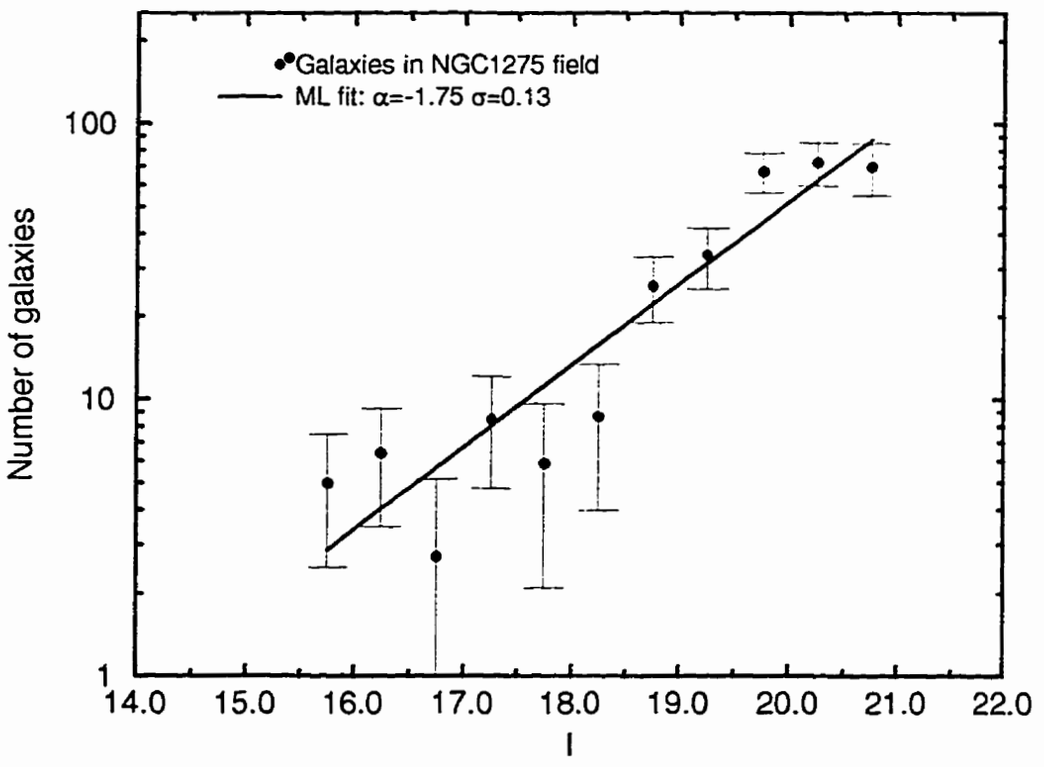

Figure 6.17: Radial distribution of galaxies in NGC1275 *I* field

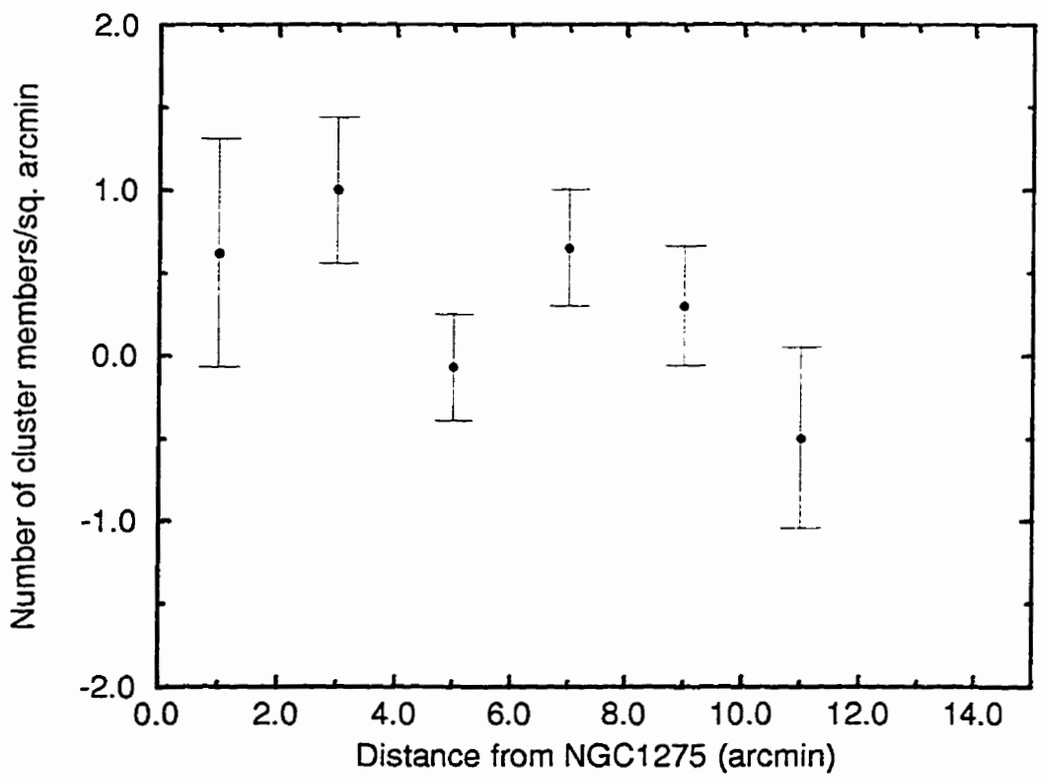

Figure 6.18: Number of galaxies in inner 5′ of NGC1275 *I* field

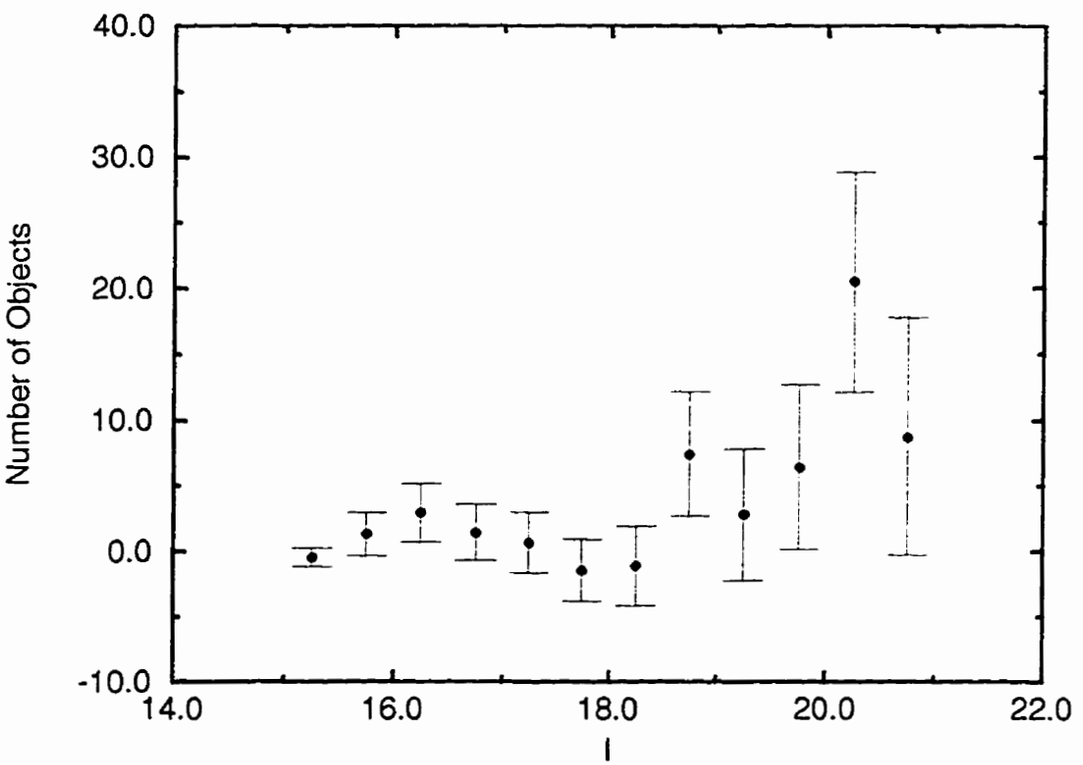

Figure 6.19: Number of galaxies outside of 5′ from NGC1275

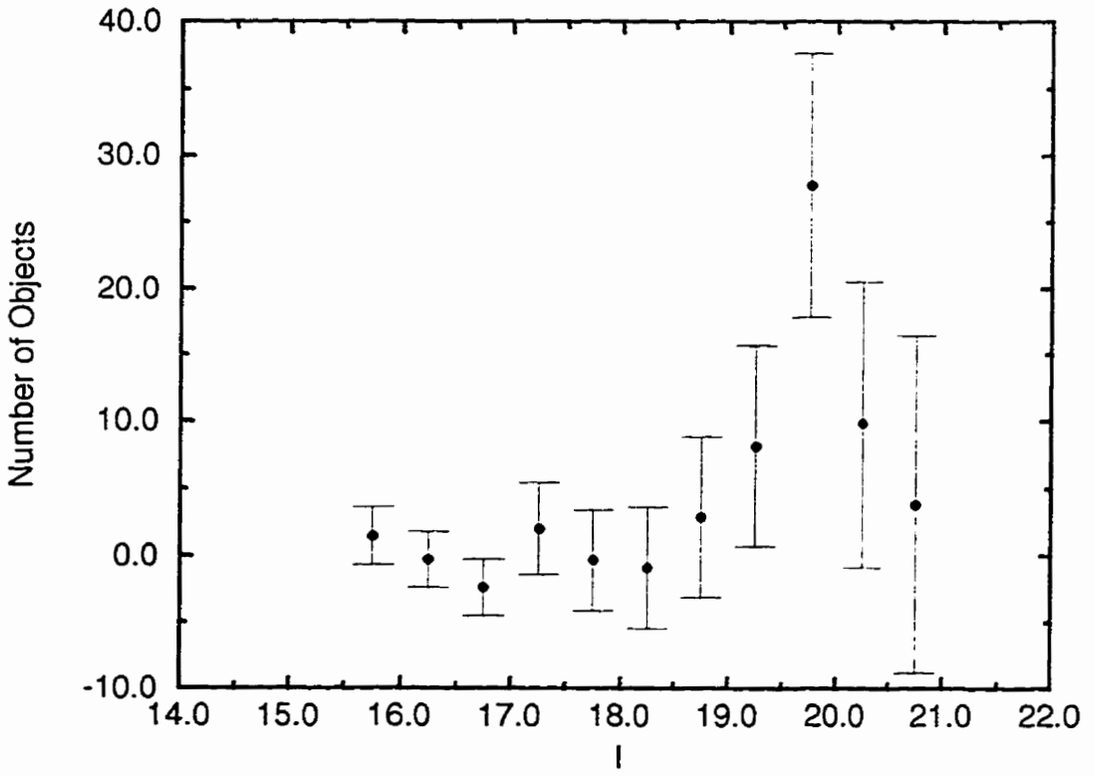

Figure 6.20: Comparison of inner and outer fields

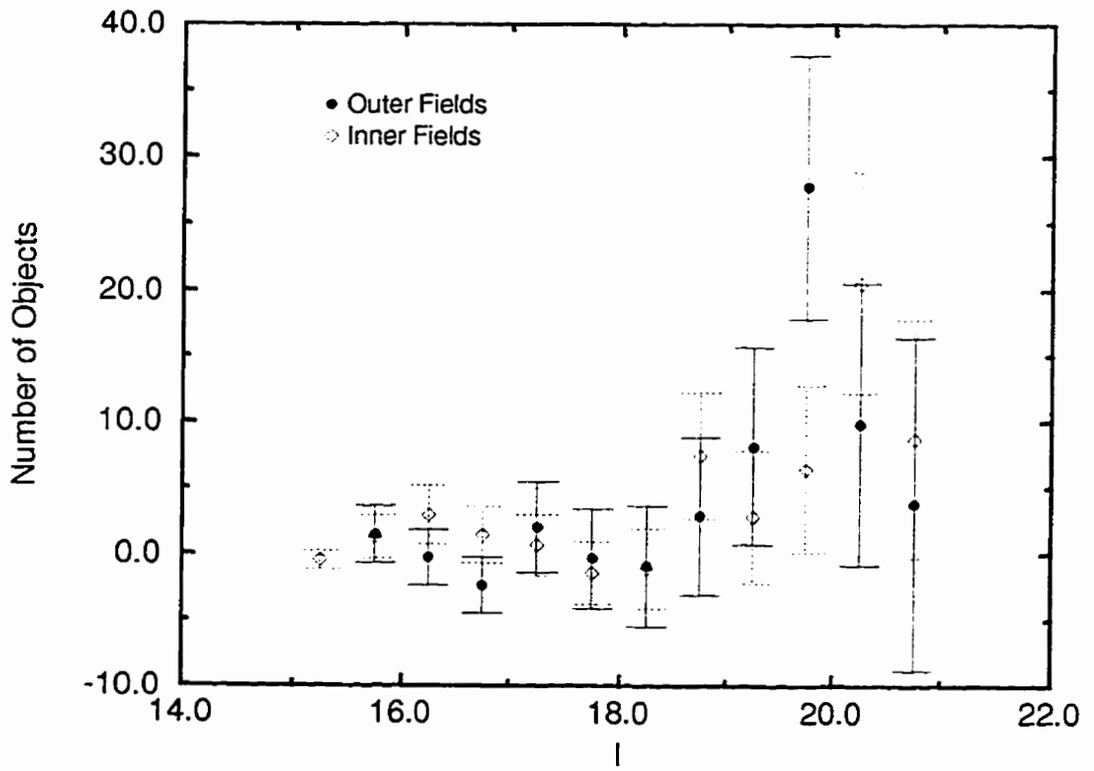

Figure 6.21: LF for galaxies in inner 5′ of NGC1275 field

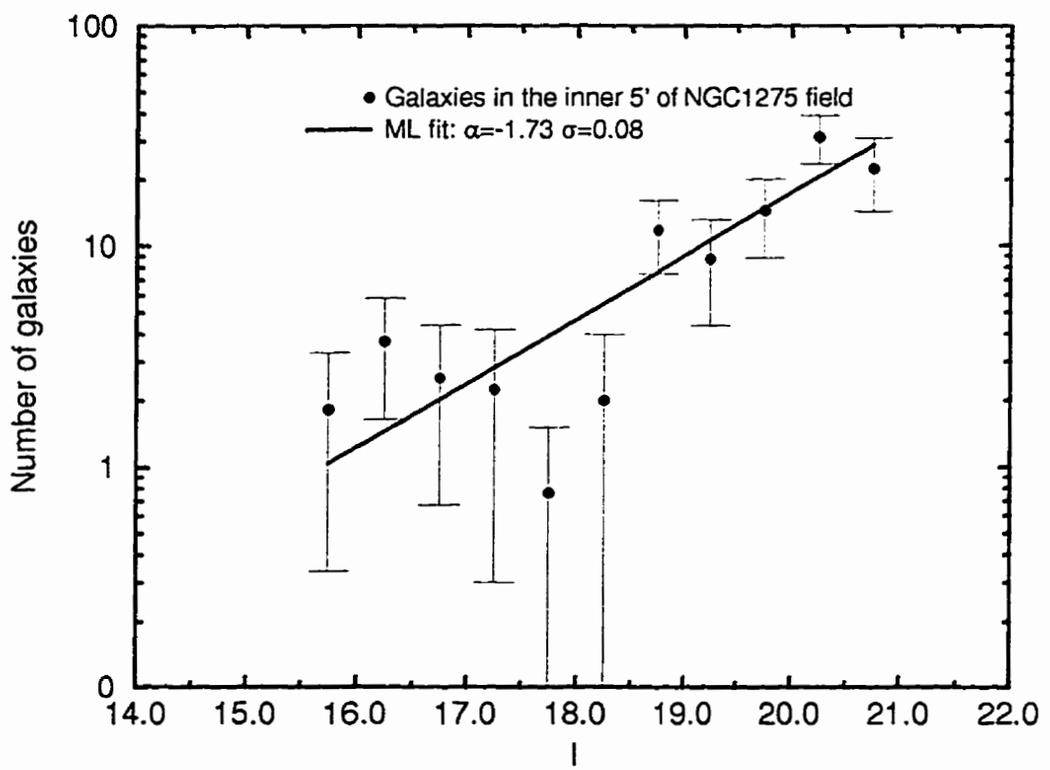

Figure 6.22: LF for galaxies in the outer region of NGC1275 field

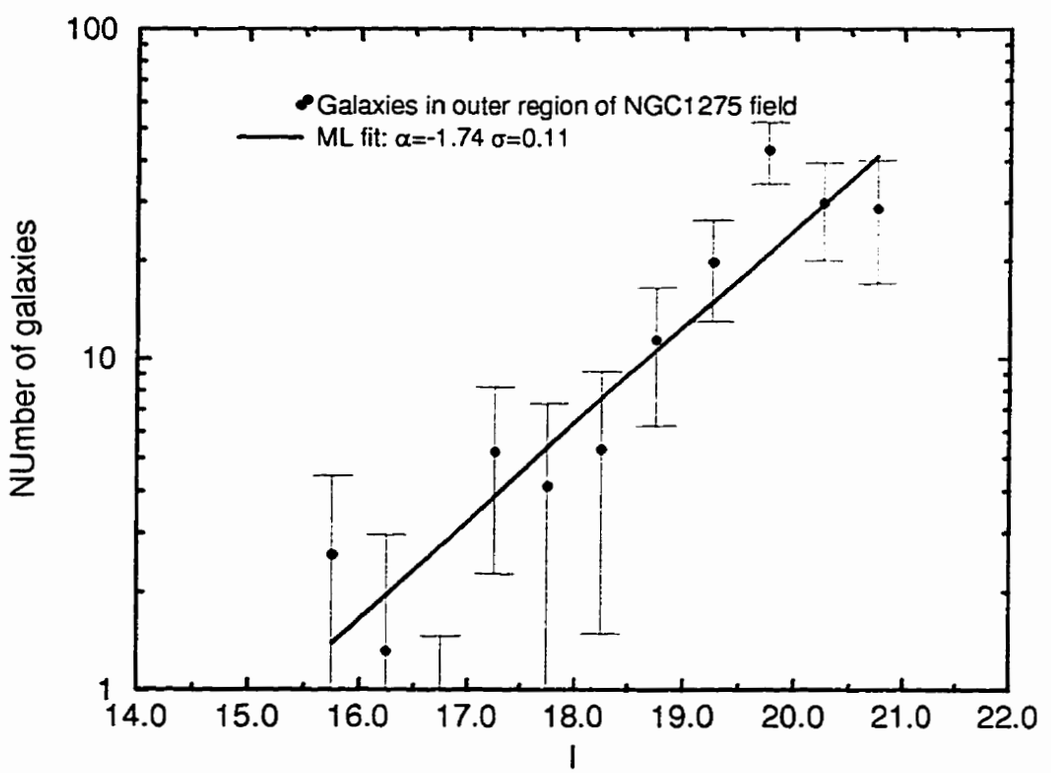

Figure 6.23: Color magnitude diagram for galaxies in NGC1275 field

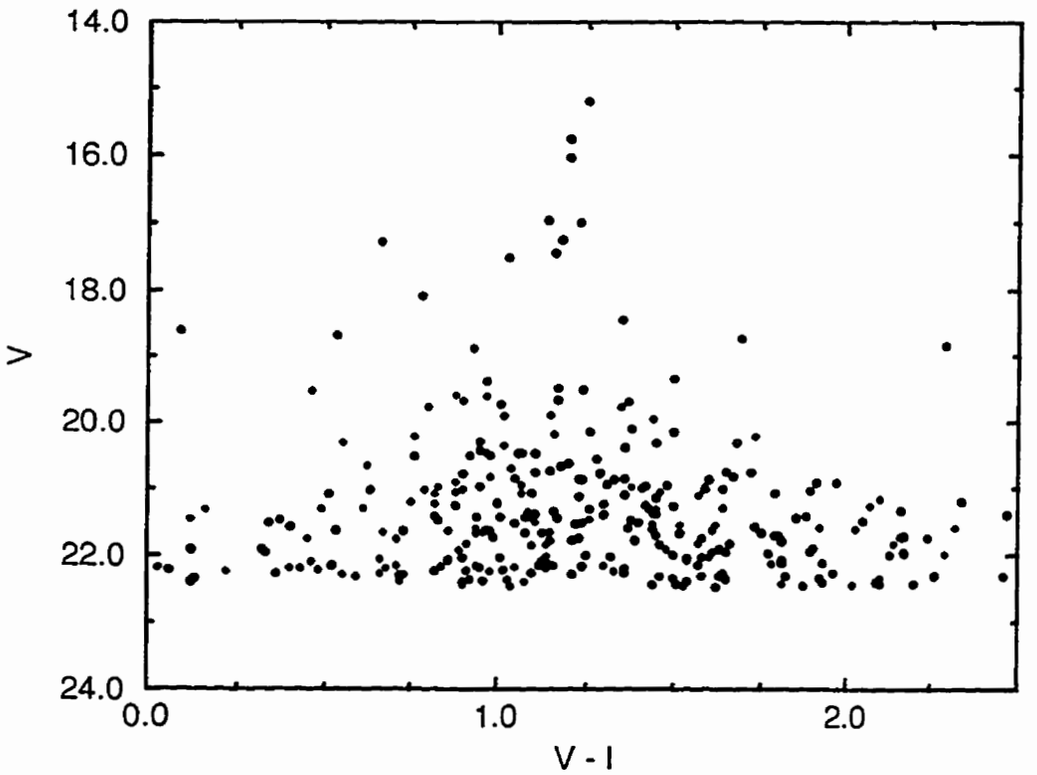

Figure 6.24: Histogram of galaxy colors for NGC1275 field

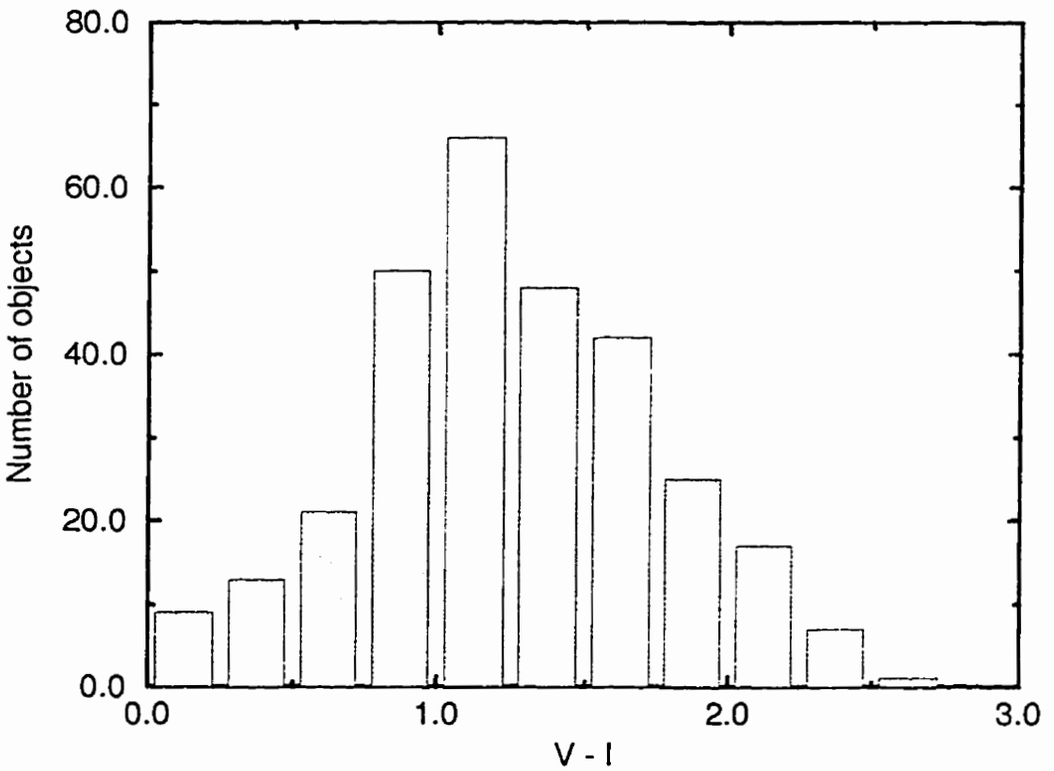

Figure 6.25: Radial distribution of average galaxy colors in NGC1275 field

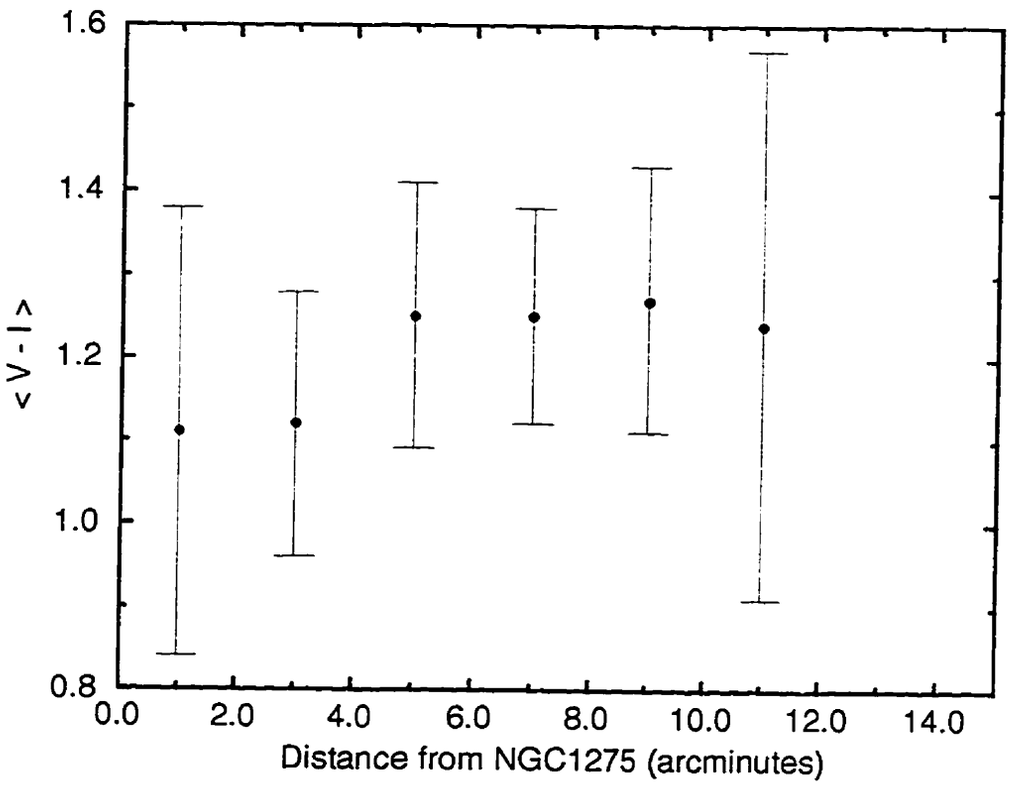

Figure 6.26: Color magnitude diagram for cluster members in NGC1275 field. See text for explanation.

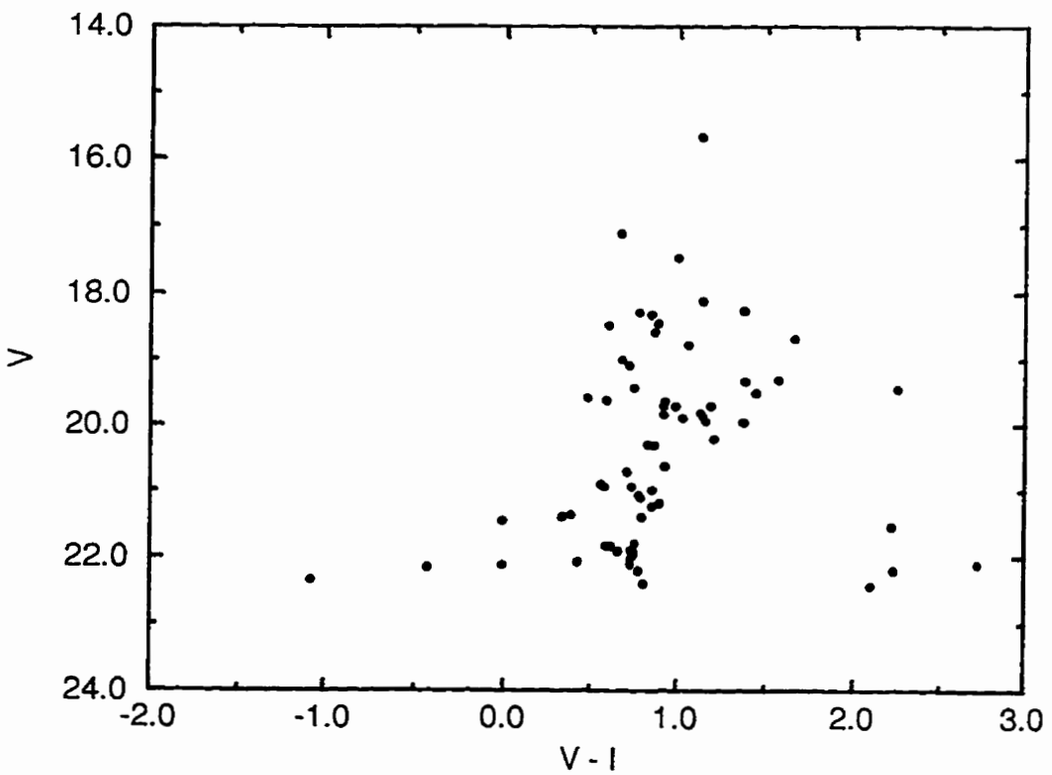

Figure 6.27: Color magnitude diagram for cluster members in NGC1275 field, as obtained with simulations. See text for further details

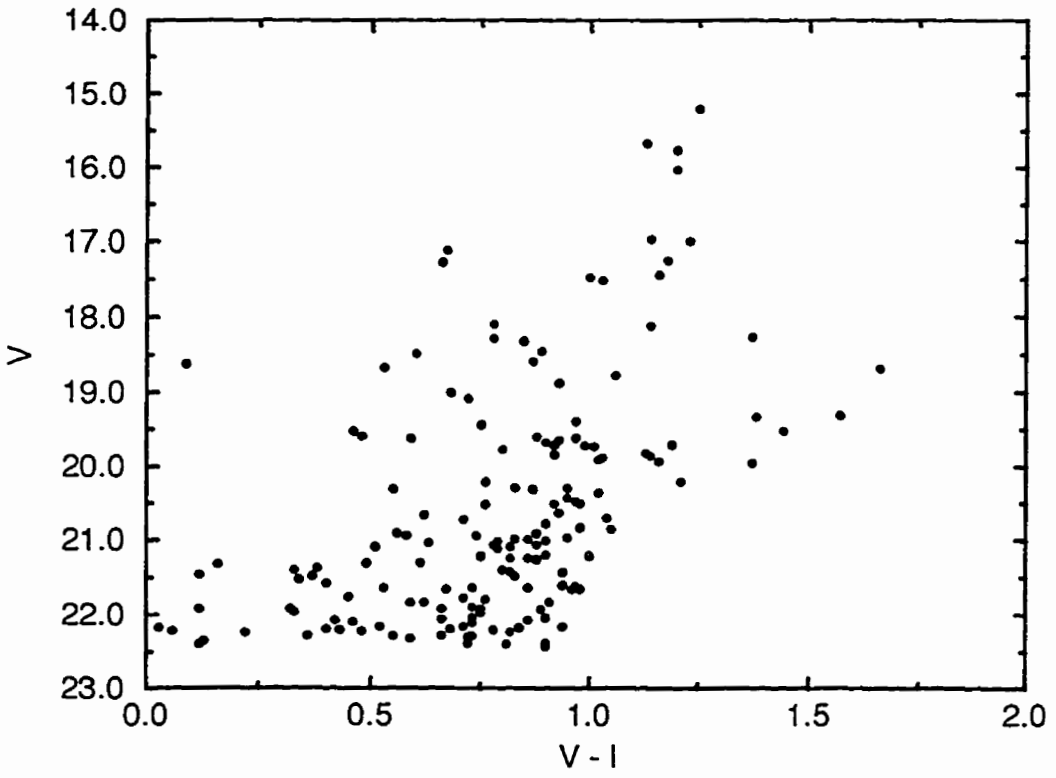

Figure 6.28: Color magnitude histogram for cluster members in NGC1275 field. See text for explanation.

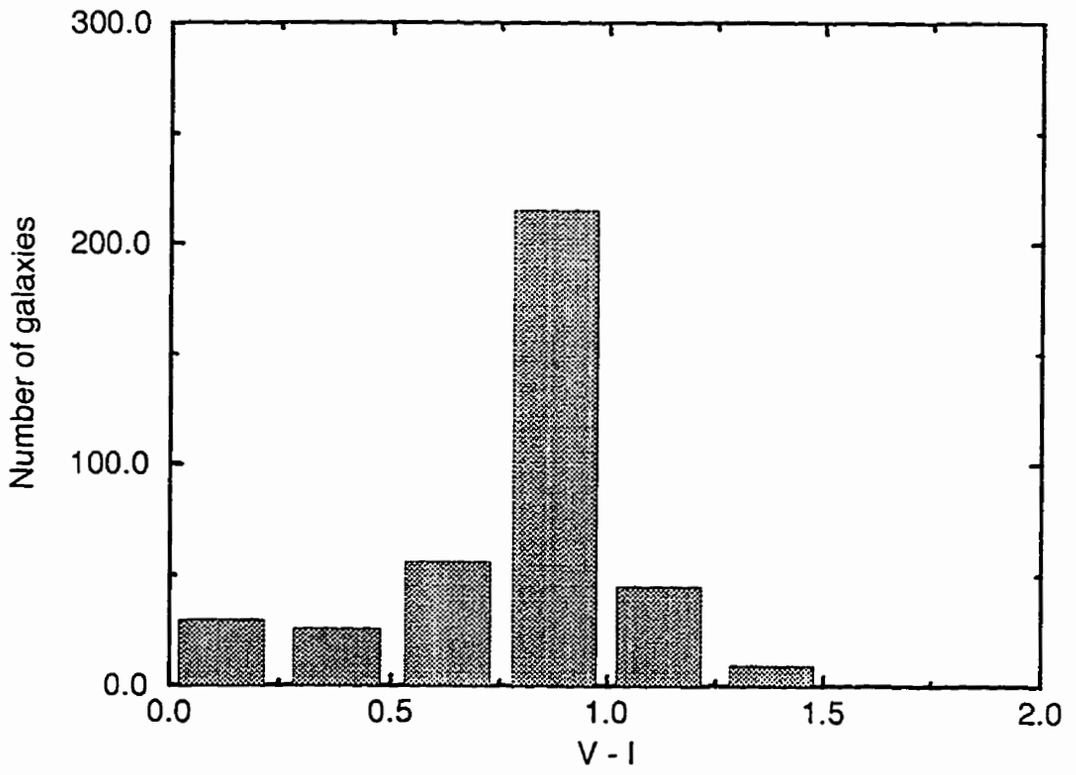

Figure 6.29: Average color vs magnitude for cluster members in NGC1275 field. See text for explanation.

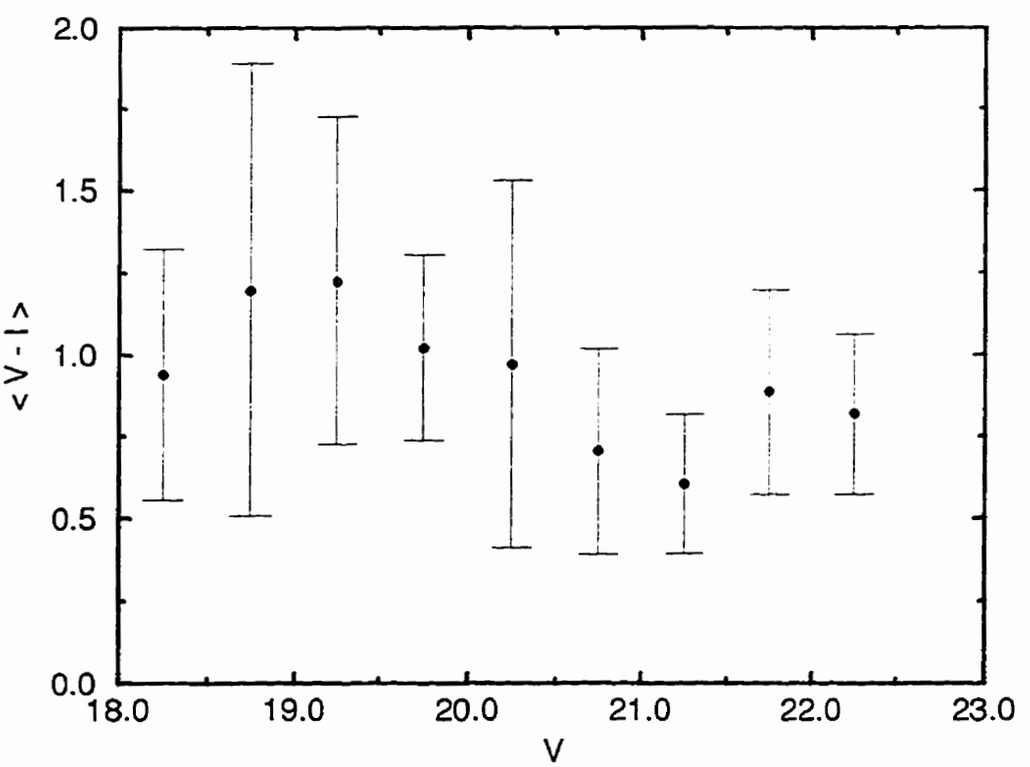

Figure 6.30: Color magnitude diagram for stars in NGC1275 field

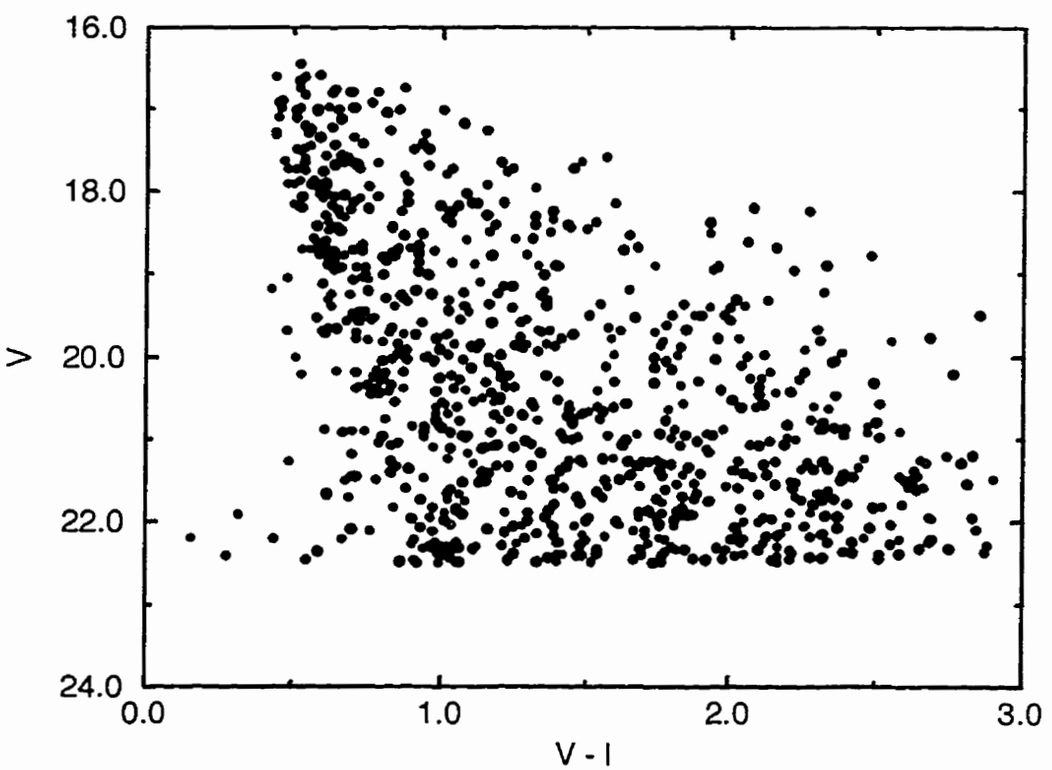

Figure 6.31: Stars in NGC1275 field and model in V

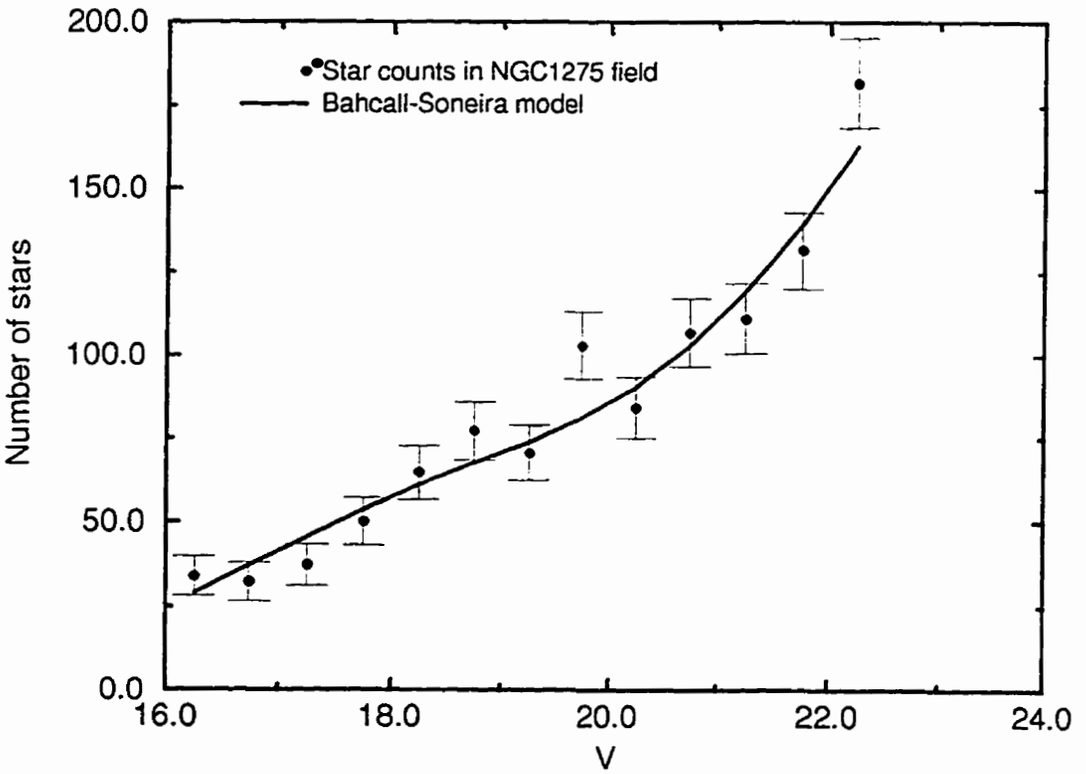

Figure 6.32: Stars in NGC1275 field and model in I

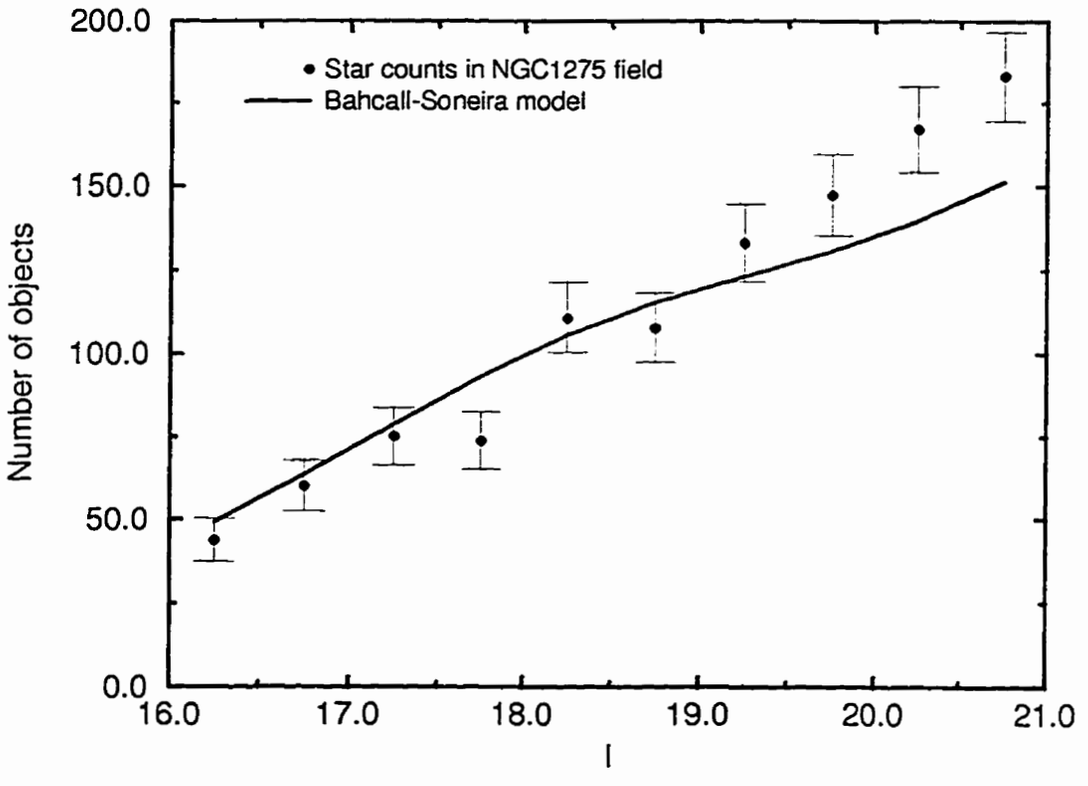

Figure 6.33: Color distribution for stars in NGC1275 field and model

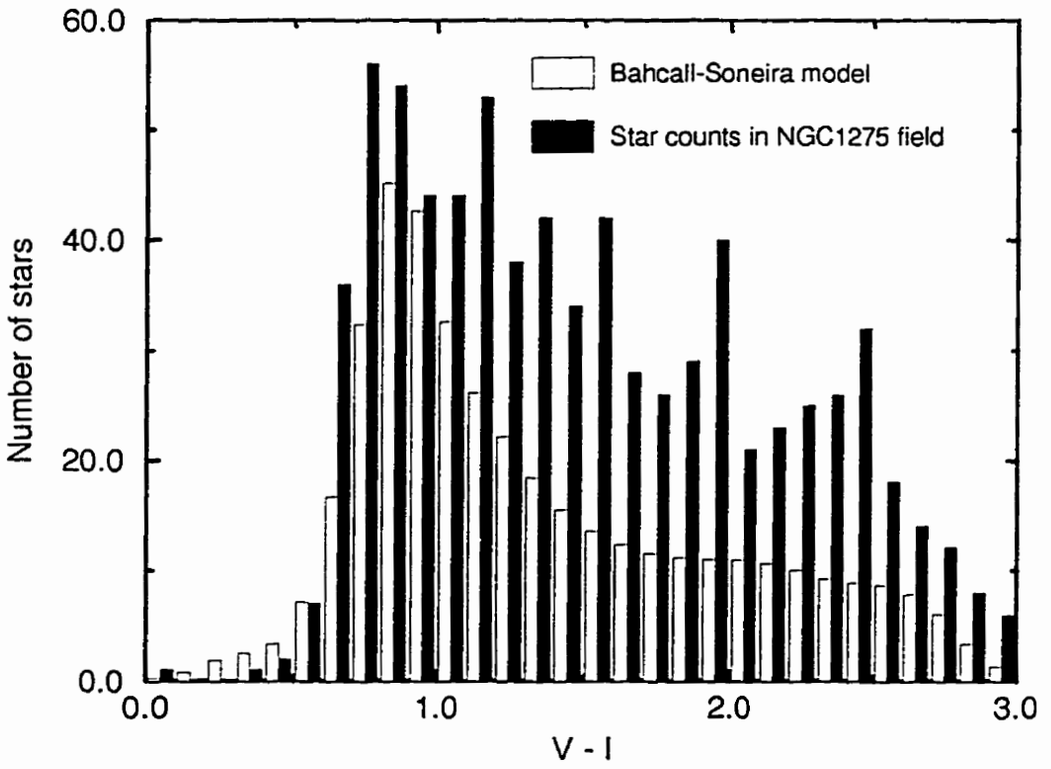

6.3 NGC1265

The giant elliptical galaxy NGC1265 is peculiar in that it is a second-ranked cluster galaxy, but it lies 20′ from the cluster core. Images were obtained in V and I, for a total of 1200s, for this object. Further information may be found in Table 4.1.

As usual, we use the r_{-2} parameter for star-galaxy separation, plotting r_{-2} vs V in Figure 6.34, where we also show the appropriate 'cut' between stars and galaxies. The 'cut' is determined in the usual way. At $V = 21.5$, $r_{-2} = 1.75 \pm 0.12$, $r_{-2} = 1.65 \pm 0.14$ and $r_{-2} = 1.6 \pm 0.20$ at $V = 22.5$. We choose $r_{-2} = 2$ at $V = 22.5$ as our 'cut' for star-galaxy separation. We tabulate the number of objects in the field, stars and galaxies in Table 6.5. These data are plotted in Figure 6.35. Table 6.6 shows the number of galaxies, background galaxies and cluster members. Figure 6.36 shows objects in this field and the estimated number of background galaxies. Note the excess above background. Table 6.6 tabulates the number of galaxies in the cluster, background objects and total number of galaxies in the field. We plot these data in Figure 6.37. The best fit LF (obtained as described above) is given by:

$$\alpha = -1.92 \pm 0.08$$

This is quite consistent with the central field for this cluster. The error quoted is 1σ. At the 99% percentile level, the LF is steeper than $\alpha = -1.73$. This is again consistent with Abell 2199 and with the field around NGC1275. The

radial distribution of objects around this galaxy is not concentrated towards NGC1265, unlike galaxies in the NGC1275 field, as shown in Figure 6.38. A plot of galaxies within 5′ and outside of 5′ from NGC1265 is shown in Figure 6.39 and 6.40, and we compare them in Figure 6.41.

We compute the LF for galaxies in these fields. In Figure 6.42 we show galaxies in the inner 5′ of this field and the LF fit. We find $\alpha = -1.75 \pm 0.22$, The error is of course large enough that a LF shallower than $\alpha = -1.5$ is only ruled out at the 10% level. The corresponding LF for galaxies outside of this area is shown in Figure 6.43. The LF is fit (by maximum likelihood methods) using $\alpha = -1.86 \pm 0.13$. The LF is steeper than $\alpha \sim -1.55$ at the 99% percentile level. As indicated by the radial profile, the LF in this field appears to be marginally steeper than in the area closest to NGC1265. It therefore appears that ellipticals may also destroy dwarfs as well.

We now consider I band images of the NGC1265 field. As usual we plot r_{-2} vs I in Figure 6.44, with the appropriate 'cut' for star galaxy separation. At $I = 20.5$, $r_{-2} = 1.62 \pm 0.12$, and at $I = 21$, $r_{-2} = 1.55 \pm 0.20$. We therefore choose $r = 1.95$ to $I = 21$ as our 'cut' for star-galaxy separation.

Table 6.7 shows the number of objects, galaxies and stars for this field and these data are plotted in Figure 6.45. We plot the number of galaxies in this field and the number of I background galaxies in Figure 6.46. Note the excess of galaxies above the background numbers. Table 6.8 shows the number of galaxies, background galaxies and cluster members for I. Figure

6.47 shows the number of cluster members and the LF. A fit to these data yields:

$$\alpha = -1.78 \pm 0.08$$

We plot the radial distribution for galaxies in this field in Figure 6.48 As we can see, the distribution is quite flat, but consistent with an increase in the number of dwarf at larger distances from NGC1265 (in I). Again, we plot the number of galaxies within $5'$ and outside of this region for NGC1265 in Figures 6.49 and 6.50. These are compared in Figure 6.51. The LF for galaxies in the inner $5'$ of this field is shown in Figure 6.52; the maximum likelihood fit yields $\alpha = -1.86 \pm 0.23$. Figure 6.53 shows the corresponding LF for galaxies in the outer region. Here $\alpha = -1.80 \pm 0.08$.

We consider colors for galaxies in this field. A plot of V vs $V - I$ for galaxies is shown in Figure 6.54. The distribution of colors for galaxies is shown in Figure 6.55. Galaxies have colors between 0.8 and 1.5 with a redder tail. The median color is about 1.2, as for the other fields. The distribution of average colors is shown in Figure 6.56. We see that galaxies have almost the same average $V - I$ at all distances from NGC1265, but there is some evidence for a blueing trend at large radii.

The color magnitude diagram for cluster members (obtained as described above) is shown in Figure 6.57. We note that most galaxies have $V - I$ between 0.7 and 1.5, despite the large scatter. Figure 6.58 shows the corresponding diagram after 10 simulations. The color histogram for cluster

members in this field is shown in Figure 6.59. Note the large contribution from galaxies at $0.75 < V - I < 1.25$. The average color as a function of magnitude is nearly constant, as shown in Figure 6.60.

For stars, the color-magnitude diagram is plotted in Figure 6.61. We note the large concentration of stars at $V - I \sim 1$. This is a 'color edge' to our distributions. The reddening line may be seen as an upper envelope to the diagram.

Figure 6.62 shows the number of galaxies in the NGC1275 and NGC1265 fields. Note that the two distributions are very similar, even in normalization, which is somewhat surprising considering that the NGC 1265 field lies outside the cluster core. The radial distributions of galaxies are compared in Figure 6.63, where we see the concentration around NGC1275, as opposed to the flatter distribution around NGC1265. Colors for galaxies in both fields are also compared in Figure 6.64, where we see that they are quite similar. Similarly, for members we see the same effect in Figure 6.65. The color histogram in Figure 6.66 shows how most galaxies have colors around $V - I \sim 1$, with a quasi Gaussian spread, which is consistent with all galaxies having approximately the same color and being scattered into different color bins by errors.The average color as a function of magnitude for both fields is also constant, as shown in Figure 6.67. Figure 6.68 shows the color histogram for all galaxies in both fields; it can be easily seen that the two distributions are virtually identical.

Figures 6.69 and 6.70 show the star counts in V and I in the NGC1265 field and compare them with the model by Bahcall & Soneira. We see that while the shape is again in good agreement, the normalization of the model is too large by about 50% (again, here normalization is arbitrary). Color distributions shown in Figure 6.71 are again well matched, with a small excess of red objects. As above, if we artificially bring the number of stars in the 'red' part in agreement, there is an excess of blue stars.

Finally, we can compare star counts in V and I for all observed fields in this region, in Figures 6.72 and 6.73. Note the excellent agreement of these star counts.

Figure 6.34: Plot of r_{-2} vs V for NGC1265 field

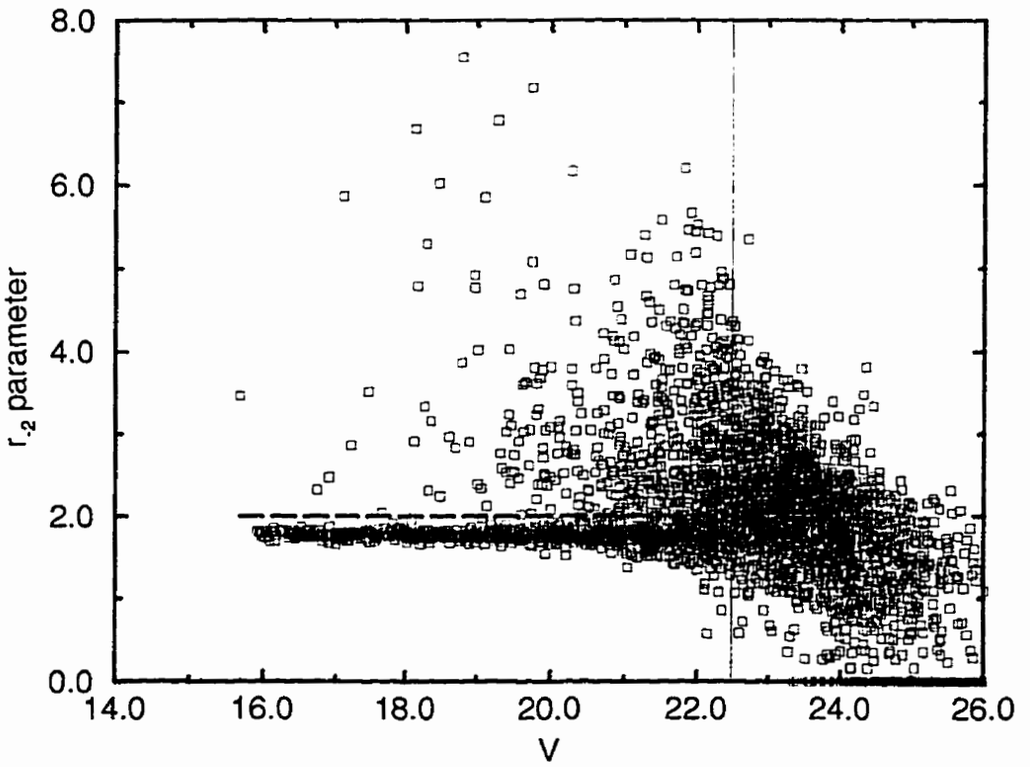

Table 6.5: NUMBER COUNTS FOR NGC1265 FIELD IN V

V	N. of objects	N. of galaxies	N. of stars	Completeness
15.25	1.00 ± 1.00	1.00 ± 1.00	0.00 ± 0.00	1
15.75	5.49 ± 2.34	1.21 ± 1.10	4.28 ± 2.07	1
16.25	31.81 ± 5.64	0.00 ± 0.00	31.81 ± 5.64	1
16.75	51.71 ± 7.19	3.42 ± 1.85	48.28 ± 6.95	1
17.25	53.16 ± 7.29	3.14 ± 1.77	50.02 ± 7.07	1
17.75	50.79 ± 7.13	0.00 ± 0.00	50.79 ± 7.13	1
18.25	76.62 ± 8.75	9.84 ± 3.14	66.78 ± 8.17	1
18.75	73.75 ± 8.59	8.63 ± 2.94	65.11 ± 8.07	1
19.25	93.71 ± 9.68	18.04 ± 4.25	75.67 ± 8.70	1
19.75	103.23 ± 10.16	30.82 ± 5.55	72.41 ± 8.51	1
20.25	133.16 ± 11.54	30.81 ± 5.55	102.34 ± 10.12	1
20.75	176.53 ± 13.29	56.62 ± 7.52	119.90 ± 10.95	1
21.25	189.68 ± 13.77	80.10 ± 8.95	109.58 ± 10.47	1
21.75	231.44 ± 15.21	116.24 ± 10.78	115.20 ± 10.73	1
22.25	414.43 ± 20.36	242.82 ± 15.58	171.59 ± 13.10	0.9

Figure 6.35: Number counts of objects, stars and galaxies in NGC1265 V field

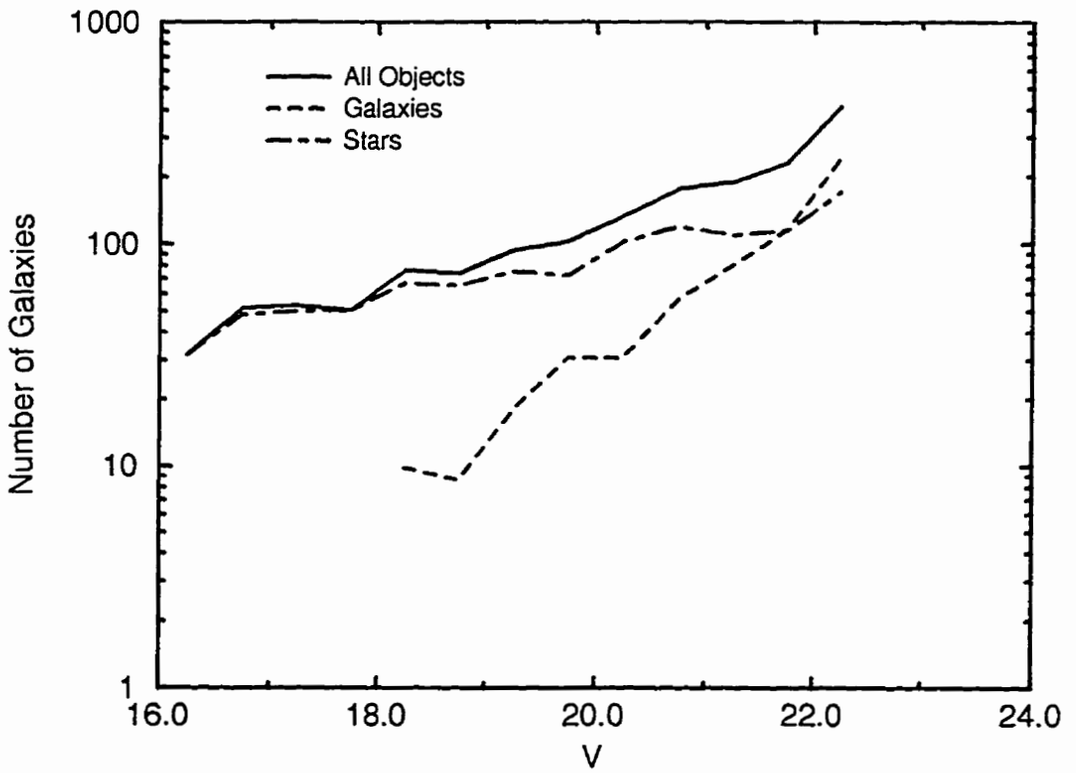

Table 6.6: NUMBER COUNTS OF GALAXIES AND BACKGROUND OBJECTS FOR NGC1265 FIELD IN V

V	N. of galaxies	Background counts	N. of cluster members
15.25	1.00 ± 1.00	0.18	0.82 ± 1.09
15.75	1.21 ± 1.10	0.29	0.92 ± 1.22
16.25	0.00 ± 0.00	0.46	-0.46 ± 0.68
16.75	3.42 ± 1.85	0.72	2.70 ± 2.04
17.25	3.14 ± 1.77	1.15	1.99 ± 2.07
17.75	0.00 ± 0.00	1.82	-1.82 ± 1.35
18.25	9.84 ± 3.14	2.88	6.96 ± 3.57
18.75	8.63 ± 2.94	4.57	4.06 ± 3.63
19.25	18.04 ± 4.25	7.24	10.80 ± 5.03
19.75	30.82 ± 5.55	11.48	19.34 ± 6.50
20.25	30.81 ± 5.55	18.20	12.61 ± 7.00
20.75	56.62 ± 7.52	28.84	27.78 ± 9.24
21.25	80.10 ± 8.95	45.71	34.39 ± 11.22
21.75	116.24 ± 10.78	72.44	43.80 ± 13.74
22.25	242.82 ± 15.58	114.82	128.00 ± 18.91

Figure 6.36: Number counts of galaxies and background galaxies in NGC1265 V field

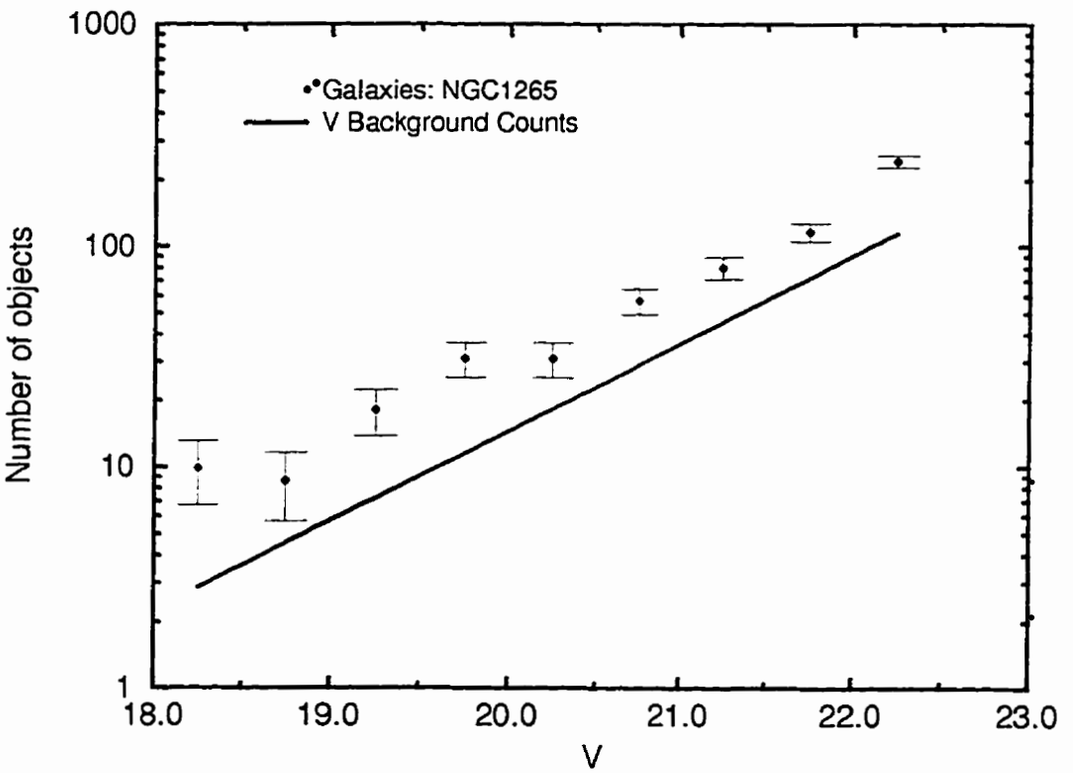

Figure 6.37: Number counts of galaxies and LF in NGC1265 V field

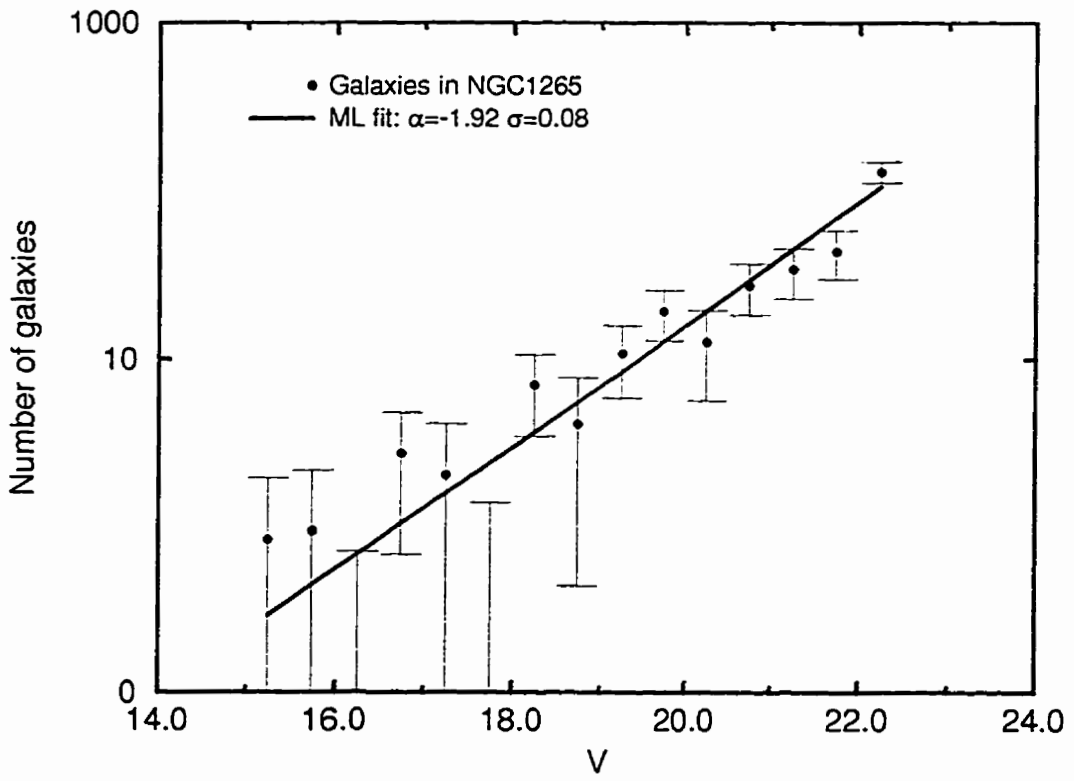

Figure 6.38: Radial distribution of objects in NGC1265 V field

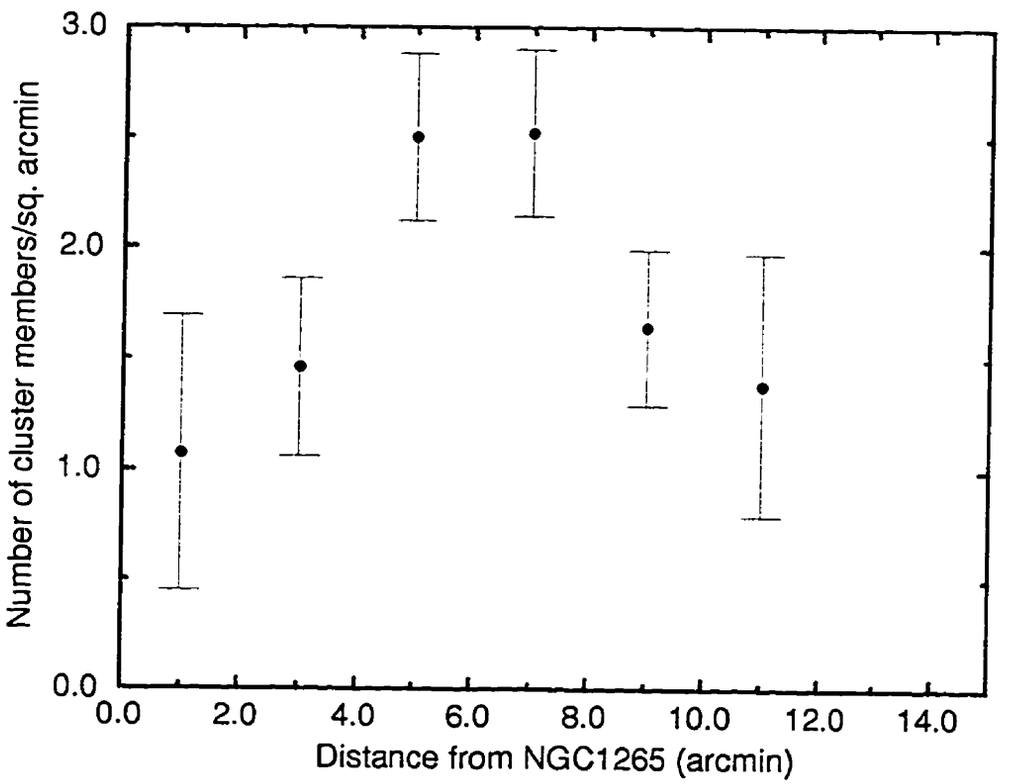

Figure 6.39: Number counts of galaxies in inner 5′ of NGC1265 field in V

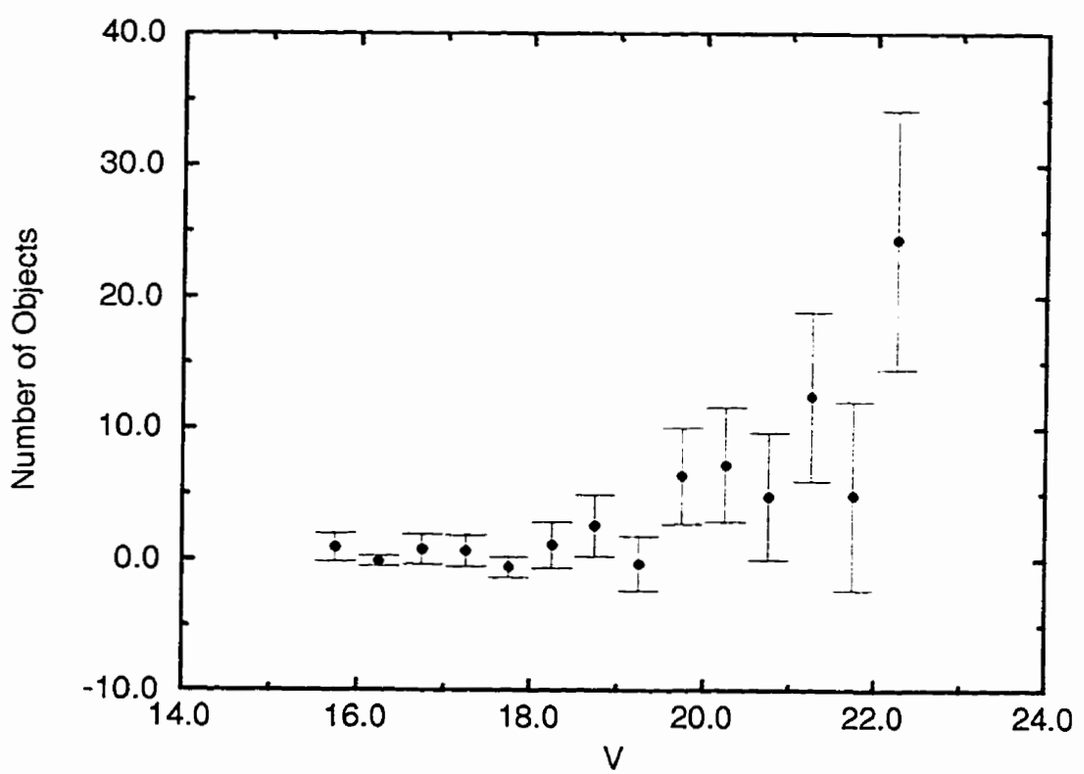

Figure 6.40: Number counts of galaxies more distant than 5′ from NGC1265

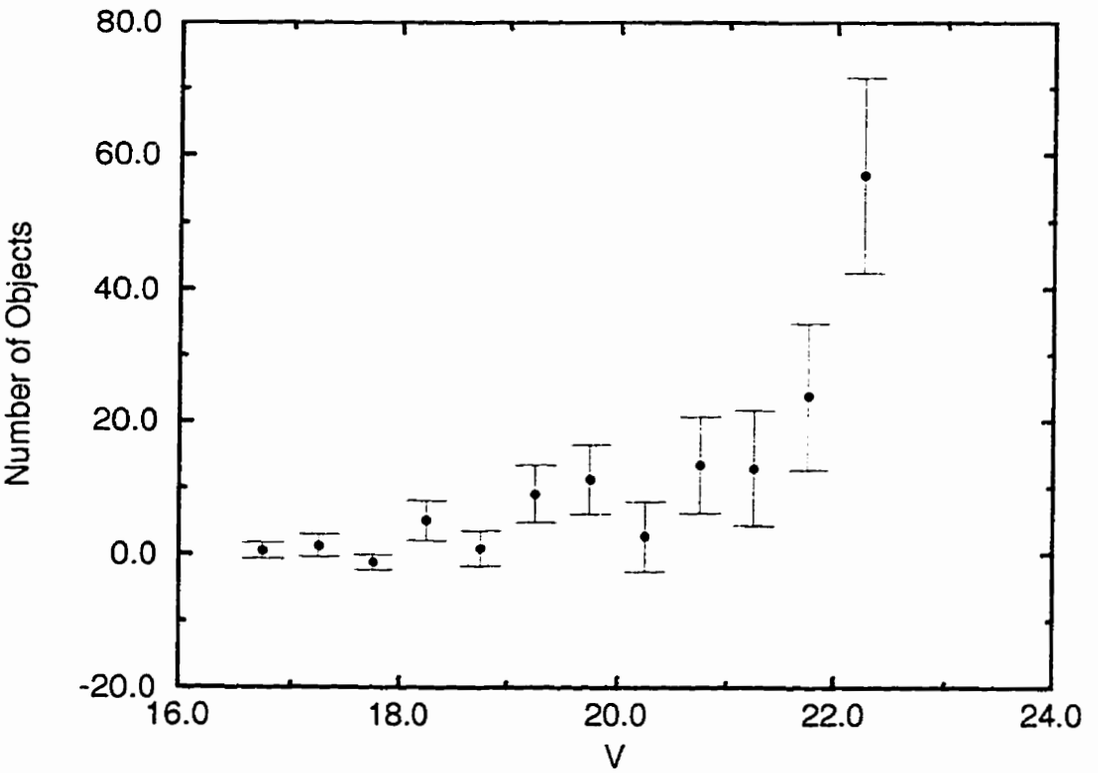

Figure 6.41: Comparison of inner and outer fields

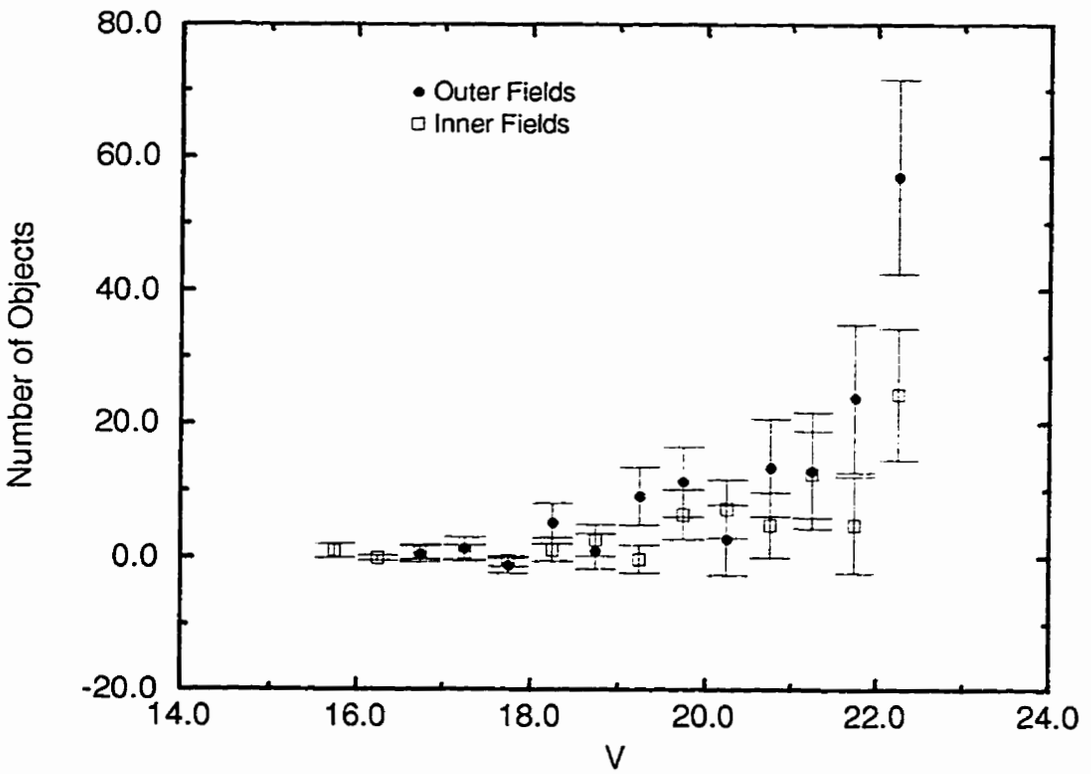

Figure 6.42: LF for galaxies in inner 5′ of NGC1265 field

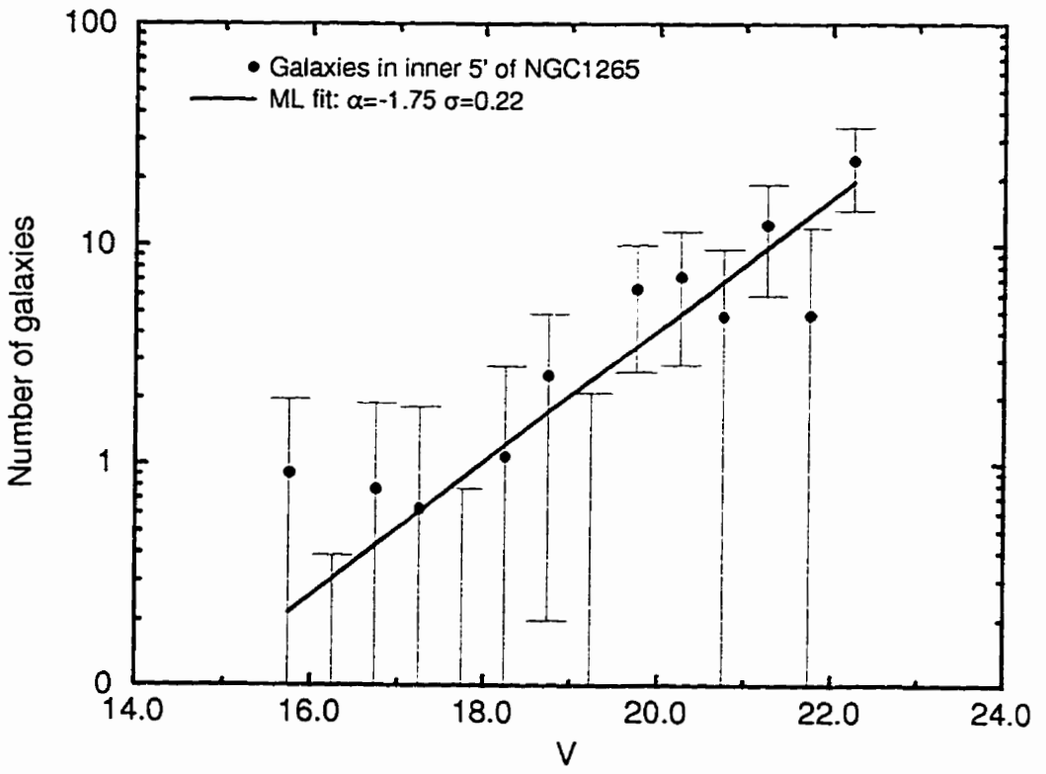

Figure 6.43: LF for galaxies in inner 5′ of NGC1265 field

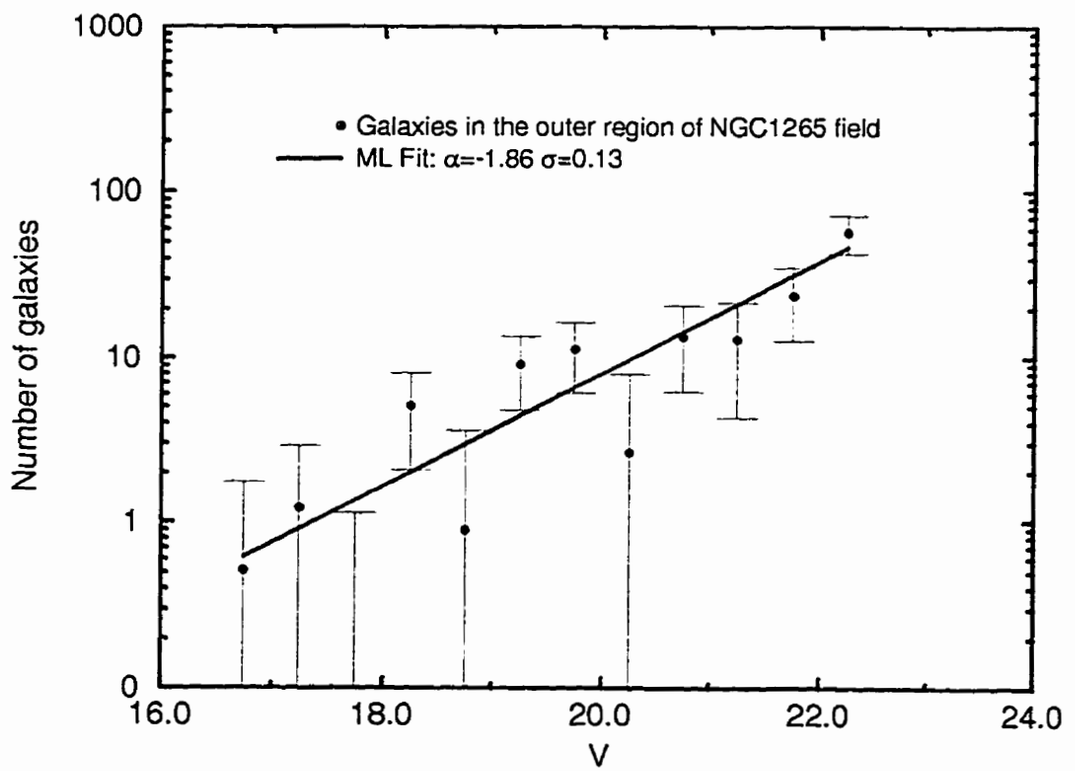

Figure 6.44: Plot of r_{-2} vs I for NGC1265 field

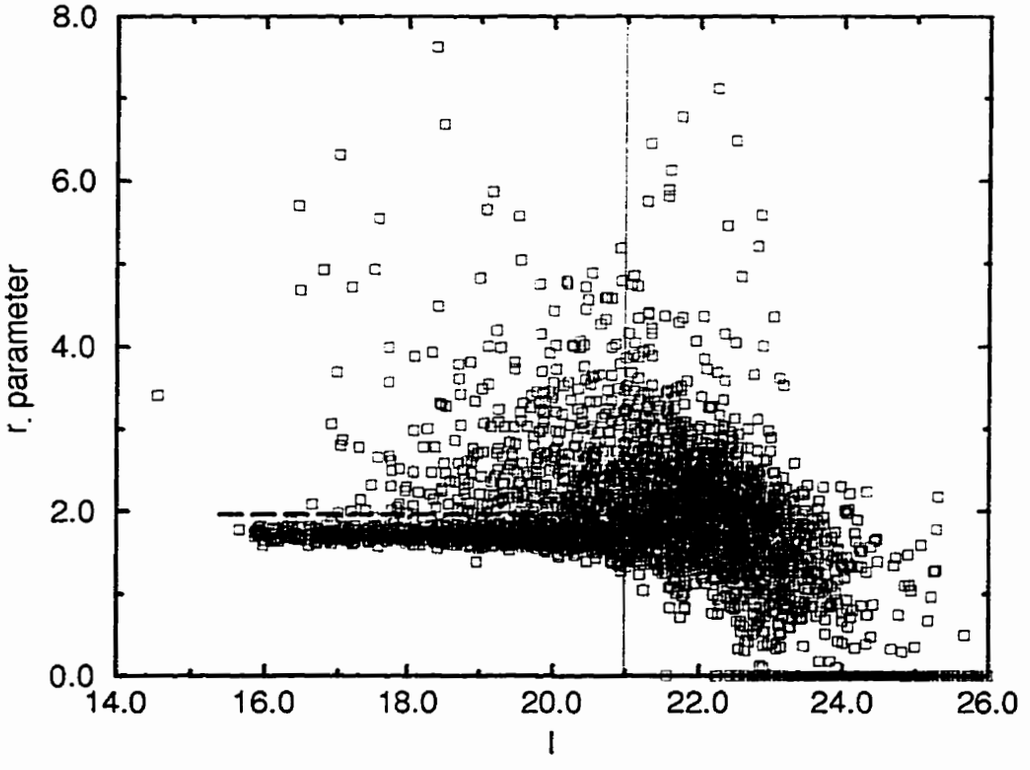

Table 6.7: NUMBER COUNTS FOR NGC1265 I

I	N. of objects	N. of galaxies	N. of stars	Completeness
15.75	18.03 ± 4.25	0.00 ± 0.00	18.05 ± 4.25	1
16.25	53.99 ± 7.35	2.08 ± 1.44	52.03 ± 7.21	1
16.75	65.34 ± 8.08	4.29 ± 2.07	61.25 ± 7.83	1
17.25	86.79 ± 9.32	10.77 ± 3.28	76.27 ± 8.73	1
17.75	94.54 ± 9.72	21.03 ± 4.59	73.74 ± 8.59	1
18.25	129.55 ± 11.38	25.24 ± 5.02	104.70 ± 10.23	1
18.75	155.74 ± 12.48	36.48 ± 6.04	119.79 ± 10.94	1
19.25	197.75 ± 14.06	57.62 ± 7.59	140.85 ± 11.87	1
19.75	226.97 ± 15.07	85.08 ± 9.22	142.53 ± 11.94	1
20.25	294.69 ± 17.17	133.69 ± 11.56	161.82 ± 12.72	1
20.75	349.33 ± 18.69	184.66 ± 13.59	167.38 ± 12.94	1

Figure 6.45: Number of objects, stars and galaxies vs I for NGC1265 field

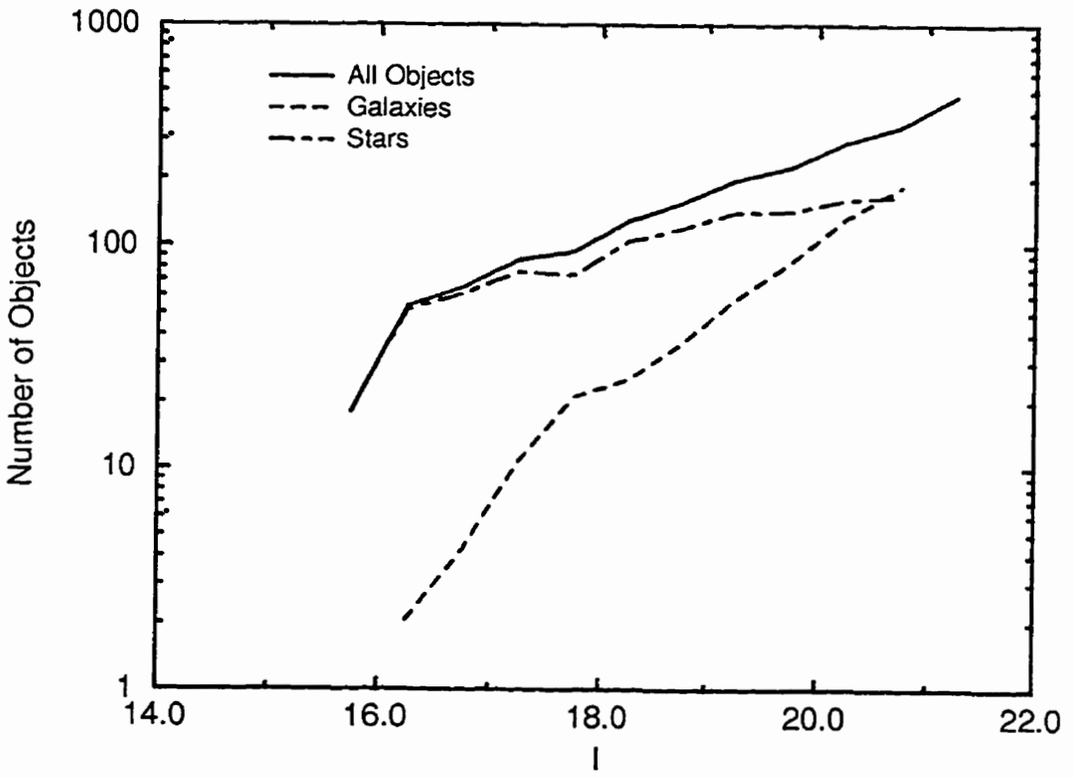

Table 6.8: NUMBER COUNTS FOR GALAXIES AND BACKGROUND OBJECTS FOR NGC1265 *I*

I	N. of galaxies	Background counts	N. of cluster members
17.25	10.77 ± 3.28	7.33	3.44 ± 4.25
17.75	21.03 ± 4.59	10.84	10.19 ± 5.65
18.25	25.24 ± 5.02	16.03	9.21 ± 6.42
18.75	36.48 ± 6.04	23.71	12.77 ± 7.76
19.25	57.62 ± 7.59	35.08	22.54 ± 9.63
19.75	85.08 ± 9.22	51.88	33.20 ± 11.70
20.25	133.69 ± 11.56	76.74	56.95 ± 14.51
20.75	184.66 ± 13.59	113.50	71.16 ± 17.27

Figure 6.46: Number of galaxies and background counts vs I for NGC1265 field

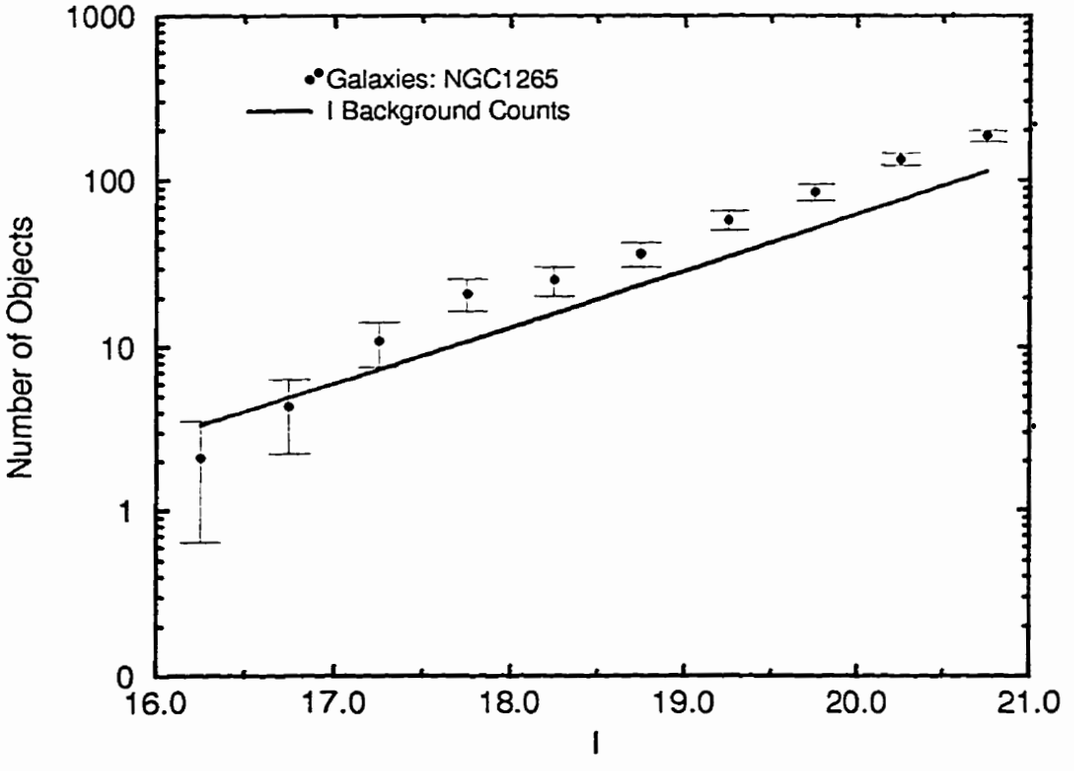

Figure 6.47: Number of cluster members vs I and LF for NGC1265 field

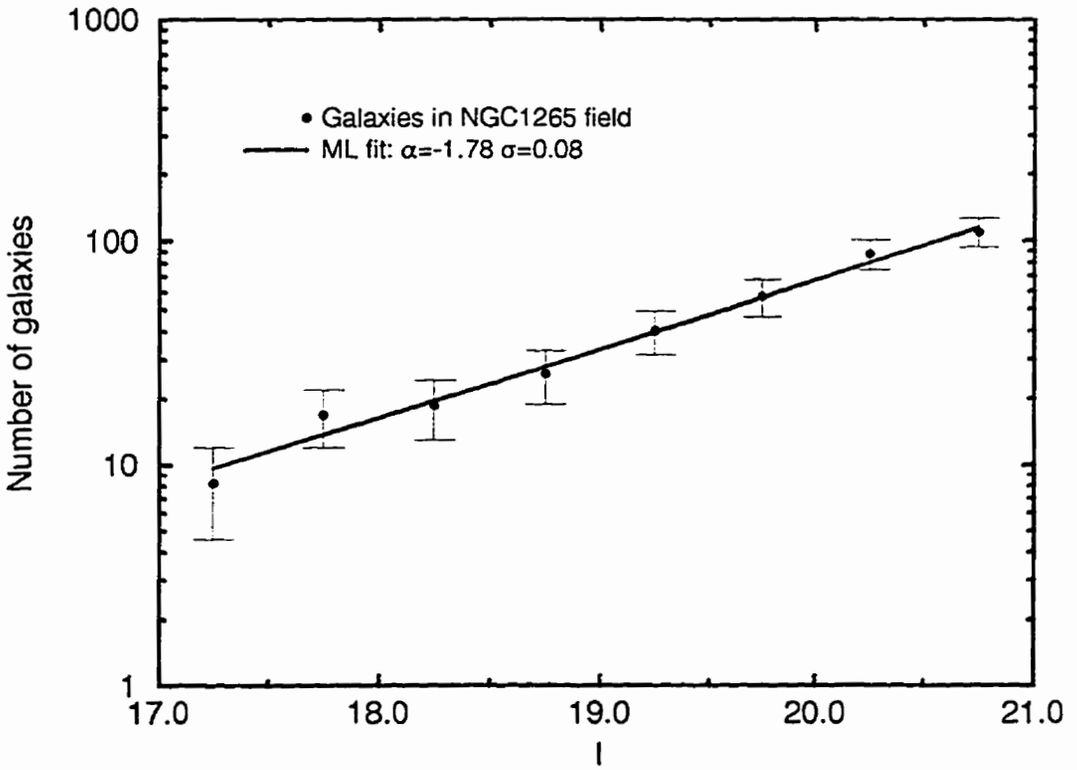

Figure 6.48: Radial distributions of galaxies for NGC1265 field

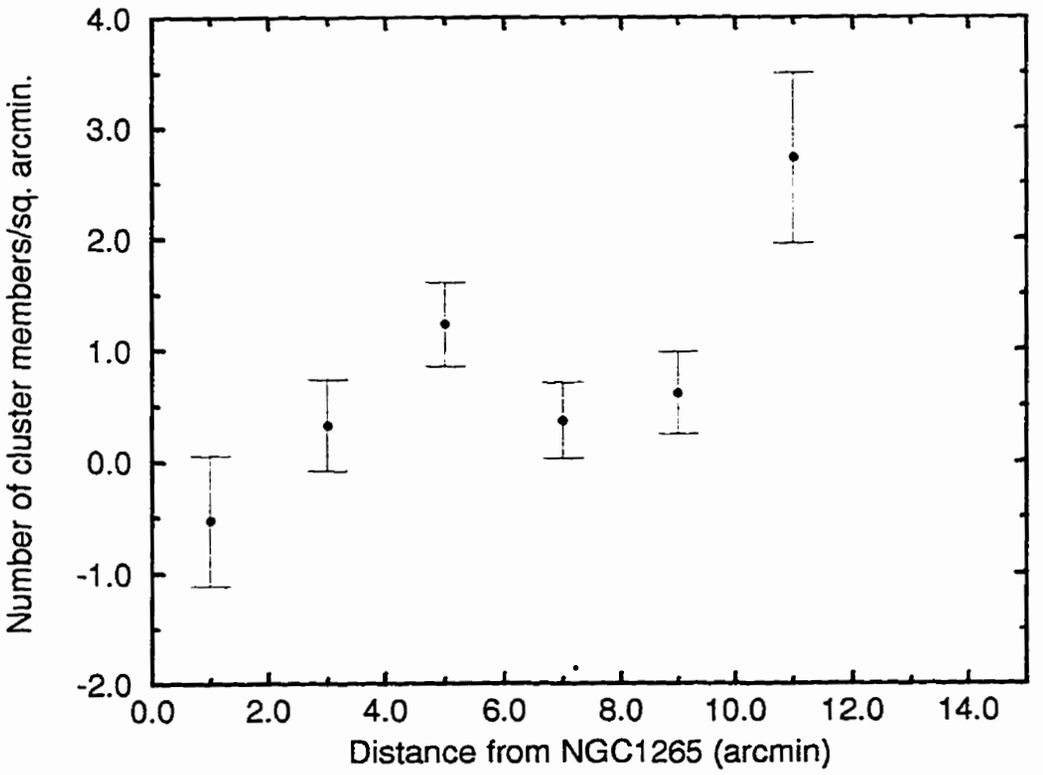

Figure 6.49: Number of objects in inner 5′ of NGC1265 field

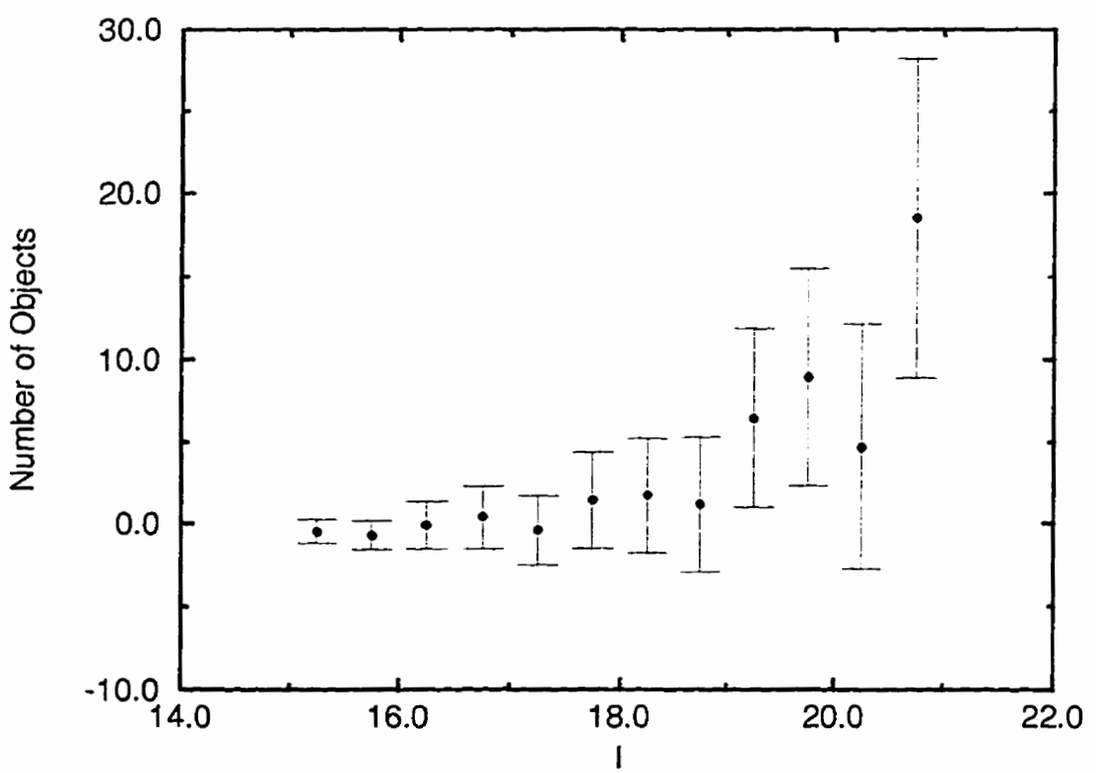

Figure 6.50: Number of objects more distant than 5′ from NGC1265

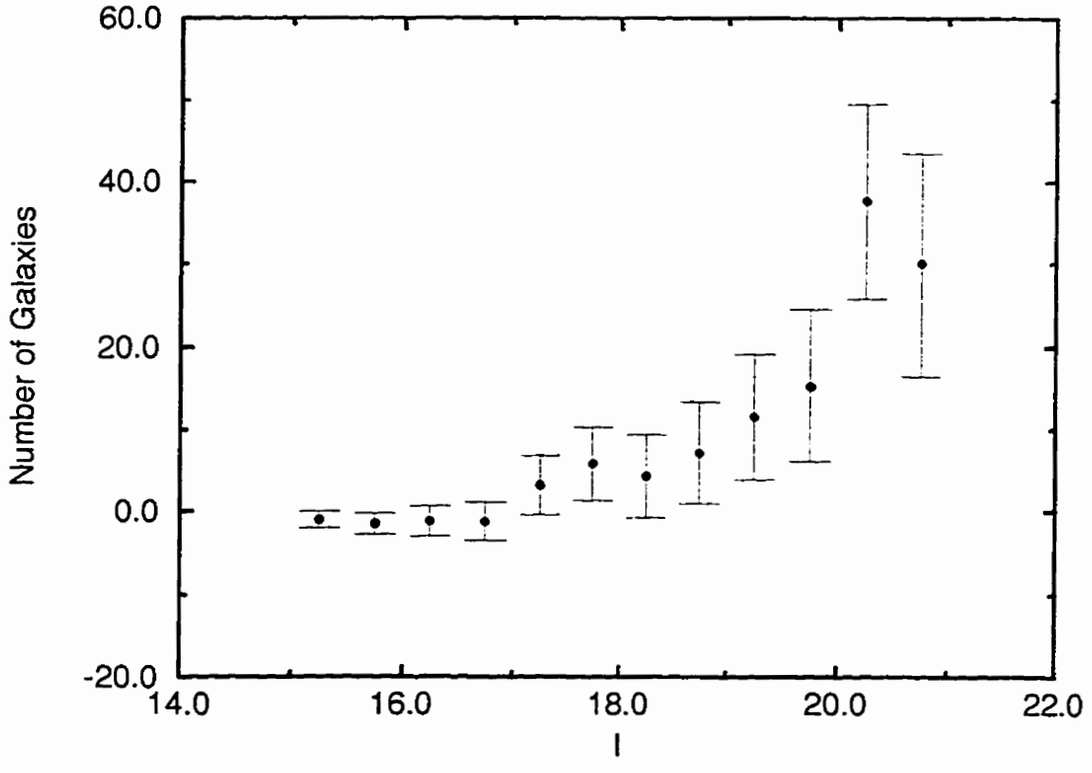

Figure 6.51: Comparison of inner and outer fields

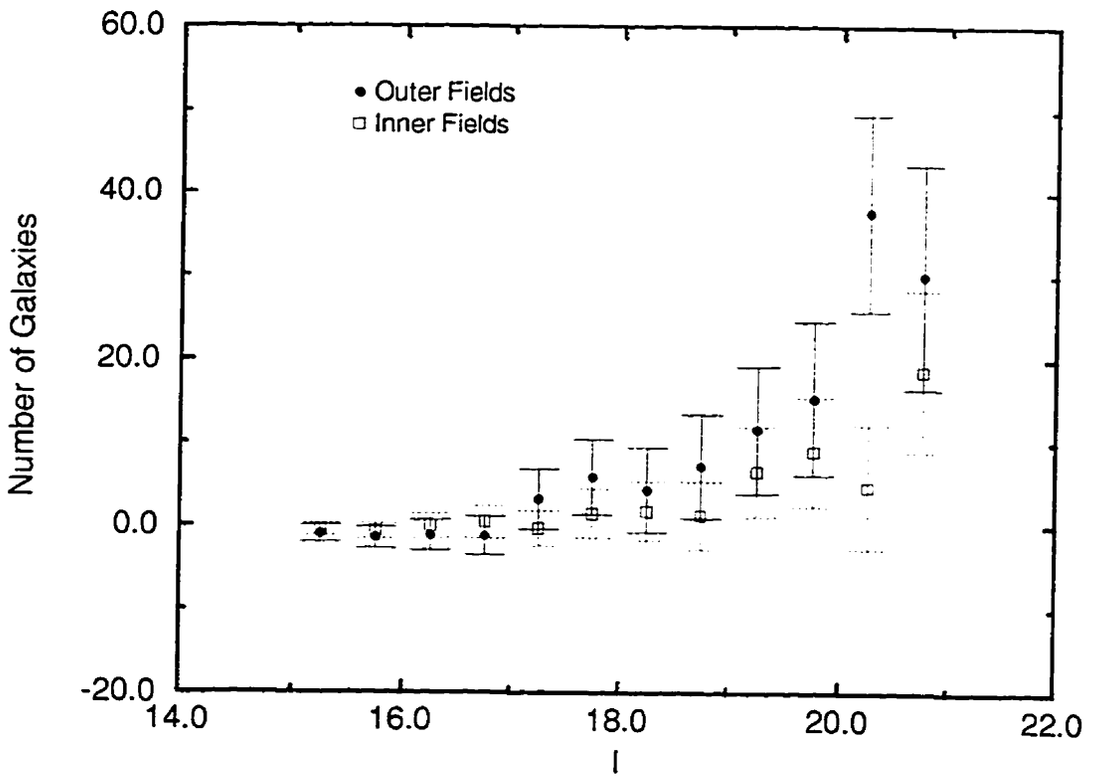

Figure 6.52: The LF for the inner 5' of NGC1265 field

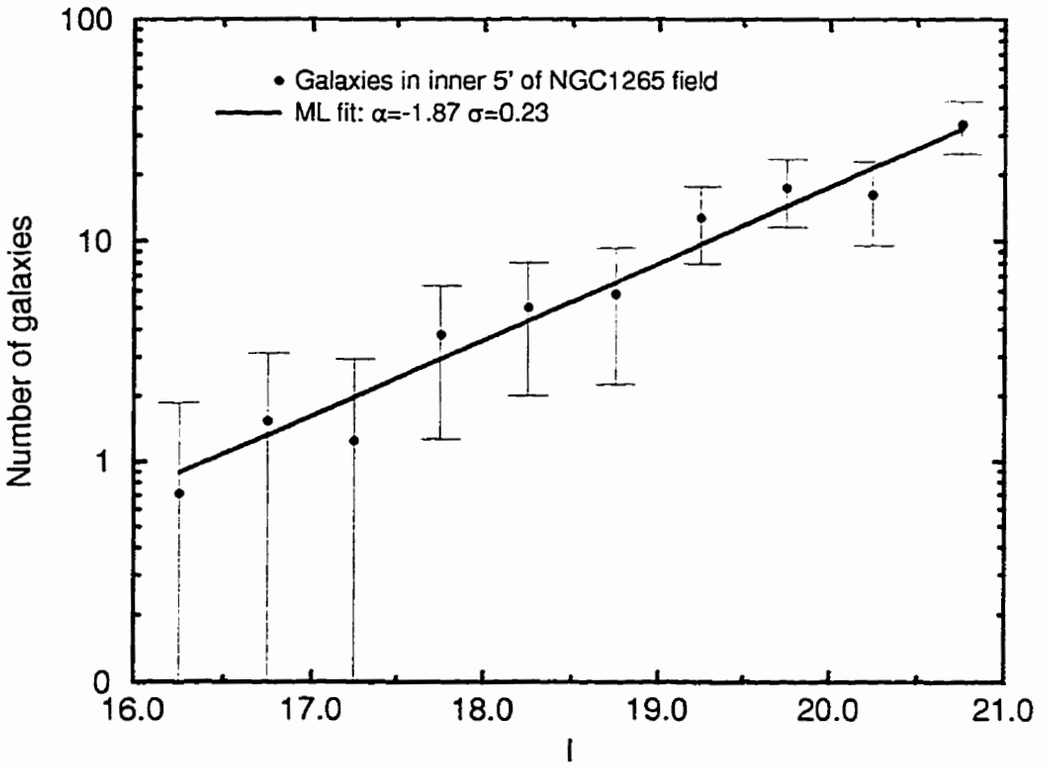

Figure 6.53: The LF for the outer region of NGC1265 field

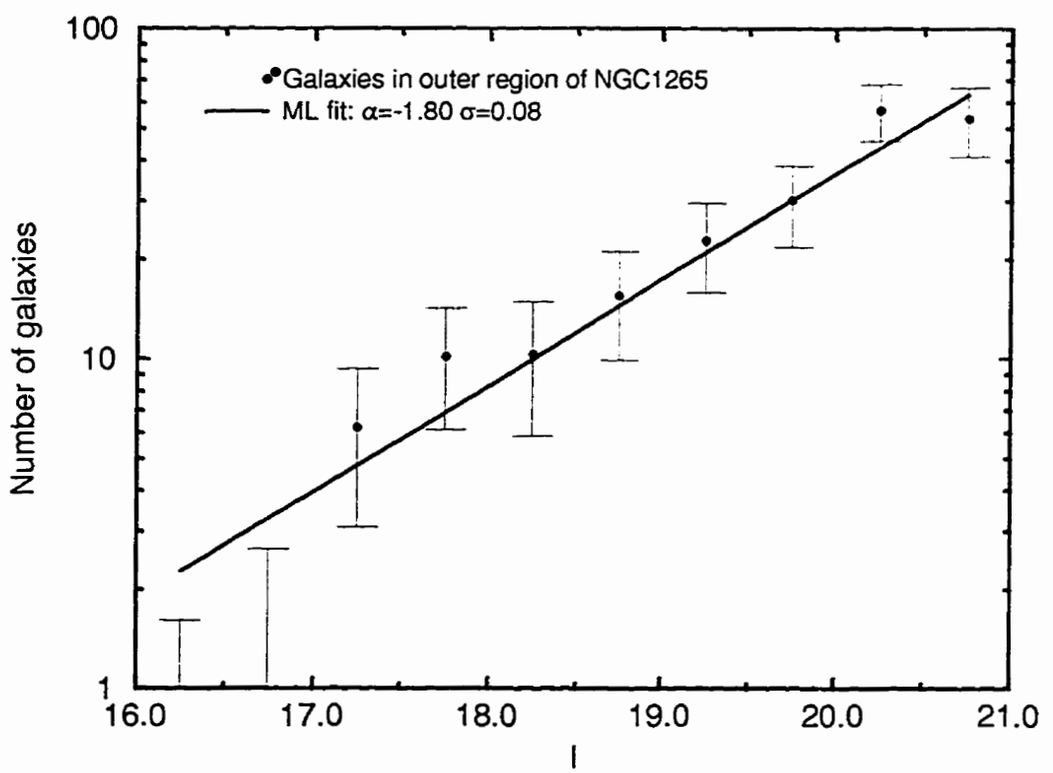

Figure 6.54: Color magnitude diagram for galaxies in NGC1265 field

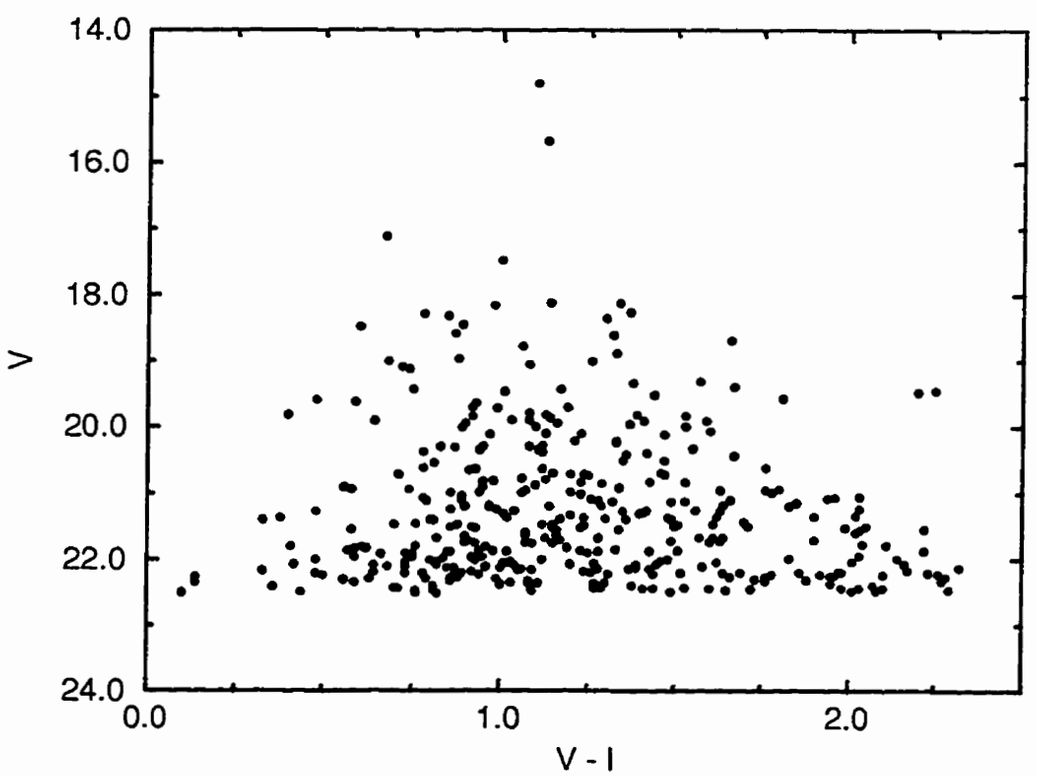

Figure 6.55: Histogram of galaxy colors for NGC1265 field

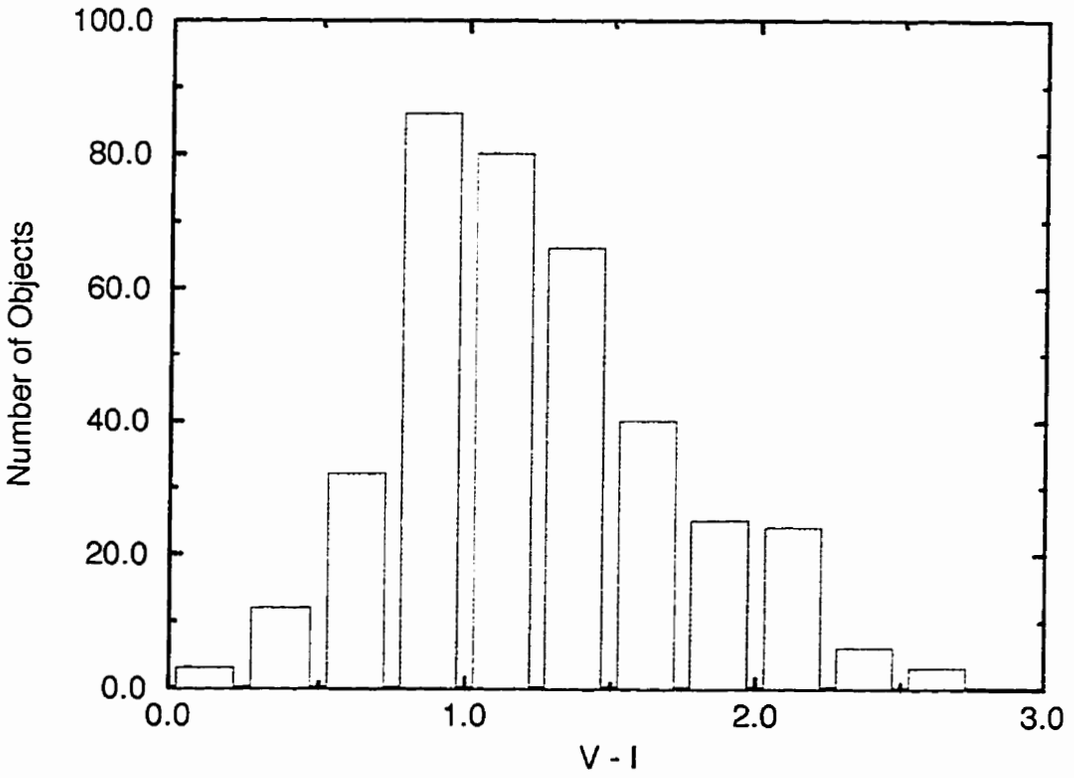

Figure 6.56: Radial distribution of average colors for galaxies in NGC1265 field

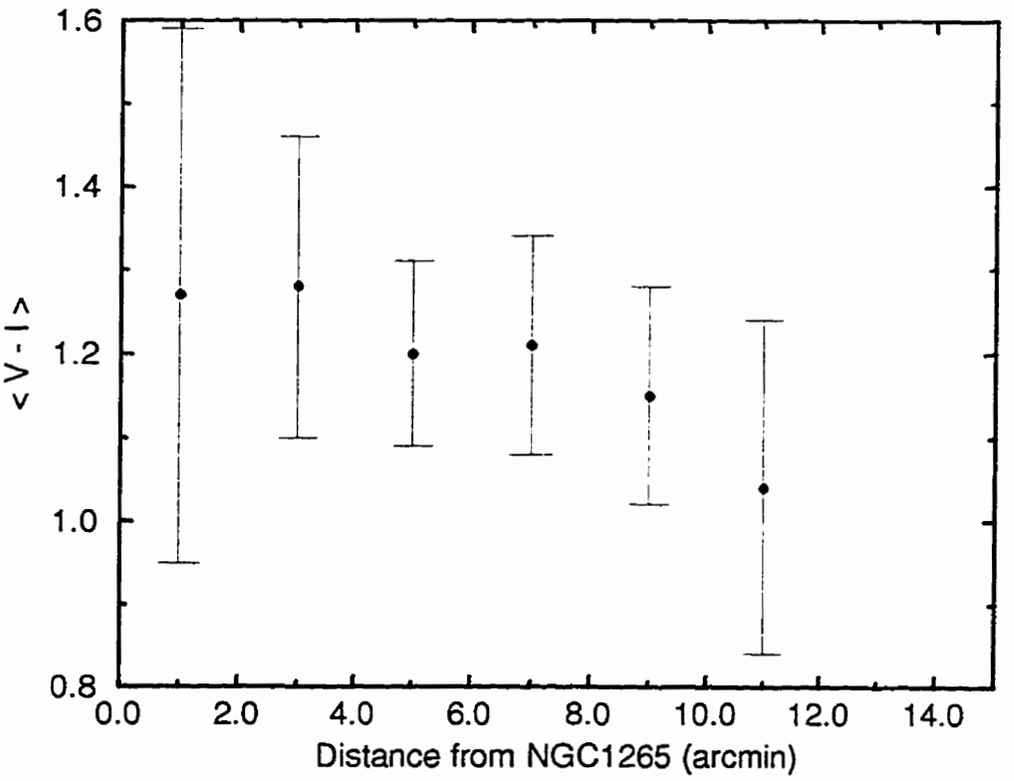

Figure 6.57: Color magnitude diagram for cluster members in NGC1265 field

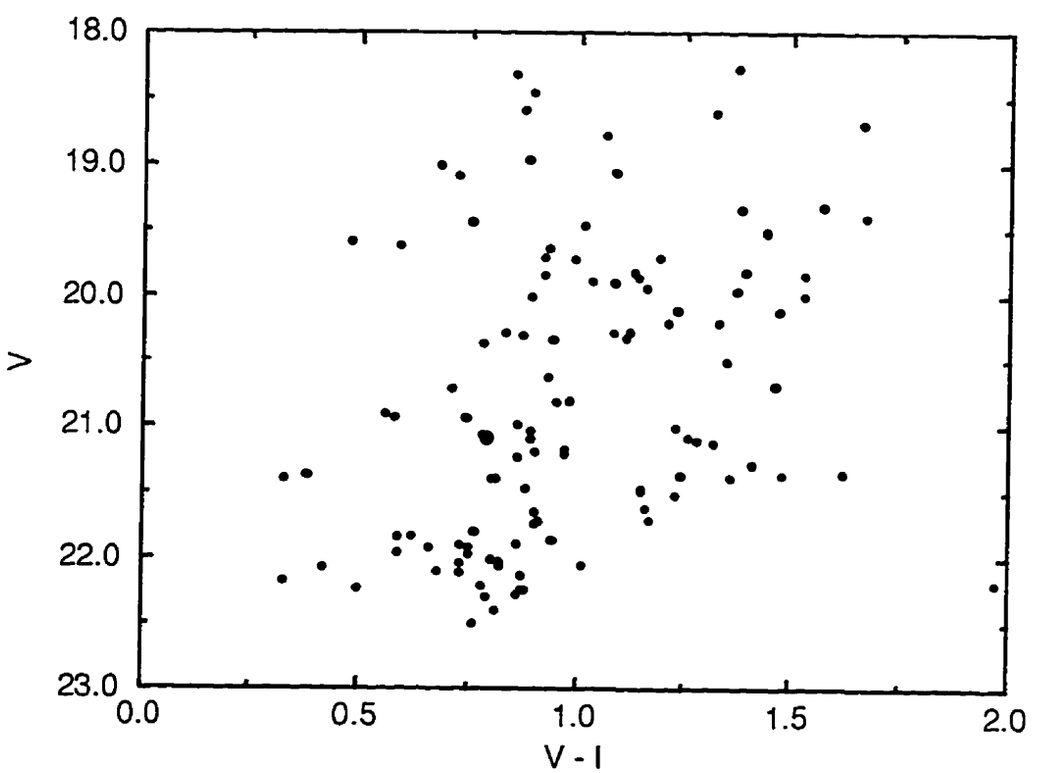

Figure 6.58: Color magnitude diagram for cluster members in NGC1275 field, as obtained by simulations

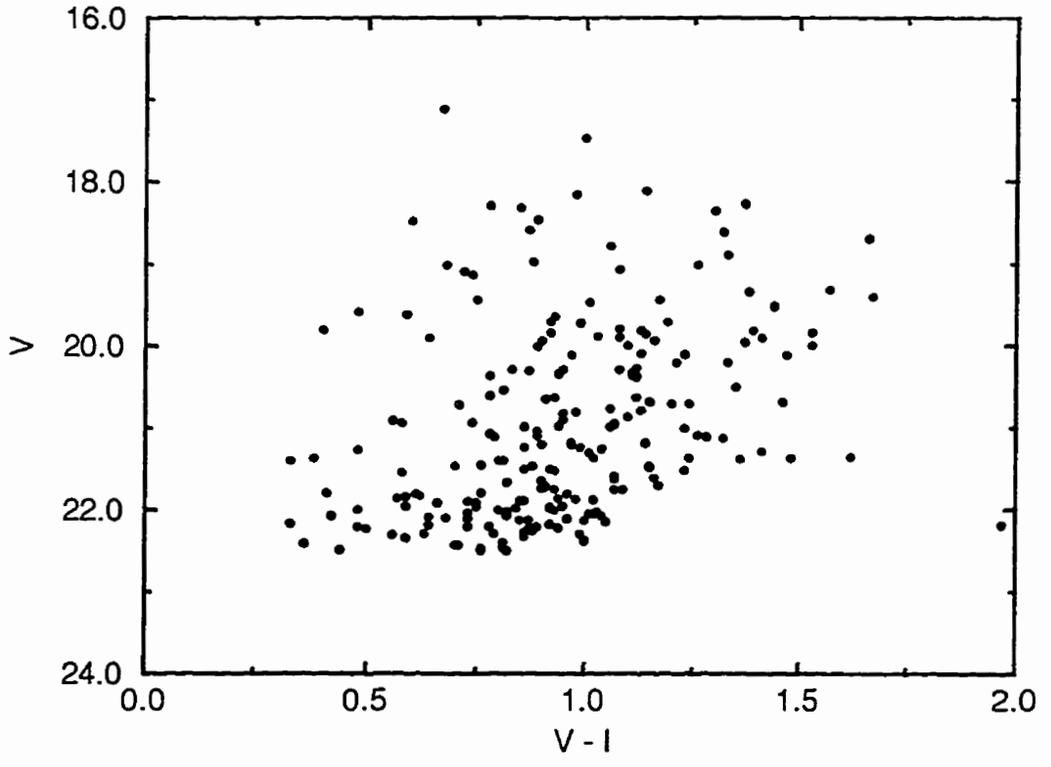

Figure 6.59: Color histogram for cluster members in NGC1265 field

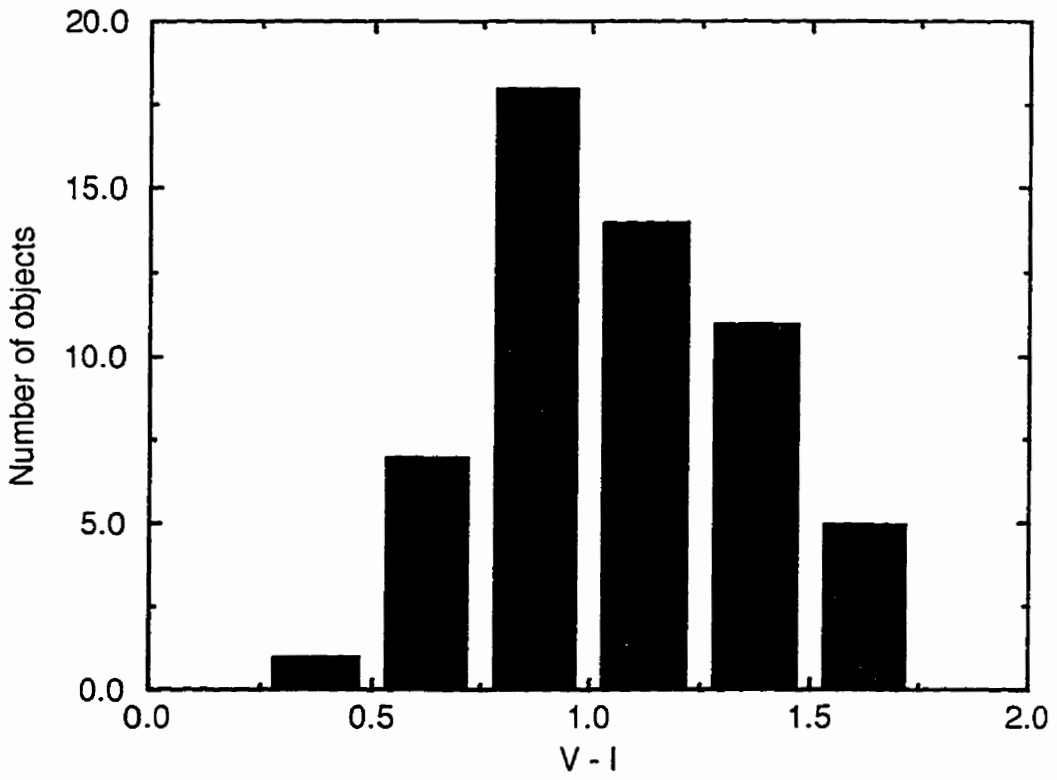

Figure 6.60: Average color as a function of magnitude in NGC1265 field galaxies

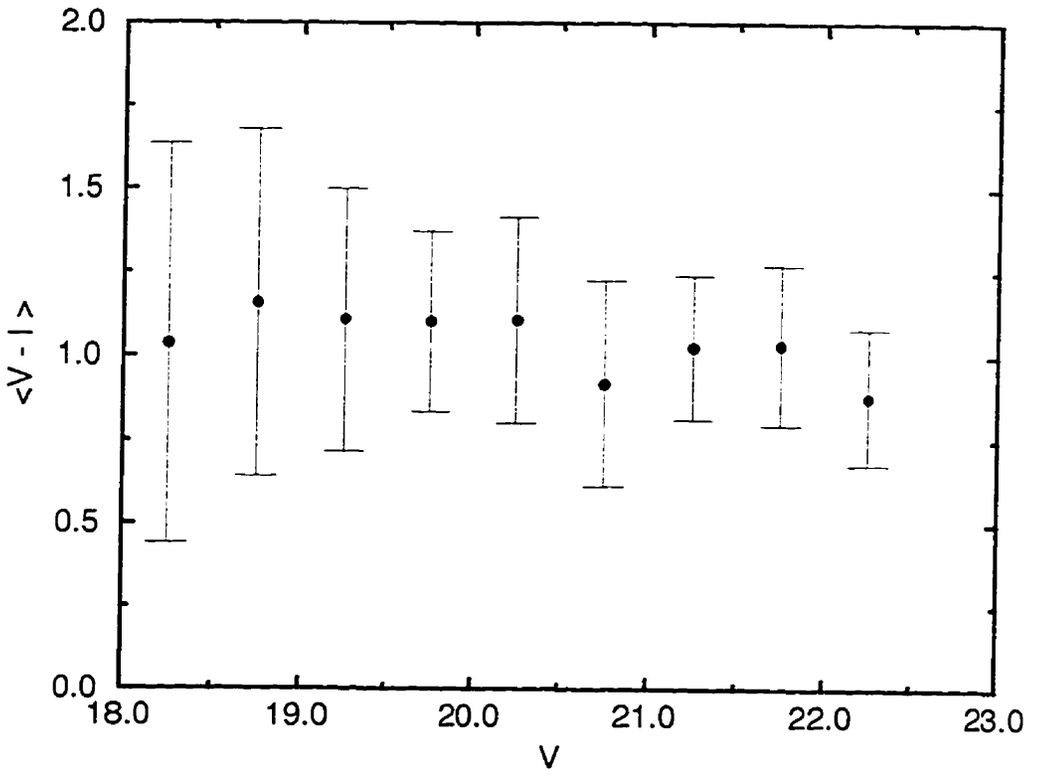

Figure 6.61: Color magnitude for stars in NGC1265 field

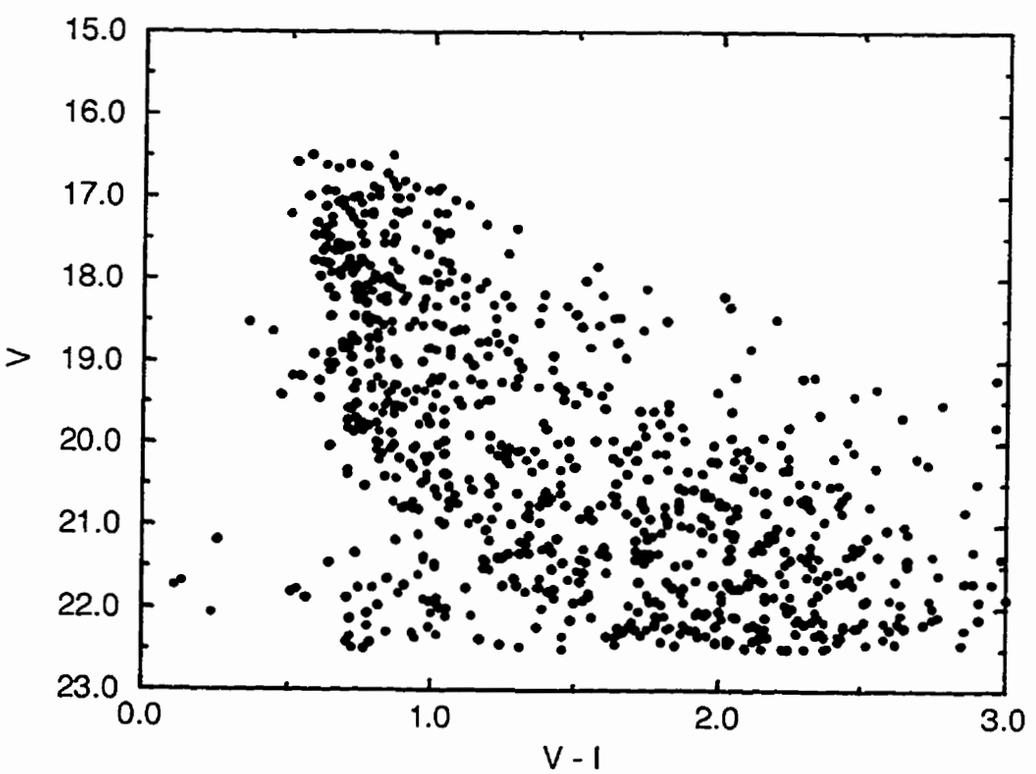

Figure 6.62: Comparison of V LF for NGC1275 and NGC1265

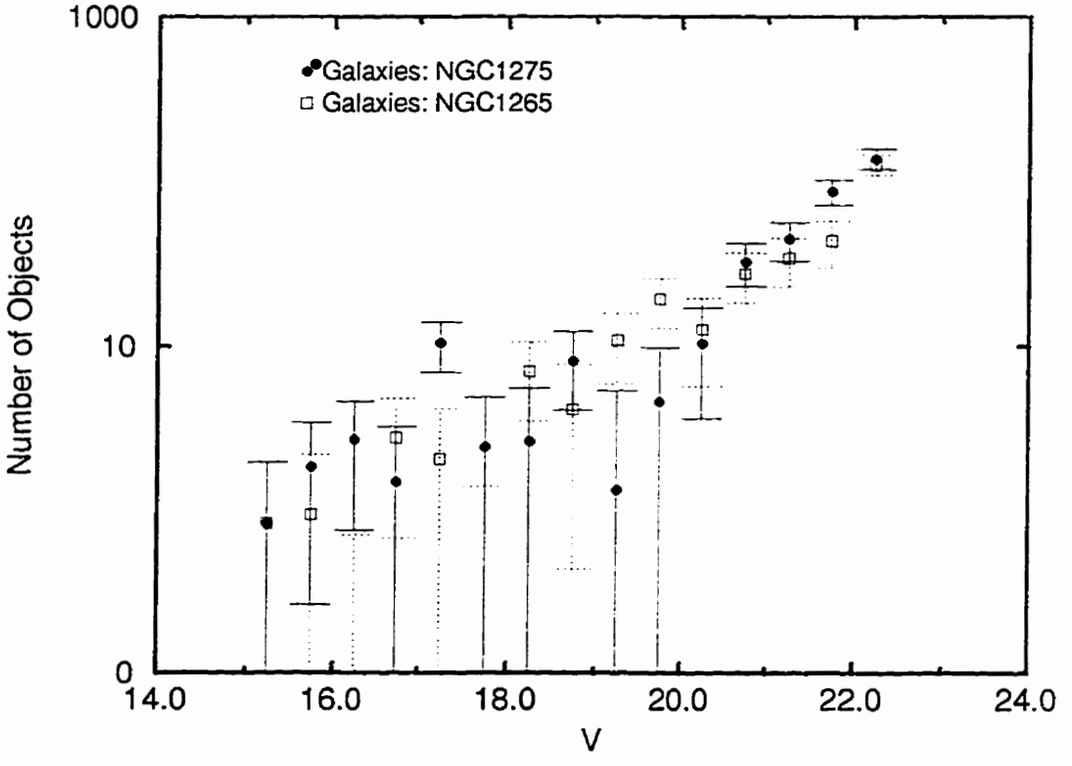

Figure 6.63: Comparison of radial distributions for NGC1275 and NGC1265 fields (V data only)

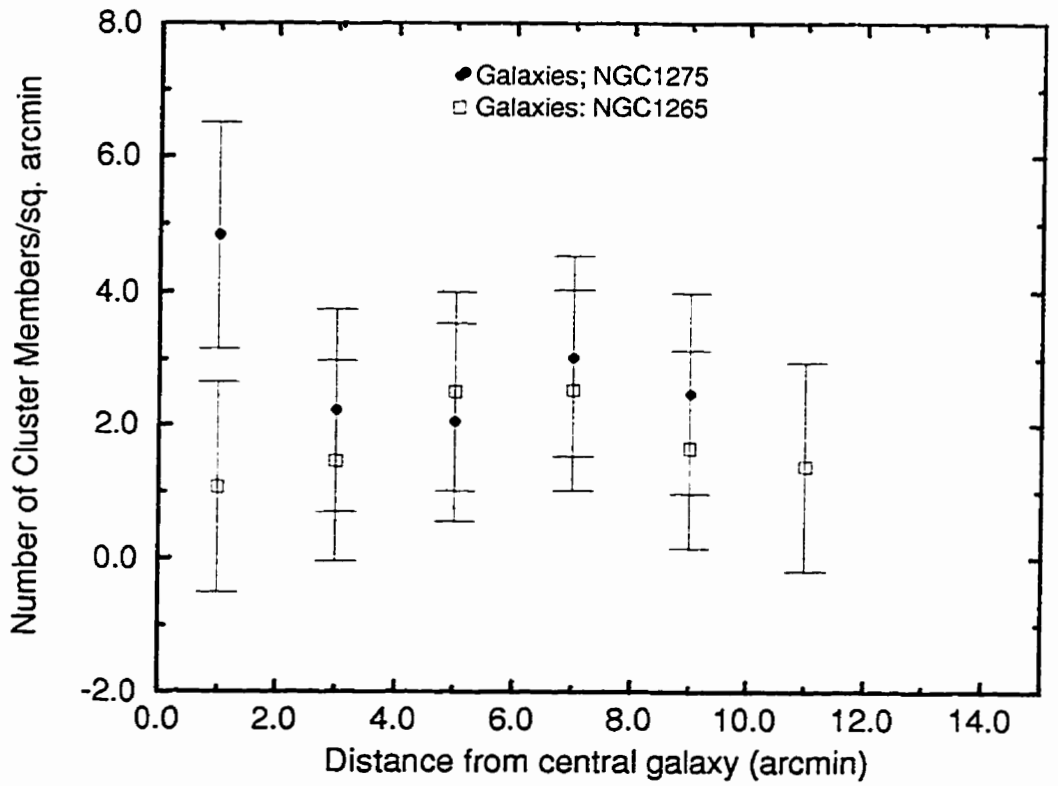

Figure 6.64: Color magnitude diagram for galaxies in NGC1275 and NGC1265 fields

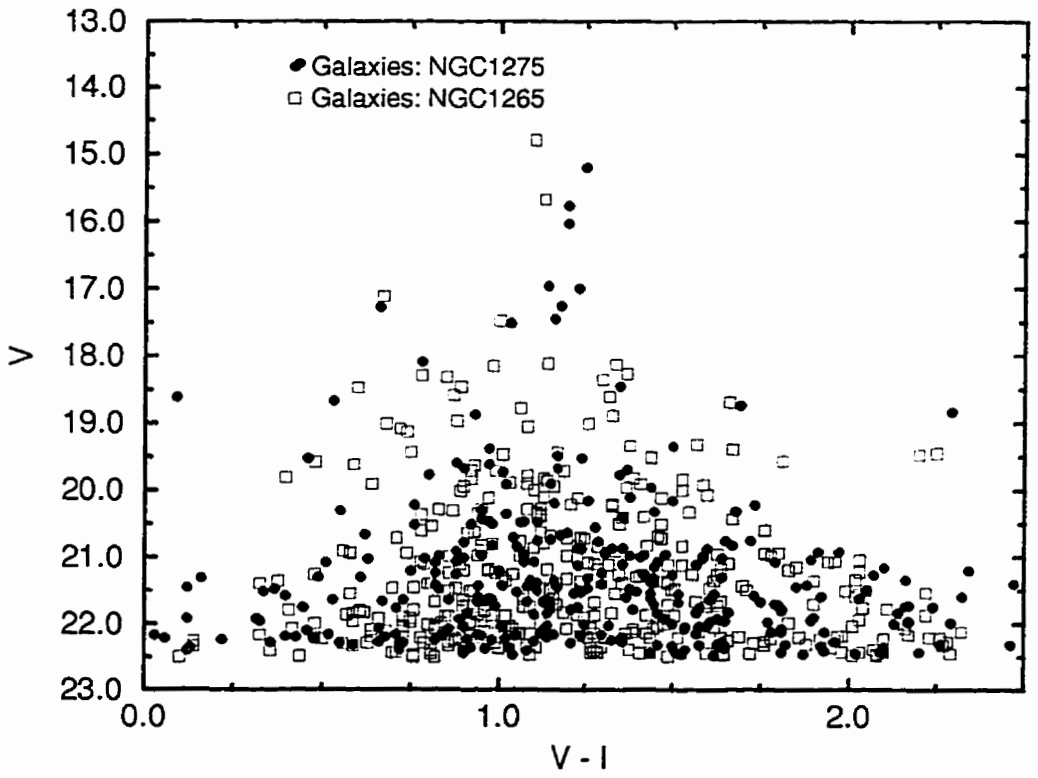

Figure 6.65: Color magnitude diagram for cluster members in NGC1275 and NGC1265 fields

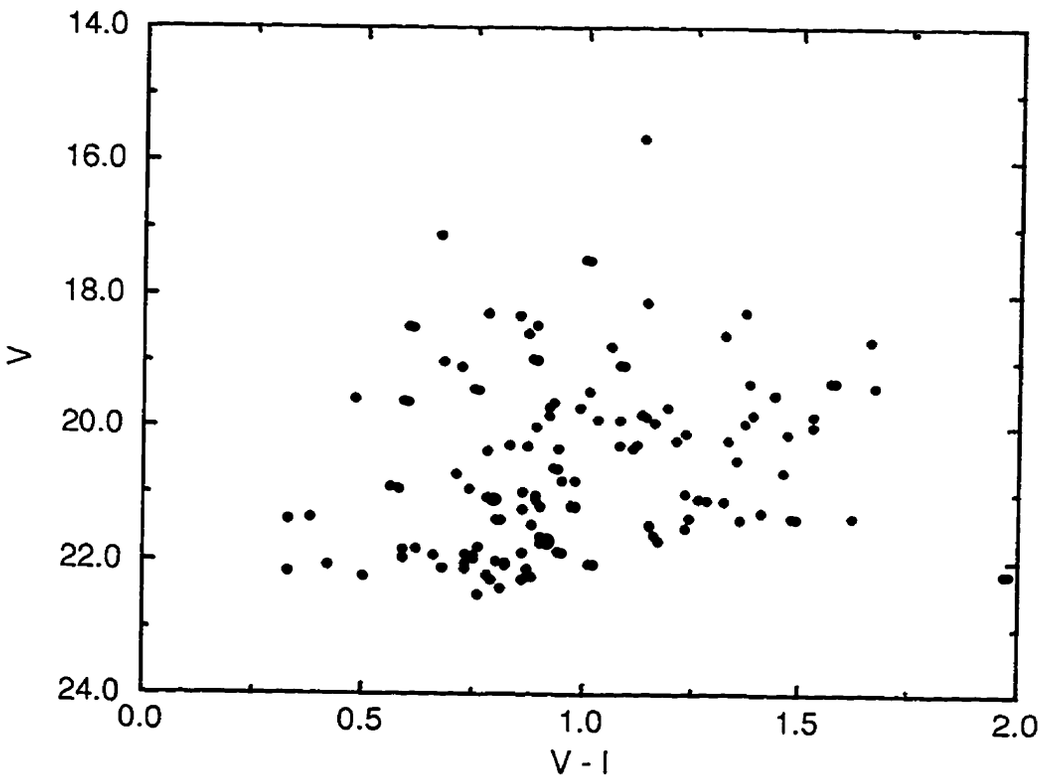

Figure 6.66: Color magnitude histogram for cluster members in NGC1275 and NGC1265 fields

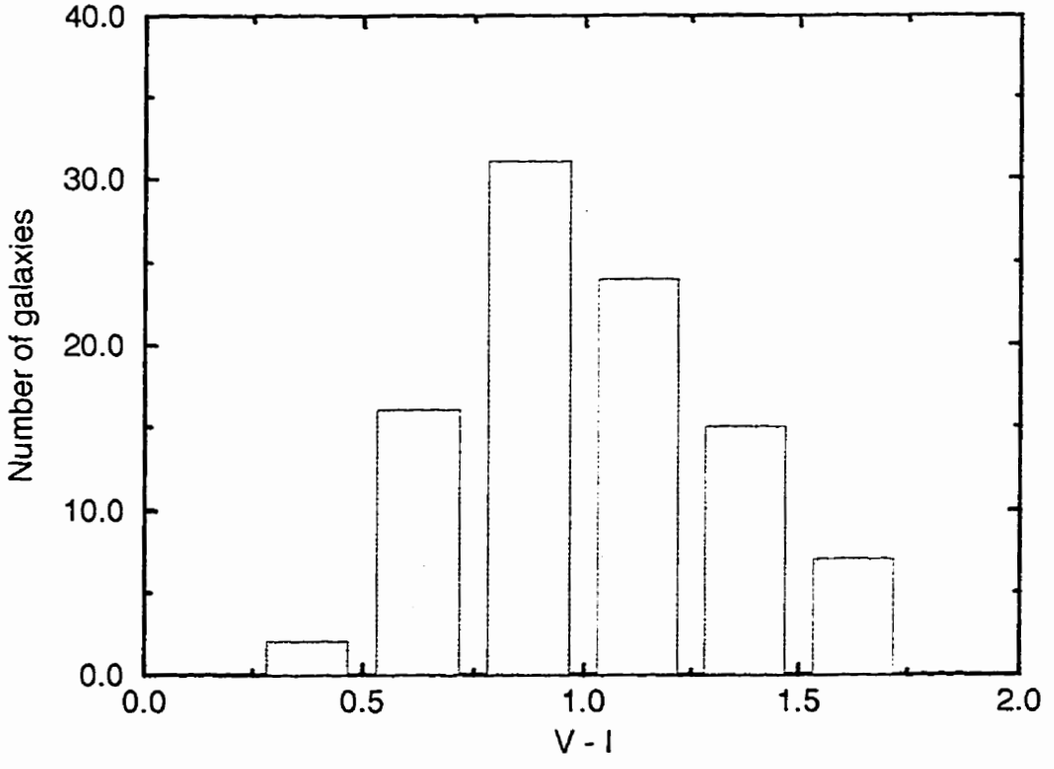

Figure 6.67: Average color vs V for cluster members in NGC1275 and NGC1265 fields

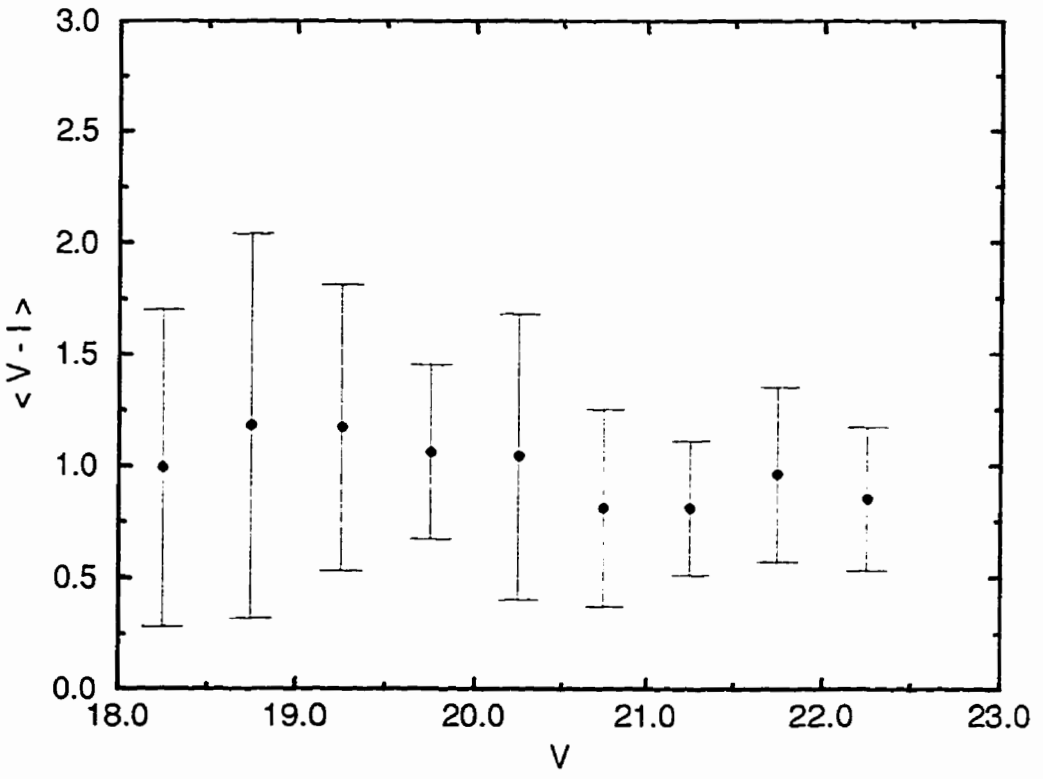

Figure 6.68: Comparison of color histograms for NGC1275 and NGC1265

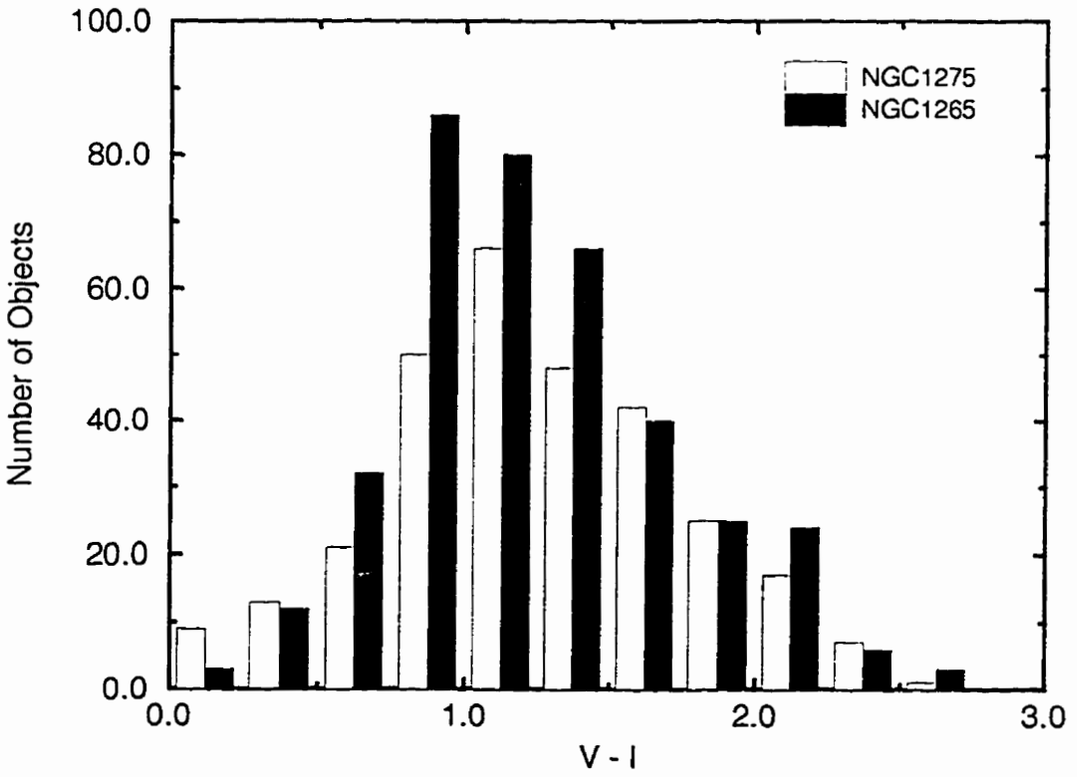

Figure 6.69: Stars and model for NGC1265 field in V

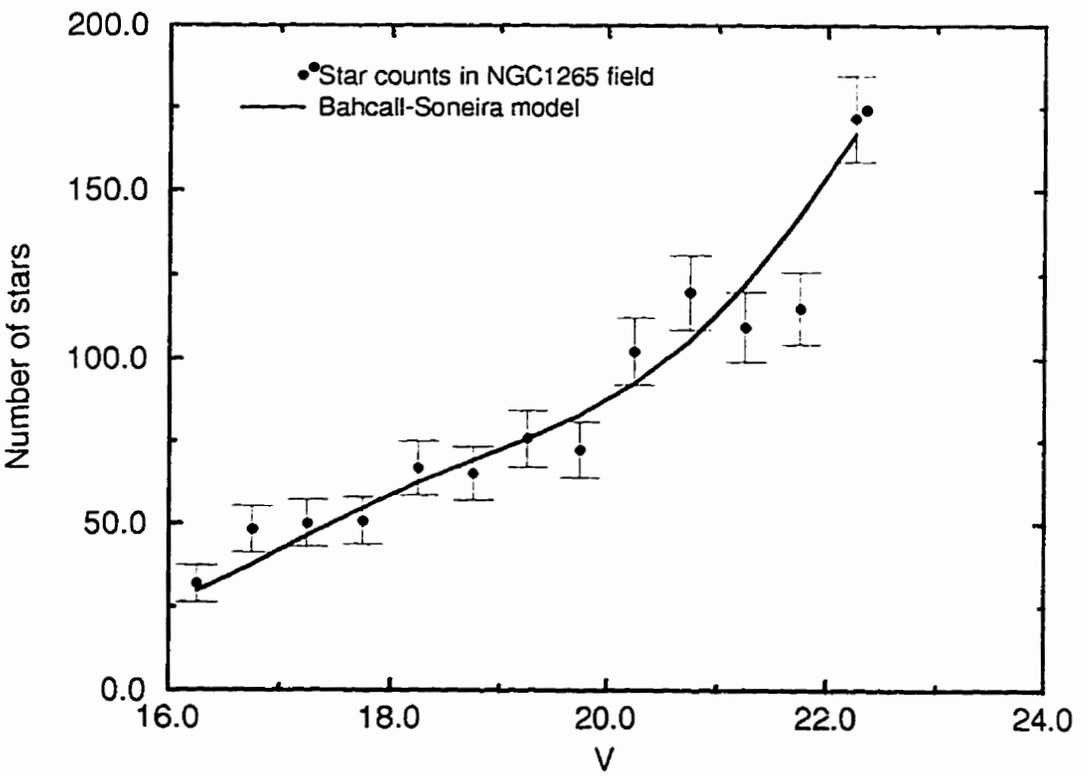

Figure 6.70: Stars and model for NGC1265 field in I

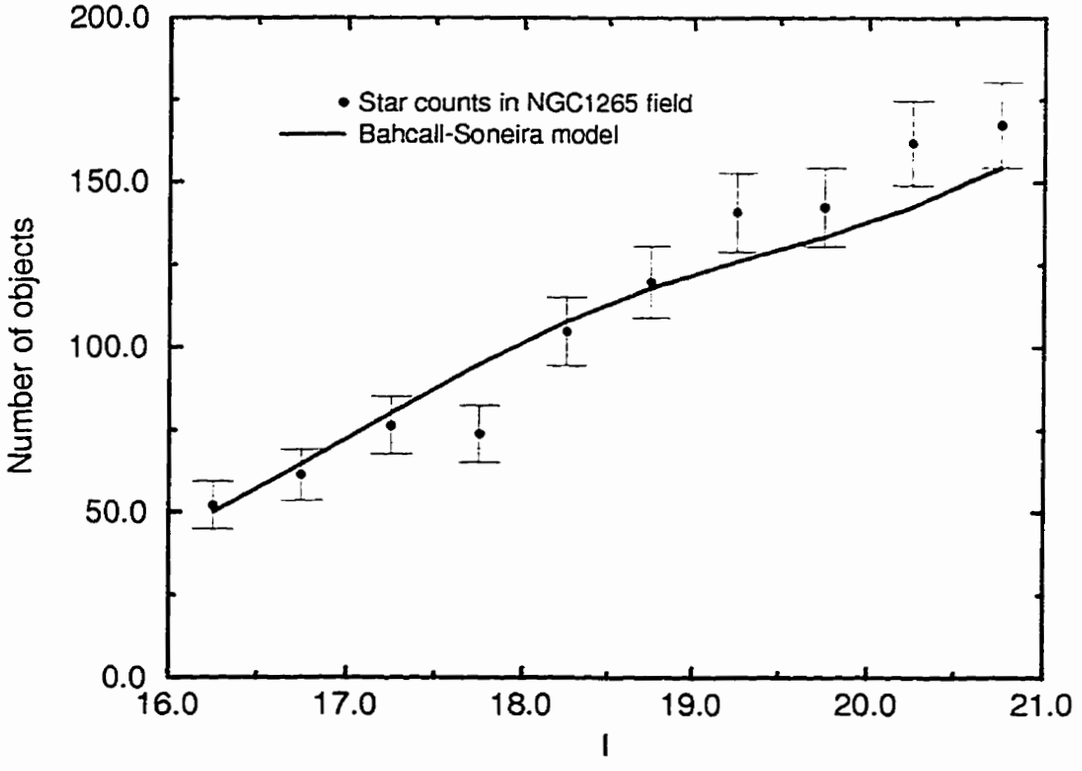

Figure 6.71: Color distribution of stars and model in NGC1265 field

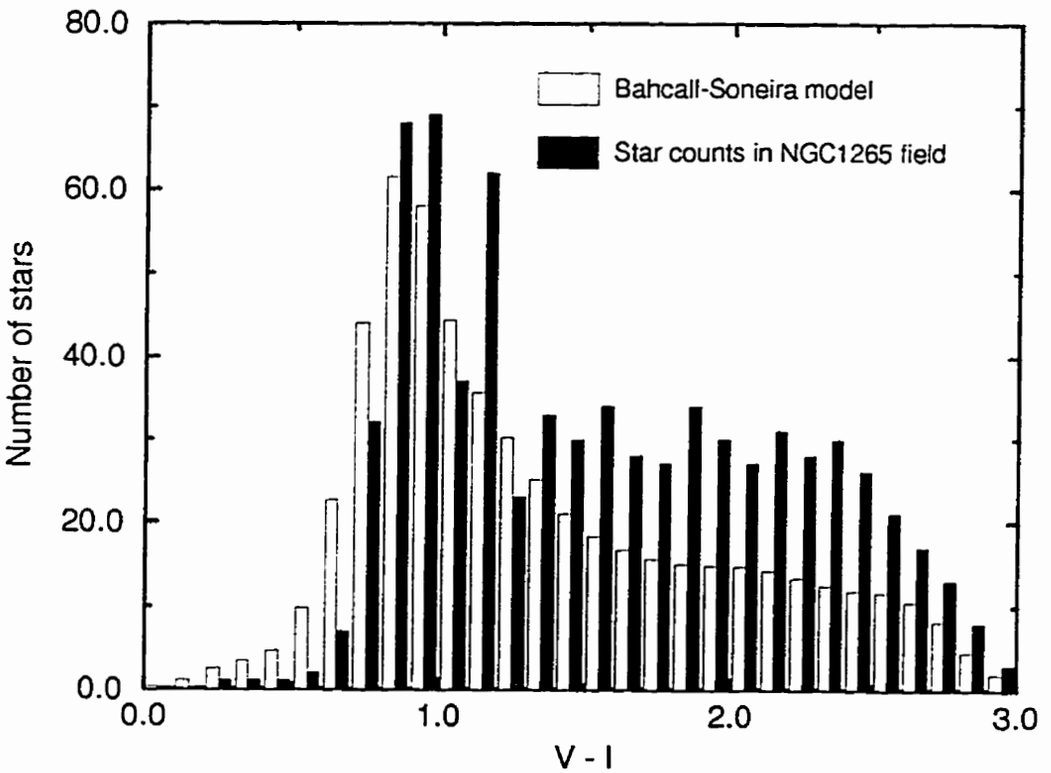

Figure 6.72: V star counts for NGC1275, NGC1265 and background field

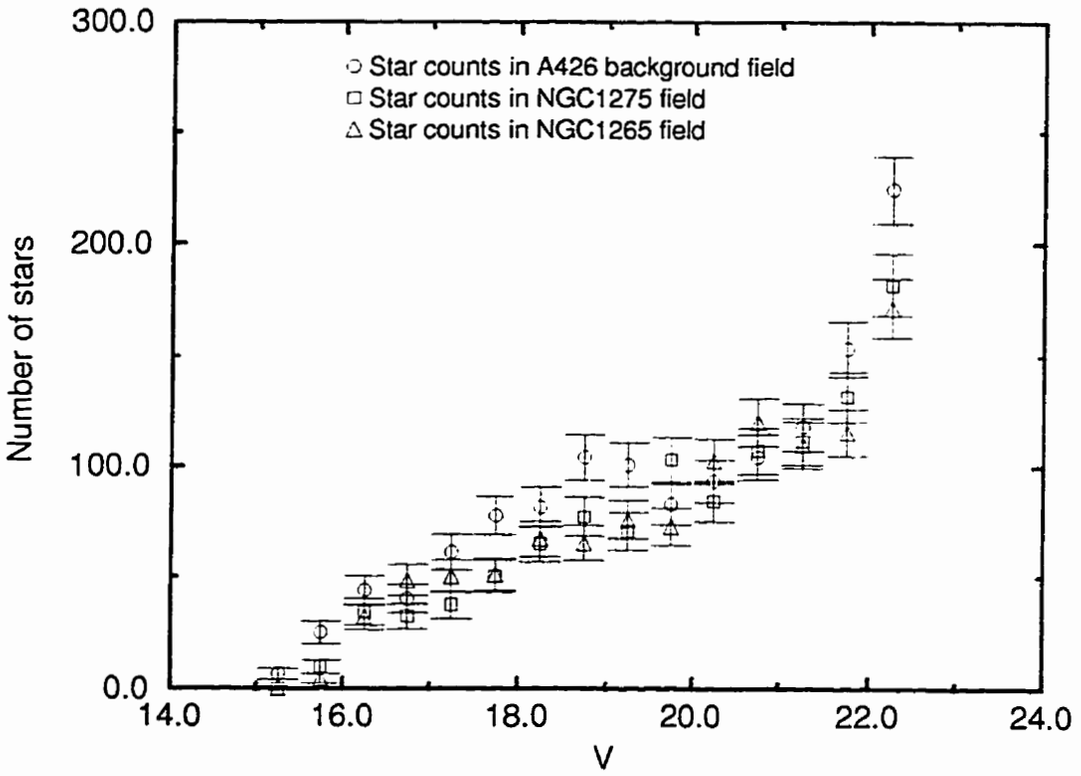

Figure 6.73: *I* star counts for NGC1265 and NGC1275 fields

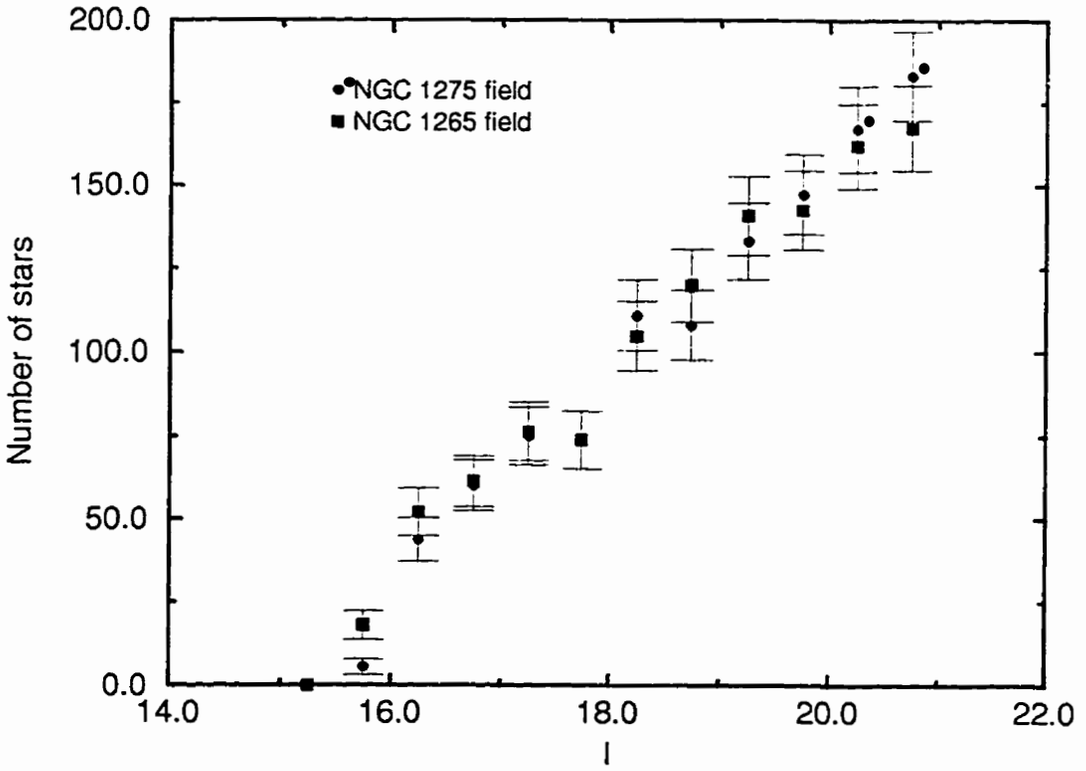

6.4 Discussion

Determination of the LF for two fields in the Abell 426 cluster has yielded: (i) the LF for both fields, in V, is well fit by a power law with $\alpha \sim -1.9$; (ii) galaxies appear to be concentrated around NGC1275 but not around NGC1265. No color gradient is detected (in average $V - I$) except some indication of a blueing in the central region of the NGC1275 field toward NGC1275, and a reddening of galaxies in the proximity of NGC1265. Both effects are quite weak.

This behavior is reminiscent of Abell 2199 (De Propris et al. 1995), and we shall comment on this in Chapter 9. It is interesting to note that the strong color gradients seen in Coma are not apparent here. On the other hand, contamination by background galaxies may dilute the signal from cluster objects.

Chapter 7

Abell 539

7.1 Introduction

The cluster Abell 539 lies at $l = 195.7$ and $b = -17.7$ at a redshift of 0.027. It has not been classified by Jones & Forman (1984), but it has a low X-ray luminosity ($L_X \sim 10^{43}$ ergs/s), although UGC3274 lies at the bottom of the cluster potential well (e.g., Ulmer et al. 1992). This cluster is dominated by early-type galaxies. It is likely to represent a transition object. It may be an early XD cluster that has undergone considerable dynamical evolution.

7.2 UGC3274

Images of the UGC3274 field were taken in the V and I for a total exposure time of 1200s. We show this field before and after removal of giant galaxies in Figures 7.1 and 7.2. As usual we consider the r_{-2} for star-galaxy separation, plotting this vs V in Figure 7.3. As above, our simulations show that at

$V = 21.00$, $r_{-2} = 1.66 \pm 0.10$, at $V = 21.5$, $r_{-2} = 1.65 \pm 0.12$ and $r_{-2} = 1.58 \pm 0.18$ at $V = 22.5$. We therefore choose $r_{-2} = 2.00$ as our 'cut' for star-galaxy separation to $V = 22.5$. All data were dereddened by 0.36 magnitudes in V and by 0.20 magnitudes in I. Table 7.1 shows the number of objects stars and galaxies in this field and these data are plotted in Figure 7.4. Note again the large number of stars in this field, which is projected over the bulge of our galaxy. We compare the number of galaxies in this field with the number of background objects in Figure 7.5. Table 7.2 shows the number of objects, background galaxies and cluster members. We plot these data in Figure 7.6, with the best power-law fit:

$$\alpha = -1.42 \pm 0.09$$

We consider the radial distribution of objects in this field and plot it in Figure 7.7, While we see a strong concentration near UGC3274, the distribution is approximately flat at large radii. Galaxies within 5′ of UGC3274 and outside of this area are plotted in Figures 7.8 and 7.9. A comparison is shown in Figure 7.10. The LF for galaxies within 5′ of UGC3274 is shown in Figure 7.11 where we see that $\alpha = -1.37 \pm 0.10$. The corresponding plot for the outer region of this field is shown in Figure 7.12, where we see that $\alpha = -1.21 \pm 0.11$. This is flatter than in the inner field (although the significance of the result is not high) and therefore implies that some environmental effect is favoring survival or creation of dwarfs in the vicinity of the giant elliptical UGC3274.

The plot of r_{-2} vs I for UGC3274 is shown in Figure 7.13 and we tabulate

the number of objects, stars and galaxies in Table 7.3. As above, we use simulations to determine an appropriate 'cut' for star-galaxy separation. At $I = 20.75$ we find $r_{-2} = 1.60 \pm 0.11$. At $I = 21.25$ we find $r_{-2} = 1.58 \pm 0.18$ and at $I = 21.75$ we find $r_{-2} = 1.54 \pm 0.18$. Therefore we choose $r_{-2} = 1.85$ as our 'cut' for star-galaxy separation.

These data are plotted in Figure 7.14. The number of cluster members is estimated in the usual way and tabulated in Table 7.4. We plot the number of cluster members and I band counts in Figure 7.15; we see that there is an excess over background. The number of cluster members is plotted vs I in Figure 7.16. We are unable, in this case, to estimate a value for α, because of the noisiness of the data. Their surface density distribution is plotted in Figure 7.17. We see that except for a strong concentration in the proximity of UGC3274, the distribution of galaxies in this field is approximately flat. We plot the numbers of galaxies within $5'$ of UGC3274 and outside of this region in Figure 7.18 and 7.19. A comparison is shown in Figure 7.20, where the two distributions do not appear to be significantly different.

We consider the distribution of galaxy colors in Figure 7.21. Note the strong signal from the bright cluster members in the V vs $V - I$ plot. This is readily apparent after contaminating galaxies have been removed as described previously, in Figure 7.22. There is a small blueing trend at low luminosities, of about 0.1 magnitudes, but this not likely to be very significant.

A histogram is shown in Figure 7.23. We see that most galaxies have

colors between 0.8 and 1.5, with a median of 1.15.

The plot of average color as a function of magnitude is shown in Figure 7.24, where we see the small blueing trend.

The plot of average $V - I$ versus distance from UGC3274 is shown in Figure 7.25. We note that there is a small blueing trend at small distances from UGC3274. This is somewhat surprising, considering that dwarfs in Coma show a reddening trend toward giant galaxies.

A color magnitude diagram for stars in this field is shown in Figure 7.2, where we see the usual 'envelope' due to the reddening line and the color edge.

As in previous fields, the shape of the luminosity distribution of field stars in this field as a function of magnitude in V and I (see Figures 7.27 and 7.28) is well fit by the Bahcall-Soneira model, although the model appears to overestimate the number of stars in this field by about 30% (the normalization in the above figures is arbitrary). The color distribution as shown in Figure 7.29 shows a good match between model predictions and observations, except perhaps for a few more red objects than predicted. This trend is consistent with that recorded in the Abell 426 fields. Note again that these are raw data, with no reddening correction assumed.

Figure 7.1: The V image of the UGC3274 field (one of three chips)

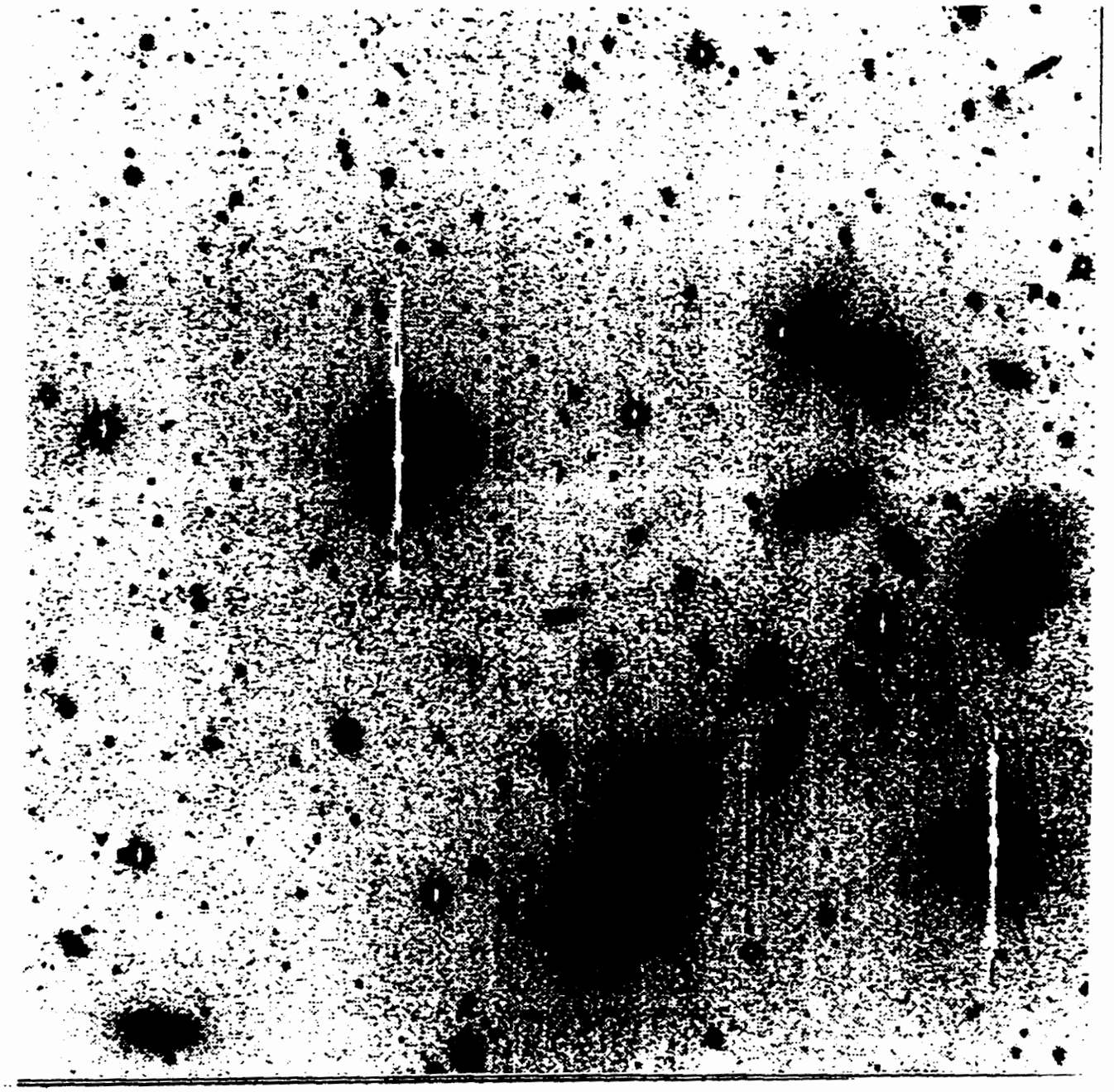

Figure 7.2: The *V* image of the UGC3274 field after removal of bright galaxies

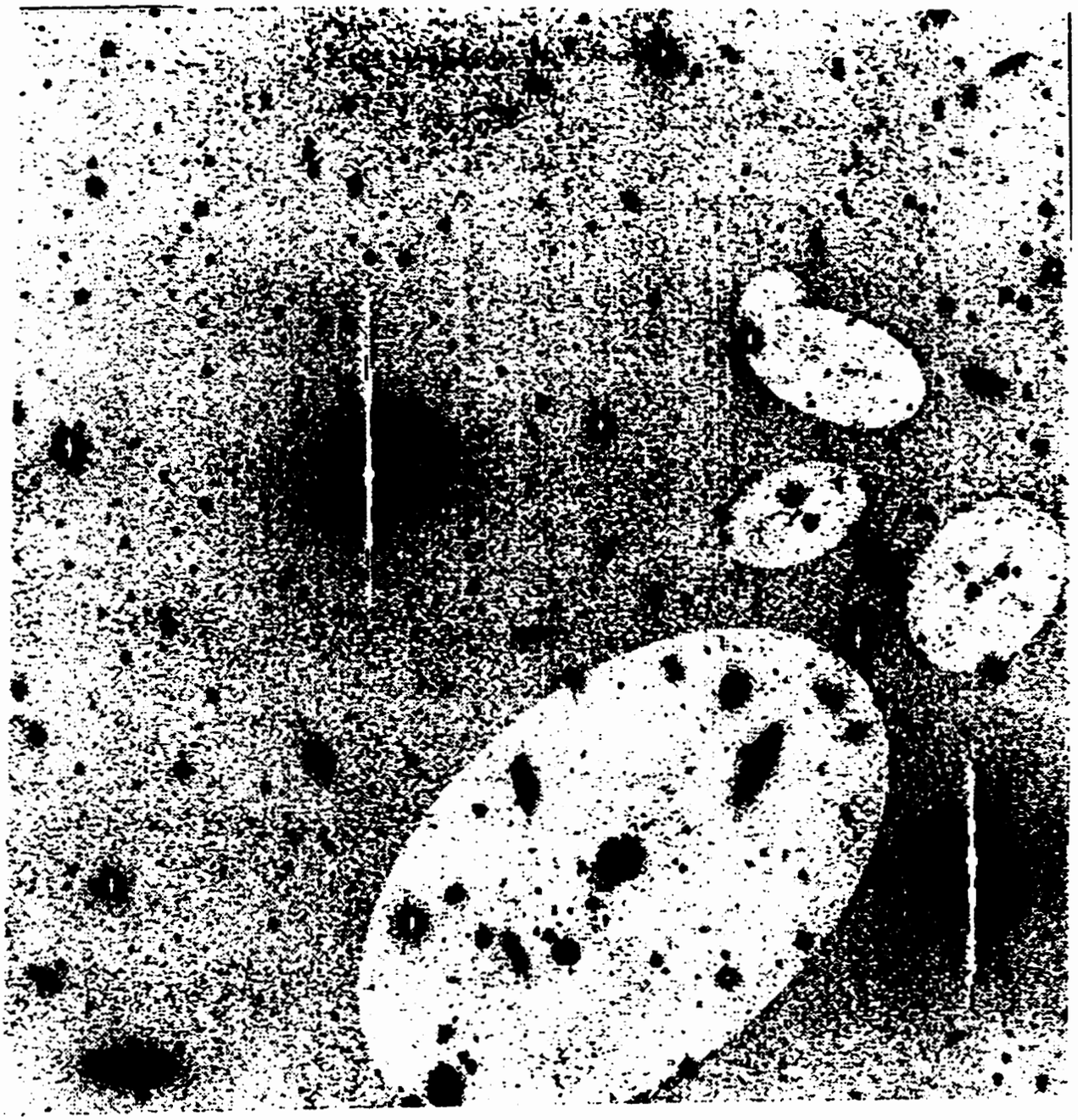

Figure 7.3: Plot of r_{-2} vs V for UGC3274 field and cut for star galaxy separation

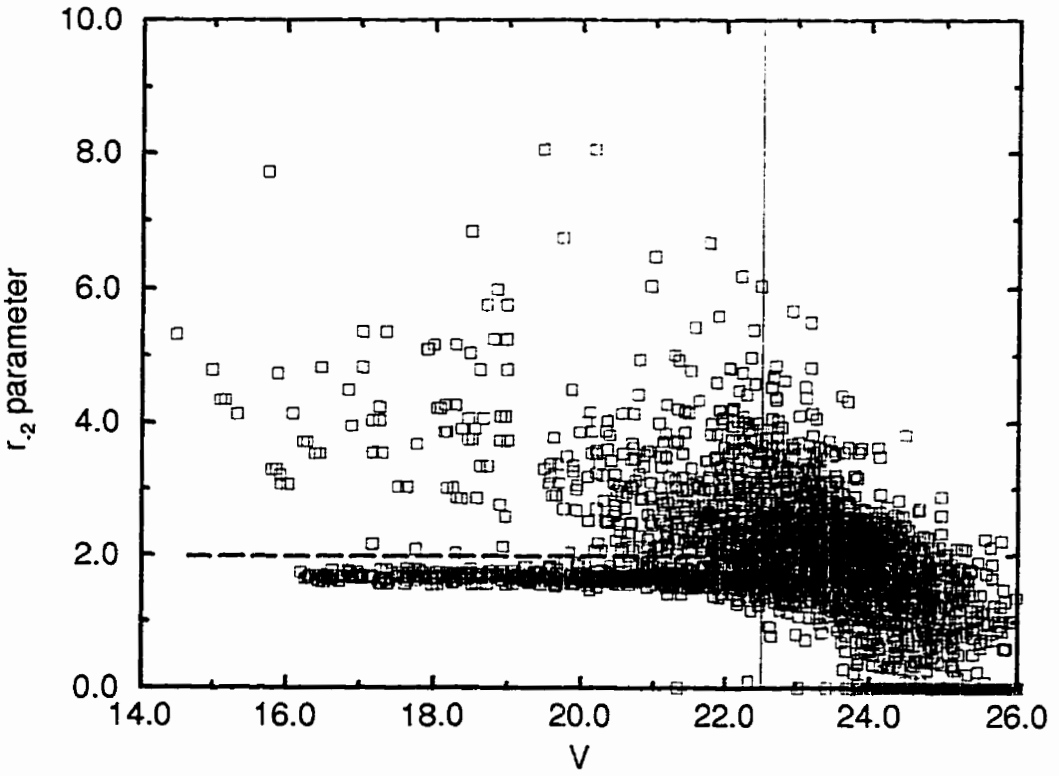

Table 7.1: NUMBER COUNTS FOR UGC3274 FIELD

V	N. of objects	N. of galaxies	N. of stars	Completeness
15.25	3.40 ± 1.84	3.40 ± 1.84	0.00 ± 0.00	1
15.75	6.57 ± 2.56	6.57 ± 2.56	0.00 ± 0.00	1
16.25	17.03 ± 4.13	8.97 ± 3.00	8.05 ± 2.84	1
16.75	32.61 ± 5.71	2.40 ± 1.55	30.21 ± 5.50	1
17.25	32.36 ± 5.69	10.16 ± 3.19	22.20 ± 4.71	1
17.75	43.59 ± 6.60	7.97 ± 2.82	35.62 ± 5.97	1
18.25	56.31 ± 7.50	17.73 ± 4.21	38.58 ± 6.21	1
18.75	53.88 ± 7.34	22.13 ± 4.70	31.74 ± 5.63	1
19.25	63.84 ± 7.99	2.38 ± 1.54	61.46 ± 7.84	1
19.75	80.17 ± 8.95	21.35 ± 4.62	58.82 ± 7.67	1
20.25	101.98 ± 10.10	31.58 ± 5.62	70.39 ± 8.39	1
20.75	134.46 ± 11.60	49.08 ± 7.01	85.38 ± 9.24	1
21.25	162.48 ± 12.75	78.78 ± 8.88	83.70 ± 9.15	1
21.75	202.99 ± 14.25	110.74 ± 10.52	93.53 ± 9.67	1
22.25	341.24 ± 18.47	217.16 ± 14.74	138.68 ± 11.78	1

Figure 7.4: Number of objects, stars and galaxies for UGC3274 V field

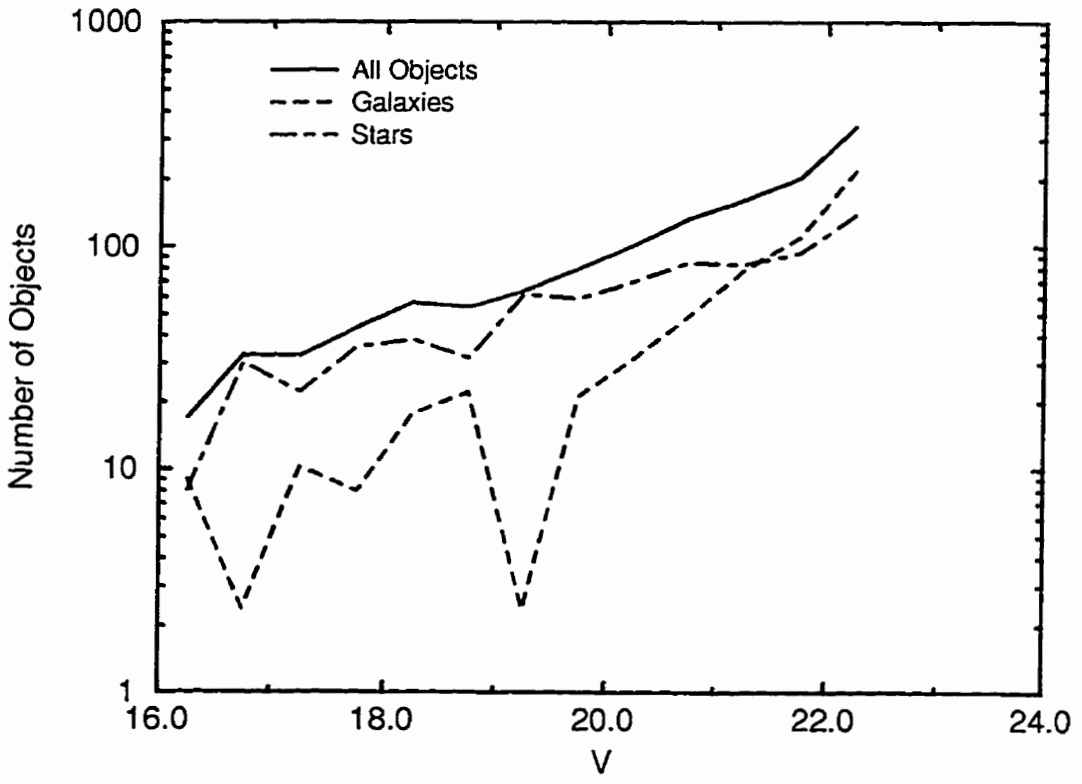

Table 7.2: NUMBER COUNTS FOR GALAXIES AND BACKGROUND OBJECTS IN UGC3274 FIELD

V	N. of galaxies	Background counts	N. of cluster members
15.25	3.40 ± 1.84	0.18	3.22 ± 1.89
15.75	6.57 ± 2.56	0.29	6.28 ± 2.62
16.25	8.97 ± 3.00	0.46	8.51 ± 3.07
16.75	2.40 ± 1.55	0.72	1.68 ± 1.77
17.25	10.16 ± 3.19	1.15	9.01 ± 3.36
17.75	7.97 ± 2.82	1.82	6.15 ± 3.13
18.25	17.73 ± 4.21	2.88	14.85 ± 4.54
18.75	22.13 ± 4.70	4.57	17.56 ± 5.17
19.25	2.38 ± 1.54	7.24	-4.56 ± 3.10
19.75	21.35 ± 4.62	11.48	9.87 ± 5.73
20.25	31.58 ± 5.62	18.20	13.38 ± 7.06
20.75	49.08 ± 7.01	28.84	20.24 ± 8.83
21.25	78.78 ± 8.88	45.71	33.07 ± 11.16
21.75	110.74 ± 10.52	72.44	38.30 ± 13.53
22.25	217.16 ± 14.74	114.82	102.34 ± 18.22

Figure 7.5: Number of galaxies and background objects for UGC3274 V field

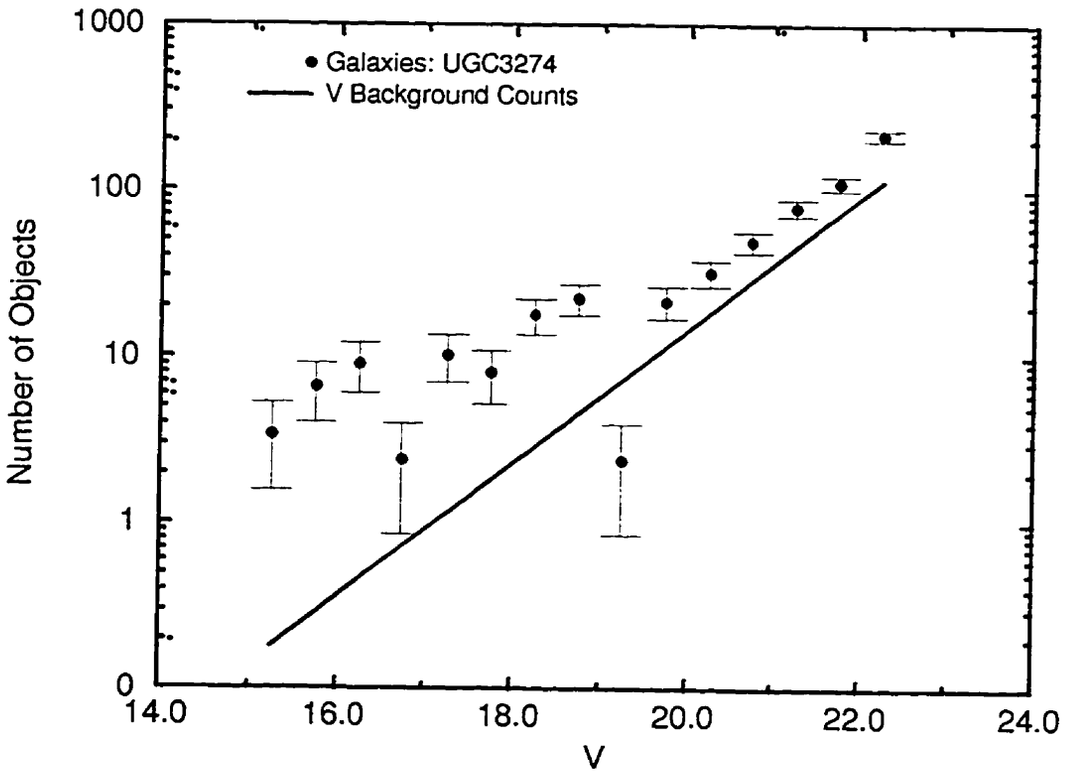

Figure 7.6: Number of cluster members and LF for V field

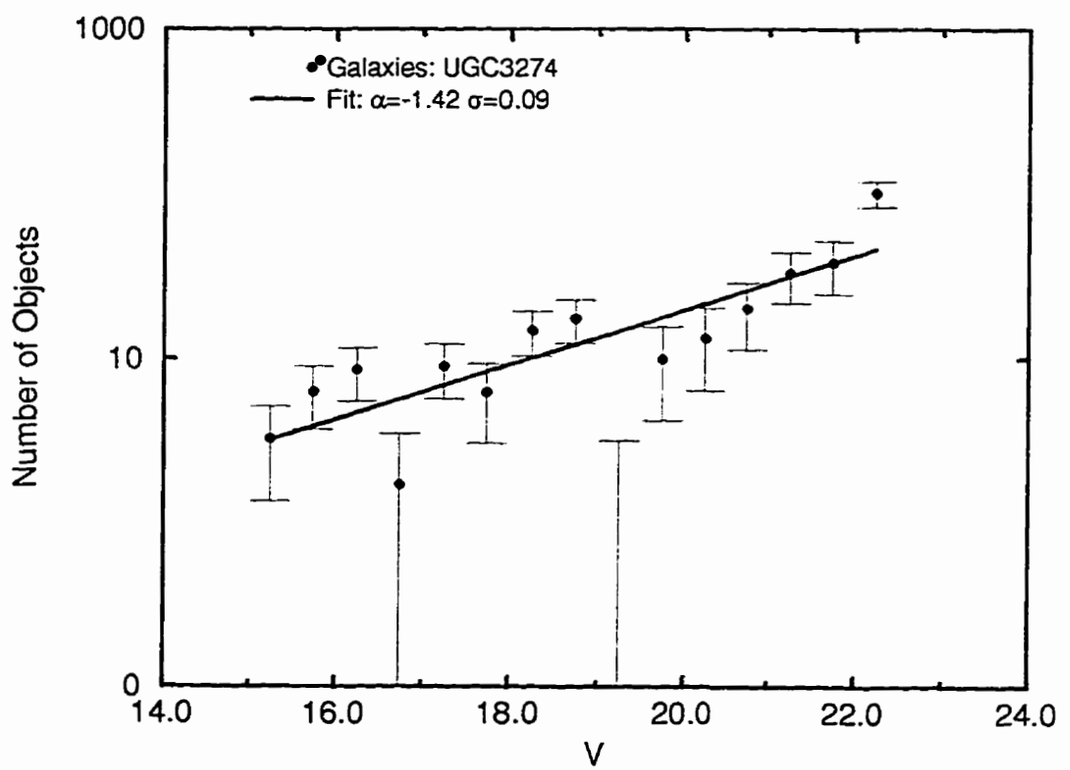

Figure 7.7: Radial distribution of cluster members in UGC3274 V field

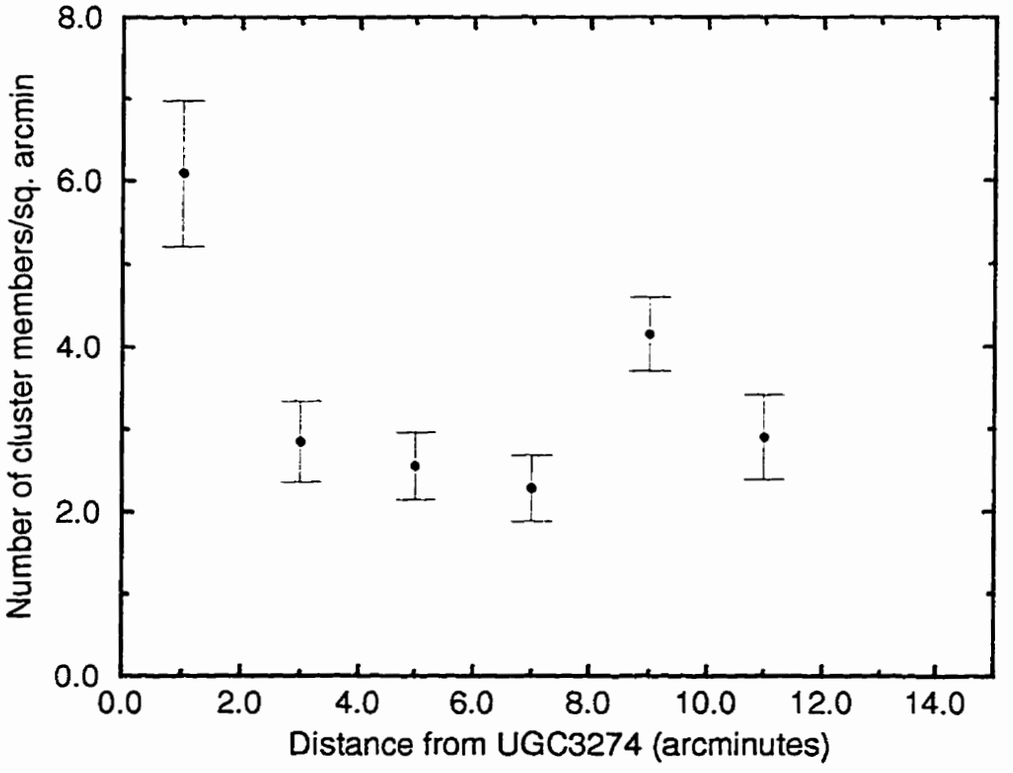

Figure 7.8: Number counts of cluster members in inner 5′ of V field

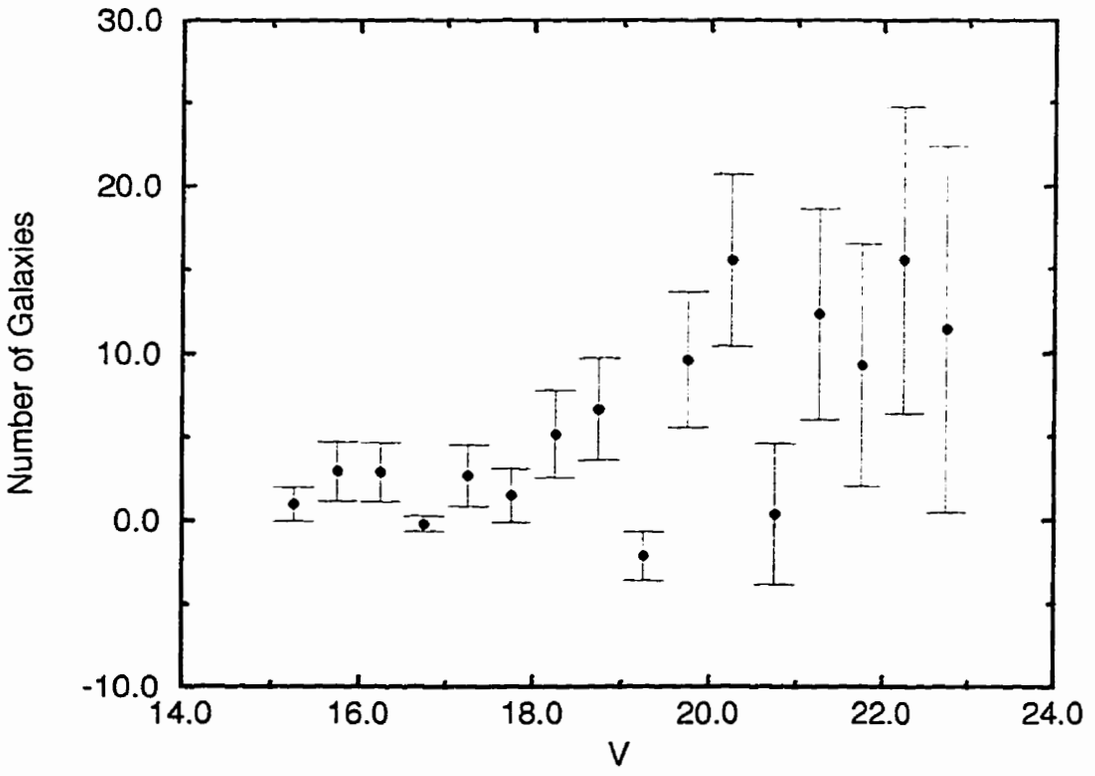

Figure 7.9: Number counts of cluster members more distant than 5′ from UGC3274

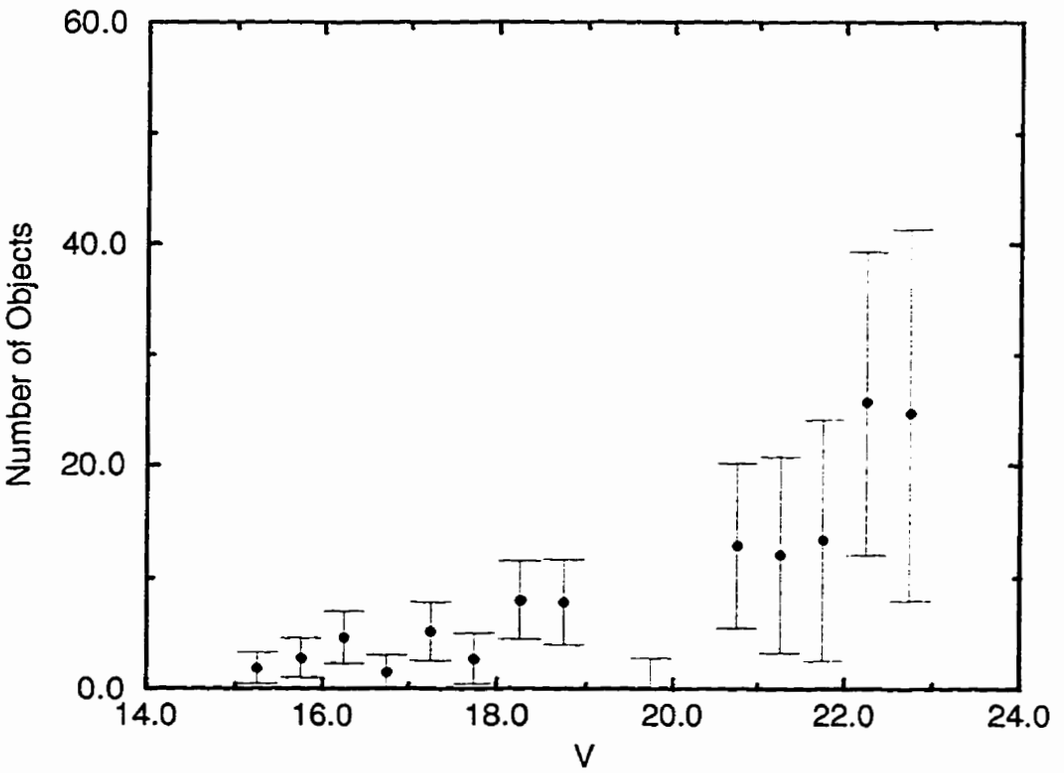

Figure 7.10: Comparison of inner and outer fields

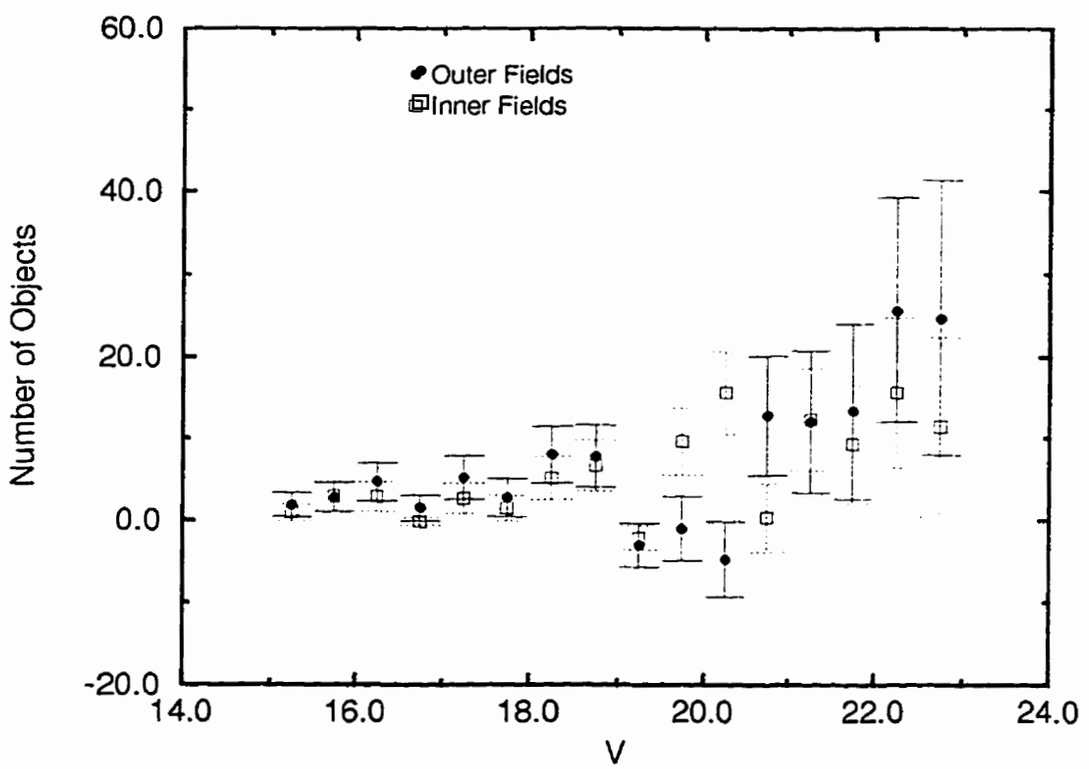

Figure 7.11: LF for inner 5' of UGC3274 field

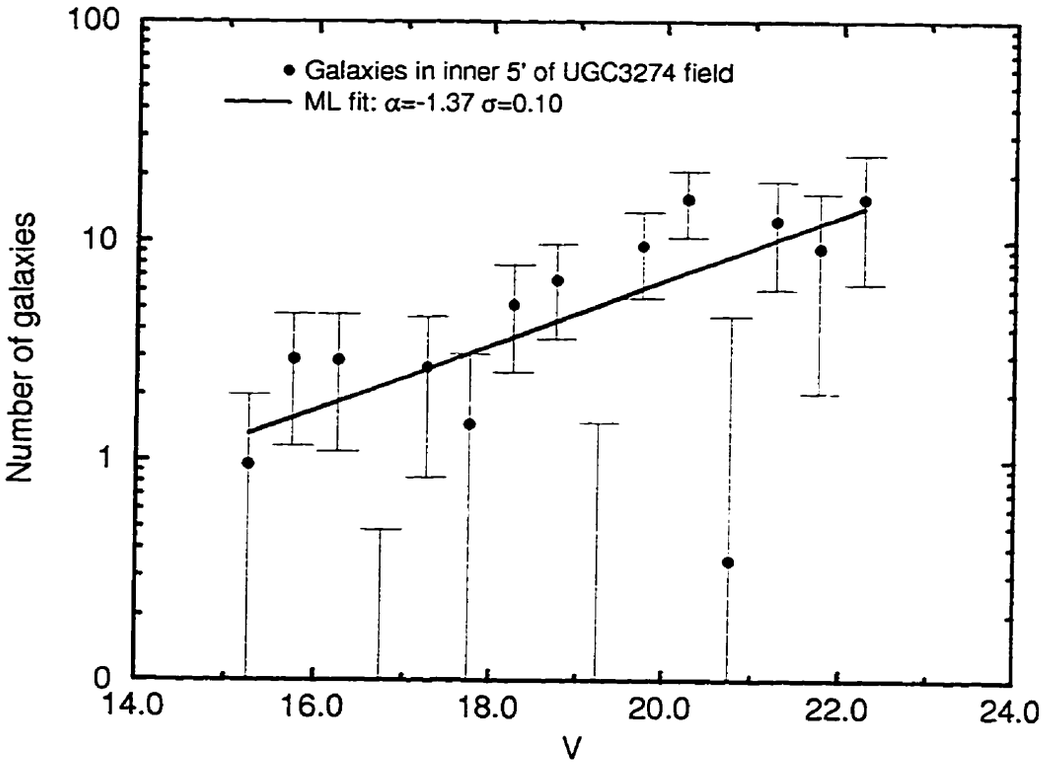

Figure 7.12: LF for inner 5' of UGC3274 field

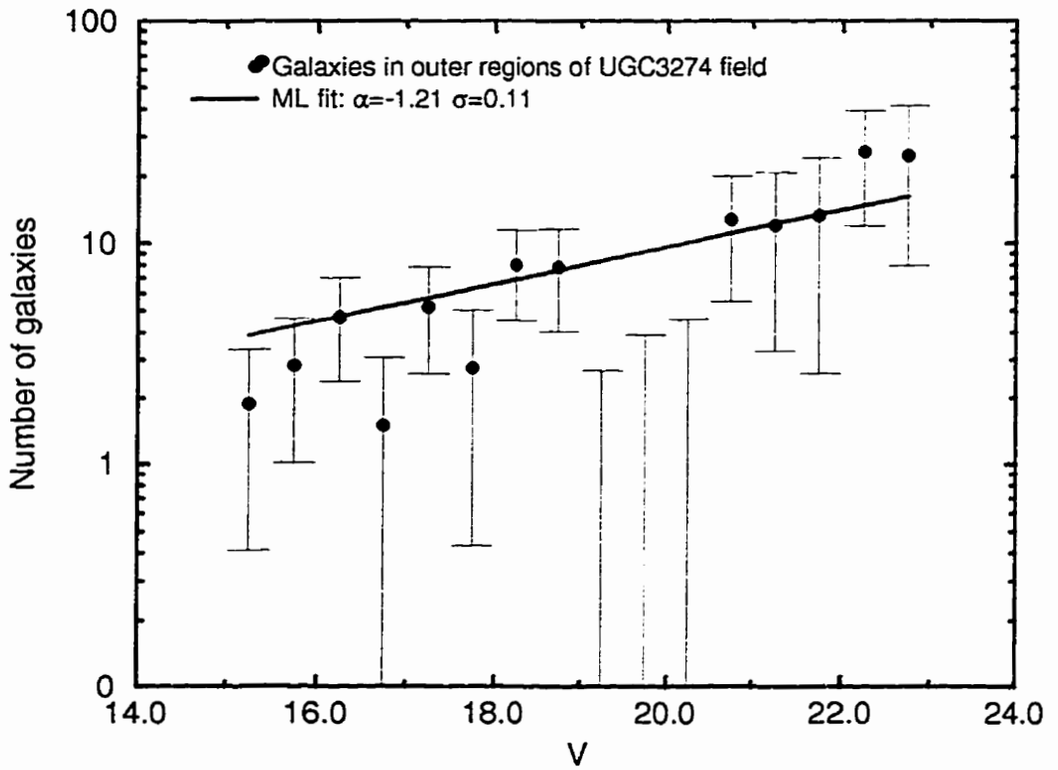

Figure 7.13: Plot of r_{-2} vs I for UGC3274 field

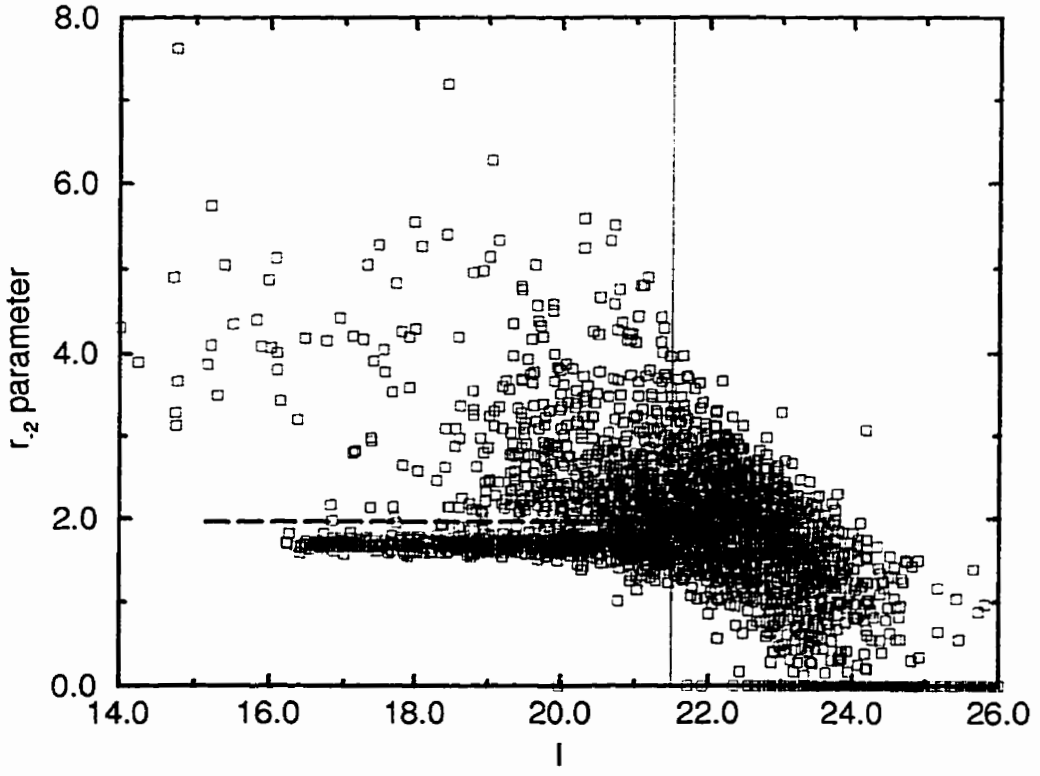

Table 7.3: NUMBER COUNTS FOR UGC3274 *I*

I	N. of objects	N. of galaxies	N. of stars	Completeness
15.25	5.30 ± 2.30	5.30 ± 2.30	0.00 ± 0.00	1
15.75	4.80 ± 2.19	4.80 ± 2.19	0.00 ± 0.00	1
16.25	19.65 ± 4.43	7.45 ± 2.73	12.20 ± 3.49	1
16.75	41.10 ± 6.41	4.30 ± 2.07	36.80 ± 6.07	1
17.25	59.10 ± 7.69	10.70 ± 3.27	48.40 ± 6.96	1
17.75	61.10 ± 7.82	12.55 ± 3.54	48.55 ± 6.97	1
18.25	66.50 ± 8.15	13.35 ± 3.65	53.15 ± 7.29	1
18.75	121.75 ± 11.03	26.30 ± 5.13	95.45 ± 9.77	1
19.25	138.90 ± 11.79	55.10 ± 7.42	83.80 ± 9.15	1
19.75	187.20 ± 13.68	97.60 ± 9.88	89.60 ± 9.47	1
20.25	250.25 ± 15.82	111.40 ± 10.55	138.85 ± 11.78	1
20.75	289.30 ± 17.01	174.90 ± 13.22	114.40 ± 10.70	1
21.25	418.11 ± 20.45	239.71 ± 15.48	182.21 ± 13.50	1

Figure 7.14: Number of objects, galaxies and stars for UGC3274 *I* field

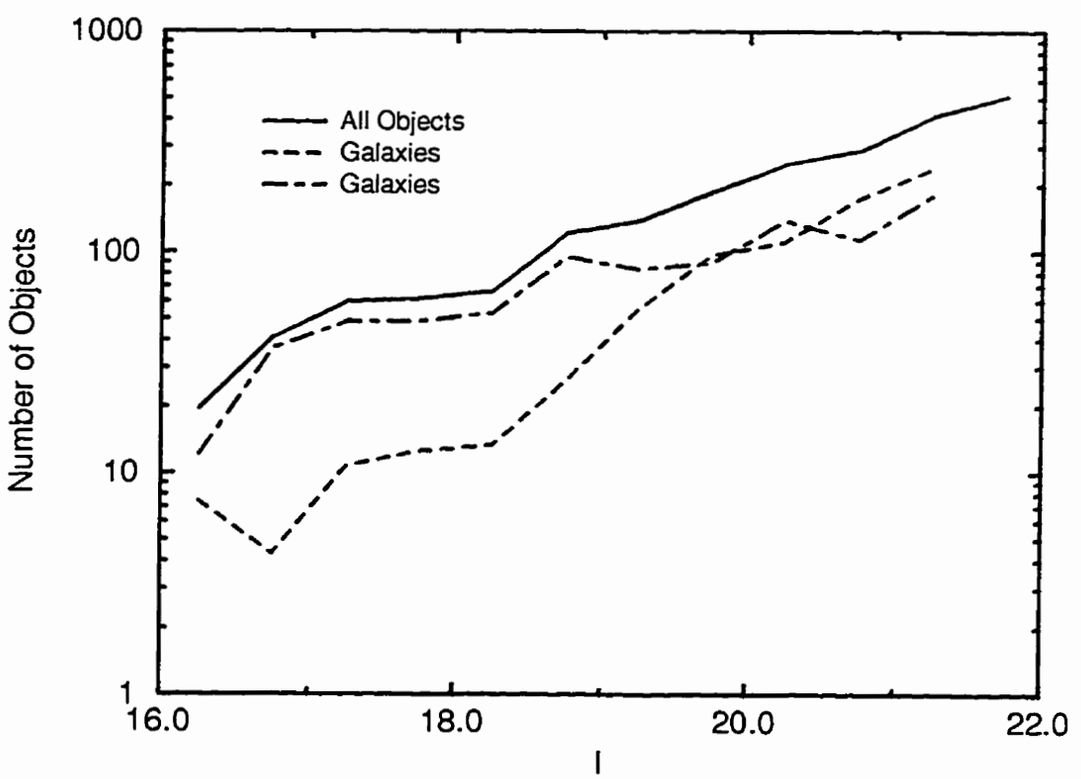

Table 7.4: NUMBER COUNTS FOR GALAXIES AND BACKGROUND OBJECTS IN UGC3274 *I*

I	N. of galaxies	Background counts	N. of cluster members
15.25	5.30 ± 2.30	1.53	3.77 ± 2.61
15.75	4.80 ± 2.19	2.26	2.54 ± 2.66
16.25	7.45 ± 2.73	3.35	4.10 ± 3.29
16.75	4.30 ± 2.07	4.95	-0.65 ± 3.04
17.25	10.70 ± 3.27	7.33	3.37 ± 4.25
17.75	12.55 ± 3.54	10.84	1.71 ± 4.84
18.25	13.35 ± 3.65	16.03	-2.68 ± 5.42
18.75	26.30 ± 5.13	23.71	2.59 ± 7.07
19.25	55.10 ± 7.42	35.08	20.02 ± 9.50
19.75	97.60 ± 9.88	51.88	45.72 ± 12.23
20.25	111.40 ± 10.55	76.74	34.66 ± 13.72
20.75	174.90 ± 13.22	113.50	61.40 ± 16.98
21.25	239.71 ± 15.48	167.88	71.83 ± 20.19

Figure 7.15: Number of galaxies and background objects for UGC3274 *I* field

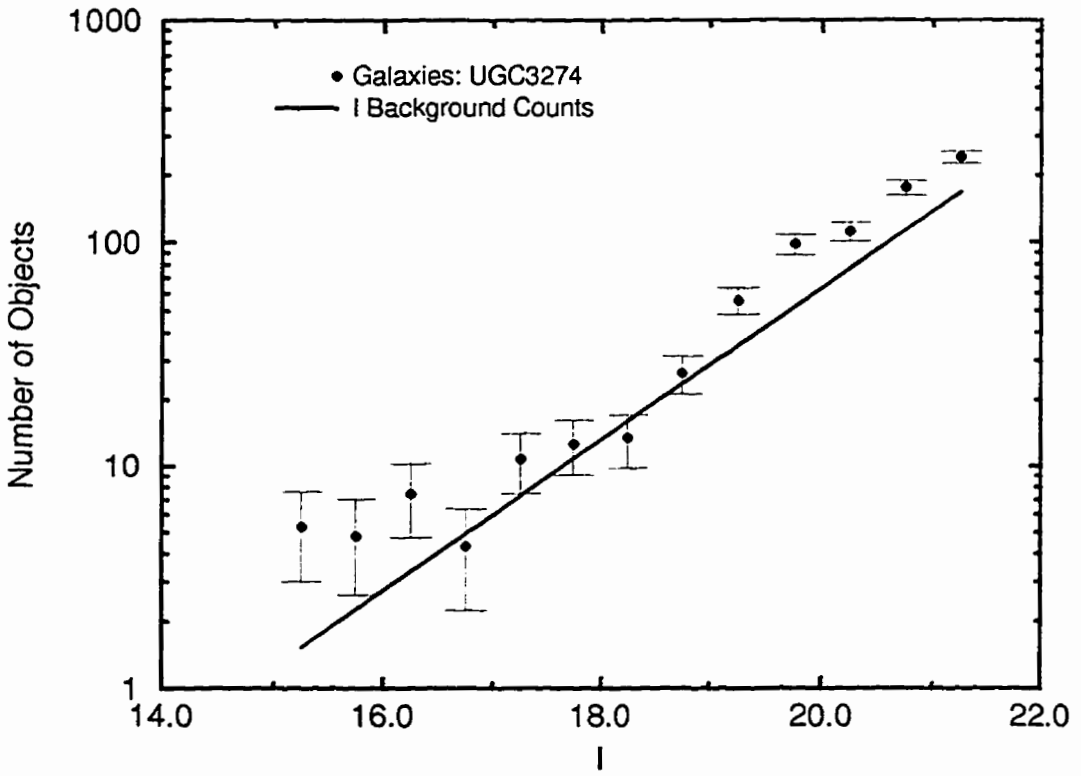

Figure 7.16: Number of cluster members and LF for UGC3274 *I* field

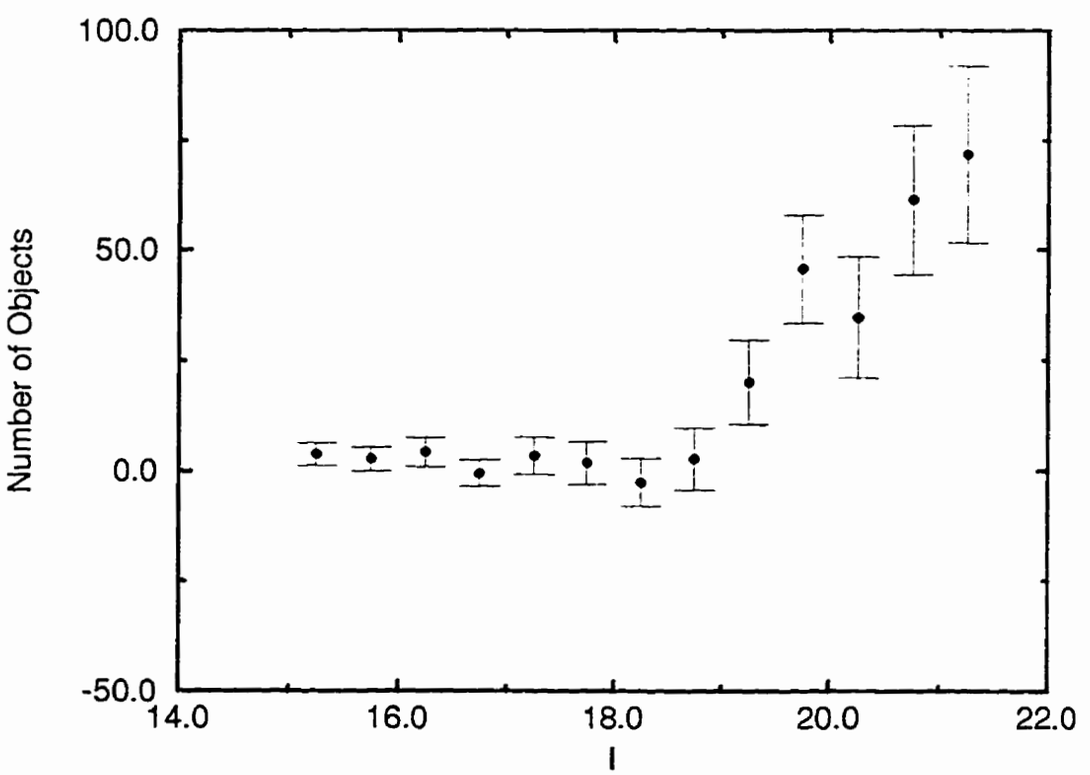

Figure 7.17: Radial distribution of cluster members for UGC3274 *I* field

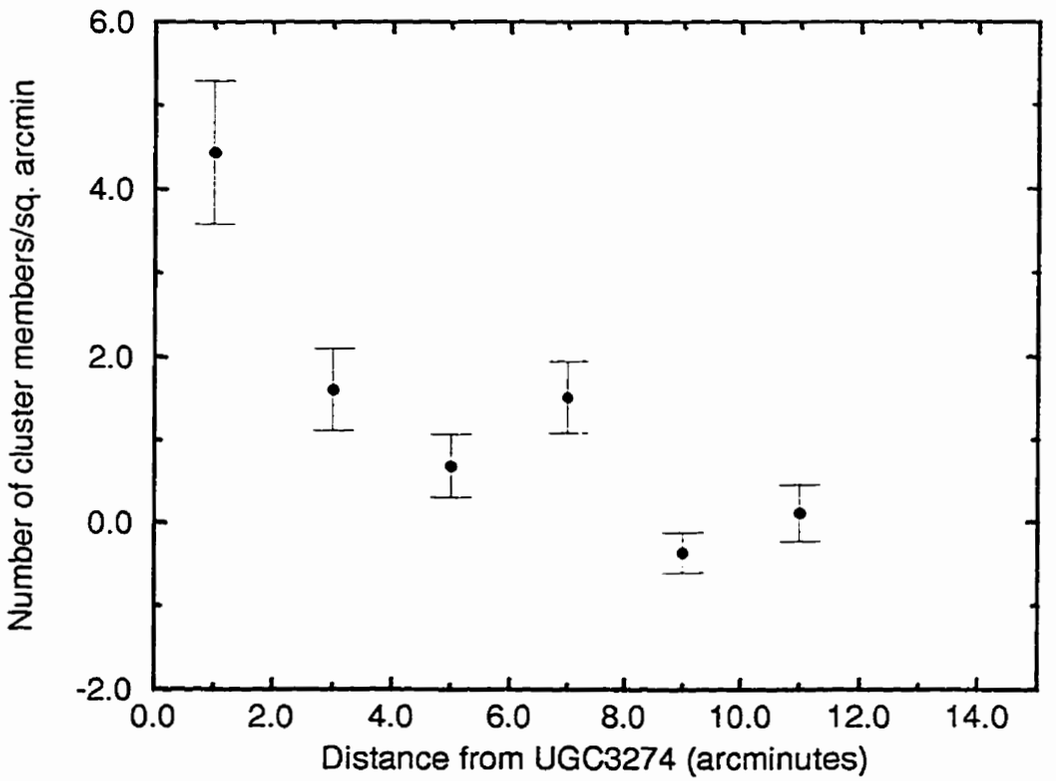

Figure 7.18: Number of objects in inner 5′ of UGC3274 *I* field

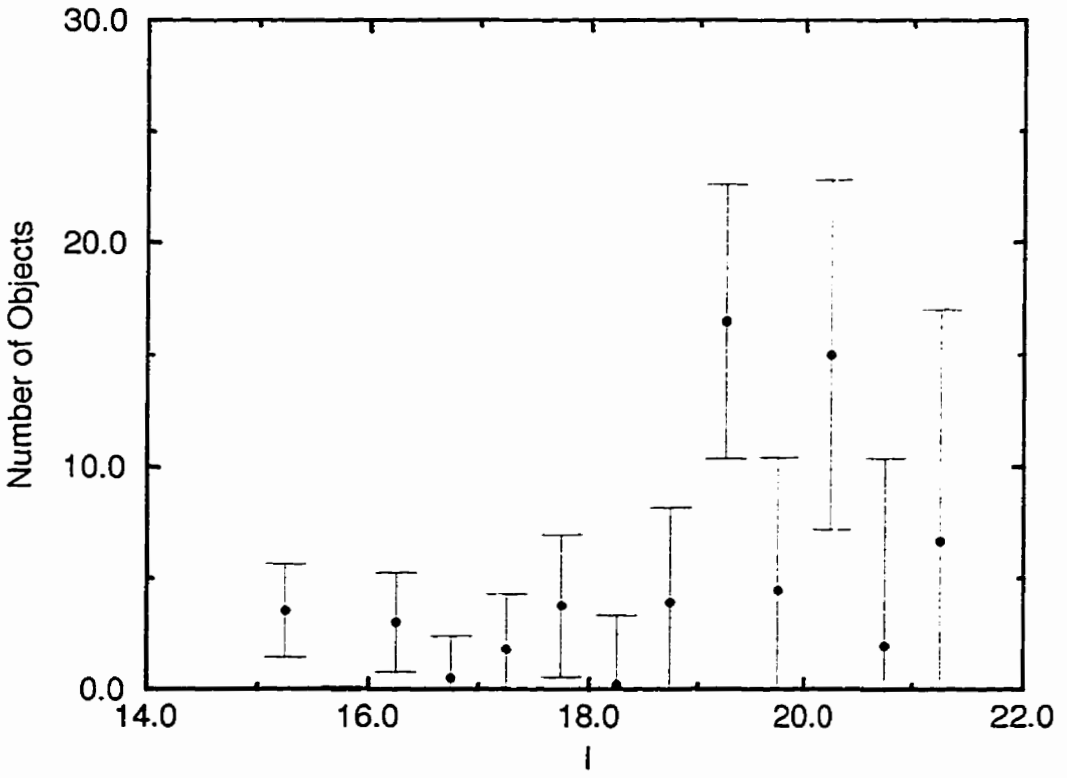

Figure 7.19: Number of objects more distant than 5′ from UGC3274

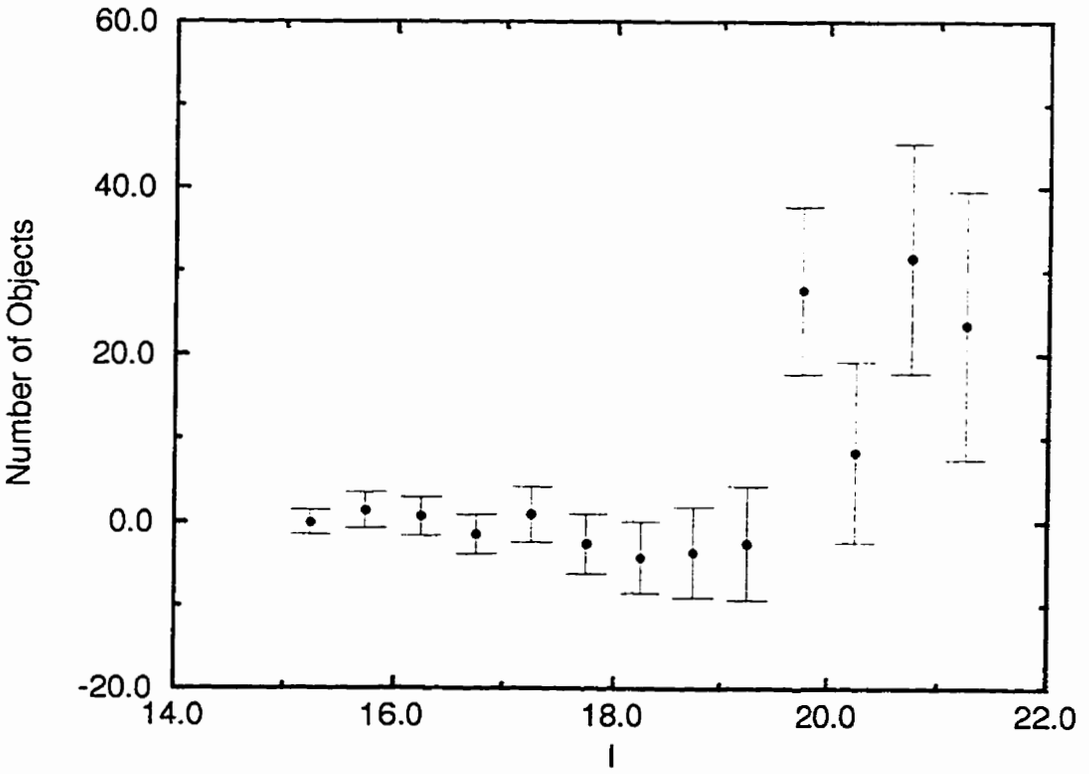

Figure 7.20: Comparison of inner and outer fields

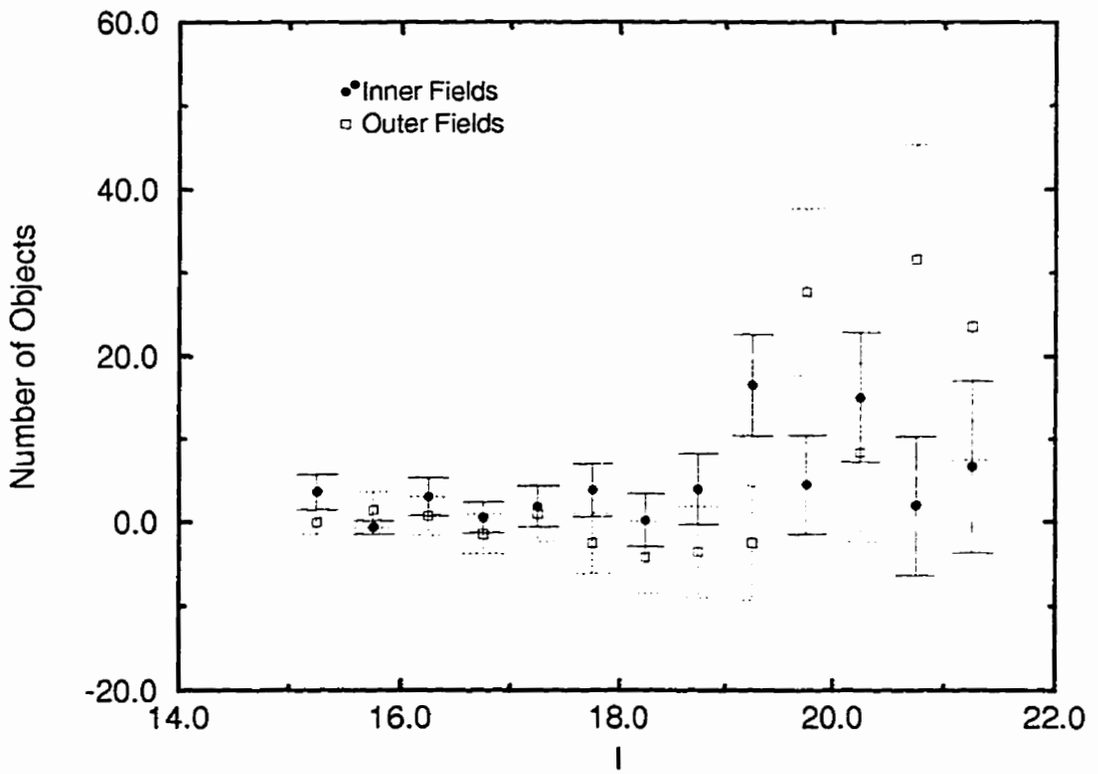

Figure 7.21: Color magnitude diagram for galaxies in UGC3274

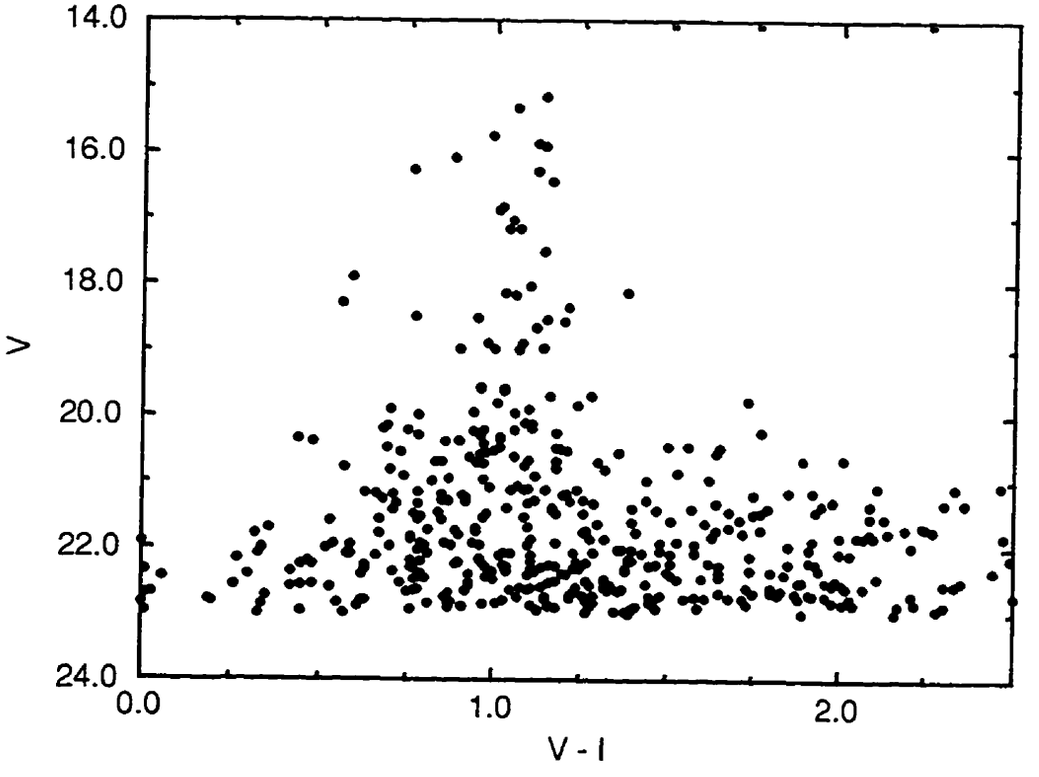

Figure 7.22: Color magnitude diagram for cluster members in UGC3274 field

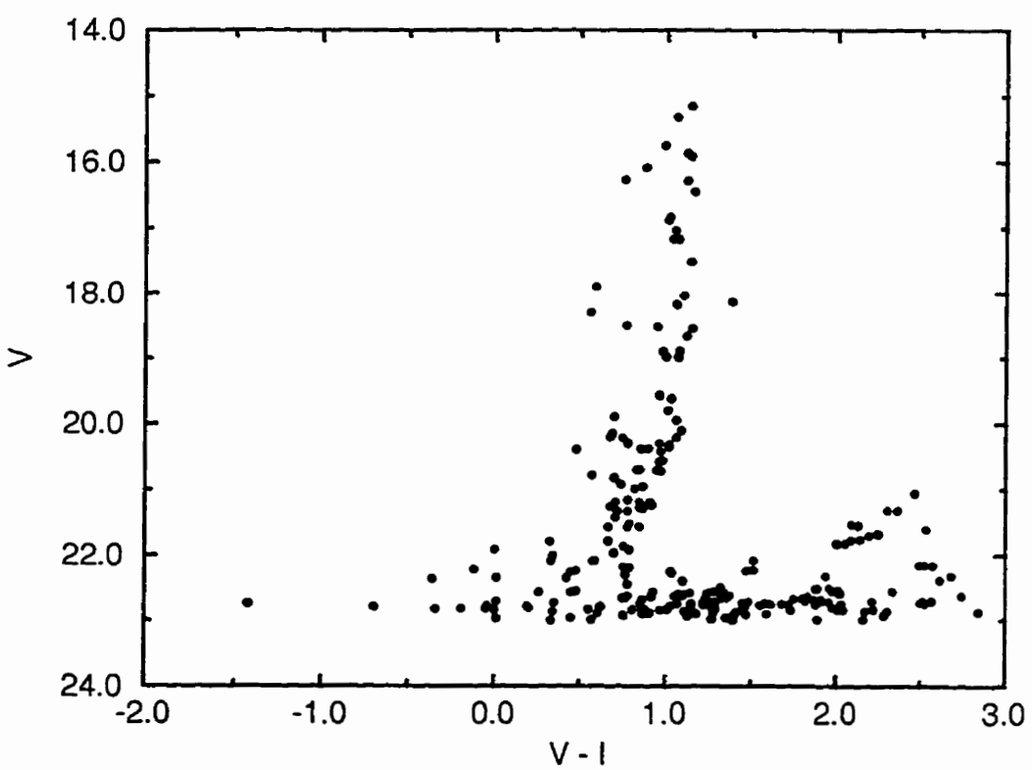

Figure 7.23: Color magnitude histogram for cluster members in UGC3274 field

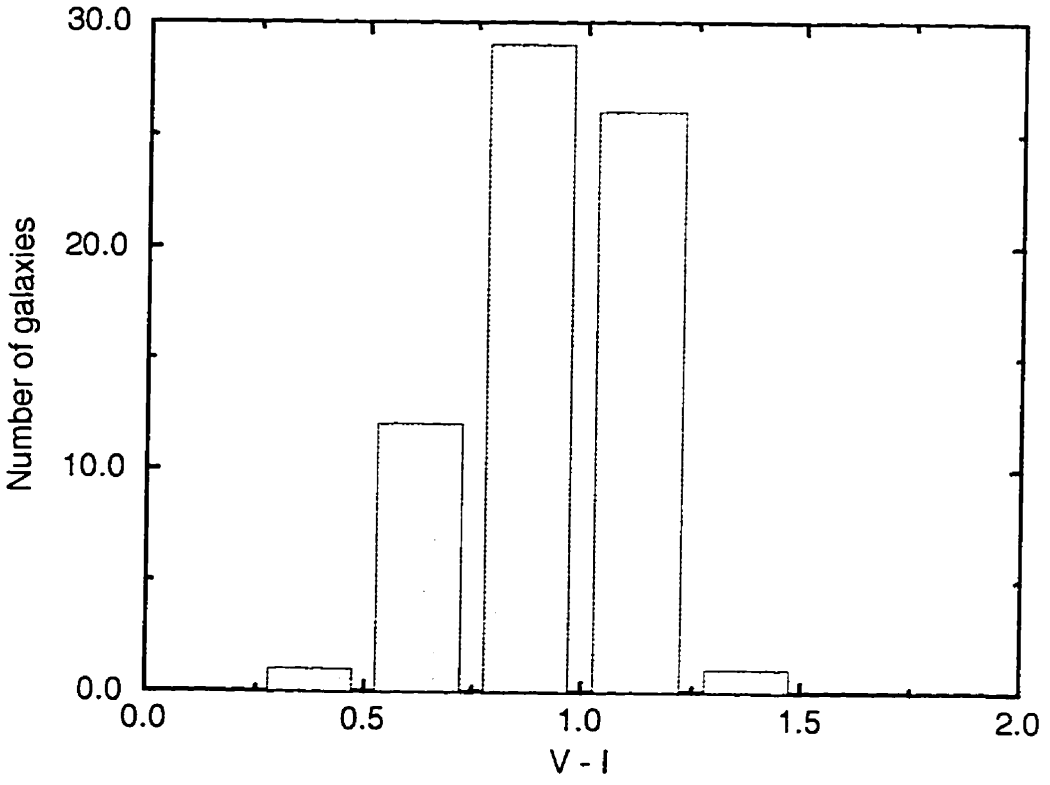

Figure 7.24: Average color as a function of magnitude for cluster members in UGC3274 field

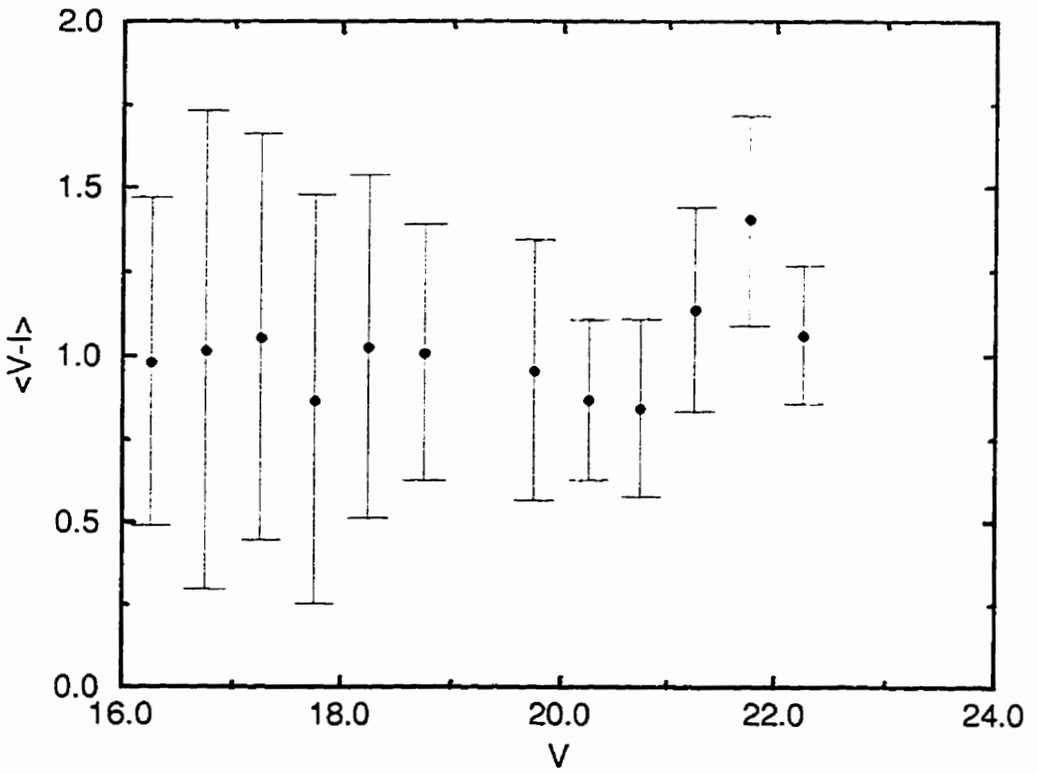

Figure 7.25: Radial distribution of average color in UGC3274

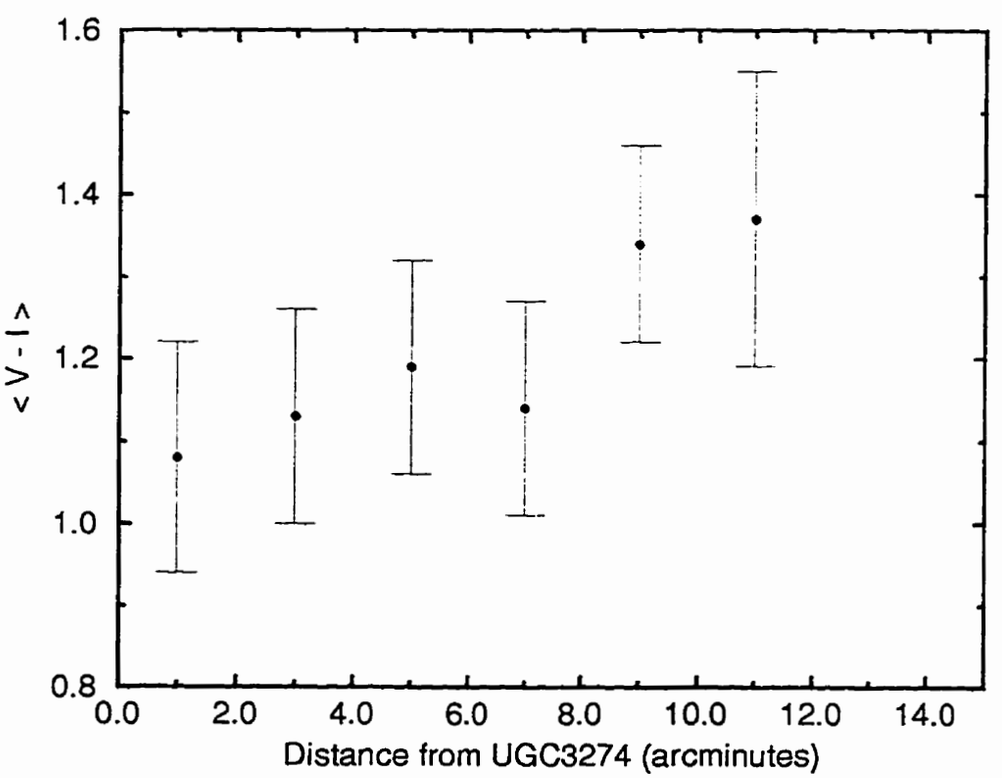

Figure 7.26: Color magnitude diagram for stars in UGC3274 field

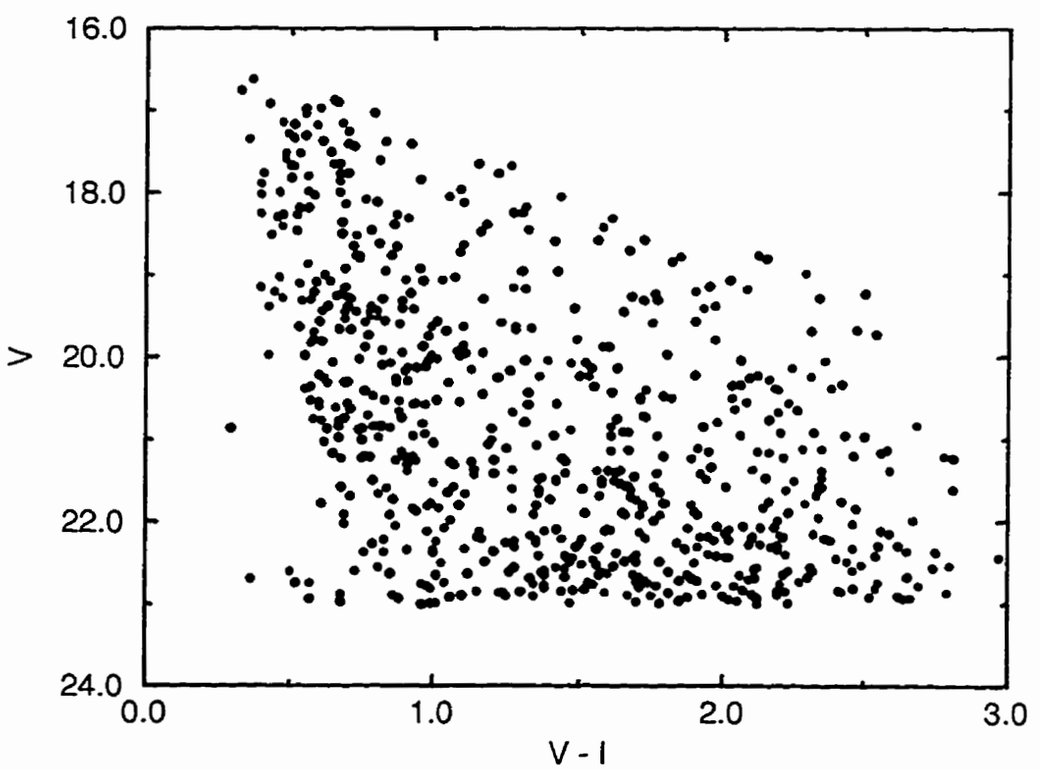

Figure 7.27: Number of stars and model for UGC3274 field in V

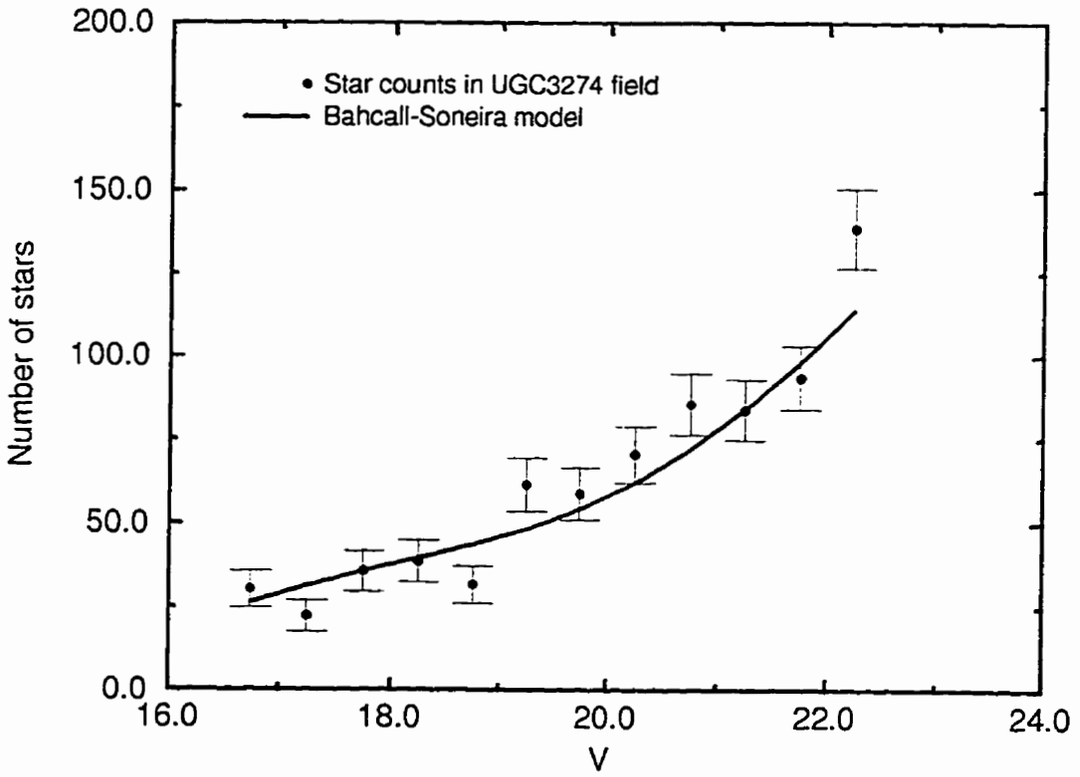

Figure 7.28: Number of stars and model for UGC3274 field in I

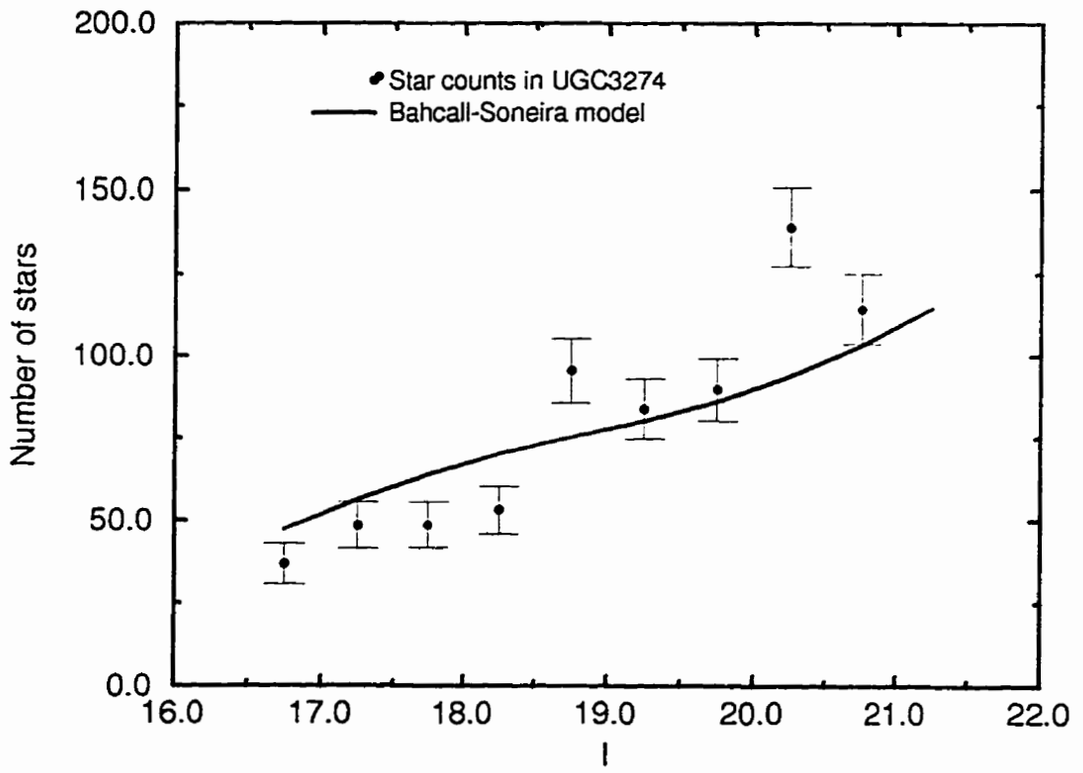

Figure 7.29: Color distribution for stars in UGC3274 model

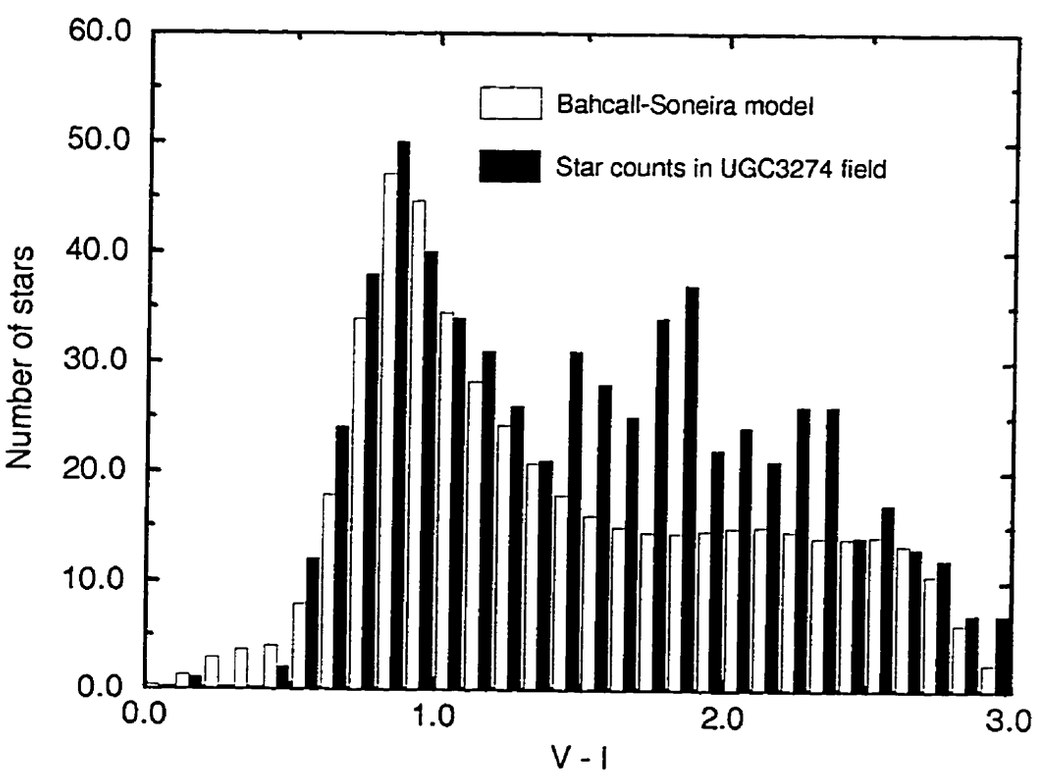

Chapter 8

A2151

8.1 The Hercules Cluster

Observations of part of the Hercules cluster were taken at the Kitt Peak National Observatory 4.2m Mayall telescope. Three images were taken in R covering a total of $17' \times 17'$ each, for a total field of 867 square arcminutes. These images were taken by Drs. Robin Ciardullo (of Pennsylvania State University) and Chris Pritchet during a program to image novae in M51 and M101. Seeing and weather conditions were not appropriate for their program and these images of Hercules were kindly taken.

The total exposure time for these images was 300s and seeing was very mediocre ($1''.5$). Weather was not photometric. Calibration for these data was therefore carried out using R band aperture photometry of galaxies in A2151 and other clusters by Strom & Strom (1978). The standard deviation of our calibration (instrumental vs. Strom photometry) is 0.14 magnitudes,

which is not unexpected, given the weather conditions and uncertainties in Strom photometry.

As usual, we plot r_{-2} vs R to remove stars from the sample. This is shown in Figure 8.1. We tabulate the number of objects, stars and galaxies in Table 8.1. We plot the number of stars. galaxies and objects in Figure 8.2. We eliminate background objects using Tyson (1988) counts in R and tabulate the number of objects, background galaxies and cluster members in Table 8.2. We plot the number of objects and background galaxies in Figure 8.3 where we see an excess of objects above background. The LF is plotted in Figure 8.4. Here we fit to N^* (normalization), α and M^* simultaneously, to get:

$$M_R^* = -23.5 \; R = 12.2 \pm 0.5$$

$$\alpha = -1.48 \pm 0.10$$

These values are consistent with values from Lugger (1986) and Oemler (1974) for which $M^* = -23.2$ and $\alpha = -1.40$. Unfortunately, no color information is available for this cluster, so we cannot compare it fully with other objects studied here.

Figure 8.1: Plot of r_{-2} vs R for Hercules

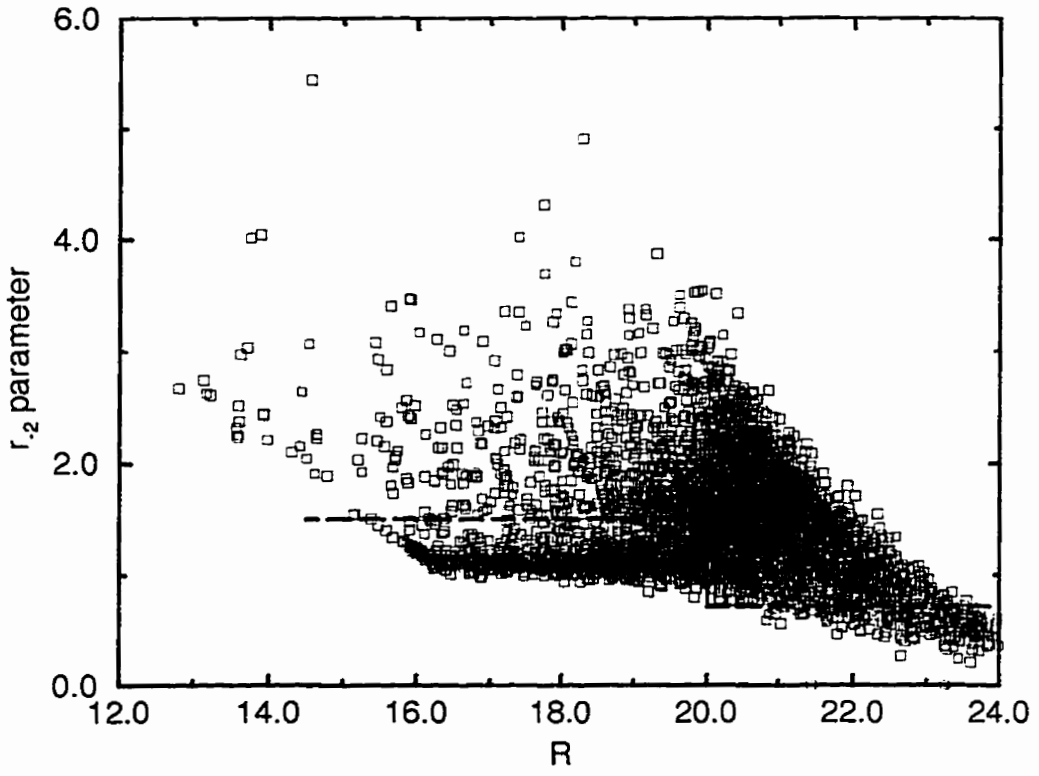

Table 8.1: NUMBER COUNTS FOR HERCULES R FIELDS

R	N. of objects	N. of galaxies	N. of stars
12.25	0.00 ± 0.00	0.00 ± 0.00	0.00 ± 0.00
12.75	1.00 ± 1.00	1.00 ± 1.00	0.00 ± 0.00
13.25	3.00 ± 1.73	3.00 ± 1.73	0.00 ± 0.00
13.75	11.00 ± 3.32	12.00 ± 3.46	0.00 ± 0.00
14.25	3.00 ± 1.73	3.00 ± 1.73	0.00 ± 0.00
14.75	8.00 ± 2.83	8.00 ± 2.83	0.00 ± 0.00
15.25	8.00 ± 2.83	10.00 ± 3.16	0.00 ± 0.00
15.75	32.00 ± 5.66	21.00 ± 4.58	12.00 ± 3.46
16.25	84.00 ± 9.17	23.00 ± 4.80	63.00 ± 7.94
16.75	104.00 ± 10.20	27.00 ± 5.20	78.00 ± 8.83
17.25	120.00 ± 10.95	38.00 ± 6.16	85.00 ± 9.22
17.75	131.00 ± 11.45	53.00 ± 7.28	86.00 ± 9.27
18.25	172.00 ± 13.11	66.00 ± 8.12	112.00 ± 10.58
18.75	229.00 ± 15.13	106.00 ± 10.30	125.00 ± 11.18
19.25	304.00 ± 17.44	151.00 ± 12.29	159.00 ± 12.61
19.75	451.00 ± 21.24	287.00 ± 16.94	181.00 ± 13.45

Figure 8.2: Number of objects, stars and galaxies in Hercules

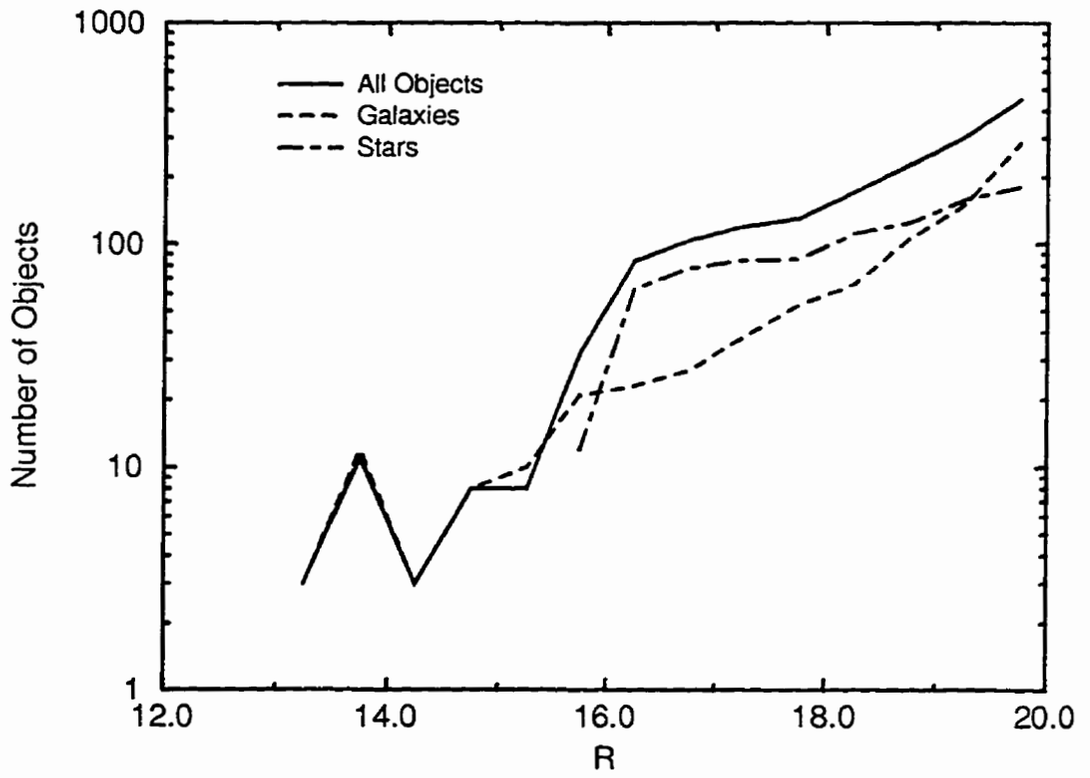

Table 8.2: Number counts for galaxies and background objects in Hercules R fields

R	N. of galaxies	Background counts	N. of cluster members
12.75	1.00 ± 1.00	0.23	0.77 ± 1.11
13.25	3.00 ± 1.73	0.36	2.64 ± 1.83
13.75	12.00 ± 3.46	0.57	11.43 ± 3.54
14.25	3.00 ± 1.73	0.89	2.11 ± 1.97
14.75	8.00 ± 2.83	1.39	6.61 ± 3.06
15.25	10.00 ± 3.16	2.18	7.82 ± 3.49
15.75	21.00 ± 4.58	3.41	17.59 ± 4.94
16.25	23.00 ± 4.80	5.34	17.66 ± 5.32
16.75	27.00 ± 5.20	8.37	18.63 ± 5.95
17.25	38.00 ± 6.16	13.12	24.88 ± 7.15
17.75	53.00 ± 7.28	20.55	32.45 ± 8.58
18.25	66.00 ± 8.12	32.20	33.80 ± 9.91
18.75	106.00 ± 10.30	50.45	55.55 ± 12.51
19.25	151.00 ± 12.29	79.04	71.96 ± 15.17
19.75	287.00 ± 16.94	123.83	163.17 ± 20.27

Figure 8.3: Number of galaxies and background counts in Hercules fields

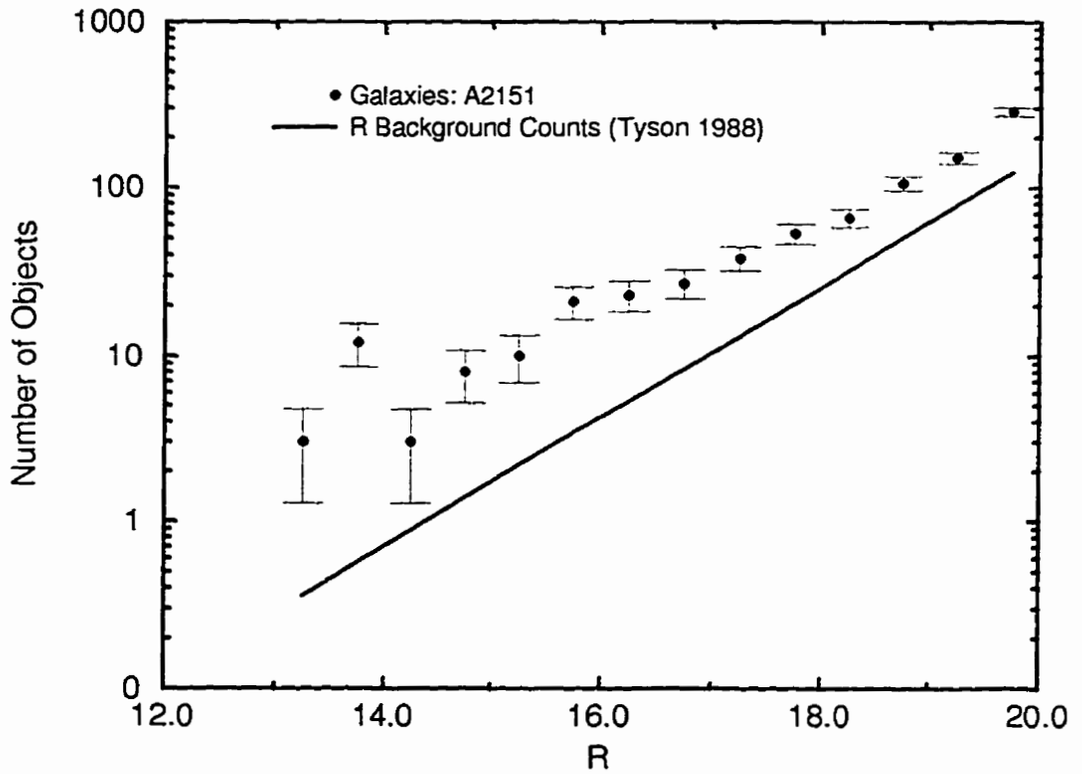

Figure 8.4: Galaxies and LF for Hercules

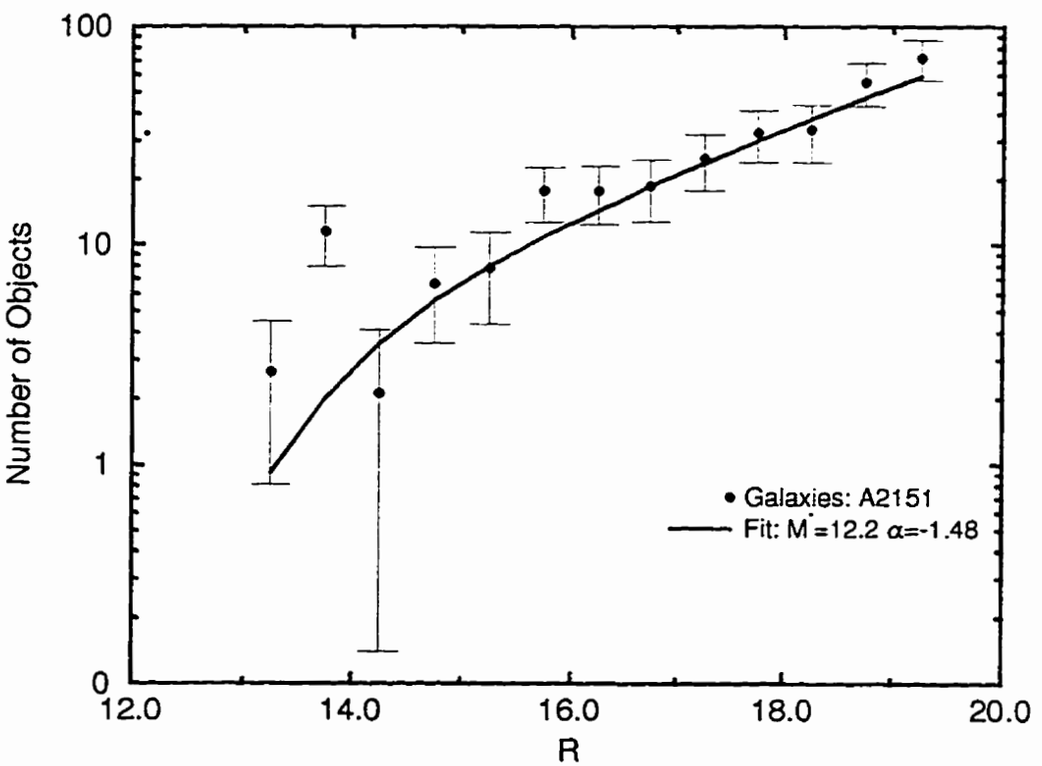

Chapter 9

Conclusions

9.1 Summary of Main Results

We have analyzed the luminosity function of dwarf galaxies in eight clusters, in order to determine the shape of the LF at low luminosities, examine the color distribution of dwarfs and derive their clustering properties in the neighbourhood of giant galaxies.

- For the four clusters (Abell 2052, 2107, 2199 and 2666) observed with HRCAM in 1988-1990, we find that the LF is well fit by a power-law with $\alpha \sim -2.2 \pm 0.2$. This result appears to be robust against errors in background subtraction and in our completeness estimates. The large number of dwarf galaxies in these fields may be due to an upward inflection of the LF at low luminosities or to the very special environment of these cluster fields, which lie within $2'$ of cD galaxies or dominant ellipticals. A population of satellites may also be invoked

to explain this result, by analogy with the populous globular cluster systems often found in the neighbourhood of giant elliptical galaxies in the centres of clusters.

- For galaxies in the centre of Abell 262, around the dominant giant elliptical NGC708, we are unable to derive a V luminosity function (I band data could not be used, as all point spread functions were being distorted into doughnut shapes by focussing problems). This is somewhat surprising, if we consider that this object occupies the centre of the cluster's X-ray gas distribution. There is some evidence for a concentration of faint galaxies in the proximity of NGC708 (within 5′ of the central galaxy), but number counts are not sufficient to derive a reliable LF even by using maximum likelihood methods. Even subtracting number counts directly from the appropriate background field, without any assumption for star-galaxy separation, is found to return a meaningless value of α.

  For the field in the neighbourhood of UGC1308, an elliptical galaxy in the vicinity but outside of the cluster core, we are able to derive a V Lf with $\alpha = -1.38 \pm 0.09$. This is consistent with values for α found in similar clusters, such as Virgo or Coma, and brighter cluster work.

  Data in I are not adequate to derive an accurate LF, especially considering the strong discrepancy between literature counts and our counts, which may be due to the fact that we are sampling considerably brighter

galaxies than Tyson (1988) or Lilly et al. (1991).

Colors for galaxies in this field were also derived and a CMD extracted for this field. It was impossible to use methods of statistical subtraction on the color-magnitude data because of the small number of galaxies in this field. We detect a contribution from cluster galaxies in the form of a dwarf galaxy sequence at $V-I \sim 1.1$. This sequence does not appear to be as tight as for Coma galaxies or for galaxies in UGC3274. This may be due to dilution of the cluster signal by background galaxies, that dominate the counts in this field, or it may mean that cluster galaxies in the outskirts of clusters do not follow the tight color magnitude sequences found in Coma and Abell 539. This may imply a different star formation history for dwarfs outside of the cluster core. On the other hand, no significant color gradient is found to occur in this field towards UGC1308.

Dwarf galaxies in this field are concentrated towards UGC1308. The LF in the inner 5′ of this field (100 kpc at this distance) is essentially the same as for the entire field, whereas the LF in the outer regions of this field cannot be derived, as there are too few galaxies above the contribution by background objects. This suggests that a population of satellites may be responsible for the LF we derived, rather than cluster galaxies. These objects do not appear to have a significantly different $V-I$ color from objects in the outer regions of the field.

It is puzzling that a LF may be derived for the UGC1308 field but not for the central field around NGC708. This may be due to destruction of dwarf galaxies in the core of Abell 262 following dynamical evolution. Very dense environments may be inimical to dwarf galaxies, as shown by the 'turnover' in the LF of compact groups (De Oliveira & Hickson 1991). Yet, our previous work seems to indicate that rich environments may favor survival of faint galaxies in accordance with the Babul & Rees (1992) paradigm. This point will be further elaborated following our discussion of other clusters.

- For galaxies in the centre of the Perseus cluster (Abell 426), centred on the peculiar elliptical NGC1275, we derive a V band LF (by maximum likelihood methods), with $\alpha = -1.93 \pm 0.08$. This is considerably steeper than in other clusters, although it is consistent with our earlier result in cD clusters, and particularly in A2199. As for our previous result we need to consider whether an erroneous background subtraction is responsible. If we decrease the background this just increases the significance of our result. If we assume 125% of background this still yields $\alpha = -1.90$. An error of 50% in background correction yields $\alpha = -1.80$. Such a large error in background estimation is very unlikely.

  The surface density distribution of galaxies in this field is nearly flat, with a central peak in the immediate vicinity of NGC1275. The LF in

two fields chosen to lie within 5′ of NGC1275 and outside of this region is very similar, with $\alpha = -1.90$, which is essentially consistent with the result for the entire field.

For the I band data, we find that $\alpha = -1.74 \pm 0.13$, which is consistent, within errors, with the result found for the V band. Even in this band, the result is robust again variations of 25% in the background, but not for larger variations. It should be recalled that our I background estimation is different from that obtained by extrapolation of data by Tyson (1988) to brighter magnitudes and is based on a single field. We again find that the distribution of galaxies as a function of radius is approximately flat, with a central peak. We find that the LF for galaxies in the inner 5′ and outside of this region is essentially identical.

Colors for galaxies in this field have also been derived. We see a contribution from cluster galaxies at $V - I \sim 1.1$, although this is again not very strong. If we 'clean' the diagram as explained above, we see that most cluster members lie at $V - I \sim 1$ (in the color histogram). This is again consistent with previous work in Coma or in A262 (above), although the sequence is much less tight than for the Coma cluster or UGC3274. This may be due to patchy extinction or be a real difference in the star formation history of galaxies in this field.

We cannot detect any strong color gradient as a function of distance from NGC1275; there is evidence for a blueing trend towards NGC1275

but this is too weak to be considered as firmly established. This is in contrast with the reddening trend reported for Coma.

A second field was observed for this object, in the vicinity of the giant elliptical NGC1265. This is an interesting object, as it is the second ranked cluster galaxy but lies about 20′ from the cluster centre. In the V band, we find that $\alpha = -1.92 \pm 0.08$, which is again consistent with data for the inner field. The same points we made above concerning variation of the background counts from our estimates applies here as well. Galaxies in this field are not concentrated around NGC1265, they rather appear to avoid the immediate neighbourhood of this galaxy. For galaxies within 5′ of the elliptical, we find a LF with $\alpha = -1.75 \pm 0.13$ and for those outside of this region $\alpha = -1.86 \pm 0.22$. Thus, galaxies more distant than 100 kpc from NGC1265 have a a marginally steeper LF, but this is not likely to be significant.

In the I band we find that the LF is again well fit by a power-law with $\alpha = -1.90 \pm 0.06$. If we have underestimated the background counts by 25% we find that $\alpha = -1.73 \pm 0.08$ and $\alpha = -1.69 \pm 0.10$ of the background is raised by 50%. Even a factor of 2 error in background counts yields $\alpha = -1.54 \pm 0.12$. The same caveats as described above are of course valid for this object as well. Galaxies in this field do not appear to be concentrated in the proximity of NGC1265. For galaxies within 5′ of NGC1265 we see that $\alpha = 1.87 \pm 0.23$ and $\alpha = -1.80 \pm 0.08$ for the outer regions. These results are in good agreement with those

for the entire field.

Color magnitude diagrams have been produced for galaxies in this field as well. We see that there is a contribution from a dwarf galaxy sequence at $V - I \sim 1.1$. When this is 'cleaned' as for the other clusters we see a definite sequence at about this color, which is also apparent in the NGC1275 field. The same comments as made for the previous field are also applicable here. Galaxy colors in this field show a reddening trend towards NGC1265.

We can compare LFs and color distributions in the NGC1275 and NGC1265 fields and we see that they are essentially identical.

- For the cluster Abell 539 we were only able to obtain V and I band images of the field centred on the giant elliptical UGC3274. The V band LF for this cluster is well fit by $\alpha = -1.42 \pm 0.09$. Galaxies in this field are not concentrated toward UGC3274. There is a density peak near UGC3274 and the distribution at larger radii is flat, as for the other clusters. In the inner 5′ of this cluster we find $\alpha = -1.37 \pm 0.10$, whereas $\alpha = -1.21 \pm 0.11$. Thus galaxies in the 'outer' field have a marginally flatter LF than in the 'inner' regions of the cluster.

  For this field, the I band data are quite noisy and it is difficult to derive an adequate LF.

  The color magnitude diagram for this cluster shows a very strong dwarf galaxy sequence, in agreement with previous results in Coma, which

this cluster resembles. If we eliminate contamination by background objects, we see a very strong dwarf sequence at $V - I \sim 1.0$. There is evidence of a small blueing trend with decreasing luminosity, although this is not likely to be very significant. Most galaxies lie between $0.75 < V - I < 1.25$. Therefore, in this cluster we can clearly identify a sequence of cluster dwarfs, with very similar stellar populations. There is a radial color gradient in which galaxies nearer to UGC3274 are bluer than those further away. This suggests that either these galaxies are more metal poor or they have had more recent episodes of star formation.

- Finally, we derived a LF for galaxies within the Hercules cluster. Here, the LF is sampled to brighter magnitudes than in our previous work, but our field size is much larger. We obtain $M_R^* = 12.2$ and $\alpha = -1.48$. These results are consistent with previous results for this object (e.g., Oemler 1974). Since we are working in a different passband and we have no color information for this object, we cannot fully compare our findings in this cluster to the other objects we studied.

- The Bahcall-Soneira model for the structure of our Galaxy was also tested at low galactic latitudes, using stars detected in the background fields and in the cluster field and identified as described above. The model appears to overestimate the number of stars at low galactic latitudes by about 40% in nearly all fields. Color distributions are very

well matched in all cases.

In consideration of the length of the previous discussion it is useful to further summarize the above conclusions into a 'summary of the summary' to conclude this section:

In four cD cluster cores (A2052, 2107, 2199 and 2666) we find very steep LFs, with $\alpha \sim -2.2$.

We find that in the center of Abell 262, near the central elliptical NGC708, there are very few dwarf galaxies. There is a small excess of faint galaxies near NGC708. In the field around UGC1308 we are able to derive a LF with $\alpha \sim -1.4$. Galaxies are concentrated within 5′ of the elliptical, so that a population of satellites may be responsible. No color gradient as a function of distance from UGC1308 may be detected.

In Abell 426 we find steep LFs both in the field around the central elliptical NGC1275 and in the field around the bright elliptical NGC1265, with $\alpha \sim -1.9$. In the NGC1275 field galaxies follow a flat distribution as a function of distance from NGC1275, with a central peak in the inner 3′ (60 kpc). LFs have essentially the same slope within 100 kpc of NGC1275 and outside of this region. It is possible to see a sequence (at constant color) in the V vs. $V - I$ plane, although this is much less tight than for Coma or Abell 539. There is a small blueing trend towards NGC1275.

In the NGC1265 field we also find a steep LF, but galaxies avoid the proximity of this elliptical. The LF is marginally steeper outside of a 100

kpc region from NGC1265 than inside of it. While we can see a weak sequence in the V vs. $V-I$ plot this is again less tight than in other clusters. Finally, we see a reddening gradient near NGC1265.

It is interesting that the LFs are very similar both in the NGC1275 field and in the NGC1265 field. Color distributions are also quite similar in both fields.

In Abell 539, we derive a LF with $\alpha \sim -1.5$. Again, the distribution of galaxies as a function of radius is flat, except for a central 'spike' near UGC3274. The LF is marginally steeper near UGC3274 than about 100 kpc away from this central elliptical. We find a very tight sequence of galaxies in the V vs. $V-I$ plot. There is blueing trend toward UGC3274.

Finally, in Hercules we obtain a LF with $\alpha \sim -1.5$ from R band data.

9.2 Discussion

The above results show that there is an *environmental effect on dwarf galaxies in clusters.* In clusters such as Abell 262 and in the neighbourhood of galaxies such as NGC708 (A262) and NGC1265 (A426) fainter galaxies appear to be missing from the LF. These objects may be destroyed by the central galaxy, or their formation may be inhibited by the formation of the giant elliptical. It is not surprising that this should happen, as it is to be expected that tidal interactions with the giant and cannibalism will destroy galaxies in its neighbourhood. One example is provided by the recently discovered dwarf

spheroidal Sagittarius (Ibata et al. 1994; 1995), which shows evidence of tidal disruption. In the compact groups reviewed by De Oliveira & Hickson (1991), that are believed to merge into a giant ellipticals on timescales shorter than a Hubble time, one sees a 'turnover' in the LF, which is evidence for destruction of faint galaxies by the brighter members.

On the other hand we see that in clusters such as Abell 2199 and Abell 426 the LF is very steep and there is, therefore, a large number of dwarf galaxies in these clusters. Therefore it appears that whatever mechanism is operating in A262 is not effective in the proximity of the giant cD galaxies dominating A426 and A2199. Even in A539 there is no evidence for such an effect. The same is also true of the field in the proximity of UGC1308.

One possibility is that this is due to the so-called Babul-Rees effect. Clusters where gas density is highest should show a stronger effect than other objects, where it is lower. Both Abell 426 and Abell 2199 are late XD clusters, in the Jones & Forman (1984) classification scheme and may therefore be considered to have very high gas densities. In these objects, pressure confinement from the intracluster medium may favor survival of dwarf galaxies. In other objects dwarfs perish because of starburst-induced winds or because they are destroyed by tidal interactions and cannibalism.

One objection to this is that high gas densities should ram-strip dwarfs and therefore destroy them, unless dwarf galaxies are all moving downstream, i.e., are more or less at rest with respect to the cluster gas. This may also

explain why they are not cannibalized by the giant elliptical in the cluster centre.

Of course the effect is not detected in Coma and A539. Coma has a high X-ray luminosity but a large core radius, so that its central gas density is lower than in clusters such as A2199 and A426. There have been claims that the LF in the Coma centre is as steep as that in our cD clusters, with $\alpha = -1.8$ (Biviano et al. 1996c). This LF becomes shallower in the proximity of the brightest cluster galaxies NGC4874 and NGC4889, which may argue for some destruction of dwarfs by the giant galaxies as in NGC708 and perhaps NGC1265. Since these galaxies are not at rest with respect to the cluster X-ray gas, they may behave as 'bulls in a china shop' with respect to the fragile dwarf galaxies, as they move down the cluster potential well towards an eventual merger.

In our data dwarfs are not concentrated towards the giants, but their distribution is much more extended, being almost flat as a function of distance from the giant. There is a central density peak but this may be related to the presence of satellite objects to the giant or to the fact that in all of our clusters the giant galaxy coincides with the X-ray center of the cluster. Galaxies avoid the immediate proximity of the bright normal elliptical NGC1265 in Perseus. They are, on the other hand, concentrated towards UGC1308 in A262, but this is likely due to satellites. Thus it appears that while giant ellipticals may destroy dwarfs (as they are expected to), these galaxies sur-

vive well in cluster cores when the giant elliptical is at rest, as these galaxies likely are.

Biviano et al. (1995b) suggest that dwarf galaxies are the true nucleus of the Coma cluster, and have a steep LF. Giant galaxies have dropped into the cluster at a later epoch, together with their associated groups. Their addition provides the 'Gaussian' part of the LF and flattens its slope when it is fitted by a single Schechter function. If the groups associated with the brighter galaxies resemble Hickson compact groups, their faint LF is extremely shallow (De Oliveira & Hickson 1991), and this would flatten the cluster LF. Thus, all clusters may have steep LFs and these may only be visible at very faint magnitudes. A possibility is that in some clusters, such as Perseus, the giant members have formed concurrently with the dwarfs instead of infalling into an environment populated by fragile dwarfs and destroying them.

This approach may be confirmed by the fact that a steep LF is seen not only for the central field of Abell 426 (NGC1275) but also for galaxies outside of the central field, and around the giant elliptical NGC1265, which suggests that the process responsible for the steep LF is cluster wide (i.e., not limited to central region only). Another argument in favor of this point is that color distributions are very similar in both fields.

Information is also provided by colors. In Coma, Secker & Harris (1995) have claimed that dwarf galaxies obey a very tight color magnitude relation (which may also be used for membership discrimination). These galaxies are

also found to obey a radial gradient in color from the central region, which is taken as evidence for the Babul & Rees (1992) effect. This may also imply uniform stellar populations, i.e., similar star formation histories (see later for more comments), although broadband colors not including U are degenerate in that respect.

In Perseus we cannot detect such a strong dwarf galaxy sequence. There is a contribution from dwarfs with a relatively small range of colors. The larger spread may be due to patchy extinction or color errors, but if real it would suggest that dwarfs in Perseus have had a complex and disparate star formation history, with multiple epochs of dwarf galaxy formation or very different metallicities. It may of course be argued that the lack of a strong dwarf galaxy sequence implies that no dwarfs are truly present in this cluster and an erroneous estimation of background contamination is responsible for our steep LF, although we have shown that large variations in background estimation do not affect our value of α.

In Abell 539 we see a strong sequence of dwarf galaxies at $V - I \sim 1.1$, in agreement with previous work in the Coma cluster. The same arguments as described above for Coma are valid here as well. In neither object are we able to confirm the radial color gradient claimed for Coma by Secker & Harris (1995). Rather, we detect a blueing trend towards NGC1275 and UGC3274. A reddening trend is confirmed for the field around NGC1265. This may suggest that dwarf galaxies in the very dense environments in the

neighbourhood of these giant galaxies, that lie at the center of the cluster gas distribution, may accrete gas from the intracluster medium as well (Silk et al. 1987). It is interesting that a reddening trend is visible for galaxies in the vicinity of NGC1265. As for Coma, galaxies closest to this giant elliptical have a flatter LF than galaxies which are more distant. This may imply that that Babul & Rees effect is operating in this field as well, and that accretion of gas and the relative star formation masks the reddening trend in the NGC1275 field.

Finally, we should consider the suggestion by Bassino et al. (1994) that dwarf galaxies may supply the large populations of globular clusters that are sometimes encountered in the neighbourhood of central cluster ellipticals. In this scheme the nuclei of dwarfs become members of the giant's cohort of globular clusters once the stars in the parent dwarf are destroyed or stripped away. Conversely, it is also possible that the bright nuclei of dwarf galaxies are mistaken for globular clusters, whereas the fainter low surface brightness envelope is missed. If this interpretation is correct, we might expect steep LFs to be correlated with normal globular cluster systems and flatter LFs with anomalous ones. The cluster system of NGC6166 (A2199) is 'normal' and the LF is steep, whereas the LF is flatter in Virgo, where the globular cluster system of M87 is very large. More data on the globular cluster and deep LF of galaxies in clusters is needed.

In summary, we propose that the steep LFs we encounter in some clusters

are due to the Babul & Rees (1992) effect, and that dwarfs in environments where gas density is highest (i.e., late XD clusters in the classification by Jones & Forman 1984) may be more affected by this process. These objects may as well accrete gas from the intracluster medium, which would explain the mild blueing trend in the proximity of NGC1275 and UGC3274. Of course this may imply that galaxies in the immediate vicinity of these giant galaxies are more metal poor. We will discuss this, with reference to the Coma cluster in the next section.

We also see that some giant ellipticals may destroy dwarfs. This is clear in the case of NGC708 and possibly NGC1265. The flattening of the LF in the proximity of the two giant galaxies in Coma (Biviano et al. 1996c) also hints to this. It is interesting that in NGC1265 we detect a reddening trend towards the giant galaxy, as in the Coma work by Secker & Harris (1995).

An alternate possibility is that dwarf galaxies, as in Coma (Biviano et al. 1996b), may constitute the main body of the cluster, and have all a steep LF. This would be consistent with the steep LF for Coma by Biviano et al. (1996c) and with the flat surface density distribution seen in the present work. The flatter LFs found in other clusters would be due to the infall of groups (with inverted LFs, such as in compact groups surveyed by De Oliveira & Hickson 1991) and the fitting of a single Schechter function to a two component luminosity distribution. It is likely that these dwarfs are at rest with respect to the cluster gas, especially if the Babul & Rees (1992)

effect is truly at work. In clusters in which steep LFs are seen the central elliptical is at rest as well, occupying the bottom of the cluster potential well. This may favor survival of the fragile dwarfs, as the presence of giant galaxies moving at relatively large speeds through the cluster core may well disrupt many of them.

Further observations are needed to resolve these issues. More information will also be derived in a later work concerning the structure of dwarf galaxies in these clusters and the distance of these clusters (De Propris et al. 1996, in preparation). To conclude our exposition we wish to discuss future prospects for this project.

9.3 Future Work

One obvious extension to this project would be to study a larger number of clusters, chosen to span a large range of evolutionary stages and X-ray properties. It would be interesting to survey some clusters in which the central galaxy does not lie at the bottom of the cluster potential well. Color and spatial information would also be very useful. The new UH 8K camera, now available on CFHT, is very well suited to this project and a collaboration with a French group (Mazure et al. 1996, private communication) has now been formed to address these issues.

The claim that a color gradient is present in Coma is very interesting (Secker & Harris 1994). This may not be due to a metal abundance gradient.

Age gradients may mimic such a gradient, as well as population gradients, in which bluer irregulars are rarer at small clustercentric distances, which is consistent with the observed preference for late type objects to avoid the cluster core (e.g., Giovanelli et al. 1986). In order to do so it would be extremely interesting to obtain colors for dwarf galaxies in the Virgo cluster (which are relatively bright and whose membership is well established) and carry out spectroscopy to determine their metal abundance. This would also allow us to explore their dynamics.

Finally, determination of cluster luminosity functions in high redshift clusters would be very useful. This would allow us to derive M^* and α for clusters at $z = 0.3$ and determine whether these quantities have evolved in the last few billion years.

9.4 Conclusions

We have observed eight clusters of galaxies and derived LFs, surface density distributions and color distributions for faint galaxies in these objects. The main result of this survey is that dwarfs are affected by the cluster environment. While this is not unexpected (Einasto et al. 1974; Giovanelli et al. 1986), the above results shed new light on the behavior of dwarfs in clusters.

The likeliest interpretation of these data is that all clusters have a steep LF at low luminosities, but that this LF is then flattened by the infall of bright galaxies. These objects destroy dwarf galaxies and introduce a population

of dwarf galaxies with very shallow LFs (as in Hickson compact groups — De Oliveira & Hickson 1991). Steep LFs survive in those clusters where the giant galaxies have rapidly fallen to the bottom of the cluster potential well.

It is not unlikely that high gas densities in some clusters also help dwarf galaxies to survive, as predicted by Babul & Rees (1992). Galaxies may also accrete gas from the intracluster medium (Silk et al. 1987) to fuel further star formation as shown by the mild blueing trends towards NGC1275 and UGC3274. Of course metal abundance gradient are another possible explanation.

We discuss perspectives for future work on these subjects.

Bibliography

Abell, G. O. 1958, Astrophysical Journal Supplement Series, 3, 211

Abell, G. O. 1962, in *Problems of Extragalactic Research*, ed. G. C. McVittie, p. 232, New York: Macmillan

Abell, G. O. 1964, ApJ, 140, 1624

Abell, G. O. 1972, in *External galaxies and Quasi Stellar Objects*, IAU Symposium 44, ed. D. S. Evans, p. 341

Abell, G. O., Corwin, H. C. & Olowin, R. 1989, ApJS, 70, 1

Babul, A. & Rees, M. J. 1992, MNRAS, 255, 346

Bahcall, J. & Soneira, R. 1980, ApJS, 44, 73

Bahcall, J. & Soneira, R. 1981, ApJS, 47, 357

Bassino, L. P., Muzzio, J. C. & Rabolli, M. 1994, ApJ, 431, 634

Baum, W. A. et al. 1995, AJ, 110, 2537

Bernstein, G. M., Nichol, R. C., Tyson, J. A., Ulmer, M. P. & Wittman, D., AJ, 110, 1507

Binggeli, B. 1986, in *Star Forming Dwarfs and Related Objects* ed. D. Kunth, T. X. Thuan & J. Tran Tranh Van (Gif-Sur-Yvette: Editions Frontieres), p. 53

Binggeli, B., Tarenghi, M. & Sandage, A. 1990, A&A, 228, 42

Binggeli, B., Sandage, A. & Tammann, G. A. 1988, ARA&A, 26, 509

Binggeli, B., Sandage, A. & Tarenghi, M. 1984, AJ, 89, 64

Biviano, A. et al. 1995a, A&A, 297, 610

Biviano, A. et al. 1995b, preprint

Bothun, G. D., Mould, J. R., Wirth, A. & Caldwell, N. 1985, AJ, 90, 697

Bothun, G. D., Impey, C. D. & Malin, D. F. 1991, ApJ, 376, 404

Buonanno, R., Corsi, C. E., Fusi Pecci, F., Hardy, E. & Zinn, R. 1985, A&A, 152, 65

Broadhurst, T. J., Ellis, R. S. & Shanks, T. 1988, MNRAS, 235, 827

Bucknell, M. J., Godwin, J. G. & Peach, J. V. 1979, MNRAS, 188, 579

Burstein, D. & Heiles, C. 1982, AJ, 82, 1165

Caldwell, N. 1983, AJ, 88, 804

Caldwell, N. & Bothun, G. D. 1987, AJ, 94, 1126

Christian, C. A. et al. 1985 PASP, 97, 363

Colless, M., Ellis, R. S., Taylor, K. & Hook, R. N. 1990, MNRAS, 244, 408

Colless, M., Ellis, R. S., Broadhurst, T. J., Taylor, K. & Peterson, B. A. 1993, MNRAS, 261, 19

Cowie, L. L., Songaila, A. & Hu, E. M. 1991, Nature, **354**, 460

Cuillandre, J. C. 1995, preprint

Da Costa, L. N. et al. 1994, ApJ, 424, L1

Davies, J. I., Phillipps, S. & Disney, M. J. 1988, MNRAS, 231, 69

Davies, J. I. & Phillipps, 1988, MNRAS, 233, 533

Dekel, A. & Silk, J. 1986, ApJ, 303, 39

De Oliveira, C. M. & Hickson, P. 1991, ApJ, 380, 30

De Propris, R., Pritchet, C. J., Harris, W. E. & McClure, R. D. 1995, ApJ, 450, 534

Disney, M. J. 1976, Nature, **263**, 573

Dressler, A. 1978, ApJ, 223, 765

Dressler, A. 1980, ApJ, 236, 351

Eddington, A. S. 1940, MNRAS, 100, 354

Eder, J. A., Oemler, A., Schombert, J. & Dekel, A. 1989, ApJ, 340, 29

Efstathiou, G., Ellis, R. S. & Peterson, B. A. 1988, MNRAS, 232, 431

Eggen, O. J., Lynden-Bell, D. & Sandage, A. 1962, ApJ, 136, 748

Einasto, J., Saar, E., Kaasik, A. & Chernin, A. D. 1974, Nature, **252**, 111

Faber, S. M. & Lin, D. N. C. 1983, ApJ, 266, L17

Felten, J. E. 1977, AJ, 82, 861

Felten, J. E. 1985, Comments on Astrophysics and Space Science, **11**, 53

Ferguson, H. C. & Sandage, A. 1988, AJ, 96, 1520

Ferguson, H. C. 1992, in *The Physics of Nearby Galaxies: Nature or Nurture ?* ed. T. X. Thuan, C. Balkowski & J. T. T. Van, Editions Frontieres, p. 442

Ferguson, H. C. & Binggeli, B. 1994, Astronomy and Astrophysics Reviews, 6, 67

Giovanelli, R., Haynes, M. & Chincarini, G. 1986, ApJ, 300, 77

Jedrzejewski, R. I., 1987, MNRAS, 226, 747

Johnson, H. L. 1965, ApJ, 141, 923

Jones, C. & Forman, W. 1984, ApJ, 276, 38

Harris, W. E. 1991, ARA&A, 29, 543

Harris, W. E., Pritchet, C. J. & McClure, R. D. 1995, ApJ, 441, 120

Hartwick, F. D. A. 1995, preprint

Holmberg, E. 1950, Publications of the Lund Observatory, Series 2, 128

Hubble, E. 1936a, ApJ, 84, 158

Hubble, E. 1936b, ApJ, 84, 270

Hubble, E. 1936c, *The Realm of the Nebulae*, New Haven: Yale University Press

Hubble, E. & Humason, M. L. 1931, ApJ, 74, 43

Hunter, D. A. & Gallagher, J. S. 1985, ApJS, 58, 533

Impey, C., Bothun, G. & Malin, D. 1988, ApJ, 330, 634

Kashikawa, N. et al. 1995, ApJ, 452, 99

Kiang, T. 1961, MNRAS, 122, 263

Kirshner, R. P., Oemler, A., Schchter, P. & Schechtman, S. A. 1983, ApJ, 88, 1285

Koo, D. C. & Kron, R. G. 1992, ARA&A, 30, 613

Koo, D. C., Gronwall, C. & Bruzual, A. G. 1993, ApJ, 415, L21

Kron, R. G. 1980, ApJS, 43, 320

Ibata, R. A., Gilmore, G. & Irwin, M. J. 1994, Nature, **370**, 194

Lavery, R. J. & Mighell, K. J. 1992, AJ, 103, 81

Lilly, S. J. 1993, ApJ, 411, 501

Lilly, S. J., Cowie, L. L.& Gardner, J. P. 1991, ApJ, 369, 79

Lilly, S. J., Tresse, L., Hammer, F., Crampton, D. & Le Fevre, O. 1995, ApJ, 455, 108

Lin, D. N. C. & Faber, S. M. 1983, ApJ, 266, L21

Lin, H. et al. 1995, preprint

Loveday, J., Peterson, B. A., Efstathiou, G. & Maddox, S. J. 1992, ApJ, 390, 338

Lugger, P. M. 1986, ApJ, 303, 535

Lynden-Bell, D. 1982, Observatory, **102**, 202

Majewski, S. 1994, ApJ, 431, L17

Majewski, S., Munn, J. A. & Hawley, S. 1994, ApJ, 427, L37

Marlowe, A. T., Heckman, T. M., Wyse, R. F. G. & Schommer. R. 1995, ApJ, 438, 563

Marzke, R. O., Huchra, J. P. & Geller, M. J. 1994a, ApJ, 428, 43

Marzke, R. O., Geller, M. J., Huchra, J. P. & Corwin, H. G. 1994b, AJ, 108, 437

McClure, R. D. 1991, PASP, 101, 1156

Metcalfe, N., Shanks, T., Fong, R. & Jones, L. R. 1991 MNRAS, 249, 498

Meurer, G. R., Freeman, K. C., Dopita, M. A¿ & Cacciari, C. 1992, AJ, 103, 60

Montgomery, K. A., Marschall, L. A. & Janes, K. A. 1993, AJ, 106, 181

Nilson, P. 1973, *The Uppsala General Catalogue of Galaxies*, Nova Acta RegiæSocietatis Scientiarum Upsaliensis, Ser V:A, 1

Oemler, A. 1974, ApJ, 194, 1

Peebles, P. J. E. 1975, ApJ, 196, 647

Peebles, P. J. E. 1980, *The Large Scale Structure of the Universe*, Princeton: Princeton University Press

Phillips, S., Davies, J. I. & Turner, J. A. 1994, in IAU Symposium 161 *Wide Field Imaging*; ed. R. West, Kluwer, Dordrecht

Postman, M. & Geller, M. J. 1984, ApJ, 281, 95

Pritchet, C. J. 1983, AJ, 88, 1476

Pritchet, C. J. & Harris, W. E. 1990, ApJ, 355, 410

Pritchet, C. J. & Infante, L. 1992a, ApJS, 83, 237

Pritchet, C. J. & Infante, L. 1992b, ApJ, 399, L35

Ribeiro, A. L. B., De Carvalho, R. R. & Zepf, S. E. 1994, MNRAS, 267, L13

Sandage, A., Tammann, G. A. & Yahil, A. 1979, ApJ, 232, 352

Sandage, A., Binggeli, B. & Tammann, G. A. 1985, AJ, 90, 1759

Sarajedini, A. & Layden, A. C. 1995, AJ, 109, 1086

Scott, E. L. 1957, AJ, 62, 248

Secker, J. & Harris, W. E. 1995, preprint

Shapley, H. 1938, Bull. Harv. Coll. Obs., No. 908

Silk, J., Wyse, R. F. G. & Shields, G. A. 1987, ApJ, 322, L59

Smecker-Hane, T. A., Stetson, P. B., Hesser, J. E. & Lehnert, M. D. 1994, AJ, 108, 507

Songaila, A., Cowie, L. L., Hu, E. M. & Gardner, J. P. 1994, ApJS, 94, 461

Steidel, C., Dickinson, M. & Persson, S. E. 1994, ApJ, **437**, L75

Thompson, L. A. & Gregory, S. A. 1993, AJ, 106, 2197

Tresse, L., Hammer, F., Le Fevre, O. & Proust, D. 1993, A&A, 277, 53

Tully, R. B. 1988, AJ, 96, 73

Tyson, J. A. 1988, AJ, 96, 1

Vader, J. P. & Sandage, A. 1991, ApJ, 379, L1

van den Bergh, S. 1992, MNRAS, 255, 29p

van den Bergh, S. 1994, in *The Local Group: Comparative and Global Properties*, ESO/CTIO workshop.

White, S. D. M. & Frenk, C. S. 1991, ApJ, 379, 52

Whitmore, B. C., Gilmore, D. M. & Jones, C. 1993a, ApJ, 407, 489

Whitmore, B. C., Schweizer, F., Leitherer, C., Borne, K. & Carmelle, R. 1993b, AJ, 106, 1354

Wirth, A. & Gallagher, J. S. 1984, ApJ, 282, 85

Zepf, S. E. 1995, preprint

Zinn, R. 1993, in *The Globular Cluster-Galaxy Connection*, Astronomical Society of the Pacific Conference Series, **48**, 302 edited by G. Smith & J. Brodie

Zwicky, F. 1942, Physical Review, **61**, 489

Zwicky, F. 1957, *Morphological Astronomy*, Berlin: Springer-Verlag

Zwicky, F. 1964, ApJ, 140, 1467

Zwicky, F., Herzog, E., Wild, P., Karpowicz, M. & Kowal, C. 1961-1968, *Catalog of Galaxies and Clusters of Galaxies*, Pasadena: California

Institute of Technology